EUROENGEO ATHENS 2020

Editors
V. P. MARINOS
C. LOUPASAKIS
C. SAROGLOU
N. DEPOUNTIS
G. PAPATHANASSIOU

3RD EUROPEAN REGIONAL CONFERENCE OF THE INTERNATIONAL ASSOCIATION FOR ENGINEERING GEOLOGY & THE ENVIRONMENT

Leading to Innovative Engineering Geology Practices

VOLUME 2
Full Papers
Proceedings

Organised by the National Group of Greece of IAEG

EUROENGEO ATHENS 2020

Leading to Innovative Engineering Geology Practices

EDITORS

Vassilis P. Marinos
Chairman of the Conference
Vice President of IAEG for Europe
Assistant Professor National Technical University of Athens, Greece

Constantinos Loupasakis
Co-Chairman of the Conference
President of Greek NG of IAEG
Associate Professor National Technical University of Athens, Greece

Charalampos Saroglou
Co-Chairman of the Conference
Secretary of Greek NG of IAEG
Dr. Engineering Geologist National Technical University of Athens, Greece

Nikos Depountis
IAEG NG of Greece
Assistant Professor University of Patras, Greece

George Papathanassiou
IAEG NG of Greece
Assistant Professor Aristotle University of Thessaloniki, Greece

ORGANIZING COMMITTEE

Vassilis P. Marinos
Chairman of the Conference-Vice President of IAEG for Europe

Constantinos Loupasakis
Co-Chairman of the Conference- President of Greek NG of IAEG

Charalampos Saroglou
Co-Chairman of the Conference – Secretary of Greek NG of IAEG

Georgios Stoumpos
Secretary of the Conference – NG of IAEG

Andreas Kaplanidis
Treasurer of the Conference – NG of IAEG

Nikos Depountis
IAEG NG of Greece

George Papathanassiou
IAEG NG of Greece

Stratis Karantanellis
IAEG NG of Greece – YEG Chair

Rafig Azzam
President of IAEG – Germany

Faquan Wu
Secretary of IAEG – China

Eugene Vosnesensky
Vice President of IAEG for Europe- Russia

Louise Vick
Chairman of YEG of IAEG-Norway

ADVISORY COMMITTEE

Ferentinou Maria
Representative of IAEG NG of South Africa

Fleurisson Jean – Alain
Treasurer of IAEG-France

Giordan Daniele
President of Italian NG of IAEG

Hutchinson Jean
Vice President of IAEG for N. America

Johnson Doug
Vice President of IAEG for Australasia – IAEG NG of New Zealand

Kazilis Nikos
IAEG NG of Greece

Kurosch Thuro
Representative of IAEG NG of Germany

Reeves Helen
Representative of IAEG NG of UK

Stavropoulou Maria
IAEG NG of Greece

Ulusay Resat
Editor in chief of BOEG- President of ISRM-IAEG NG of Turkey

Verhoef Peter
Representative of IAEG NG of Nederland

Vlachopoulos Nikos
Representative of IAEG NG of Canada

Waeber Julien
Representative of IAEG NG of USA

Zangerl Christian
Representative of IAEG NG of Austria

SCIENTIFIC COMMITTEE

Abolmasov Biljana
Alexiadou Chara
Ann Williams
Azzam Rafig
Baynes Fred
Benardos Andreas
Bozzano Francesca
Burns Scott F.
Christaras Vassilis
Cohen-Waeber Julien
Dahal Ranjan Kumar
Delgado Carlos
Depountis Nikos
Dong, Jia-Jyun
Evelpidou Niki
Giordan Daniele
Gkanas Athanassios
Gkouvailas Alkis
Huiming Tang
Hutchinson Jean
Jang Bo-An
Kaplanidis Andreas
Kazilis Nikos
Kiril Angelov
Kontoes Charalampos
Kosović, Ivan
Koukis George
Kurosch Thuro
Lawrence James
Lekkas Efthimios
Lollino Giorgio
Loupasakis Constantinos
Marinos Paul
Marinos Vassilis
Mark Eggers
Mavrouli Olga
Mazzanti Paolo
Murphy Bill
Ngan-Tillard Dominique
Nikolaou Nikolaos
Nomikos Pavlos
Nomikou Paraskevi
Oliveira Ricardo
Papathanassiou George
Papoutsis Ioannis
Paraskevopoulou Chrysothemis
Parharidis Isaak
Perleros Vassilis
Rozos Dimitrios
Sabatakakis Nikos
Saroglou Charalampos
Simeon Abam Tamunoene Kingdom
Stavropoulou Maria
Steiakakis Manolis
Stoumpos George
Torok Akos
Tsagaratos Paraskeyas
Tsiambaos Georgios
Tsifoutidis Georgios
Ulusay Resat
Vassilakis Manolis
Verhoef Peter
Vick Louise
Vilneuve Marlene
Vlachopoulos Nikos
Vosnesensky Eugene
Wasoski Janusz
Wu Faquan
Yiouta-Mitra Paraskevi
Zangerl Christian

Thank you to our SPONSORS

TERNA GEK TERNA GROUP

AVAX

ΑΤΤΙΚΕΣ ΔΙΑΔΡΟΜΕΣ

Hellas GOLD

intrakat

ATTIKO METRO S.A.

METRICA

geo STAND

Edafomichaniki S.A.

geotest

NEOTEK

ΔΕΗ

ATENEIA

OmikronKappa Consulting

GEOGNOSI S.A.
GEOTECHNICAL - GEOLOGICAL INVESTIGATIONS & DESIGN CONSULTANT ENGINEERS & GEOLOGISTS

Ο.Α.Σ.Π.

ΟΛΥΜΠΙΑ ΟΔΟΣ

MACCAFERRI

EDAFOS S.A.
ENGINEERING CONSULTANTS

OTM SA
Engineering Consulting Company

Under the auspices

HELLENIC REPUBLIC
MINISTRY OF INFRASTRUCTURE AND TRANSPORT

Endorsed by

CITY OF ATHENS

National Technical University of Athens

Aristotle University of Thessaloniki

Technical University of Crete

DEMOCRITUS UNIVERSITY OF THRACE

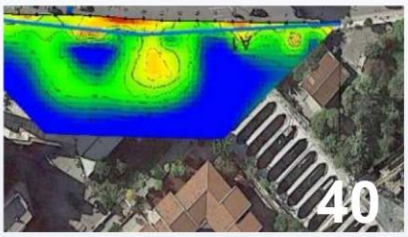

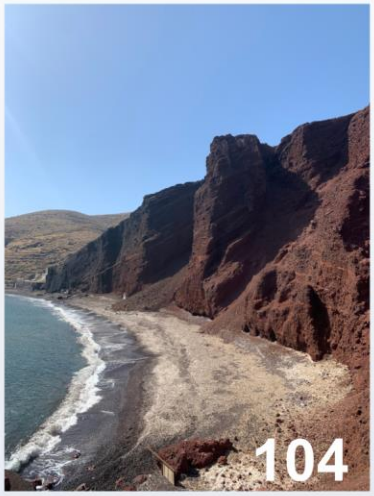

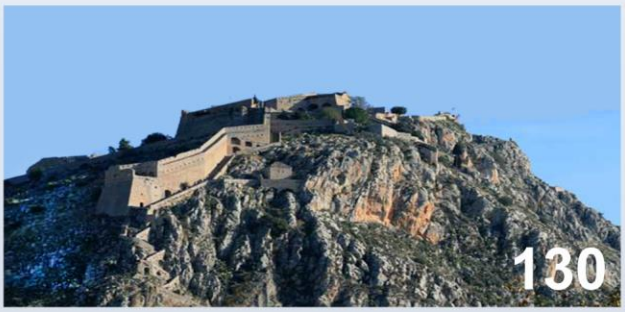

THEMES

Theme 1 - Characterisation and Behaviour of Soils and Rocks.....01

Theme 2 - Environmental Engineering Geology.....31

Theme 3 - Advances in Site Investigation for Engineering Geology.....40

Theme 4 - Engineering Geology for Engineering Works.....46

Theme 5 - Engineering Geology for Urban Environment.....96

Theme 6 - Analysis and Mitigation of Geo-hazards.....104

Theme 8 - Engineering Geology and Cultural Heritage Protection.....130

Theme 10 - Aggregates and Construction Materials.....139

TABLE OF CONTENTS

THEME 1 - CHARACTERISATION AND BEHAVIOUR OF SOILS AND ROCKS 1

Sandstone Intact Rock Strength - A focus on the comparison between uniaxial and triaxial laboratory tests in tunnelling design 2
Lorenzo Paolo Verzani, Giordano Russo

The influence of subjective factors on the accuracy of graphical constructions to interpret the preconsolidation pressure in IL-tests 10
Vladimir Matveev, V.V. Shanina

Investigation of the mechanical properties of tectonized limestones in western Lefkada Island, Greece, via field methods, laboratory testing and back-analyses of a co-seismic landslide 18
Vassilis Kallimogiannis, Charalampos Saroglou

The Behaviour of Sand Stabilized with Colloidal Silica in Triaxial Compression and Extension 24
Eleni-Maria Pavlopoulou, Vassiliki Georgiannou, Filippos Chortis

THEME 2 - ENVIRONMENTAL ENGINEERING GEOLOGY 31

Assessment of Human Exposure to Polycyclic Aromatic Hydrocarbons in Groundwater near Municipal Landfills 32
Alexandru Balint

THEME 3 - ADVANCES IN SITE INVESTIGATION FOR ENGINEERING GEOLOGY.....40

Prediction of the hydrogeological conditions in the Snowy 2.0 deep tunnels by means of temperature measurements 41
Antonio Dematteis, Manfred Thuering, Francisco Alvarado, Gabriele De Carli

THEME 4 - ENGINEERING GEOLOGY FOR ENGINEERING WORKS.....46

Combination of cementitious and chemical grouting in the transition zone of unlined and concrete-lined tunnel: a case from Upper Tamakoshi Hydroelectric Project, Nepal 47
Sanjib Sapkota, Renos Christakis, Jharendra KC, Mahesh Raut

Engineering Geological Aspects of Pipelines, an Australian Prospective 62
Graeme Jardine

Investigation of the Effects of Hydraulic Connection Between Neighboring Valleys and Geologic Structure on Dam Site Selection 74
Remzi Karagüzel, H. T. Yalçın, Cenk Yaltırak

Performance of different chemical soil stabilisers in the presence of sulphates 82
Maria Mavroulidou, Chris Gray, Mike J. Gunn

A comparative study of different biocementation implementation methods for embankment foundation soil 89
M.U. Safdar, Maria Mavroulidou, Mike J. Gunn, D. Purchase, I. Payne, J. Garelick

THEME 5 - ENGINEERING GEOLOGY FOR URBAN ENVIRONMENT 96

Geotechnical Evaluation of Acıpayam Basin (Denizli-Turkey) by Using A Geological and Geotechnical Information System (GEO-GIS) 97
Halil Kumsar, T. Sarayköylü, Y. Say

THEME 6 - ANALYSIS AND MITIGATION OF GEO-HAZARDS.....104

Merge historical documents digitalisation with LiDAR: a method for assessing and disseminating rockfall mitigation strategies.....105
Davide Notti, Daniele Giordan, Diego Guenzi, Rosa Lasponara

The application of empirical rainfall thresholds towards shallow landslide probability estimation in fire-affected areas 113
Spyridon Lainas, Nikolaos Depountis, Nicholas Sabatakakis

Rock mass characterisation for rock slope instabilities using aerial photogrammetry and 3D Point Cloud Model interpretation 121
Charalampos Saroglou, Deheng Kong, Faqua Wu, Vassilis Kallimogiannis, Athina Tsirogianni, Neil Bar

THEME 8 - ENGINEERING GEOLOGY AND CULTURAL HERITAGE PROTECTION .. 130

Profiling of the recent deposits of Nafplio coastal plain (Greece) from engineering geological modelling and geophysical surveys 131
Charalampos Saroglou, Francesca Bozzano, Salvatore Martino, Aggelos Mouzakiotis, Vassilis Karastathis, Athina Tsirogianni, Benedetta Antonielli, Paolo Ciampi, Matteo Fiorucci, Roberto Iannucci, Daniele Inciocchi, Charilaos Maniatakis, Stefano Rivellino, Andreas Antoniou, Achilleas Papadimitriou, Renzo Carlucci, Alessio Di Iorio

THEME 10 - AGGREGATES AND CONSTRUCTION MATERIALS 139

Importance of Engineering Geological Studies in Resource and Reserve Reporting for Aggregates 140
Atiye Tuğrul, Murat Yilmaz

Author Index 148

THEME 1 - CHARACTERISATION AND BEHAVIOUR OF SOILS AND ROCKS

Sandstone Intact Rock Strength - A focus on the comparison between uniaxial and triaxial laboratory tests in tunnelling design

Lorenzo Paolo Verzani[1], Giordano Russo[1]

[1]*GEODATA Engineering, Turin, Italy*
lpv@geodata.it , grs@geodata.it

ABSTRACT: A complex hydropower project, with many underground structures, requires a lot of investigations and studies for a whole understanding of the rock mass behaviour. A recent large underground project in Andean Cordillera offers opportunity for a focus on the comparison between the laboratory data obtained from uniaxial and triaxial compressive tests on sandstone samples, with main reference to the Hoek-Brown failure criterion. These results drive the geomechanical characterization, with a direct consequence on the design, as the behaviour of the excavated rock masses strongly depends on the intact-rock proprieties. The knowledge of field geology based on site observations, surveys and investigations, is also fundamental for the interpretation of laboratory data. The availability of tens of confined compressive strength tests (→ σci) on sandstone and their analysis through many rupture envelopes are of interest for a better understanding on the results of the laboratory data, possibly affected by different behaviour of the rock samples when tested through the unconfined compressive test (→ UCS). The sharp difference between the Hoek-Brown strength criterion parameter σci and the UCS parameter is shown.

Keywords: Intact Rock Strength, UCS, Triaxial Tests (σci)

1. Introduction

The intact rock strength is a parameter that strongly influence the characterization of the rock mass with a direct consequence on tunnelling design.

Bewick et Al. (2015) and Kaiser (2016) focused on the conceptual difference between UCS and the Hoek-Brown parameter σ_{ci} derived by fitting in the main stresses plane the results of triaxial compressive tests. Moreover, the same Authors recommended the basic reference to σ_{ci} while indicating the Hoek-Brown failure envelope for the design.

The purpose of this paper is to take advantage of the large number of laboratory tests performed on the Cretaceous sandstones in the Andean Cordillera to analyse these rock parameters, possibly to individuate a rational procedure for assessing the most appropriate and representative design values of the intact rock strength.

2. Geological setting

The study area is in the central part of the Andean Cordillera, which is known as a double vergence chain controlled by the subduction of the Nazca Plate below the continental plate of South America. The convergence of these plates is the main responsible for the geodynamic setting and the tectonic structures of the site. Figure 1 shows a block-diagram view of the interpreted deep structures of the Andes representative of the interest area, located in the eastern side of the chain, in the Sub-Andeans area between the Eastern Cordillera and the Amazonian plain.

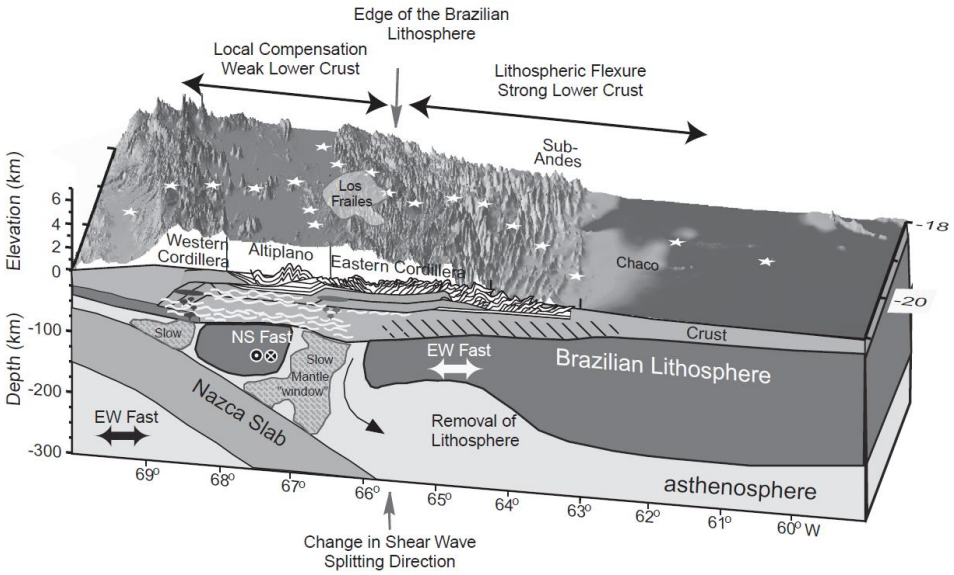

Figure 1. Regional scale interpretation of the crust and mantle structures in the Central Andes (McQuarrie et al., 2005)

The main works of the project are in a sedimentary sequence belonging to an asymmetric anticline, with the long side dipping toward SW. The bedrock is mostly covered by a thin layer of Quaternary deposits, mainly composed by coarse debris and alluvial cobbles. The tropical vegetation densely covers the whole area.

The bedrock sequence is composed by three geological formations tectonically stacked and separated by sliding planes with medium dipping. The direction of these plans is approximately parallel to the stratification and perpendicular to the longitudinal axis of the underground works. Figure 2 shows a 3D geological model of the project area.

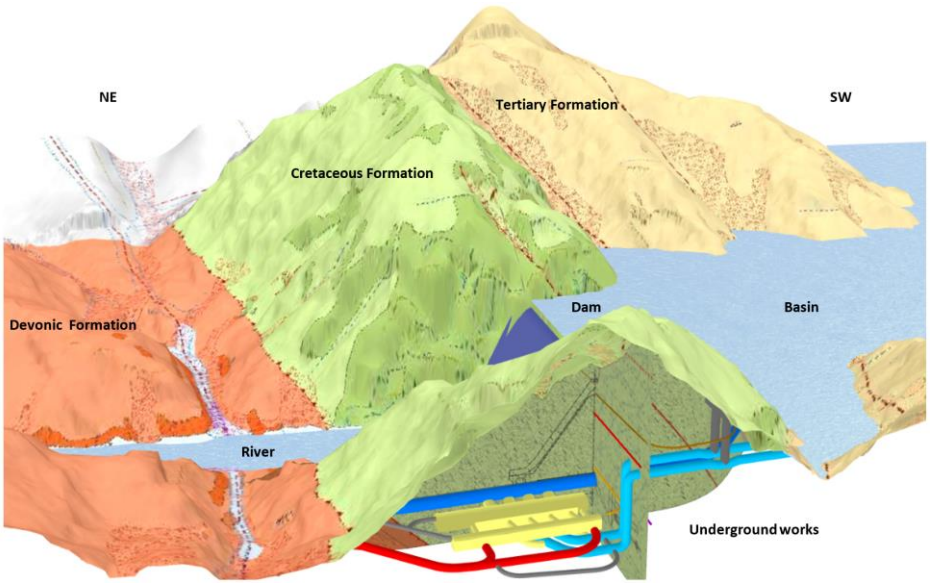

Figure 2. 3D geological model of the project area

Starting from upstream, at the top of the sequence outcrops the Tertiary Formation, with fractured sandstone interbedded to shales and claystone layers. The morphology is hilly with plain areas.

Moving downstream, in a mountain context, massive banks of quartzite-sandstone, belonging to the Cretaceous Formation, are exposed along the steep sides of the gorge (Figure 3); some high angle minor faults and master joints were detected during the geological survey.

Figure 3. The sandstone of Cretaceous Fm. outcropping along the riverbanks. Sandstone outcrop in massive banks; the original layering includes cross-bedding structure. Large collapsed blocks are locally piled on the edge of the river, fallen from the rocky slope

In this area there are the main underground works and external structures, therefore the Cretaceous sandstones were strongly investigated and tested during the two main investigation campaigns. Three major discontinuity-sets were measured in the sandstone rock masses (Table 1).

Table 1. Main discontinuity-sets measured in the sandstone Cretaceous Formation

Discontinuity set	Dip-Direction (-)	Dip (°)
Bedding (St)	SW	50 - 70
Joint set (Jn1)	E	20 - 50
Joint set (Jn2)	NNW	75 - 90

The fracturing degree, observed in the core samples and loggings (e.g. acoustic BHTV and optical OPTV tele-viewer images) from several vertical and inclined boreholes, is moderately low.

Moving further downstream, in the last part of the work, the Devonian Formation outcrops. It is an intensely folded sequence of sandstone alternated with shales, more fractured due to the proximity to a regional anticline axis which bends the described sedimentary sequence.

The tectonic discordance contact between Devonian and Cretaceous formations is marked by a pre-Cretaceous over thrust, while the tectonic contact between Cretaceous and Tertiary formations is given by low to medium-angle reverse fault.

3. Analysis of laboratory tests

By the analysis of the data obtained from the laboratory tests, some differences were observed between the sandstone samples (Cretaceous Fm.) collected in the boreholes located close to river area and those collected deeper inside the slope to investigate the cavern area. This condition even emerged from the analysis of the values of the unit weight (γ), where the higher values belong to the sandstones of the river area (Figure 4).

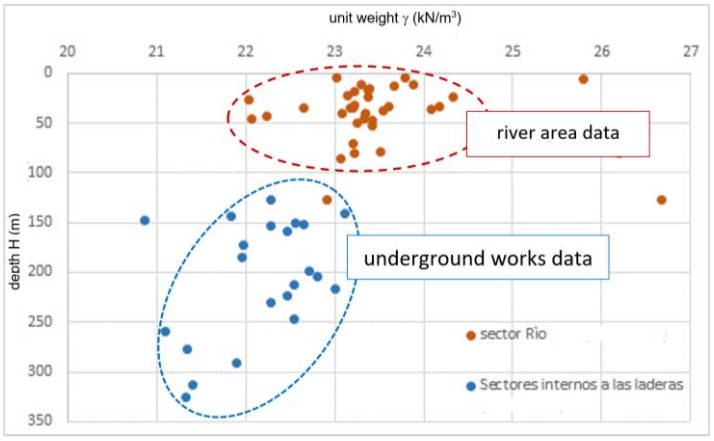

Figure 4. Cretaceous Fm.: unit weight (γ) vs depth (H), from different sectors

By the comparison of the results of the triaxial tests, the higher strength of the sandstones from the river area was also observed (Figure 5). The difference is related to the sedimentation process and the tectonic setting, since even by the comparison between the data from the samples collected at deeper levels on the two sides of the river (distance ~400m), a total similarity of the results was obtained. While the shallow sandstones of the river area showed a different behaviour (Figure 6).

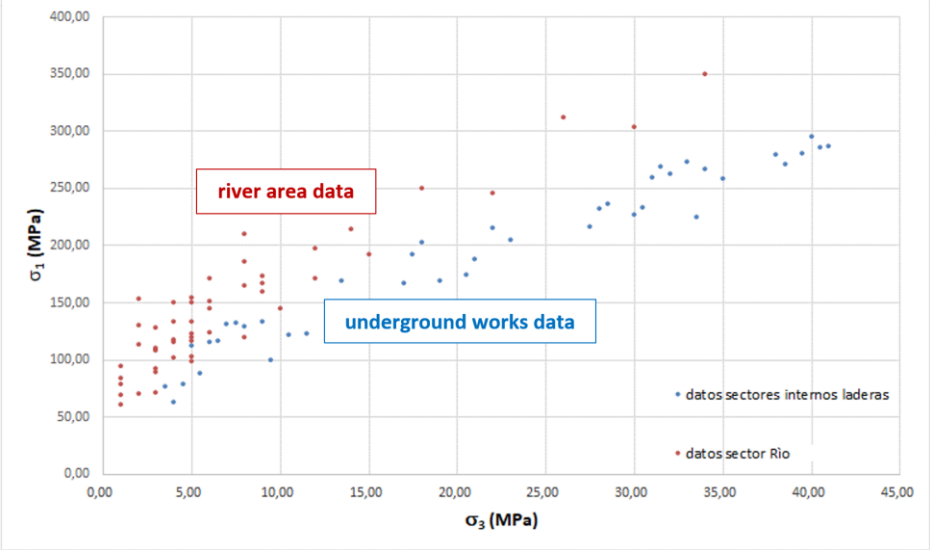

Figure 5. Cretaceous Fm.: triaxial test data, from different sectors

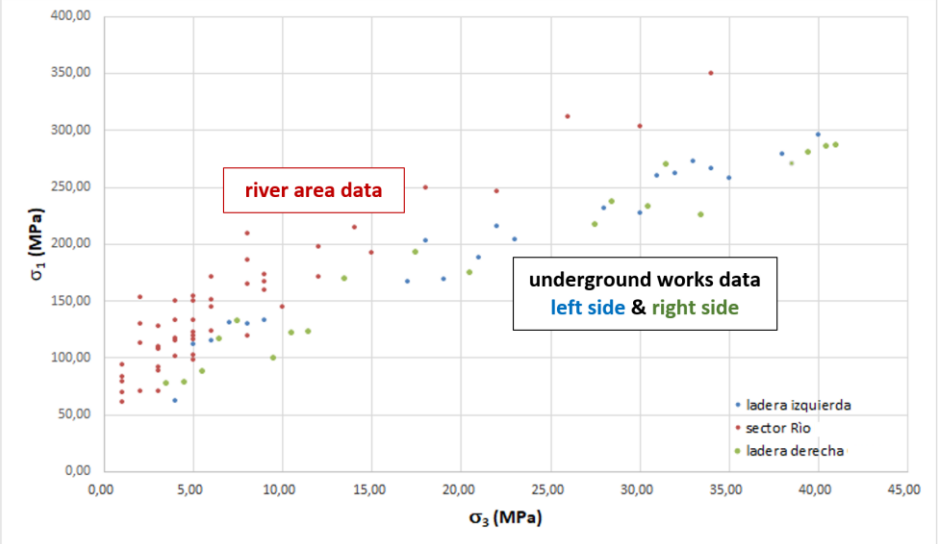

Figure 6. Cretaceous Fm.: triaxial test data, differentiation of left and right sides for deeper rock

The UCS data have a high range of variability (~10 to 65MPa, Figure 7), since many factors as the failure mechanism and testing procedure significantly affected the strength-values. Generally, the lower values, not representative, were associated to sampling disturbance and the partial rupture of the sample, while the higher ones to the shear-failure across the whole sample.

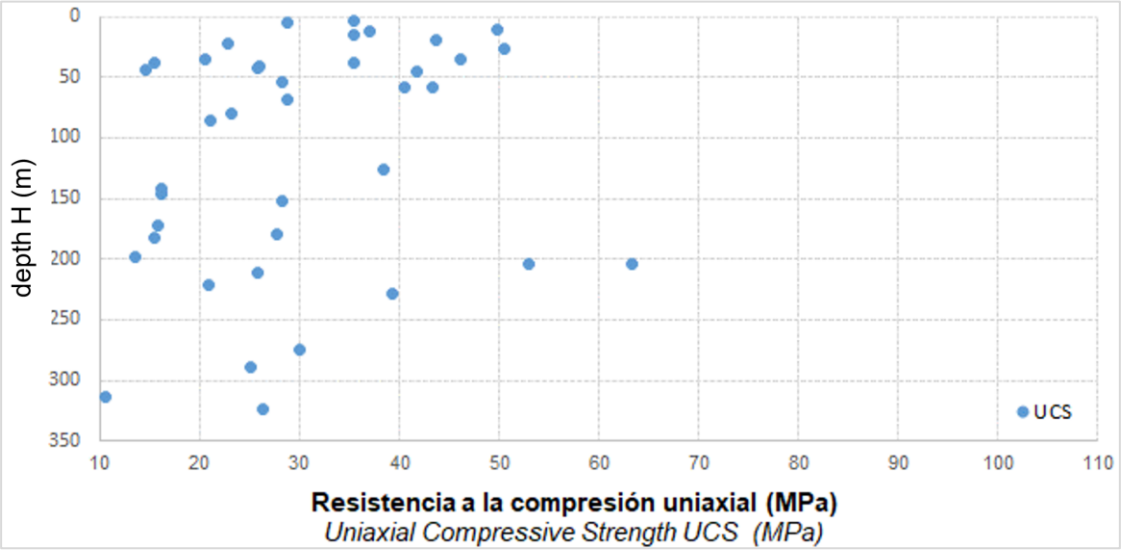

Figure 7. Cretaceous Fm.: Uniaxial Compressive Strength (UCS) vs depth (H)

From the comparison between the results of the compressive strength obtained with Uniaxial (→UCS) and the Triaxial (→ σ_{ci}) tests a clear difference was observed, by deriving in prevalence high values from the latter (UCS<<σ_{ci}). Furthermore, considering the different trends σ_1/σ_3 obtained from the samples collected in different sites (river area and underground structures), the triaxial data were analysed separately.

For the Cretaceous Formation 91 triaxial tests are available, 41 sandstone-samples were collected from the deeper levels (underground works) and 50 from the river area. According to the Hoek-Brown failure-criterion, the intact rock parameter "m_i" (material constant) and "σ_{ci}" (i.e. the resulting σ_1 value with σ_3=0) are thus calculated.

Different analyses (RocLab, by Rocscience) were performed, to define the representative values of the parameters.

For the river area, the 50 TX-tests have confinement values in the range 1<σ_3<34MPa; different combinations of the value pairs of the main stresses (σ_1/σ_3), give values of m_i variables approximately between 14 and 24 and values of σ_{ci} variables from 70MPa to approximately 116MPa (Figure 8). The representative values of the parameters are:

- m_i 18 (14-22)
- σ_{ci} 90 (70-110) MPa.

For the underground work sectors, the 41 TX-tests have confinement values in the range 4<σ_3<41MPa (Figure 9), by the combinations of the value pairs of the main stresses the representative parameters are:

- m_i 23±1 (22-24)
- σ_{ci} 65 (50-80) MPa.

The average σ_{ci} value, between 90MPa and 65MPa, is exactly the value obtained from the analysis of all the 91 TX-tests plus one sound and representative UCS value obtained from a reliable test with the shear-failure across the whole sample (Figure 10):

- m_i 18.5
- σ_{ci} 77.8 MPa.

The m_i values obtained from different combinations of triaxial test data is consistent with the range indicated in the Literature for sandstone rocks (m_i=17±4, Hoek-Brown failure criterion).

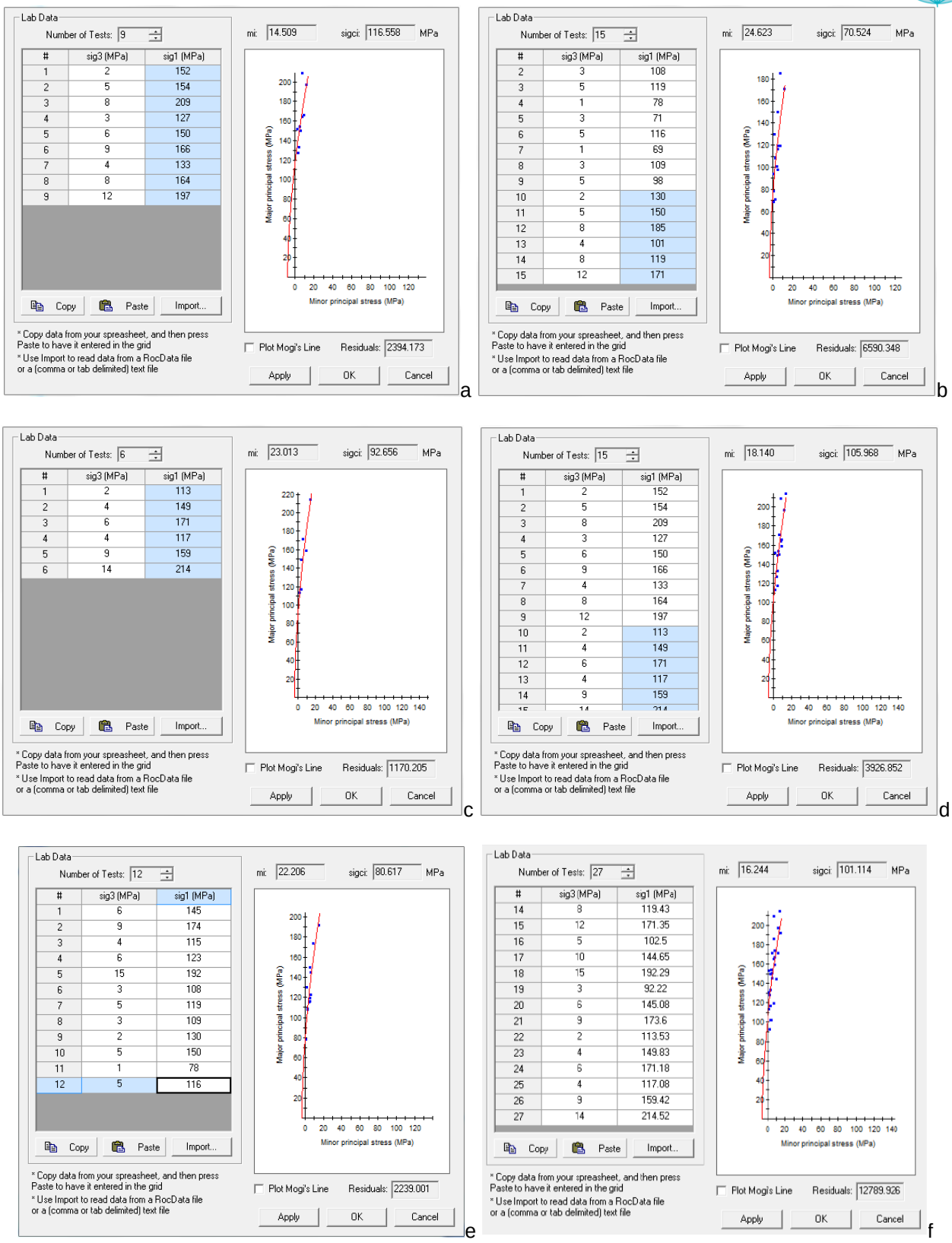

Figure 8. Cretaceous Fm., river area: combinations of value-pairs σ1 / σ3 to define the rupture envelope and the constants mi and σci - (a-b-c-d) right river side; (e) left river side; (f) 27 triaxial tests (RocLab, Rocscience)

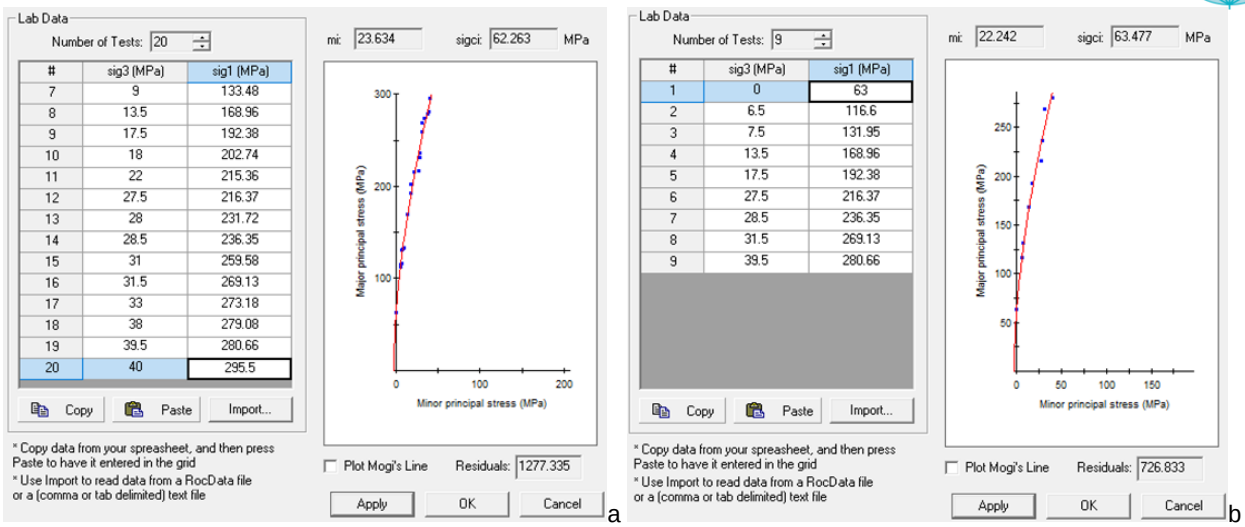

Figure 9. Cretaceous Fm. underground sectors: combinations of value-pairs σ1 / σ3 to define the rupture envelope and the constants mi and σci (RocLab, Rocscience)

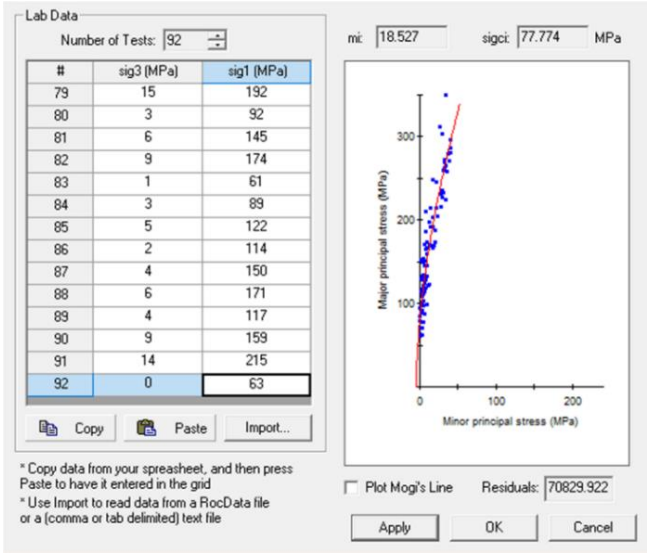

Figure 10. Cretaceous Fm.: envelope and constants mi and σci 91 triaxial data and 1 UCS (RocLab, Rocscience)

4. Conclusions

The difference between UCS and σ_{ci} derived from uniaxial and triaxial compressive strength tests, respectively, can have a significant impact in geomechanical modelling.

As indicated in the Literature, the values of uniaxial compressive strength resulting through the triaxial tests (σ_{ci}, confined test), are generally higher than those obtained through the uniaxial compressive tests (UCS, unconfined test). Therefore, as also remarked by Kaiser (2016), for characterizing the Hoek-Brown failure envelope, the value of σ_{ci} should be considered, in place of the UCS value.

For example, in the frame of the discussed data analysis, by the comparison between the values of the rock mass strengths (σ_c and σ_{cm}) resulting from three different sets of INPUT data (Table 2, from RocLab, by Rocscience) we observe that those obtained with UCS=30MPa without a Disturbance Factor (D=0), are close to those obtained applying the Disturbance Factor (D=1) with σ_{ci}=65MPa. This seems to confirm that the UCS-values are more affected by sampling disturbance, while the σ_{ci} values (from triaxial tests) are more representative of the undisturbed rock.

For the specific case analysed, the rock mass behaviours resulting as a function of the two different input data of the intact rock strength (UCS and σ_{ci}) are sharply different. From numerical analysis calculations it can be observed, for example, that considering the UCS as input the plastic zones induced by tunnel excavations extend for about hundred metres, while the reference to σ_{ci} provides a more realistic rock mass behaviour, showing the development of a few meters of plastic zone around the tunnels, as observed in similar cases.

Table 2. Comparison between rock mass strengths (σ_c σ_{cm}), from different INPUT data (σ_{ci}, UCS, m_i, D, GSI)

σ_{ci} (MPa)	UCS (MPa)	m_i (-)	D (-)	GSI	σ_c (MPa)	σ_{cm} (MPa)
65	-	23	0	70	12.2	25.8
			1		5.3	14.7
-	30		0		5.6	11.9

Disclosure statement

The Authors show the laboratory data and relevant analysis on behalf of the scientific community of engineering-geology, without mentioning the project for confidentially reasons. All the triaxial tests have been performed according to the requirements and supervision of the Authors.

References

Hoek, E., Carranza Torres C., Corkum B., 2002 Edition. Hoek-Brown failure criterion.

Hoek, E. and Diederichs, M. S., 2005. Empirical estimation of rock mass modulus. Internal Journal of Rock Mechanics and Mining Sciences 43 (2006): 203–215.

RocLab 2007 Rocscience Inc. Rock mass strength analysis using the Hoek-Brown failure criterion. User's Guide.

Kaiser P. K., December 2008. Rock mechanics challenges in underground construction and mining. ACG Australian Centre for Geomechanics, Volume No.31.

Bewick R.P., Amann F., Kaiser P. K., Martin C. D., ISRM Congress 2015 Proceedings. Symposium on Rock Mechanics. ISBN:978-1-926872-25-4. Interpretation of UCS test results for engineering design.

Kaiser P. K., 2016. Challenges in rock mass strength determination for design of deep underground excavations. Laurentian University, ISRM.

McQuarrie N., Horton B.K., Zandt G., Beck S., Decelles P., 2005. Lithospheric evolution of the Andean fold-thrust belt, Bolivia, and the origin of the Central Andean Plateau. Tectonophysics. 399. 15-37.

The influence of subjective factors on the accuracy of graphical constructions to interpret the preconsolidation pressure in IL-tests

Vladimir. Matveev[1], V.V. Shanina[2]

[1]*Geotechnical Graduate Lab LLC, Moscow, Russia,*
vladimir@matveev.email

[2]*Lomonosov Moscow State University, Moscow, Russia,*
viosha@mail.ru

ABSTRACT: This article discusses various factors that affect the accuracy of determining the preconsolidation pressure using graphical methods in increment loading (IL) tests. The study aims to identify subjective factors in graphical constructions and assess their impact on the accuracy of methods. The tests were performed on ground pastes of a fluid consistency with a given preconsolidation pressure. Clay slurries were made from moraine and fluvioglacial soils selected in Salaryevo (Moscow, Russia). A series of 12 oedometric IL-tests with loading, unloading, reloading and unloading was carried out. Then the obtained data were processed by nine methods (Casagrande, Pacheco Silva, Burland, Boone, bi-logarithmic, Becker, Nagaraj & Shrinivasa, Senol & Saglamer, Wang & Frost), the set and received values were compared, after that, the methods were ranked according to their accuracy. In the process of data processing, the influence of graphical constructions on the obtained result was evaluated. It turned out that almost all methods have approximately the same accuracy, and the discretisation makes the most significant contribution to the accuracy of measurements of steps. From the obtained results, it is recommended to reduce the steps or approximate the obtained points with analytical curves.

Keywords: preconsolidation pressure; graphical constructions; increment loading test

1. Introduction

Currently, the issue of determining the parameters of soil overconsolidation is very relevant. Over the past 85 years, many methods have been proposed to interpret preconsolidation pressure.

Preconsolidation pressure (σ_p) is a pseudo-elastic limit which separates 'elastic' pre-yield from 'plastic' post-yield behaviour of a soil. This is a key parameter in geotechnical engineering for analysing and predicting settlement behavior (Umar & Sadrekarimi, 2016).

Estimates of preconsolidation stress σ_p are normally made on the basis of oedometer test results. By interpreting the stress–strain curve during initial loading, the preconsolidation stress σ_p, is normally determined using the different methods (Grozic et al., 2003).

However, the processing methods proposed by different researchers can give significantly different results from each other. Existing inaccuracies, shortcomings, and discrepancies in determining these soil parameters affect the accuracy of the determination of stress-strain state.

2. Empirical methods for predicting preconsolidation pressure

2.1 Semi-logarithmic methods

Casagrande's method

This method uses an empirical construction from the *e* – log σ curve, where e is the void ratio and σ is the effective stress (Casagrande, 1936). On a logarithmic scale, idealised compression curve in width range of effective stresses is linear for normal consolidated (NC) clays, or bilinear for overconsolidated (OC) clays: the first section corresponds to branch of recompression, second – branch of normal consolidation (Figure. 1a).

Pacheco Silva's method

Similarly to Casagrande's (1936) method, Pacheco Silva's method uses an empirical construction from the *e* – log σ curve (Pacheco Silva, 1970). Graphic constructions consist of drawing a horizontal line at e_0. A vertical line is drawn at the intersection of this horizontal line and the tangent to the NCL until it intersects with the compression curve. Then, a second horizontal line is drawn from this intersection point until it intersects with the tangent to the NCL. The stress at this intersection defines σ_p (Figure 1b). This method is straightforward to use, requiring subjective interpretation (Clementino, 2005).

Burland's method

The Burland method uses a graph of the dependence of the porosity index I_V on stresses σ (Figure 1c). The porosity index is determined by the formula $I_V = (e - e^*_{100})/(e^*_{100} - e^*_{1000})$, or for weaker soils: $I_V = (e - e^*_{10})/(e^*_{10} - e^*_{100})$, where e^*_{10}, e^*_{100} and e^*_{1000} void ratio at loads of 10, 100 and 1000 kPa. This construction space is equivalent to the e — log σ space.

Boone's method

Boone's method uses a compression curve in the *e* — log σ space (Figure 1d). This method uses the unloading and reloading loop in construction. The preconsolidation stress is determined by the intersection point of the tangent to the final section and the line parallel to the unloading and reloading loop.

2.2 Bi-logarithmic methods

Bilogarithmic methods have been proposed by Butterfield (1979), Oikawa (1987), Shridharan et al. (1989), Onitsuka et al. (1995). These methods suggest using a bilogarithmic plot of the *e*+1 on the stress σ (Figure 1e). The methods offer the same constructions among themselves, which do not depend on the scale of the axes. Since the methods differ only in the scale of the axes, their accuracy is the same.

In this study, these methods will be considered as the same method.

2.3 Strain energy methods

Tavenas's and Becker's methods

Tavenas et al. (1979) and Becker et al. (1987) have presented a method for interpreting the oedometer test data using work per unit volume as the criterion for determining the preconsolidation pressure σ_p of clays.

An arithmetic plot of cumulative work per unit volume *W* and applied effective stress σ will define a generally bilinear plot. The intersection of these lines will define the preconsolidation pressure σ_p (Figure1f) (Becker et al., 1987).

Nagaraj & Shrinivasa Murthy's method

Nagaraj & Shrinivasa Murthy's method is similar to Becker's method; it differs by using the log *W* — log σ space (Figure 1g) (Nagaraj & Shrinivasa Murthy, 1991).

Senol & Saglamer's method

Senol & Saglamer's method is similar to Becker's method; it differs by using the *W* — log σ space (Figure 1h) (Senol & Saglamer, 2000).

Wang & Frost's method (dissipated strain energy method DSEM)

This method uses the unloading and reloading loop in construction and can account for sample disturbance effects to a certain degree. Compared to other energy methods, such as Becker's, this method uses dissipated strain energy (Wang & Frost, 2004).

The total strain is the sum of plastic and elastic strain. Therefore, it is sufficient to subtract the elastic strain from the total strain to separate the plastic strain from the total strain.

Figure 1i is represented by the compression curve (RUYX), recompression line (RU), NCL (UY), unloading line (YX). Line UY corresponds to total strain energy, and the line parallel to YX is elastic strain energy. The difference of the obtained lines is the dissipated strain energy line, the intersection of which with the abscissa axis will give the preconsolidation pressure.

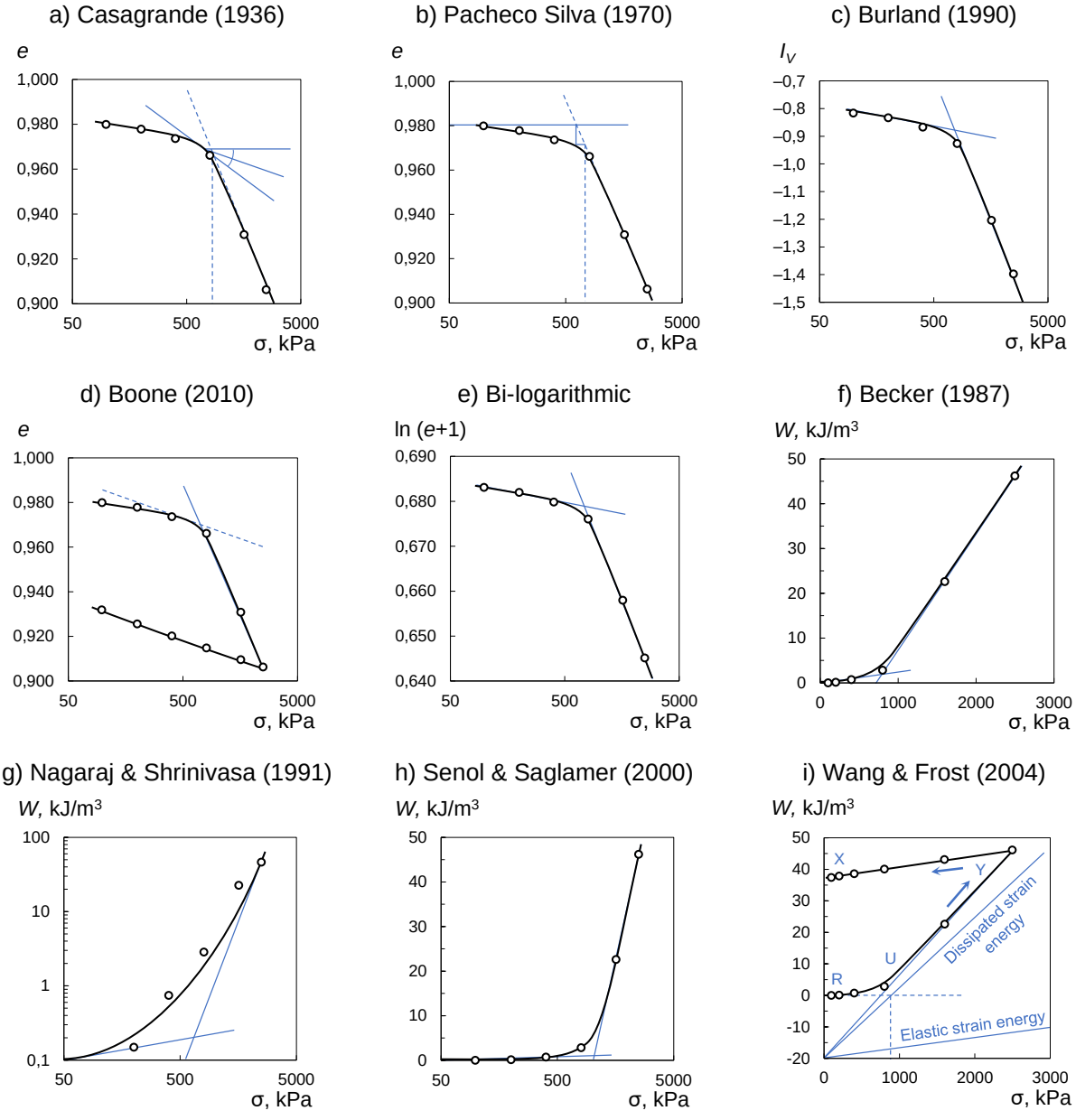

Figure 1. Graphical constructions for determination preconsolidation pressure

3. Experimental procedure

3.1 Tested clays

For the tests, samples were prepared from the soils selected at the engineering and geological surveys in Salaryevo (Moscow, Russia). Moraine and fluvioglacial quaternary clays were chosen for this study. Their characteristics are presented in Table 1.

Table 1. Basic characteristics of the clay samples used in this study

Sand (%)	Silt (%)	Clay (%)	w_p (%)	w_L (%)	I_p (%)
19–70	21–59	8–23	11–19	20–44	9–25

In order to further study the samples, an X-ray Diffraction (XRD) analyses was performed. The predominant minerals are quartz (41.6–51.2 %), smectite (9–21.5 %), feldspar (5.6–10.3 %), illite (4.9–10.2 %) plagioclase (3.8–17.0 %) and kaolinite (1.4–4.6 %)

3.2 Specimen preparation

Clay slurries were made from the soil samples. First, the soil was ground and then saturated to a liquid state with an exceeding 1½ – 2 times the liquid limit. Then, the resulting paste's moisture content was determined. Clay slurries are expected to have no stress history as they are nearly fluid, and thus they do not reflect any inherent relict stress or soil fabric effects (Becker et al., 1987).

3.3 Increment load test

For determining the preconsolidation pressure used oedometric testing following GOST 12248.4-2020 "Soils. Determination of deformation parameters by compression testing" on GEOTEK R&D Enterprise LLC (Penza, Russia) equipment at maximum load stages up to 10 kN. The tests were carried out in two types of oedometer is 72×20 mm and 86×25 mm.

The first stage test scheme was designed in such a way as to model the growth of stress in the ground during its sedimentation, its achievement of a given maximum historical stress during the advance of the glacier. This is followed by decompression, which corresponds to the retreat of the glacier and the extraction of the sample to the surface during sampling. Finally, at the second stage, the laboratory compression test of the soil in the odometer was modelled.

For this purpose, the ground paste was loaded with steps starting from 6 kPa. The axial stress was increased stepwise at a load increment ratio (LIR) of 1. The maximum stress on the first load branch was 800 or 600 kPa. The choice of such values is due to the limitations of the test setup. The first loading branch corresponds to the NCL. Then the specimen was completely unloaded. After that, the specimen was loaded again at LIR of 1, 0.5 or 0.3, up to a maximum stress of 1.5 or 2.5 MPa. The stabilisation criterion for each step was 0.01 mm in 12 hours.

The inflexion on the second branch should correspond to the transition of the sample from the recompression to the normal compression. With such a sequence of actions, it is possible to show the entire history of loads and recreate in detail the natural stresses under which the soil existed.

4. Experimental results and interpretations

Imposed preconsolidation pressure (600 or 800 kPa) and predicted by some methods are presented in Table 2, and their comparison is shown in Figure 2.

Table 2. Imposed and Predicted Preconsolidation Pressure

Specimen	LIR	Max. stress, MPa	Imposed σ_{pi}, kPa	Predicted σ_{pp}, kPa								
				Casagrande (1936)	Pacheco Silva (1970)	Becker (1987), Tavenas (1979)	Wang & Frost (2004)	Bi-logarithmic	Boone (2010)	Burland (1990)	Senol & Saglamer (2000)	Nagaraj (1991)
GJ6835	1.0	2.5	800	702	758	752	796	733	763	732	764	729
GJ6838	0.5	2.5	600	716	622	682	693	668	671	664	724	670
GJ6890	1.0	2.5	600	663	628	622	655	553	605	545	697	507
GJ6874	1.0	2.5	600	712	657	656	659	627	641	621	718	551
GJ6864	1.0	2.5	800	798	706	798	765	798	798	798	798	798
GJ6898	0.5	2.5	600	658	575	635	606	621	606	614	703	618
GJ6888	0.5	2.5	600	636	511	629	607	606	593	596	669	609
GJ68A0	0.5	2.5	600	670	535	653	574	625	597	621	680	625
GJ6895	0.3	1.5	800	876	788	847	893	830	842	828	866	833
GJ6840	0.3	1.5	800	942	871	904	904	893	896	892	903	887
GJ6885	0.3	1.4	800	870	704	841	774	828	806	826	852	816
GJ68B3	0.3	1.5	800	916	788	886	825	880	872	878	908	887
GJ6835	1.0	2.5	800	702	758	752	796	733	763	732	764	729

For evaluating the accuracy of the methods, absolute and relative error and root-mean-square error (RMSE) were used, calculated using the following formulas:

$$\text{Absolute Error} = \frac{1}{n}\sum \sigma_{pp} - \sigma_{pi} \quad [1]$$

$$\text{Absolute RMSE} = \sqrt{\frac{1}{n}\sum(\sigma_{pp} - \sigma_{pi})^2} \quad [2]$$

$$\text{Relative Error} = \frac{1}{n}\sum \frac{\sigma_{pp} - \sigma_{pi}}{\sigma_{pp}} \quad [3]$$

$$\text{Relative RMSE} = \sqrt{\frac{1}{n}\sum \left(\frac{\sigma_{pp} - \sigma_{pi}}{\sigma_{pp}}\right)^2} \quad [4]$$

For ranking the methods by accuracy, such values as the ranking index and the ranking distance determined by the following formulas were used (Sadrekarimi, 2017, Kootahi, 2017):

$$\text{RI} = \mu\left|\ln\left(\frac{\sigma_{pp}}{\sigma_{pi}}\right)\right| + \sigma\left[\ln\left(\frac{\sigma_{pp}}{\sigma_{pi}}\right)\right] \quad [5]$$

$$\text{RD} = \sqrt{\left[1 - \mu\left(\frac{\sigma_{pp}}{\sigma_{pi}}\right)\right]^2 + \left[\sigma\left(\frac{\sigma_{pp}}{\sigma_{pi}}\right)\right]^2} \quad [6]$$

After analysing the values presented in Table 3, it can be concluded that the accuracy estimate for all methods is approximately equal; absolute RMSE was from 40 to 58 kPa, relative RMSE was from 5.4 % to 8.5 %, which is consistent with the results of previous studies (Grozic et al., 2004; Umar & Sadrekarimi, 2016).

The most accurate methods were simple graphical constructions, such as bi-logarithmic, Boone, Burland, Becker, Wang & Frost (RI is less 0.12; RD is less 0.09).

Table 3. Accuracy of methods for determination of preconsolidation pressure (σ_p) for the IL-test

Method	Absolute Error, kPa	Absolute RMSE, kPa	Relative Error, %	Relative RMSE, %	Ranking index RI	Ranking distance RD
Casagrande	63	64	9.5	8.8	0.16	0.13
Pacheco Silva	−22	58	−2.9	8.4	0.12	0.09
Becker, Tavenas	42	41	6.2	5.5	0.11	0.08
Wang & Frost	29	50	4.3	7.1	0.11	0.08
Bi-logarithmic	22	47	3.1	6.5	0.09	0.07
Boone	24	40	3.4	5.4	0.09	0.06
Burland	18	48	2.5	6.6	0.09	0.07
Senol & Saglamer	73	49	11.2	7.6	0.17	0.14
Nagaraj & Shrinivasa	11	58	1.3	8.5	0.12	0.09

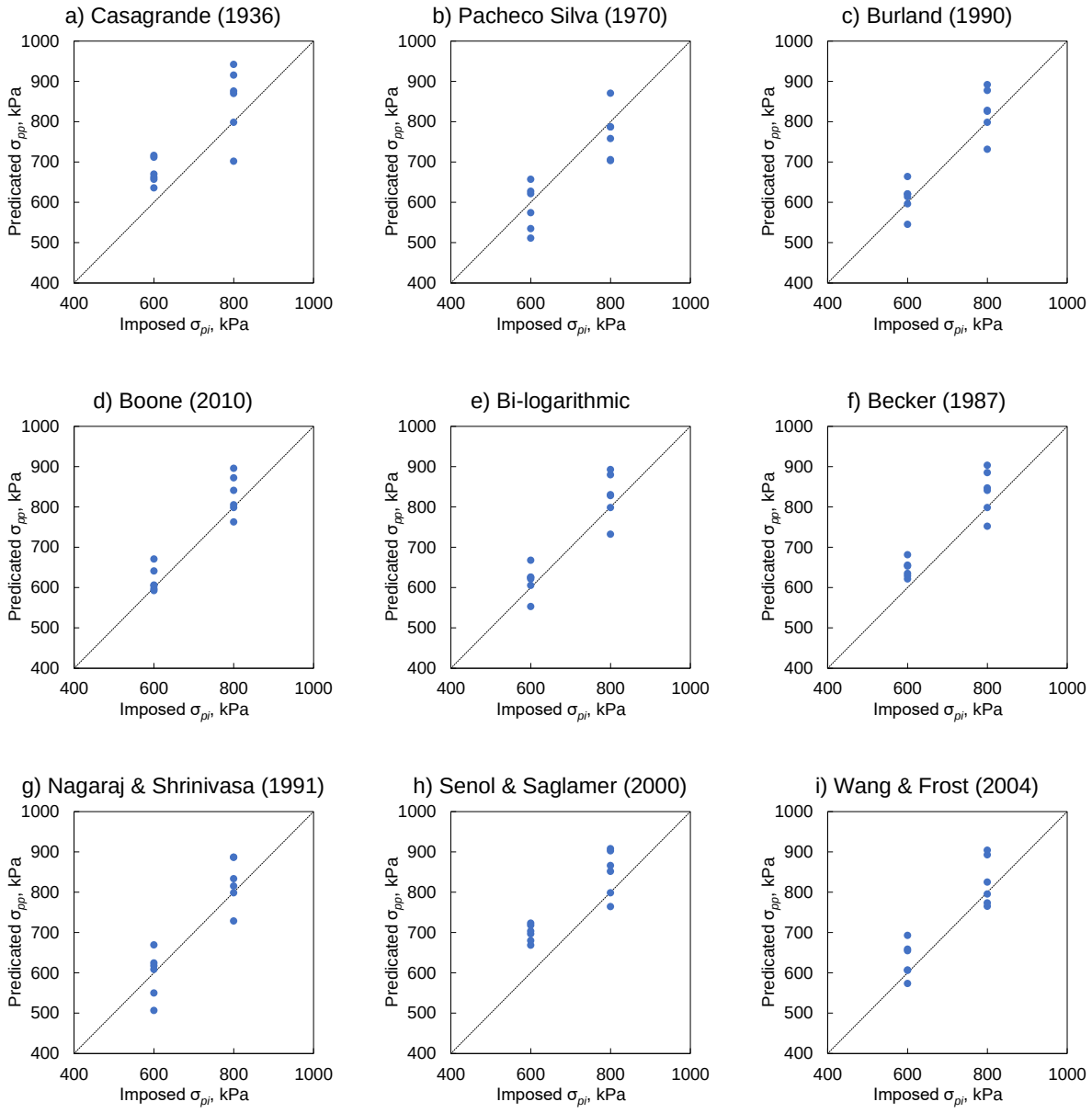

Figure 2. Comparisons of imposed preconcolidation pressure σp with predictions

5. Discussion of subjective factors

For all graphical methods, the accuracy of the constructions directly depends on the number of experimental points, and the accuracy of determining the preconsolidation pressure directly depends on the density of points in the area of the estimated preconsolidation pressure. However, the LIR at pressures sufficiently close to the preconsolidation pressure must be constant. Otherwise, nonlinear distortions of the deformability dependence graph will be observed. At the same time, the LIR should be completely small so as not to destroy the structure of the soil (Crawford, 1960) and simplify graphical constructions.

Some graphical constructions, such as Casagrande (1936) and Pacheco Silva (1970), require a smooth continuous line. Interpolation, both linear and cubic, does not give significant advantages. The approximation of the compression curve on a given section of some analytical curve seems to be the most suitable solution. In strain energy methods, the transition from strain to strain energy by direct integration, rather than by the trapezoidal rule, will also increase the accuracy of the constructions.

All graphical methods use a tangent to the final section. To correctly draw the tangent to the final section, it is reliable to go to the NCL. That is, the maximum load should be several times higher than the expected preconsolidation pressure. It should be noted that sometimes, at high stresses, a reverse curve of the graph is observed. This may be indicated that the linear law of deformability is beyond the limits of applicability. Also, a similar effect can be observed when the LIR is not a constant in the test scheme but decreases with increasing effective stress. In such cases, the tangent to the finished section should be carried out in the steepest part.

In methods that use a tangent to the initial section in their graphical constructions, the subjective factors carry out this tangent. Such methods include bilogarithmic, Burland (1990), Becker (1987), Senol (2000), and Nagaraj (1991). The tangent to the initial section is often also difficult to draw. In the case of images of unsatisfactory preservation, the bend between the lines of recompression and NCL turns out to be rounded and smooth. However, the inflexion is not easy to detect even in high-quality samples because the decompression and recompression lines do not coincide but form a loop. Reconsolidation is strongly recommended when testing samples. The tangent should not be carried out at the beginning of the compression curve but closer to the inflexion point in the area exceeding the maximum pressure.

When using the Casagrande method, there are significant difficulties in determining the point of maximum curvature. Casagrande (1936) proposed to choose the point with the smallest radius of curvature in the original work. There is also a method of withdrawing tangents to the initial and final sections and lowering the bisector on the compression curve (GOST R 58326-2018). In the approximation of the compression curve of some analytical curve, the search for the point of maximum curvature becomes a trivial task.

Drawing a bisector to a space of different dimensions seems absurd. Instead, it is proposed to use the median since, at small angles, the tangent of the half argument is approximately equal to half the tangent of the whole argument. With this construction, the intersection point will not depend on the selected axis scale. Thus, the scale factor of the axes can be excluded.

In Wan-Frost's (2004) and Boone (2010) methods, a decompression line is used instead of a recompression line. When drawing a tangent to the decompression line, the recommendations are similar to tangents to the recompression line. The tangent should not be carried out on the initial part of the unloading and the entire interval.

6. Conclusions

Some weaknesses of laboratory methods for determining the preconsolidation pressure σ_p are revealed, such as difficulties with the choice of tangents in graphical constructions and the subjective factor in such a choice.

Test interpretation requires the high qualification of the researcher. In addition, you must use at least two independent constructions performed in parallel for each method to process the data.

For increasing confidence in determining the overconsolidation characteristics, it is necessary to use several methods of processing the compression curve in parallel. This approach will ensure mutual control of the results and eliminate gross errors in interpreting the tests.

References

Becker D.E., Crooks J.H.A., Been K., Jefferies M.G. (1987) Work as a criterion for determining in situ and yield stresses in clays. Canadian Geotechnical Journal. Vol. 24. No. 4. P. 549–564.

Boone S.J. (2010) A critical reappraisal of “preconsolidation pressure” interpretations using the oedometer test. Canadian Geotechnical Journal. Vol. 47. No. 3. P. 281–296. https://doi.org/10.1139/T09-093.

Butterfield R. (1979) A natural compression law for soils (an advance on e — log p’). Géotechnique, 24(4): 469-480.

Burland J. B. (1990) On the compressibility and shear strength of natural clays. Géotechnique, 40(3), 329-378.

Casagrande A. (1936) The determination of the preconsolidation load and its practical significance. Proceedings of the 1st International Conference on soil mechanics and foundation engineering. Cambridge, UK: Harvard Printing Office, Vol. 3. P. 60–64.

Clementino R. V. (2005) Discussion of “An oedometer test study on the preconsolidation stress of glaciomarine clays.” Canadian Geotechnical Journal, 42(3), 972–974. doi:10.1139/t05-010

Crawford C.B. (1964) Interpretation of the consolidation test. Journal of Soil Mechanics and Foundations Division, ASCE, 90(5): 87–102.

GOST 12248.4-2020 Soils. Determination of deformation parameters by compression testing.

GOST R 58326-2018 Soils. Laboratory method for determining the overconsolidation charateristics.

Grozic J. L., Lunne T., & Pande S. (2003) An oedometer test study on the preconsolidation stress of glaciomarine clays. Canadian Geotechnical Journal, 40(5), 857–872. doi:10.1139/t03-043

Kootahi K. (2017) Discussion of “Accuracy of determining pre-consolidation pressure from laboratory tests”. Canadian Geotechnical Journal, 54(3): 441-450.

Nagaraj T. S., Shrinivasa Murthy B. R., Vatsala A. (1991) Prediction of soil behaviors – part II – saturated uncemented soil. Canadian Geotechnical Journal. Vol. 21. No. 1. P. 137-163.

Onitsuka K., Hong Z., Hara Y., & Yoshitake S. (1995) Interpretation of Oedometer Test Data for Natural Clays. Soils and foundations, 35(3), 61–70. doi:10.3208/sandf.35.61

Oikawa H. (1987) Compression curve of soft soils. Journal of the Japanese Geotechnical Society, Soils and Foundations. Vol. 27. No. 3. P. 99–104.

Pacheco Silva F. (1970) A new graphical construction for determination of the preconsolidation stress of a soil sample. Proceedings of the 4th Brazilian Conference on soil mechanics and foundation engineering. Rio de Janeiro, Brazil. Vol. 2. No. 1. P. 225–232.

Sadrekarimi A. (2017) Reply to the discussion by Kootahi on “Accuracy of determining pre-consolidation pressure from laboratory tests”. Canadian Geotechnical Journal, 54:1799-1801. doi.org/10.1139/cgj-2017-0349.

Senol A., Saglamer A. (2000) Determination of Preconsolidation Pressure with a New Strain Energy-Log Stress Method. Electronic Journal of Geotechnical Engineering. Vol. 5.

Sridharan J. B. T. (1991) Improved technique for estimation of preconsolidation pressure. Géotechnique. Vol. 41. No. 2. P. 263–268.

Tavenas F., Des Rosier J.P., Leroueil S. et al. (1979) The use of strain energy as a yield and creep criterion for lightly overconsolidated clays. Géotechnique. Vol. 29. P. 285–303.

Umar M., Sadrekarimi A. (2016) Accuracy of determining pre-consolidation pressure from laboratory tests. Canadian Geotechnical Journal. Vol. 54. No. 3. P. 441–450. https://doi.org/10.1139/cgj-2016-0203.

Wang L., Frost J.D. (2004) Dissipated strain energy method for determining preconsolidation pressure. Canadian Geotechnical Journal. 2004. Vol. 41. No. 4. P. 760–768. https://doi.org/10.1139/t04-013.

Investigation of the mechanical properties of tectonized limestones in western Lefkada Island, Greece, via field methods, laboratory testing and back-analyses of a co-seismic landslide

Vassilis Kallimogiannis[1], Charalampos Saroglou[1]

[1]*National Technical University of Athens, Greece*
vkallim@hotmail.com, saroglou@central.ntua.gr

ABSTRACT: The main objective of the present study is to investigate the mechanical properties of tectonized limestones in western Lefkada Island, Greece. The aforementioned region is frequently impacted by severe landslides due to the presence of weak limestone formations and the impact of strong earthquakes. Processes of tectonic origin have resulted in the formation of tectonic limestone breccias and tectonized limestones with poor mechanical properties and complex behavior. Conventional laboratory methods to determine their mechanical properties are unsuitable. Laboratory testing is usually impractical due to the great extent of disintegration during sampling whereas the most common classification systems do not fully apply to such tectonized materials. In the present study, an in-situ investigation, a novel sample preparation and laboratory testing technique and a Limit Equilibrium 3D back-analysis of a co-seismic landslide that occurred during the M6.5 earthquake in November 2015, are employed to better understand, characterize and predict the mechanical behavior of these formations. The findings from laboratory scale tectonic breccia specimens reveal a wide range of the material's Uniaxial Compressive Strength that is due to its complex, composite nature. The 3D back-analysis proves that the shear strength of the in-situ material has been extensively reduced, hence, it obtains a behavior similar to that of soils. Further research is needed to better understand the governing factors that control the mechanical properties of the tectonized materials.

Keywords: Tectonized Limestones, Lefkada Island, Mechanical properties, 3D back-analysis, Landslide, Uniaxial Compressive Strength, Laboratory testing

1. Background

Lefkada Island consists of carbonate rock masses of the Ionian Zone, limestones of the Paxos Zone and sporadic developments of Ionian flysch, sandstones and marls (Bornovas, 1964; Rondoyanni-Tsiambaou, 1997). The Ionian Zone, which comprises the majority of the Island, is composed of late Triassic formations while the Paxos zone emerges in the southwest part of the Island and is composed of Late Jurassic to Oligocene carbonate rocks (Bathrellos et al., 2009).

The island's tectonic structure is highly associated with the presence of the Cephalonia Transform Fault (CFT), which links the continental subduction to the north with the oceanic subduction to the south, along the Hellenic Subduction Zone. Neotectonic faults are mainly NE-SW to NNE-SSW while some minor faults appear with a NW-SE exhibit left-lateral component (Papathanassiou et al., 2013).

The impact of fault systems along the Western part of Lefkada Island has resulted in intense tectonization of the limestone rock masses. Consequently, their mechanical properties are affected and can be characterized as poor in certain locations. The combination of the island's high seismicity, the reduced strength of the ground and the relatively steep slopes on the west part of the Lefkada Island have resulted in many co-seismic landslides, especially during the 2003 and 2015 earthquakes, with magnitude M_w 6.2 and M_w 6.5, respectively.

The behavior of weak and tectonized rock masses has not been adequately studied since most of the areas are remote and steep. Moreover, laboratory testing is extremely challenging as the material is weak and

presents disintegration problems using conventional sampling methods. Therefore, an effective approach to determine its in-situ mechanical properties is through back-analyses of existing slope failures.

2. Methodology

An in-situ investigation was conducted along the west coast of Lefkada Island to characterize the weak rock masses encountered and to perform Point Load tests. Moreover, samples of tectonic limestone breccias were retrieved to investigate the mechanical properties of the tectonic breccias in the laboratory.

To assess the response of the entire geological formations during seismic loading, a 3D limit equilibrium back-analysis of a co-seismic landslide that occurred in 2015 (Egremnoi beach) was also conducted. The pre- and post-earthquake landslide surfaces were determined using data from the Hellenic National Cadaster and field mapping with Unmanned Aerial Vehicles (UAVs) that generated a 3D Point Cloud model using the Structure-From-Motion (SfM) technique (Zekkos et al.,2018). The back-analyses results were evaluated using the Mohr-Coulomb failure criterion (Kallimogiannis et al., 2019).

3. In-situ investigation

The limestones in the study area are tectonized and are either characterized as tectonic limestone breccias or brecciated limestones depending on the degree of brecciation. A detailed map presenting the sites visited and the rock mass characterization in each one is shown in Figure 1. The location where tectonized limestone breccia blocks were collected to perform laboratory tests is included.

Based on 40 point load tests conducted in the field, a histogram of the derived I_{s50} and the correspondent indirect UCS in various study locations is presented in Figure 2. The average Uniaxial Compressive Strength (UCS) of the intact rock was 76.5 MPa.

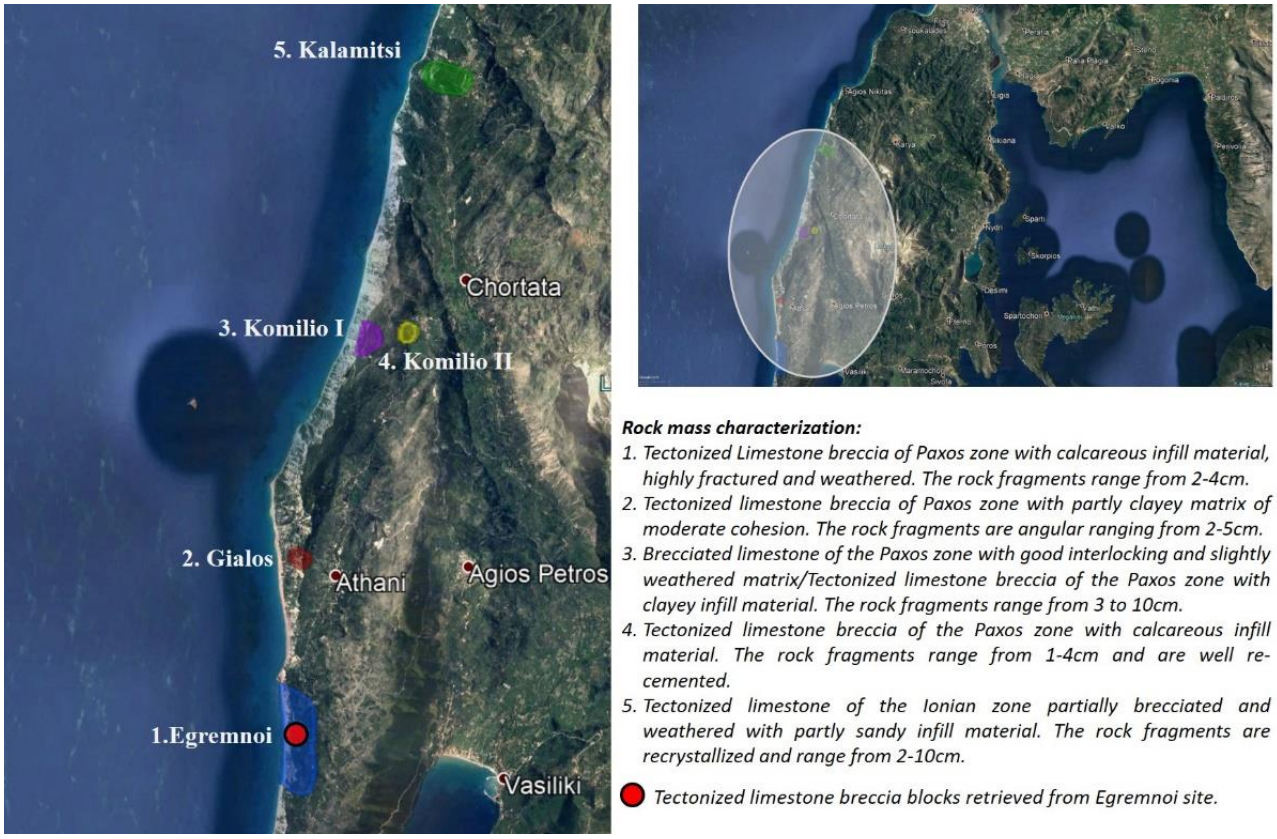

Figure 1. Rock mass characterization for the sites visited in western Lefkada

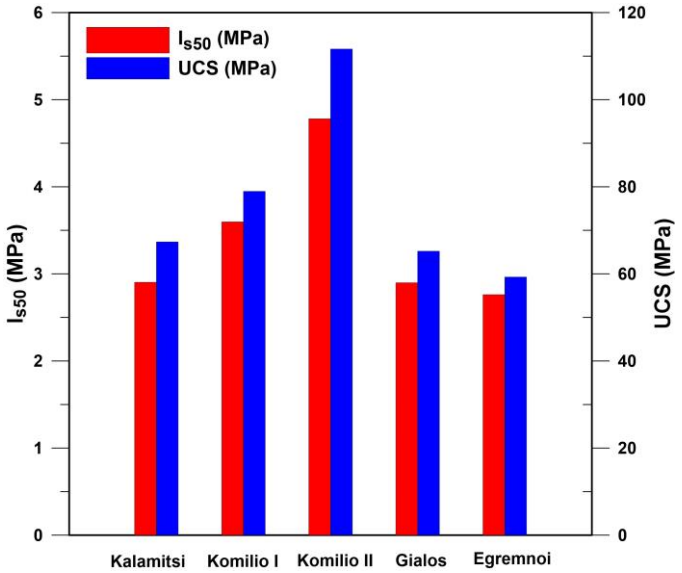

Figure 2. a) Histogram of the spatial distribution of Is50 indices and the indirect Uniaxial Compressive Strength obtained from point load tests in Western Lefkada

4. Laboratory Tests results

Intact limestones are not weak or complex formations but, extreme disintegration can result in limestone rock masses with poor mechanical properties and no memory of their initial structure (Marinos, 2010). The formations encountered in the studied areas are limestones that belong to either the Paxos or the Ionian zone. The presence of major faults striking parallel to the slopes in the western part of the island has resulted in the formation of tectonic limestone breccias and tectonized limestones with poor mechanical properties and composite nature.

In particular, the tectonic breccias consist of limestone fragments and calcite/clayey or sandy matrix. Their behavior is controlled by the mechanical properties of the fragments and matrix, the ratio between the two and the existence of secondary fractures.

Weak materials tackle intense difficulties associated with sampling, laboratory, or in-situ testing. Sampling and specimen preparation are frequently infeasible due to the material's disintegration (Nickmann et al., 2006; Marinos, 2010) whilst laboratory testing devices are rarely specialized for weak rock testing (Kanji, 2014). Moreover, the commonly used rock-mass classification systems (Q, RMR) have been developed around hard rocks and do not fully apply for the characterization of weak materials (e.g., Brook and Hutchinson, 2008; Kanji, 2014).

Three Tectonized limestone breccia rock blocks (A, B and C) were retrieved from Egremnoi beach, Lefkada Island in the vicinity of the landslide that was back-analyzed. The blocks presented higher strength than the in-situ material in which the landslide occurred; however, they belong to the weak rock type and thus, the preparation of samples in accordance with the conventional methods (e.g., ISRM, 1979; ASTM, 2014) was impossible. In particular, core drilling proved to be infeasible due to the disintegration and the detachment of the material's fragments. Therefore, an alternative method that involved a disk cutter with a diamond saw blade (400mm) was employed to obtain cubic specimens with edges of approximately 8cm. The cutting duration was short, a fact that prevented grain-matrix detachment and excess fracturing. Nonetheless, the procedure was successful in the central parts of blocks A and B from which 4 and 8 samples were retrieved, respectively. Block C was highly tectonized and dominated by calcite matrix material, hence, sample preparation was even more challenging. The cutting process resulted in only one sample.

The porosity, unit weight and wave velocity were measured for every specimen (except for the one from Block C), before uniaxial compression tests were performed. The ranges of the physical and mechanical properties derived from the dataset are presented in Table 1.

The variance of the material's physical and mechanical properties is significant proving its complex nature. According to ISRM (1978), the UCS values range from very low (<5 MPa) to moderate (25-50MPa). The structural properties of the samples (existence of microcracks, proportion of calcitic matrix to fragments) control their strength and their quantification is part of ongoing research. The correlation between UCS and the wave velocity, porosity and unit weight are given in Figures 3a to 3d.

Table 1. Physical and mechanical properties of the tectonic limestone breccia specimens

Physical and mechanical properties of the tested tectonic limestone breccias	Range		Average
	Min	Max	
Porosity (%)	9	26	15
Unit Weight (kN/m^3)	18.4	22.9	21.2
P-wave velocity (m/s)	2398	5114	3488
S-wave velocity (m/s)	1539	2975	2239
Uniaxial Compressive Strength (MPa)	2.7	33.4	12.0

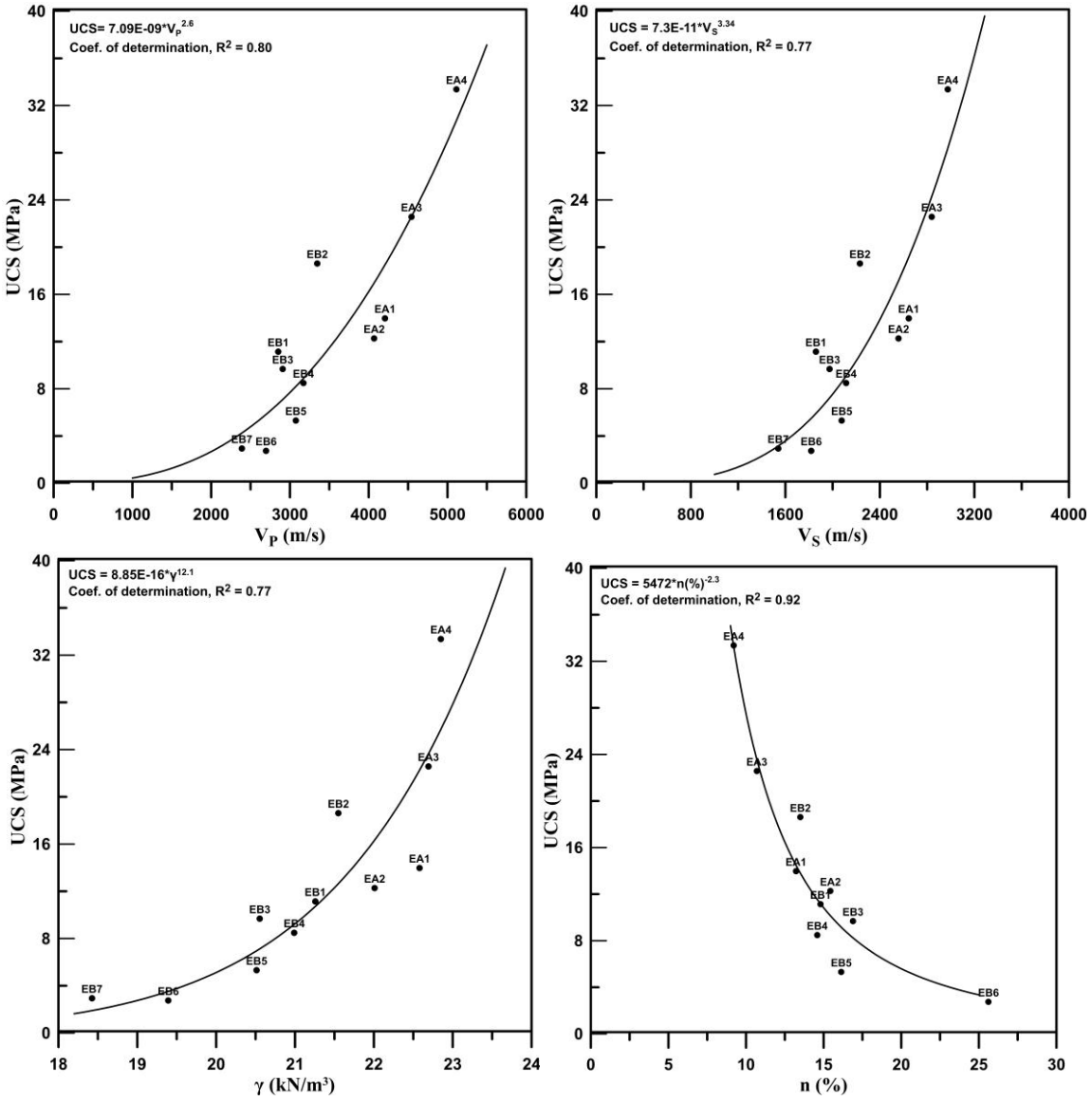

Figure 3. Correlation of the tectonic limestone breccia specimens' UCS and a) P-wave velocity, b) S-wave velocity, c) Unit Weight and d) Porosity

A multivariable regression using the UCS as the dependent variable and the P-wave velocity and porosity as independent variables results in the following equation which shows a mean absolute percentage error (MAPE) equal to 18%.

$$\mathrm{UCS\ (MPa)} = 657.67 * \mathrm{V_P}^{0.25}\ \mathrm{(m/s)} * \mathrm{n}^{-2.29}\mathrm{(\%)} \quad [1]$$

5. Back analysis of co-seismic landslide in Egremnoi, Lefkada Island

The most reliable way to obtain the shear strength of a geomaterial in an extended slope is by back-calculating its failure mechanism (Sonmez et al.,1998). Back-analysis also provides a realistic comparison between the back-calculated rock mass strength and the strength obtained by the existing failure criteria (e.g., Hoek and Brown criterion) or by laboratory testing (Ulusay and Aksoy, 1994; Min et al. 2014).

The back-calculations conducted in the Egremnoi site for a co-seismic landslide showed that the actual strength of the in-situ material is highly reduced (Kallimogiannis et al., 2019). Weathering and tectonic processes have deteriorated its mechanical properties. As a result, the material can be characterized as a weak rock-hard soil. Using the Mohr-Coulomb criterion, the 3D back-analysis yields a Uniaxial Compressive Strength between 0.20-0.23 MPa, much lower than that derived via laboratory testing.

6. Summary-Discussion

In the present study the mechanical properties of limestone rock masses in the western, coastal Lefkada Island, Greece, were investigated. Major faults striking parallel to the slopes have resulted in the formation of tectonic limestone breccias and tectonized, brecciated limestones with poor mechanical properties. An investigation to characterize the in-situ material and to perform Point Load tests was conducted. The latter enabled the indirect derivation of the spatial distribution of the intact rock Uniaxial Compressive Strength across the area of interest.

The mechanical properties of the tectonic breccias were derived via a novel laboratory testing procedure which enabled the preparation of cubic samples and via a back-analysis of a co-seismic landslide that occurred in 2015. The results of the laboratory tests prove that the tectonic breccias present relatively low strength which significantly varies depending on the correlation between the fragments and matrix content of a sample. Back-analysis showed that the strength of the material in the actual scale is even lower and resembles that of a soil. Further research to develop a methodology to derive the in-situ properties of such materials is currently ongoing.

Acknowledgments

The authors would like to thank ElxisGroup SA that performed the UAV photography for the study area.

References

ASTM D7012-14e1, (2014). Standard Test Methods for Compressive Strength and Elastic Moduli of Intact Rock Core Specimens under Varying States of Stress and Temperatures, ASTM International, West Conshohocken, PA, DOI:10.1520/D7012-14E01

Bathrellos, G.D., Antoniou, V.E., Skilodimou, H.D., (2009). Morphotectonic characteristics of Lefkas Island during the Quaternary (Ionian Sea, Greece). Geologica Balcanica 38(1—3), 23—33.

Bornovas, J., (1964). Géologie de l'île de Lefkade, vol 1, 10th edn, Geological geophysique research (IGSR). Geological Geophysique Research, Athens.

Brook, M.S. and Hutchinson, E., (2008). Application of rock mass classification techniques to weak rock masses: A case study from the Ruahine Range, North Island, New Zealand. Canadian Geotechnical Journal. 45(6): 800-811. DOI:10.1139/T08-019

ISRM, (1978). Suggested Methods for the quantitative description of discontinuities in Rock Masses. Int. J. Rock Mech. Min. Sci. Geomech., 15, 319–368.

ISRM, (1979). Suggested methods for determining the uniaxial compressive strength and deformability of rock materials, Int J Rock Mech Min Sci. 16 (2), 135-140.

Kallimogiannis, V., Saroglou, H., Zekkos, D., and Manousakis, J., (2019). Back-analysis of landslide in Egremnoi caused by the 2015 Lefkada earthquake. Proc. of 2nd Int. Conference on Natural Hazards & Infrastructure, 2019; Chania, Greece.

Kanji, M.A., (2014). Critical issues in soft rocks. Journal of Rock Mechanics and Geotechnical Engineering, 6(3), 186–195. DOI:10.1016/j.jrmge.2014.04.002

Marinos, P.V., (2010). New Proposed GSI classification charts for weak or complex rock masses. Bulletin of the Geological Society of Greece, 43(3), 1248-1258. DOI:10.12681/bgsg.11301

Min, S.N., Ashraf, M. and Abustan, I., (2014). Back Analysis of Slope Failure Using Finite Element with Point Estimate Method (FEM-PEM). Journal of Civil Engineering Research, 4(3A): 31-35, DOI:10.5923/c.jce.201402.04

Nickmann, M., Spaun, G., and Thuro, K. (2006). Engineering geological classification of weak rocks. International Association for Engineering Geology and the Environment, 492(492), 9.

Papathanassiou G., Valkaniotis S., and Pavlides S. (2013) Evaluation of the Temporal Probability of Earthquake-Induced Landslides in the Island of Lefkada, Greece. In: Margottini C., Canuti P., Sassa K. (eds) Landslide Science and Practice. Springer, Berlin, Heidelberg. DOI:10.1007/978-3-642-31427-8_27

Rondoyanni-Tsiambaou, Th., (1997). Les seismes et l'environnement geologique de l'ıle de Lefkade, Grece: Passe et Futur. In: Marinos, et al., (Eds.), Engineering Geology and the Environment. Balkema, 1469– 1474.

Sonmez H., Ulusay R., and Gokceoglu C. (1998). A practical procedure for the back analysis of slope failure in closely jointed rock masses, International Journal of Rock Mechanics and Mining Sciences, Volume 35, Issue 2, 1998, Pages 219-233, ISSN 1365-1609, DOI:10.1016/S0148-9062(97)00335-5.

Zekkos, D, Greenwood, W., Lynch J., Manousakis, J., Zekkos, A., Clark, M., Cook, K. and Saroglou, H. (2018). Lessons Learned from The Application of UAV-Enabled Structure-From-Motion Photogrammetry in Geotechnical Engineering. 4. 254. 10.4417/IJGCH-04-04-03.

Ulusay, R. and Aksoy, H., (1994). Assessment of the failure mechanism of a highwall slope under spoil pile loadings at a coal mine. Eng. Geol., 1994, 38(2), 117±134.

The Behaviour of Sand Stabilized with Colloidal Silica in Triaxial Compression and Extension

Eleni-Maria Pavlopoulou[1], Vassiliki Georgiannou[1] & Filippos Chortis[1]

[1]*Department of Geotechnical Engineering, National Technical University of Athens, Athens, Greece*
eleni-pav@hotmail.com, vngeor@civil.ntua.gr, philipposchortis@gmail.com

ABSTRACT: In this paper triaxial compression and extension tests are performed on sand stabilized with colloidal silica aqueous gel, to understand the response of the binary gel-sand system and verify whether typical sand response is shown. Drained loading conditions are considered with measurements of volumetric changes in stabilized sand. The results show that stabilized sand retains the characteristics of sand behaviour. In comparison to the untreated sand, tested under the same conditions, the effect of the gel is beneficial although to a lesser extent in extension, with the exception of the initial stiffness in compression being lower for the treated sand.

Keywords: soil stabilization, colloidal silica, sands, compression test, extension test

1. Introduction

Despite our advances in understanding the liquefaction phenomenon through testing and analysis, the severe damage in terms of destruction and fatalities observed in the recent 2018 Palu (Bradley et al., 2019) and the 2011 Christchurch (Cubrinovski, 2013) earthquakes was driven by liquefaction, and this raises important questions concerning protection against liquefaction. At undeveloped sites, the high effectiveness and low cost of various densification methods is recognised albeit their limitations in the vicinity and/or underneath existing structures. More recently a promising, non-disruptive technique of 'passive site stabilisation' has been applied to liquefiable soils in developed sites (Gallagher and Mitchell, 2002), exploiting the time-dependent properties of colloidal gels. To stabilize sand in-situ, a dilute suspension of colloidal nano-silica particles (hydrosol) is slowly injected into the ground and transported through the saturated soil mass by means of natural or enhanced groundwater flow (Gallagher et al., 2007), or by electro osmosis (Thevanayagam and Jia, 2003). The silica hydrosol has low viscosity during the injection phase and thickens in a controllable electrochemical manner to form a stable, non-toxic gel; the gel retains the pore water and supports the grain structure so it cannot collapse under cyclic and/or seismic loading.

The abovementioned response is supported by a number of laboratory studies indicating that sand stabilized with silica gel shows enhanced strength associated with extreme dilation (Georgiannou et al., 2017; Kodaka et al., 2005; Porcino et al., 2012; Porcino and Marcianò, 2017; Triantafyllos et al., 2021), as well as liquefaction resistance (Díaz-Rodríguez et al., 2008; Gallagher and Mitchell, 2002; Porcino et al., 2015, 2011), compared to untreated sand. However, in many of these studies it is also highlighted that, given the fact it does not liquefy, treated sand exhibits lower shear modulus in resonant column tests (Spencer et al., 2007) and higher rates of strain and excess pore water pressure accumulation under cyclic loading compared to untreated sand (Kodaka et al., 2005; Pavlopoulou and Georgiannou, 2021; Porcino et al., 2015, 2011). These findings indicate that gel stabilized sand does not fit into the existing frameworks of soil behaviour; offering a justification to its various characterizations in the literature e.g. regarded as a 'dense' sand (Porcino et al., 2012), a 'structured' sand (Georgiannou et al., 2020, 2017), a sand with 'cohesive' properties (Kodaka et al., 2005) and a 'single phase' material (Vranna and Tika, 2019).

Prompted by these observations, results of triaxial compression and extension tests are discussed in this paper to show whether the behaviour of the binary gel-sand system is inherently different or it is fundamentally more like sand's i.e. response much weaker and more contractive in extension than in compression due to the hosting sand's anisotropic structure.

2. Materials and test methods

All tests were performed in computer-controlled hydraulic triaxial stress path cells (Bishop and Wesley, 1975) under strain-controlled loading. Submersible LVDTs were mounted diametrically opposite over a central gauge length of the 38mm diameter and 2:1 height to diameter ratio specimens to measure local axial and radial displacements. Water pluviation was used for the formation of the specimens. The drag in water and the dilute nano-silica particles solution is similar during pluviation; subsequently, the sand specimens are subjected to a suction of 30 kPa while the hydrosol thickens to a self-supporting gel within 50 hours. Details on the dilute solution of nano-silica particles turned to gel with time can be found in Georgiannou et al. 2017. A value of $B=\Delta u/\Delta\sigma=0.95$ was measured for treated and untreated specimens 10mins after the application of $\Delta\sigma$ by measuring the pore water pressure at the base of the specimen. Measurements of pore water pressure and/or volumetric changes are feasible and should not be ignored, as they allow for an effective stress analysis of the treated sand behaviour (Georgiannou et al., 2017; Triantafyllos et al., 2021).

3. Test results

Figure 1 shows the response of M31 sand in triaxial compression and extension at an initial mean effective stress, p'_i=200kPa, for isotropically consolidated specimens included in Table 1. Typical sand response is observed i.e. extreme strength anisotropy. In Figure 1(a) the stress path in compression shows a peak strength of 500 kPa, compared to 150kPa in extension. The weaker response under extension loading is associated with the significantly higher contraction observed in extension i.e. a 60% increase compared to compression loading in Figure 1(c). The peak stress ratio along the failure envelope, $\eta=q/p'$, is also higher in triaxial compression compared to extension (1.34 cf. 1.00) in Figure 1(d), where stress ratio is plotted against axial strain. Moreover, significantly higher axial strains are observed in extension than in compression at the same pre-peak stress ratio, reflecting the sand's weak structure along the plane of deposition. Strain non-uniformities in strain distribution have resulted in specimen necking observed by the naked eye in a range of strains between 7% to 9% in extension. The weak nature of sands under triaxial extension has been repeatably observed in triaxial tests indicating that the fabric of deposited sand is anisotropic (De Gennaro et al., 2004; Georgiannou, 2006; Georgiannou and Konstadinou, 2014; Hight and Georgiannou, 1995; Miura and Toki, 1984; Vaid et al., 1990; Vaid and Chern, 1983).

Table 1. Triaxial Tests

Test	Loading Type	Drainage Conditions	Treated	e_i	p'_i(kPa)
CD	C	D	-	0.748	200
ED	E	D	-	0.737	200
SCD	C	D	T	0.751	200
SED	E	D	T	0.742	200

C=compression, E=extension, D=drained, S=stabilized

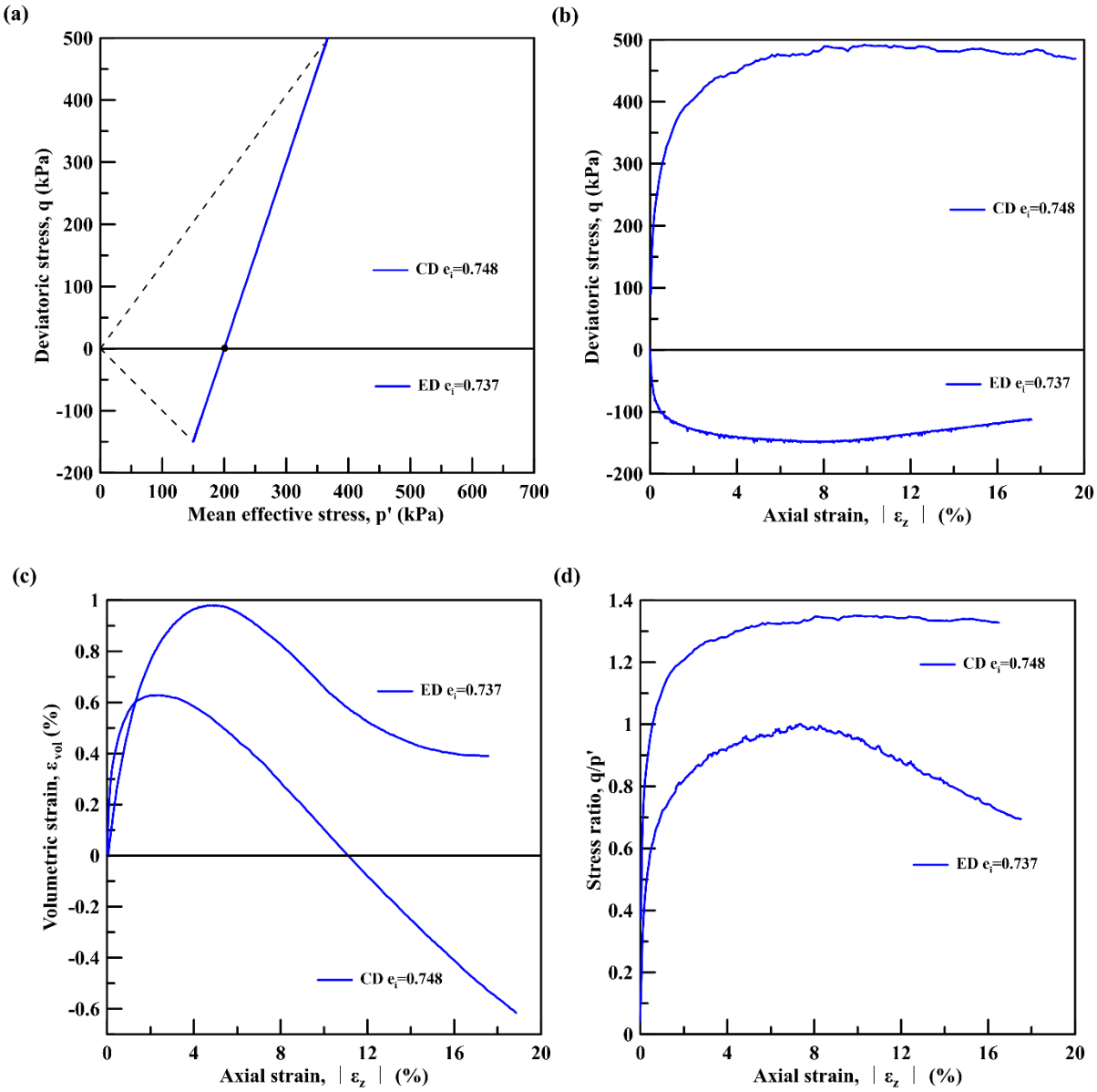

Figure 1. Drained triaxial compression and extension tests on M31 sand: (a) effective stress paths; (b) stress-strain curves; (c) volumetric strain against axial strain curves; (d) stress ratio, q/p', against axial strain curves

In Figure 2 tests on stabilized treated sand at similar densities are presented in terms of effective stress paths, Figure 2(a), stress-strain curves, Figure 2(b), and volumetric strain against axial strain curves in Figure 2(c). In Figure 2 the results for untreated sand have also been included for comparison and are shown in blue colour. For treated sand (in red colour) evidence of behaviour undergoing systematic weakening (more contractive behaviour and reduction in peak deviatoric stress) in extension is provided in Figure 2(a, b and c).

Treated sand shows higher peak strength in compression than in extension like untreated sand in Figure 2(a) and (b); however, compared to untreated sand the treated sand shows higher peak strength under both compression and extension loading while sharing the same ultimate strength at large strains. Similarly, treated sand is substantially less contractant, with volumetric changes in Figure 2(c) being approximately half the values observed in sand under both compression and extension loading, and more dilatant than the sand before and after phase transformation respectively, and reaches this phase at smaller axial strains compared to the sand. Nonetheless, for treated sand contraction in extension increased by more than twofold compared to compression; an increase higher than that observed in untreated sand. Figure 2(d) shows the stress ratio versus axial strain curves, where a similar increase of about 15% at peak strength ratios is observed in both triaxial compression and extension drained tests for treated compared to untreated sand. Note that necking is observed at about 9% for treated sand specimens.

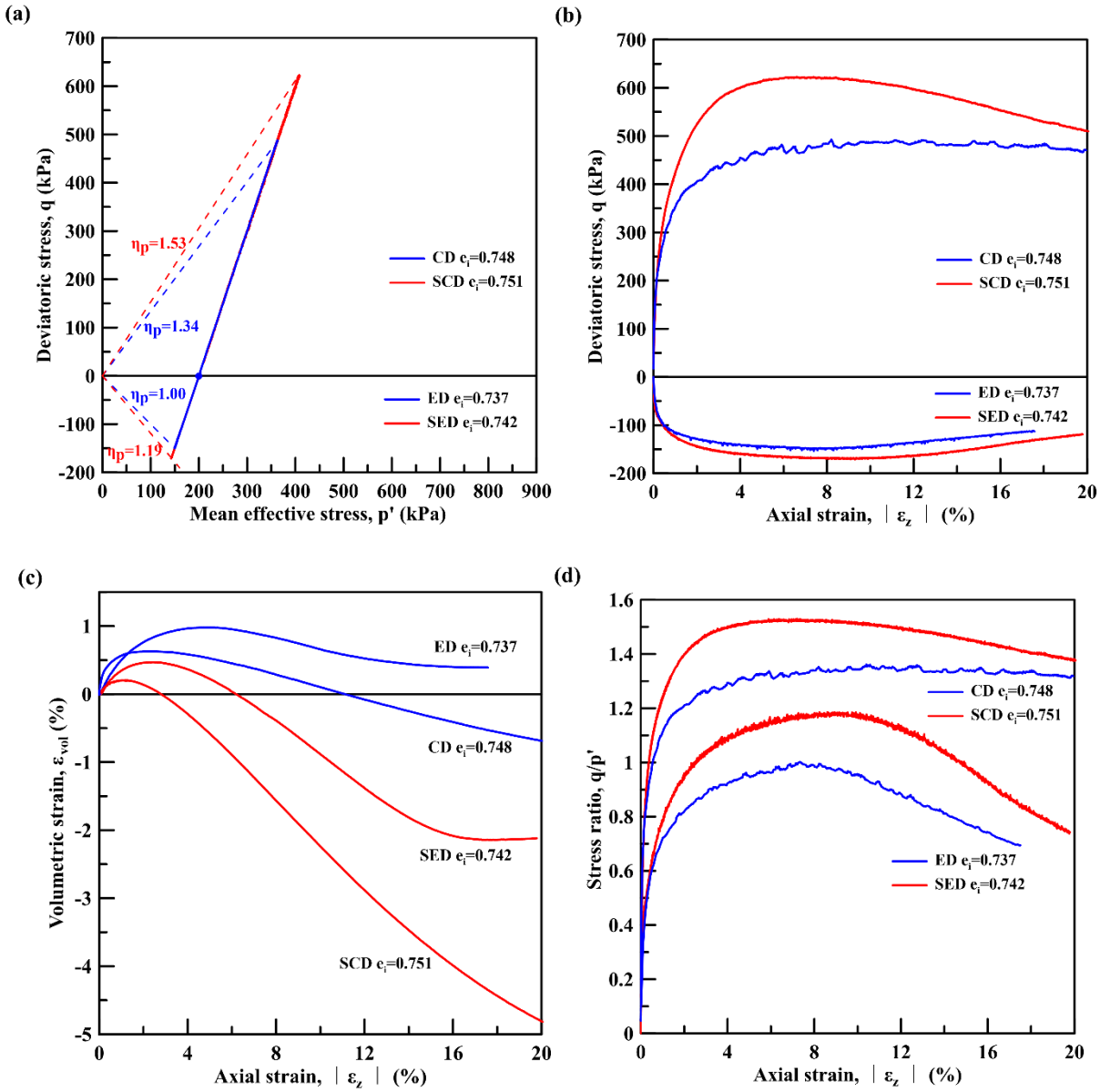

Figure 2. Drained triaxial compression and extension tests on treated (in red colour) and untreated (in blue colour) M31 sands: (a) effective stress paths; (b) stress-strain curves; (c) volumetric strain against axial strain curves; (d) stress ratio, q/p', against axial strain curves

Hence, based on the preceding observations extension tests are the key to interpret treated sand behaviour characterized by similar strength anisotropy than sand in drained tests, thus indicating the dominance of the anisotropic fabric of the sand within the sand-gel binary system. In treated sand under compression loading the gel supported sand grain skeleton is significantly more dilative than the grain load-carrying structure in sand (Figure 2 (b) & (c)). Due to dilation, the stress ratio after phase transformation is higher for treated than untreated sand at the same density (Figure 2(d)); however, at large strains, shearing takes place under the same stress ratio controlled by the granular medium.

In Figure 3 the secant stiffness values have been plotted against axial strain for the tests presented herein. It can be observed: (i) in triaxial compression the initial stiffness e.g. at 0.1% axial strain, shows a nearly twofold increase compared to stiffness in extension for both treated and untreated sand; (ii) in compression the treated sand shows significantly lower stiffness than sand for axial strain values less than 0.1% contrary to the reduced contraction and increased dilatancy observed previously with further straining in Figure 2(c); (iii) in contrast the treated sand shows an increase in stiffness in extension.

Interestingly, despite its higher strength due to dilative tendencies treated sand is less stiff than untreated sand in the initial stage of compression prior to phase transformation. It can be speculated that the soft nature of the gel reduces the stiffness of the sand-grain skeleton before dilative tendencies take over and increase the strength of treated sand. On the other hand, in extension the weak fabric of the granular

medium, due to fewer contacts in the plane of deposition, requires higher strains at the same stress ratio than in compression (Figure 2(d)); an observation made in both treated and untreated sand. In comparing treated and untreated sand the effect of the gel in extension is beneficial i.e. lower volume reduction than sand and, contrary to compression, this is also reflected in stiffness.

It appears that the gel supports the sand grain structure both in compression and extension. This macroscopic response is also confirmed by the smaller radial strains at the same axial strain level, both measured locally, developed by treated sand. However, the gel does not affect anisotropy which is dictated by the sand grain structure. Regarding treated sand stiffness at small strains, it is lower in compression and higher in extension compared to sand; the latter to a lesser degree.

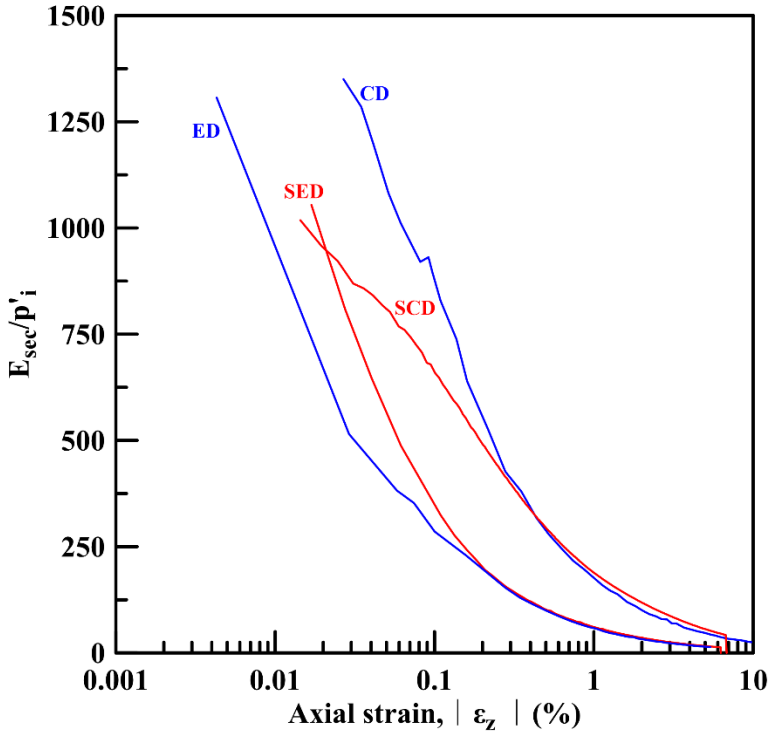

Figure 3. Stiffness characteristics of treated (in red colour) and untreated M31 sands in triaxial compression (C) and extension (E) tests under drained (D) loading conditions

4. Conclusions

Sand stabilized with colloidal silica gel holds on to characteristic sand behaviour i.e. showing in extension weaker response in terms of strength, higher contraction, and significantly lower initial stiffness compared to loading in compression. The high strength anisotropy of treated sand results from the extreme dilation introduced in compression which is relatively suppressed under triaxial extension. Hence, in comparison with clean sand, the benefit of the dilative tendencies of the gel supported sand grain structure is further accrued in compression; albeit the lower small strain stiffness of the treated sand in compression.

Acknowledgements

This research is carried out / funded in the context of the project "Experimental investigation of the anisotropic behaviour of sand before and after stabilization" (MIS 5049187) under the call for proposals "_Researchers' support with an emphasis on young researchers- 2nd Cycle_". The project is co-financed by Greece and the European Union (European Social Fund- ESF) by the Operational Programme Human Resources Development, Education and Lifelong Learning 2014-2020.

References

Bishop, A.W., Wesley, L.D., 1975. A Hydraulic Triaxial Apparatus for Controlled Stress Path Testing. Geotechnique 25, 657–670. https://doi.org/10.1680/geot.1975.25.4.657

Bradley, K., Mallick, R., Andikagumi, H., Hubbard, J., Meilianda, E., Switzer, A., Du, N., Brocard, G., Alfian, D., Benazir, B., Feng, G., Yun, S.H., Majewski, J., Wei, S., Hill, E.M., 2019. Earthquake-triggered 2018 Palu Valley landslides enabled by wet rice cultivation. Nat. Geosci. 12, 935–939. https://doi.org/10.1038/s41561-019-0444-1

Cubrinovski, M., 2013. Liquefaction - Induced Damage in The 2010-2011 Christchurch (New Zealand) Earthquakes. International Conference on Case Histories in Geotechnical Engineering. 1, 1-11. https://scholarsmine.mst.edu/icchge/7icchge/session12/1

De Gennaro, V., Canou, J., Dupla, J.C., Benahmed, N., 2004. Influence of loading path on the undrained behaviour of a medium loose sand. Can. Geotech. J. 41, 166–180. https://doi.org/10.1139/t03-082

Díaz-Rodríguez, J.A., Antonio-Izarraras, V.M., Bandini, P., López-Molina, J.A., 2008. Cyclic strength of a natural liquefiable sand stabilized with colloidal silica grout. Can. Geotech. J. 45, 1345–1355. https://doi.org/10.1139/T08-072

Gallagher, P.M., Conlee, C.T., Rollins, K.M., 2007. Full-Scale Field Testing of Colloidal Silica Grouting for Mitigation of Liquefaction Risk. J. Geotech. Geoenvironmental Eng. 133, 186–196. https://doi.org/10.1061/(asce)1090-0241(2007)133:2(186)

Gallagher, P.M., Mitchell, J.K., 2002. Influence of colloidal silica grout on liquefaction potential and cyclic undrained behavior of loose sand. Soil Dyn. Earthq. Eng. 22, 1017–1026. https://doi.org/10.1016/S0267-7261(02)00126-4

Georgiannou, V.N., 2006. The undrained response of sands with additions of particles of various shapes and sizes. Geotechnique 56, 639–649. https://doi.org/10.1680/geot.2006.56.9.639

Georgiannou, V.N., Konstadinou, M., 2014. Torsional Shear Behavior of Anisotropically Consolidated Sands. J. Geotech. Geoenvironmental Eng. 140, 04013017. https://doi.org/10.1061/(asce)gt.1943-5606.0000985

Georgiannou, V.N., Pavlopoulou, E.M., Bikos, Z., 2017. Mechanical behaviour of sand stabilised with colloidal silica. Geotech. Res. 4, 1–11. https://doi.org/10.1680/jgere.16.00017

Georgiannou, V.N., Pavlopoulou, E.M., Chortis, F.C., 2020. Aqueous Gel in Sands; a Friend or Foe? Geotech. Eng. 51, 37–43.

Hight, D.W., Georgiannou, V.N., 1995. Effects of sampling on the undrained behaviour of clayey sands. Geotechnique 45, 237–247. https://doi.org/10.1680/geot.1995.45.2.237

Kodaka, T., Ohno, Y., Takyu, T., 2005. Cyclic shear characteristics of treated sand with colloidal silica grout. Proc. 16th Int. Conf. Soil Mech. Geotech. Eng. Geotechnol. Harmon. with Glob. Environ. 2, 401–404. https://doi.org/10.3233/978-1-61499-656-9-401

Miura, S., Toki, S., 1984. Anisotropy in Mechanical Properties and its Simulation of Sands Sampled from Natural Deposits. Soils Found. 24, 69–84. https://doi.org/10.3208/sandf1972.24.3_69

Pavlopoulou, E.M., Georgiannou, V.N., 2021. The effect of colloidal silica aqueous gel on the monotonic and cyclic response of sands. J. Geotech. Geoenvironmental Eng. https://doi.org/10.1061/(ASCE)GT.1943-5606.0002641

Porcino, D., Marcianò, V., Granata, R., 2015. Cyclic liquefaction behaviour of a moderately cemented grouted sand under repeated loading. Soil Dyn. Earthq. Eng. 79, 36–46. https://doi.org/10.1016/j.soildyn.2015.08.006

Porcino, D., Marcianò, V., Granata, R., 2012. Static and dynamic properties of a lightly cemented silicate-grouted sand. Can. Geotech. J. 49, 1117–1133. https://doi.org/10.1139/T2012-069

Porcino, D., Marcianò, V., Granata, R., 2011. Undrained cyclic response of a silicate-grouted sand for liquefaction mitigation purposes. Geomech. Geoengin. 6, 155–170. https://doi.org/10.1080/17486025.2011.560287

Porcino, D.D., Marcianò, V., 2017. Bonding degradation and stress–dilatancy response of weakly cemented sands. Geomech. Geoengin. 12, 221–233. https://doi.org/10.1080/17486025.2017.1347287

Spencer, L., Rix, G.J., Gallagher, P.M., 2007. Dynamic Properties of Collodial Silica Gel and Sand Mixtures. 4th Int. Conf. Earthq. Geotech. Eng.

Thevanayagam, S., Jia, W., 2003. Electro-Osmotic Grouting for Liquefaction Mitigation in Silty Soils, in: Grouting and Ground Treatment. American Society of Civil Engineers, Reston, VA, pp. 1507–1517. https://doi.org/10.1061/40663(2003)127

Triantafyllos, P., Georgiannou, V., Pavlopoulou, E.-M., Dafalias, Y., 2021. Strength and dilatancy of sand before and after stabilisation with colloidal-silica gel. Géotechnique 1–30. https://doi.org/10.1680/jgeot.19.p.123

Vaid, Y.P., Chern, J.C., 1983. Effect of Static Shear on Resistance to Liquefaction. Soils Found. 23, 47–60. https://doi.org/10.3208/sandf1972.23.47

Vaid, Y.P., Sayao, A., Enhuang Hou, Negussey, D., 1990. Generalized stress-path-dependent soil behaviour with a new hollow cylinder torsional apparatus. Can. Geotech. J. 27, 601–616. https://doi.org/10.1139/t90-075

Vranna, A., Tika, T., 2019. Laboratory improvement of liquefiable sand via colloidal silica and weak cementation. Proc. Inst. Civ. Eng. - Gr. Improv. 1–37. https://doi.org/10.1680/jgrim.19.00019.

THEME 2 - ENVIRONMENTAL ENGINEERING GEOLOGY

Assessment of Human Exposure to Polycyclic Aromatic Hydrocarbons in Groundwater near Municipal Landfills

Alexandru Balint[1]

[1]*University of Bucharest, Romania*
alexandruioan.balint@gmail.com

ABSTRACT: The paper aims at identifying the health risks associated with the presence of polycyclic aromatic hydrocarbons (PAHs) in groundwater near municipal landfills, with a special focus on inhabited areas as receptors. The methods used in the current research may be applied in any area worldwide if appropriate care is given to the selection of parameters. Three landfills located near the capital of Romania were selected as case studies due to their significant geological and hydrogeological similarities, and due to their dissimilarities in groundwater usage by the nearby population. The study consisted of an initial assessment which confirmed the initial presumptions that polycyclic aromatic hydrocarbons (PAHs) may be determined in groundwater around landfilling sites as in the United States of America, Sweden, and Poland. Although the estimated risk associated with groundwater ingestion and daily dermal contact is minimal, the presence of PAHs in groundwater calls for legal regulations.

Keywords: Polycyclic aromatic hydrocarbons, human exposure assessment, groundwater dermal risk, groundwater ingestion risk

1. Introduction

Polycyclic aromatic hydrocarbons (PAHs) are a class of chemical substances consisting of carbon and hydrogen only, which have multiple fused ring systems (Favre H.A., 2014; IUPAC, 2014). Polycyclic aromatic hydrocarbons are generated through thermal decomposition of organic materials which may include fossil fuel or biomass, but they have also been reported as benzo[a]pyrene at concentrations higher than 0.5 ng/g in food products which include very well-cooked red meat, grilled chicken and hamburgers, popcorn and pumpkin pies (Grimmer, 1983; Forsgren, 2015; Kazerouni et.al., 2001). Given the fact that PAHs were reported in landfill leachates in the United States of America, Sweden, and Poland at various concentrations (Clarke et.al., 2015; Eggen et.al., 2010), but also in groundwater near industrial and landfilling sites (Plumb, 1991), it is presumed that they represent one of the multiple categories of potential soil and groundwater contaminants near landfills.

The national legislation concerning landfill design and operations management in Romania does not impose any specific contaminants to be monitored by landfill operators as opposed to other more developed countries, such as the US Code of Federal Regulations, Part 264, Appendix IX. Furthermore, the Romanian national legislation establishing the maximum limit values of contaminants in groundwater does not include PAHs. As a result, the human health risks generated by PAHs potentially contaminated groundwater are not considered in the Romanian legislation.

The current study aims at (1) identifying potential receptors located around the investigated landfills based on existing hydrogeological conditions; (2) identifying any presence of PAHs in groundwater near municipal landfills located around the capital city of Romania, Bucharest; (3) assessing the potential health risks generated by PAHs in groundwater and (4) providing solutions for regulating the PAHs in groundwater.

2. Methods

2.1 General Information on Selected Polycyclic Aromatic Hydrocarbons

There are more than 100 compounds classified as PAHs (Crawford B.C., 2017), although from a toxicological point of view, only 16 PAHs are frequently monitored in Europe and USA (Lerda, 2011).

PAHs are highly hydrophobic and insoluble in water, given the value of the octanol-water partition coefficient (US Department of Energy RAIS, 2020; Ma et.al., 2010). Most of the compounds have a higher density than water, except acenaphthylene, so almost all PAHs tend to accumulate at the base of the aquifer after reaching the groundwater (Haynes et.al., 2017; US Department of Energy RAIS, 2020).

From a toxicological point of view, all compounds have a boiling point higher than 200 °C, which means that boiling groundwater would not remove contaminants in the event of groundwater usage for food or hot beverages preparation (Haynes et.al., 2017; US Department of Energy RAIS, 2020).

To identify the concentration of PAHs in groundwater, one groundwater sample was collected from two wells near each landfill. The groundwater samples were sent to an ISO 17025 certified laboratory for analysis. The PAHs identified in each sample and their concentration are included in Table 1.

Table 1. Concentrations of PAHs Recorded near the Analysed Landfills (ALS Life Sciences Romania SRL, 2020)

Parameter	Limit of detection	Units	Concentration					
			CHI1	CHI2	GLI1	GLI2	VID1	VID2
Anthracene	0.001	$mg \cdot L^{-1}$	n.d.	n.d.	n.d.	n.d.	0.0013	n.d.
Fluoranthene	0.001	$mg \cdot L^{-1}$	n.d.	n.d.	n.d.	n.d.	0.0011	n.d.
Fluorene	0.001	$mg \cdot L^{-1}$	n.d.	n.d.	n.d.	n.d.	0.0037	n.d.
Naphthalene	0.007	$mg \cdot L^{-1}$	0.0201	n.d.	0.0150	0.0200	n.d.	n.d.
Phenanthrene	0.001	$mg \cdot L^{-1}$	n.d.	n.d.	n.d.	0.0024	0.0065	0.0014
Pyrene	0.001	$mg \cdot L^{-1}$	n.d.	n.d.	n.d.	n.d.	0.0030	0.0032
n.d. – concentration below limit of detection								

The largest number of PAHs compounds was identified around Vidra landfill, whereas only naphthalene was identified around Chiajna and Glina landfill. The highest concentrations were recorded around Chiajna and Glina landfill.

2.2 Identification of potential receptors

Three municipal landfills are located in the southeastern part of Romania, around the capital of the country - Bucharest city. The three landfills were named based on the name of the nearest commune as follows: Chiajna - located in the north-western part of Bucharest, Glina - located in the south-eastern part of Bucharest and Vidra - located in the southern part of Bucharest.

The groundwater in the area of Chiajna landfill is drained by the Dambovita river, with a local flow from northwest towards southeast (Ghenea et.al., 1972). The nearest receptors are the inhabitants of the Giulesti neighborhood located southeast of the landfill.

The groundwater in the area of Glina landfill is also drained by the Dambovita river, with a local flow from southwest towards northeast (Bandrabur, et al.). The nearest receptors are the inhabitants of the Glina commune located east of the landfill.

The groundwater in the area of Vidra landfill is drained by the Sabar river, with a divergent local flow from north towards south in the area of interest (Bandrabur et.al., 1970). The nearest receptors are the inhabitants of the Sintesti village, part of the Vidra commune, located south and southwest of the landfill.

2.3 Potential exposure routes, exposure pathways and qualitative risk assessment

The landfills located near Bucharest city are highly different in terms of potential receptors due to their various social and economic status. As a result, the potential exposure routes and pathways are different from one landfill to another, which enabled an assessment of various conditions of exposure.

Inhalation may occur both outdoors and indoors near all landfills, but lower exposure is expected in Chiajna and Glina, since the groundwater is not generally used for sanitary purposes. Additionally, only exposure to naphthalene is considered relevant due to its sublimation properties. As a result, the risk of PAHs inhalation

is presumed to be significantly low due to the low concentrations of naphthalene in groundwater. No further assessment was considered necessary in the current study.

Ingestion of contaminated groundwater may occur through two main pathways:

- Direct ingestion from groundwater, which is expected at a low frequency in low-income families near Glina landfill, and with a high frequency for the Vidra landfill area, where groundwater is used for sanitary and drinking purposes.
- Indirect ingestion from food washed or cooked with PAHs contaminated groundwater.
- Further assessment of the risks associated with the ingestion of groundwater was conducted only for direct ingestion, since it also covers the indirect ingestion.

Dermal contact is presumed to be lower in Chiajna and occur only during household activities when hands may meet the contaminated groundwater. A higher risk is expected around Glina and Vidra landfills, since many residents use the groundwater for sanitary purposes, including bathing, especially around Vidra landfill. Further assessment was conducted for daily dermal contact with the hands around Chiajna landfill and daily dermal contact with the entire skin around Glina and Vidra landfill.

For a more accurate prediction of health risks, 5 categories of exposed people were taken into consideration, which were described in Table 2.

Table 2. Categories of exposed people

Category no.	Description
1	people living for 70 years near the landfill and using contaminated water during their entire lifetime
2	people living near the landfills until 20 years and moving afterwards in a non-contaminated area
3	people moving at the age of 30 years near the landfills for the rest of their 70-year-old life expectancy
4	infants below 2 years old
5	children and young adults between 2 and 20 years old

2.4 Equations for estimating health risk level

2.4.1 Equations for exposure through ingestion

Risk-Based Screening Levels (RBSLs) are non-site-specific values for chemicals of concern, that are protective of human health for specified exposure pathways (ASTM, 2015).

The following equation was used to identify RBSLs for non-carcinogenic PAHs in groundwater for exposure through ingestion of contaminated groundwater (ASTM, 2015):

$$RBSL_W \left[\frac{mg}{l \cdot H_2O}\right] = \frac{THQ \cdot RfD_o \cdot BW \cdot AT_n \cdot 365 \frac{days}{year}}{IR_W \cdot EF \cdot ED} \quad [1]$$

Where THQ is the target hazard quotient for individual constituents, $\mathrm{RfD_o}$ is the oral chronic reference dose $[\mathrm{mg \cdot kg^{-1} \cdot day^{-1}}]$, BW is the body weight [kg], $\mathrm{AT_n}$ is the averaging time for noncarcinogens [years], $\mathrm{IR_W}$ is the daily water ingestion rate $[\mathrm{l \cdot day^{-1}}]$, EF is the exposure frequency $[\mathrm{days \cdot year^{-1}}]$ and ED is the exposure duration [years].

The target hazard quotient for individual constituents was considered 1. The body weight was presumed as a standard 80 kg for adults. The body weight of infants was estimated based on the World Health Organization (WHO) standard growth charts for boys and girls with 95% confidence and for children and young adults based on the Centers for Disease Control and Prevention (CDC) growth charts for boys and girls with 95% confidence.

2.4.2 Equations for exposure through dermal contact

The following equation was used to calculate the expected dermally absorbed dose for PAHs in groundwater for exposure to dermal contact (EPA, 2004):

$$DAD_W \left[\frac{mg}{kg \cdot day}\right] = \frac{DA_{event} \cdot EV \cdot ED \cdot EF \cdot SA}{BW \cdot AT} \quad [2]$$

Where $\mathrm{DAD_W}$ is the dermally absorbed dose $[\mathrm{mg \cdot kg^{-1} \cdot day^{-1}}]$, $\mathrm{DA_{event}}$ is the absorbed dose per event $[\mathrm{mg \cdot cm^{-2} \cdot event^{-1}}]$, EV is the event frequency $[\mathrm{events \cdot days^{-1}}]$, ED is the exposure duration [years], EF is

the exposure frequency $[\text{days} \cdot \text{year}^{-1}]$, SA is the skin surface area available for contact $[\text{cm}^2]$, BW is the body weight $[\text{kg}]$ and AT is the averaging time $[\text{days}]$.

When computing the DAD_W, leap years were not considered, so 1 year was presumed to have 365 days when entering the averaging time.

The absorbed dose per each event was calculated based on the event duration and the necessary time for the specific chemical to reach steady-state, using the following equation (Crank, 1975; Frasch et.al., 2007; EPA, 2004):

$$DA_{event} = \begin{cases} 2 \cdot FA \cdot K_p \cdot C_W \cdot \sqrt{\dfrac{6 \cdot \tau_{event} \cdot t_{event}}{\pi}} \quad , if\ t_{event} \leq t & [3] \\ FA \cdot K_p \cdot C_W \cdot \left[\dfrac{t_{event}}{1+B} + 2 \cdot \tau_{event} \cdot \left(\dfrac{1+3B+3B^2}{(1+B)^2}\right)\right] , if\ t_{event} > t & [4] \end{cases}$$

Where FA is the fraction absorbed water, K_p is the dermal permeability coefficient of compound in water $[\text{cm} \cdot \text{hours}^{-1}]$, C_W is the chemical concentration in water $[\text{mg} \cdot \text{cm}^{-3}]$, τ_{event} is the time lag per event $[\text{hours}]$, t_{event} is the event duration $[\text{hours} \cdot \text{event}^{-1}]$, t is the time to reach steady-state $[\text{hours}]$ and B is a dimensionless ratio of permeability coefficient of a compound through the stratum corneum relative to its permeability across the viable epidermis.

The time lag is the time required during an event for the concentration across the skin to reach a linear gradient after exposure and it may be determined graphically by plotting the cumulative concentration penetrating the skin as a function of time and the time lag is the intercept on the time axis or it may be expressed analytically through the following equation (Barrer, 1951):

$$\tau_{event} = \frac{d^2}{6D_{skin}} \quad [5]$$

Where d is the thickness of the skin $[\text{cm}]$ and D_{skin} is the diffusion coefficient of chemical in the skin $[\text{cm}^2 \cdot \text{hours}^{-1}]$.

Although multiple models were developed to estimate the diffusion coefficient of substances through the skin (Mitragotri S., 2011), the simplest possible model was considered in which skin is regarded as a homogeneous membrane (Stein, 1986):

$$D_{skin} = \frac{K_p \cdot d}{K_{sw}} \quad [6]$$

Where K_{sw} is the skin-water partition coefficient.

The dermal permeability coefficient was calculated using the following equation (Potts & Guy, 1992), valid for chemicals with a molecular weight (MW) starting from 18 to >750 and log K_{ow} between -3 and +6:

$$K_p[cm \cdot hours^{-1}] = 10^{-2.74+0.71 \cdot \log K_{ow} - 0.0061 \cdot MW} \quad [7]$$

The thickness of the human skin varies between 1.5 mm in the thigh area and 2.5 mm in the suprascapular area, with higher values for males than women and it consists of three strata: dermis, epidermis, and stratum corneum (Laurent, 2007). The main barrier that prevents physical and chemical stressors from entering the human body, as well as for avoiding excessive loss of water is the stratum corneum which is a thin layer of approximately 10-15 mm, generally described as having a brick (corneocytes) and mortar (intercellular lipids) structure. The main lipid components include ceramide, cholesterol, and fatty acids (Gopinathan et.al., 2012). A correlation between the stratum corneum lipid phase/water partition coefficient (K_{sw}) and the octanol/water partition coefficient (K_{ow}) was provided as follows (Nitsche et.al., 2018):

$$\log_{10} K_{sw} = 0.411 + 0.571 \cdot \log_{10} K_{ow} - 0.320 \cdot \alpha - 0.562 \cdot \beta + 2.137 \cdot \log_{10}\left(\frac{MW}{100}\right) \quad [8]$$

Where α and β are the Abraham solvation parameters, namely the hydrogen bond acidity α and hydrogen bond basicity β. In the specialty literature, the parameters are referred to as A and B, but Greek letters were provided to avoid confusion with B in equation [4]. The Abraham solvation parameters were selected for the chemicals of concern from the UFZ-LSER database (Ulrich, et al., 2020).

The time to reach steady-state (t) refers to the time necessary for a given contaminant to enter and exit the skin at the same rate and it is dependent on the half-life ($t_{1/2}$) of the given chemical. A useful estimate of t is obtained by the following equation (Gupta, 2016):

$$t = 4.3 \cdot t_{1/2} \quad [9]$$

The dermal half-life was considered 3 hours for all chemicals, as reported for benzo[a]pyrene in the toxicological profile of PAHs (ATSDR, 1995).

The area of the skin was estimated as a weighted average based on the mean values for combined sexes at 95th percentile classified in age groups (EPA, 2011).

3. Results

The results for groundwater ingestion were expressed using two quotients as follows:

Hazard quotient (HQ_W):

$$HQ_W = \frac{C_W \cdot IR_W}{RfD_O} \quad [10]$$

Risk quotient (RQ_W):

$$RQ_W = \frac{C_W}{RBSL_W} \quad [11]$$

An HQ_W or RQ_W value higher than 1 indicates a significant risk for the given category of receptors. By summation of all values of HQ and RQ, the cumulative hazard and risk quotients were calculated for each category of receptors and results were included in Figure 2 and 3. A total value higher than 1 indicates a significant health risk.

The highest risk associated to the ingestion of PAHs contaminated groundwater for infants (cat. 4), children and young adults (cat. 5) was identified in Glina, due to the presence of naphthalene at higher concentrations and low values of the RBSLs for cat. 4 and 5. However, both the cumulative hazard and risk quotient are well below the value of 1, which indicate a significant low risk for ingestion of PAHs contaminated groundwater.

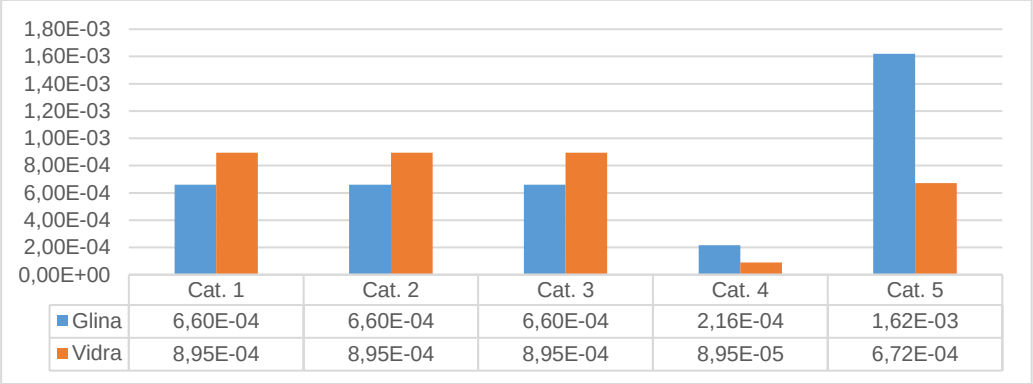

	Cat. 1	Cat. 2	Cat. 3	Cat. 4	Cat. 5
Glina	6,60E-04	6,60E-04	6,60E-04	2,16E-04	1,62E-03
Vidra	8,95E-04	8,95E-04	8,95E-04	8,95E-05	6,72E-04

Figure 2. The cumulative hazard quotient for ingestion of PAHs contaminated groundwater

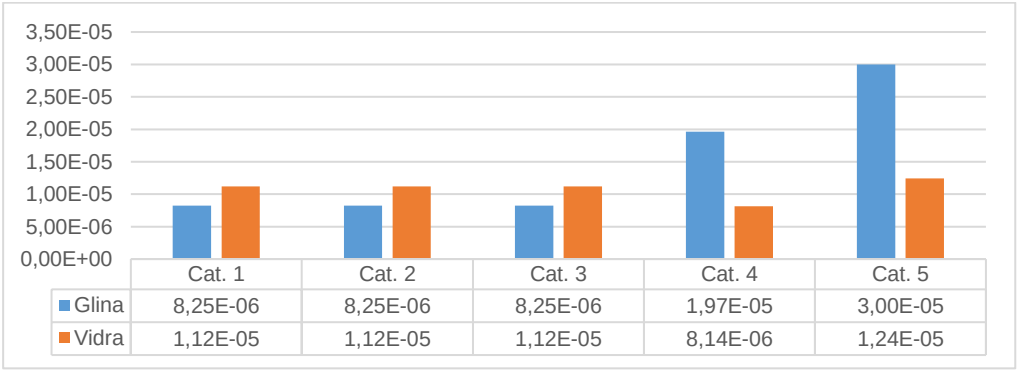

	Cat. 1	Cat. 2	Cat. 3	Cat. 4	Cat. 5
Glina	8,25E-06	8,25E-06	8,25E-06	1,97E-05	3,00E-05
Vidra	1,12E-05	1,12E-05	1,12E-05	8,14E-06	1,24E-05

Figure 3. The cumulative risk quotient for ingestion of PAHs contaminated groundwater

The hazard quotient for dermal exposure was expressed as a division between DAD_w and the absorbed reference dose (RfD_{ABS}). The RfD_{ABS} was determined based on the oral reference dose (RfD_o) - specific for a given chemical - and the fraction of contaminant which is absorbed in the gastrointestinal tract (ABS_{GI}) using the following equation (EPA, 2004):

$$RfD_{ABS} = RfD_O \cdot ABS_{GI} \quad [12]$$

The values for RfD_O were obtained from the Risk Assessment Information System (US Department of Energy RAIS, 2020) except for phenanthrene, which was considered the same as for anthracene due to their similar chemical structure. The ABS_{GI} was considered 89% as recommended by the US Environmental Protection Agency for PAHs (EPA, 2004).

The cumulative hazard quotient for dermal exposure to groundwater is higher for Vidra region, mainly due to higher exposure of receptors during showering. No significant difference was observed between the 5 categories of receptors. The main reason is the fact that at the same exposure frequency and duration, DAD_W will have approximately the same value since a decrease in the area of the skin will certainly require a decrease of the body mass. The lowest hazard quotient was identified for Chiajna area due to limited exposure to contaminated groundwater. The cumulative hazard quotient was depicted in figure 4.

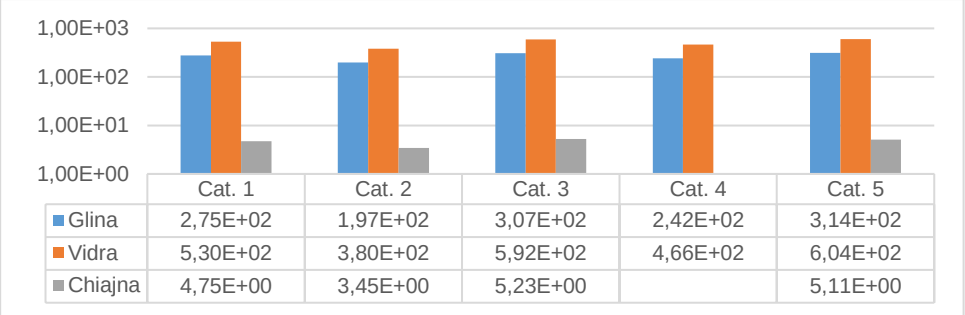

	Cat. 1	Cat. 2	Cat. 3	Cat. 4	Cat. 5
Glina	2,75E+02	1,97E+02	3,07E+02	2,42E+02	3,14E+02
Vidra	5,30E+02	3,80E+02	5,92E+02	4,66E+02	6,04E+02
Chiajna	4,75E+00	3,45E+00	5,23E+00		5,11E+00

Figure 1. The cumulative hazard quotient for exposure of receptors through dermal contact to PAHs contaminated groundwater [multiplication factor x107]

4. Conclusions and Discussions

Based on the results of the current study, it may be concluded that there is no significant risk associated with the consumption of PAHs contaminated groundwater around the three landfills located near Bucharest city. Additionally, the results of the current assessment contradicted the initial presumption that the shallow groundwater may be significantly contaminated with PAHs as reported at landfilling sites in the United States of America. However, the current study does not suggest that the shallow groundwater is suitable for human consumption or household activities due to the potential presence of other chemical and biological contaminants.

The current study is an example of a general preliminary risk assessment which should represent the basis for the design of a detailed groundwater risk assessment for assessing public health, especially in areas where groundwater used by the population might be impacted by anthropic activities. As the assessment was focused mostly on the receptors rather than the source of contamination, the degree of contamination near the landfill along with the fate and transport of the contaminants remain uncertain altogether. A future detailed assessment of the source of contamination and a groundwater flow model would clarify if higher concentrations are expected to reach the receptors in the future. Therefore, it is clear that an assessment of the receptors, without specific details of the source of contamination, may be valid only for a given point in time rather than having a comprehensive understanding of the risks associated with groundwater contamination and the total time of exposure.

Based on the results of the cumulative hazard quotients and risk quotients, it was concluded that for the same exposure frequency and duration, the risks associated with ingestion exposure should be assessed for various categories of exposed receptors, since it is more sensitive to changes in body weight. On the other hand, the risks associated with dermal exposure depends on the ratio between the skin area and body weight, thus no significant changes are expected between various categories of exposed receptors at low concentrations.

The study also revealed the necessity for a legislation improvement in Romania and other countries with similar situations, where private wells are used for groundwater supply from the shallow aquifer. Legal regulations should establish either general limit values in groundwater taking into consideration the worst-case scenario, or risk-based screening levels identified based on the local geology and hydrogeology and on the presumed exposure routes. The groundwater quality may be assessed both at the receptors' location through sampling performed by the public authorities based on a local groundwater monitoring program and at the source of the contamination, e.g. landfilling sites, by the economical operator. Additionally, the legislation should also consider the results of groundwater monitoring and risk assessment in the urban and rural planning for future development.

References

ALS Life Sciences Romania SRL. (2020). Analytical Report no. PI2004719. Ploiesti, Romania: ALS Life Sciences.

ASTM. (2015). E1739-95(2015) Standard Guide for Risk-Based Corrective Action Applied at Petroleum Release Sites. West Conshohocken, USA: ASTM International.

ASTM. (2015). E2081-00(2015) Standard Guide for Risk-Based Corrective Action. West Conshohocken, USA: ASTM International.

ATSDR. (1995). Toxicological Profile for Polycyclic Aromatic Hydrocarbons. Atlanta, United States: Agency for Toxic Substances and Disease Registry.

Bandrabur, T., Mihaila, N., Ghenea, A., Petrescu, I., Chiragosian, C., Daus, V., & Liteanu, E. (n.d.). Hydrogeological Map of Romania, scale 1:100,000, sheet L-35-125 Bucharest. Bucharest, Romania: Geological Institute of Romania.

Bandrabur, T., Petrescu, I., & Enea, G. (1970). Hydrogeological Map of Romania, scale 1:100,000, sheet 44c Vidra. Bucharest, Romania: Geological Institute of Romania.

Barrer, R. M. (1951). Diffusion In and Through solids. London: Cambridge University Press.

Clarke, B., Anumol, T., Barlaz, M., & Snyder, S. (2015). Investigating landfill leachate as a source of trace organic pollutants. Chemosphere, 269-275. doi:10.1016/j.chemosphere.2015.02.030

Crank, J. (1975). The mathematics of diffusion 2nd edition. Oxford, England: Clarendon Press.

Crawford B.C., Q. B. (2017). Microplastic Pollutants. Elsevier Science. doi:10.1016/C2015-0-04315-5

Eggen, T., Moeder, M., & Arukwe, A. (2010). Municipal landfill leachates: A significant source for new and emerging pollutants. Science of the Total Environment, 408, 5147-5157. doi:10.1016/j.scitotenv.2010.07.049

EPA. (2004). EPA/540/R/99/005 Risk Assessment Guidance for Superfund Volume I: Human Health Evaluation Manual (Part E, Supplemental Guidance for Dermal Risk Assessment). Washington, USA: US Environmental Protection Agency.

EPA. (2011). Exposure Factors Handbook 2011 Edition EPA/600/R-09/052F. Washington, DC, USA: U.S. Environmental Protection Agency.

Favre H.A., P. W. (2014). Nomenclature of Organic Chemistry: IUPAC Recommendations and Preferred Names 2013. Cambridge: The Royal Society of Chemistry. doi:10.1039/9781849733069-FP001

Forsgren, A. (2015). Wastewater Treatment: Occurrence and Fate of Polycyclic Aromatic Hydrocarbons (PAHs). Boca Raton, USA: CRC Press.

Frasch, F. H., & Barbero, A. M. (2007). The transient dermal exposure: Theory and experimental examples using skin and silicone membranes. Journal of Pharmaceutical Sciences, 1578-1592. doi:10.1002/jps.21035

Ghenea, A., Ghenea, C., Petrescu, I., Grigorescu, C., & Vlad, V. (1972). Hydrogeological Map of Romania, scale 1:100,000, sheet 43b Domnesti. Bucharest, Romania: Geological Institute of Romania.

Gopinathan, K. M., Cleary, G. W., & E., L. M. (2012). The structure and function of the stratum corneum. International Journal of Pharmaceutics, 3-9. doi:10.1016/j.ijpharm.2012.06.005

Grimmer, G. (1983). Environmental Carcinogens: Polycyclic Aromatic Hydrocarbons - Chemistry, Occurence, Biochemistry, Carcinogenity. CRC Press.

Gupta, P. (2016). Fundamentals of Toxicology. Essential Concepts and Applications. London, UK: Academic Press.

Haynes, W., Lide, D., & Bruno, T. (2017). CRC Handbook of Chemistry and Physics 97th edition. Boca Raton, USA: CRC Press.

IUPAC. (2014). Compendium of Chemical Terminology: Gold Book. Blackwell Science. doi:10.1351/goldbook

Kazerouni, N., Sinha, R., Hsu, C., Greenberg, A., & Rothman, N. (2001). Analysis of 200 food items for benzo[a]pyrene and estimation of its intake in an epidemiologic study. Food and Chemical Toxicology, 39, 423-436.

Laurent, A. e. (2007). Echographic measurement of skin thickness in adults by high frequency ultrasound to assess the appropriate microneedle length for intradermal delivery of vaccines. Vaccine, 6423-6430. doi:10.1016/j.vaccine.2007.05.046

Lerda, D. (2011). Polycyclic Aromatic Hydrocarbons (PAHs) Factsheet 4th edition. European Commission – Joint Research Centre – Institute for Reference Materials and Measurements.

Ma, Y.-G., Lei, Y. D., Xiao, H., Wania, F., & Wang, W.-H. (2010). Critical Review and Recommended Values for the Physical-Chemical Property Data of 15 Polycyclic Aromatic Hydrocarbons at 25 °C. J. Chem. Eng., 819-825. doi:10.1021/je900477x

Mitragotri S., e. (2011). Mathematical models of skin permeability: An overview. International Journal of Pharmaceutics, 115-129. doi:10.1016/j.ijpharm.2011.02.023

Nitsche, J. M., & Kasting, G. B. (2018). How Predictable Are Human Stratum Corneum Lipid/Water Partition Coefficients? Assessment and Useful Correlations for Dermal Absorption. Journal of Pharmaceutical Sciences, 727-738. doi:10.1016/j.xphs.2017.07.026

Plumb, R. (1991). The Occurrence of Appendix IX Organic Constituents in Disposal Site Ground Water. Groundwater Monitoring & Remediation, 11(2), 157-164. doi:10.1111/j.1745-6592.1991.tb00378.x

Potts, R. O., & Guy, R. H. (1992). Predicting Skin Permeability. Pharmaceutical Research, 663-669.

Stein, W. D. (1986). Transport and Diffusion across Cell Membranes. London, UK: Academic Press Inc.

Ulrich, N., Endo, S., Brown, T., N., W., Bronner, G., Abraham, M., & Goss, K. (2020, October 13). UFZ-LSER database. Retrieved from Helmholtz Centre for Environmental Research - UFZ: http://www.ufz.de/lserd

US Department of Energy RAIS. (2020, October 5). RAIS Toxicity Values and Physical Parameters Search. Retrieved from The Risk Assessment Information System: https://rais.ornl.gov/index.html

THEME 3 - ADVANCES IN SITE INVESTIGATION FOR ENGINEERING GEOLOGY

Prediction of the hydrogeological conditions in the Snowy 2.0 deep tunnels by means of temperature measurements

Antonio Dematteis[1], Manfred Thuering[1], Francisco Alvarado[2] & Gabriele De Carli[3]

[1]*Lombardi Engineering Limited, Sydney, Australia*
antonio.dematteis@lombardi.group, manfred.thuering@lombardi.group

[2]*Future Generation JV, Cooma, Australia*
f.alvarado@futuregenerationjv.com.au

[3]*Webuild S.p.A., Roma, Italia*
g.decarli@webuildgroup.com

ABSTRACT: This paper refers to recent ABSTRACT: This paper refers to recent experiences developed during the deep tunnels design studies of the Snowy 2.0 pumped-storage hydroelectric project in NSW, Australia. Long-term temperature monitoring in the boreholes has been used to infer an empirical thermal model along the tunnels. The thermal measurements and the developed models are used to design the durability of the structures and to predict the ventilation and safety conditions during excavation. A graphical interpretative method of borehole temperature logs is proposed to infer downward or upward groundwater flows and predict the hydrogeological behaviour in permeable, fractured and faulted zones. Local thermal borehole gradients are also correlated with local variations in permeability and hydraulic gradient. Furthermore, their application during tunnel excavation is proposed as an additional tool for the prediction of water inflow or identification of areas to be grouted and/or drained.

Keywords: Deep tunnels, temperature, geothermal gradient, hydrogeology.

1. Introduction

The knowledge of rock temperature is essential for planning and constructing deep tunnels. The design of the ventilation and cooling system for underground construction and operation and the structural durability design are based on this information. Water temperature measurements during tunnel excavation can also be used as an efficient and cost-effective predictor of water inflows. Fitting the observed temperature profiles on the inferred design-model during tunnel excavation makes it possible to express the potential flow rate beyond the tunnel head (Hasegawa et al., 1993; Maréchal & Perrochet, 2010). Finally, the knowledge of the thermal conditions also allows to evaluate the energy potential of the site and the possible heat recovery, complying with a sustainable management of natural resources in underground works (Wilhelm & Rybach, 2003; Dematteis et al., 2020).

The Snowy 2.0 project is a pumped-storage hydroelectric extension of the existing Snowy Scheme, in the Snowy Mountain Kosciuszko National Park, New South Wales, Australia. The plant will provide a maximum power of 2000 Megawatts and will have a storage capacity of approximately 9.1 GWh. The project connects two existing dams, Tantangara and Talbingo, through 27 km of waterway tunnels with a diameter of 9.9 m and an underground power plant with pumping capabilities. In addition to the main waterway there are additional 65 km of dry access and service tunnels around the power plant complex to be excavated. The tunnels will be excavated with 3 TBMs and lined with a segmented lining. The design is currently nearing completion, the access works have been completed and the tunnel excavation shall begin in January 2021.

2. Measurements

Today the market offers a wide range of temperature measuring devices of highly satisfactory quality with an accuracy around 0.1-0.5 °C, no particular calibration requirements during use, devices are small and can be employed even in dirty or aggressive environments, and all at a relatively low cost. All these features facilitate the measurement of the temperature in geotechnical investigation phases and during tunnel excavation.

There are 2 types of temperature measurements in Snowy 2.0: long-term monitoring by means of fixed temperature sensors, coupled to piezometric sensors in boreholes, and thermal boreholes logs performed after drilling.

Long-term temperature monitoring in Snowy 2.0 is done through a network of Vibrating Wire Piezometers (VWPs), which have been installed at different depths in boreholes to measure water pressures and temperature. The temperature is natively read in terms of a frequency, which has an accuracy of 0.5% and a resolution of 0.025% on an operating scale of -20 °C to 60°C.

Borehole temperature logging (T-log) has been performed by means of a temperature sensor for monitoring the operation of an acoustic televiewer (ATV) logging probe. Only the last logs were made with a dedicated temperature probe that measures the formation temperature. The production phase of a T-log is a delicate operation, which requires some technical measures to obtain the best result. The standard procedure requires the T-log probe to be first lowered at the bottom of the borehole and then pulled back to surface. The log is normally recorded during the ascent of the probe. If the borehole is flushed prior to the logging, e.g. when ATV imaging is also performed, before starting the T-log a careful check of the temperature balance between the probe, the injected surface flushing water and the ground is needed. The flush prior to the log is done with fresh water injected into the hole from the surface, at a temperature that may be different from the water in the borehole. The injected flushing volume is generally equal to approximately 3 times the volume of the borehole (e. g. around 1500 litres for a 750 m deep HQ hole). The temperature of the flushing water should be recorded, to improve the temperature control inside the borehole. Once the flushing has been completed, the time which is needed to completely balance the temperature of the water and the ground depends on the initial temperature difference. The ascent T-log can only be started after the complete equilibration. Many times, a temperature gradient inversion has been detected at the bottom of a hole, which was not necessarily related to a natural condition, but most likely to the presence of residual cold water at the bottom of the hole, caused by flushing.

3. Interpretation and discussion

3.1 Geothermal model along the tunnel

Long-term VWP data monitoring allows to know the temperature in equilibrium with the surrounding rock at the VWP location. The stabilized temperatures measured so far have been interpolated to determine the current temperature profile at the waterway tunnel elevation (Figure 1). Measured temperatures at the tunnel level are between 11.5°C and 25.2°C, varying from one sector to another depending on the overburden and hydrogeological conditions. The highest temperatures are expected in the deepest part of the project, where the power station complex is located (around chainage 19+300). In this area, new piezometers are being installed at the time of writing, which will allow to verify the current hypotheses.

A comparison of temperature with overburden is shown in Figure 1 and allows to identify the tunnel stretches where the temperature is lower than expected. The temperature line falling below the overburden line indicates the possible presence of a more permeable zone, such as a fracture or fault zone, which may host groundwater flowing from the surface towards depth.

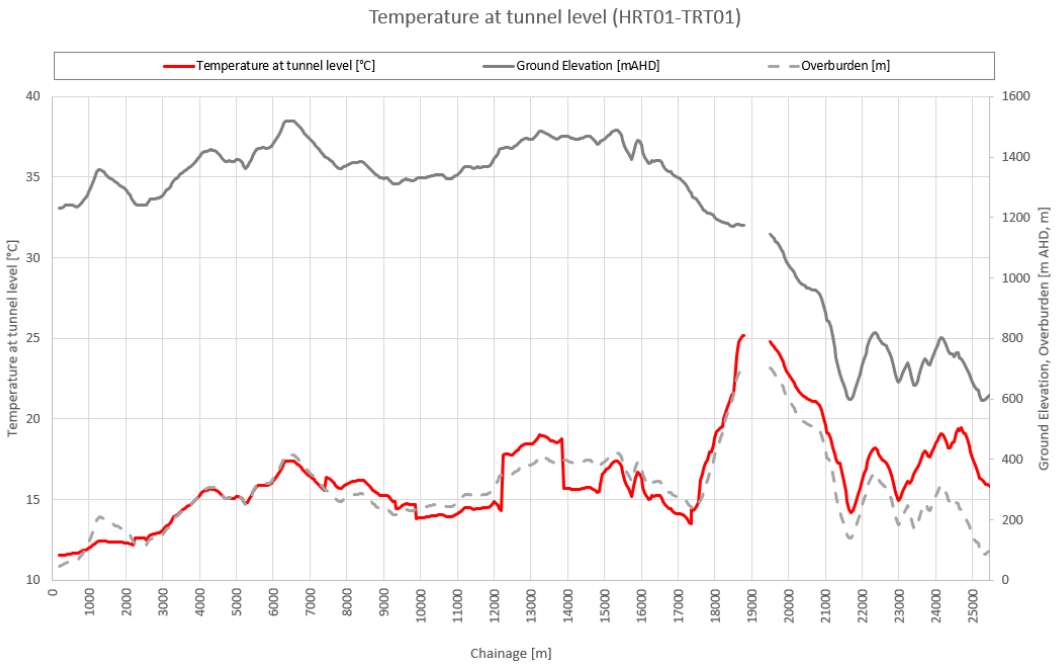

Figure 1: Temperature profile at tunnel level along the Snowy 2.0 project.

3.2 Geothermal gradients

At each borehole location the local geothermal gradient (GG) was inferred from VWP monitoring data. The measured GGs show locally a high variability, ranging from 0.9 to 4.4 °C/100 m. Three GG categories are recognized (values in °C/100m): high (GG>2.5), medium (1.5 <GG> 2.5) and low (GG<1.5). These categories are relative and not absolute, referring to the gradients found in the Snowy 2.0 project area only; a gradient that is considered high or low in this context may not be so in another geological and tectonic context.

Figure 2 shows all the temperature values measured in VWP at various depths along the Snowy 2.0 project. The data is separated into three groups, which correspond to sectors with different geothermal characteristics: Plateau area, Ravine area and Yarrangobilly River area.

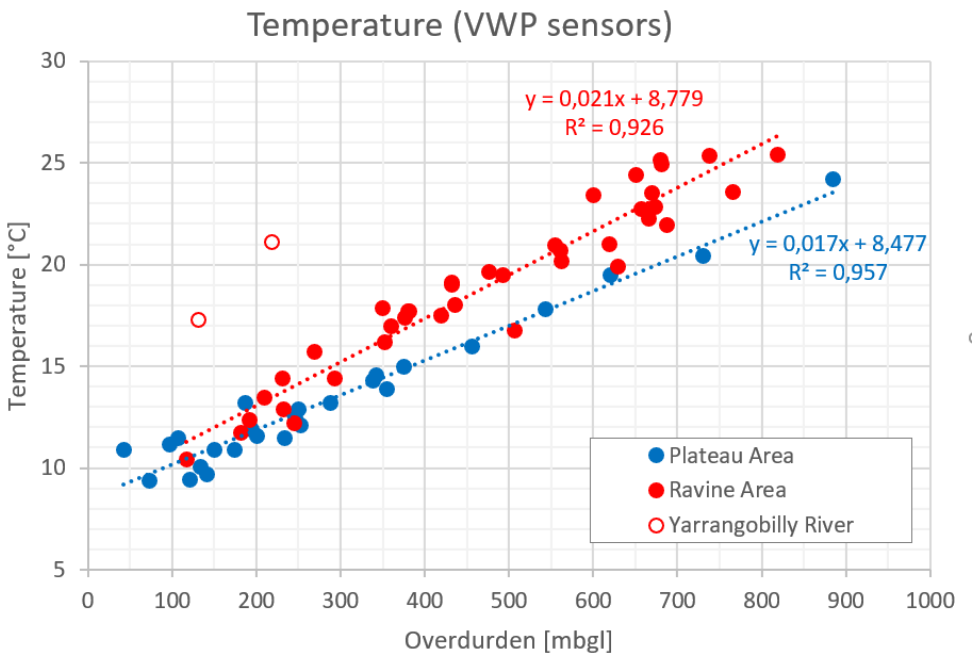

Figure 2: Temperature measurements in the Snowy 2.0 VWPs.

The Plateau area is located along the headrace tunnel between chainages 0 and 15400 m (see ground elevations and the chainages in Figure 1). The overburden on top of the tunnel varies approximately between 200 and 400 m below ground level (bgl). The Plateau area has been subject to uplift, assumed to have occurred about 20–25 Ma (Cenozoic Era) ago with differential movements causing both direct uplift and tilting. These movements have generated faults that are considered to have formed at least partly in tension and partly in strike-slip motion. They may have opened up fracture zones that extend to the tunnel level leading to poor ground conditions and groundwater connectivity. The average geothermal gradient in this area is 1.7° C/100m.

The incised Ravine area extends from an old, large fault zone called the Long Plain Fault Zone (LPFZ) to the west. The LPFZ is considered to have been initially active during the Palaeozoic and reactivated in the Cenozoic. This area was not affected by the Cenozoic uplift to the same extent as the Plateau area, but some uplift is likely to have occurred as the current terrain is an incised ridge and ravine landscape, with the Yarrangobilly and Tumut rivers 800 m below which witness the currently active erosive phase. Due to erosive process, the slopes in this area are much steeper than in the Plateau area. The overburden is more variable than in the previous area, ranging from about 700 m in the powerhouse cavern to 200-300 m along the tailrace tunnel. The average GG in this area is slightly higher with a value that reaches 2.1°C/100 m.

Two points along the Yarrangobilly river have been measured at 131 and 219 m bgl and show a high GG of 4.4°C/100m. This local anomaly is possibly due to the proximity to a deep geothermal system in the Yarrangobilly limestone (Moye et al., 1954). Although limestones have not been intercepted by the boreholes at the tunnel level, these limestones could be deeper seated, and its waters may filtrate upwards through fracture zones towards the Yarrangobilly river, that represents the hydraulic minimum of the system.

3.3 Thermal anomalies along the boreholes

T-logs are used to detect local thermal anomalies along the boreholes, which may be related to groundwater flow systems. Rather than reliable measures of the absolute temperature at specific point, the T-log evidences temperature variations along a borehole. In the upper part of Figure 3 three typical cases of T-logs are shown and below a conceptual model for the three types is suggested. The three models offer a key to interpret the anomalies, based on the shape of the T-log.

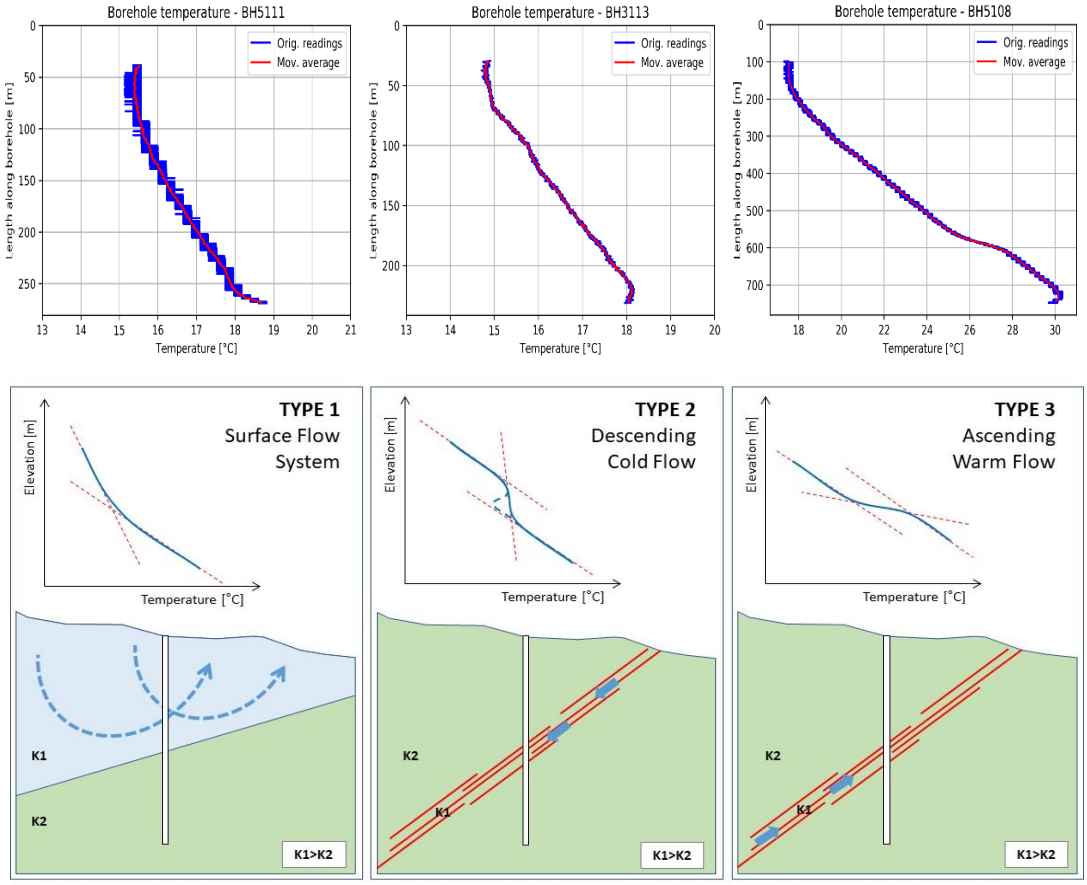

Figure 3: Conceptual models for T-log interpretation. K1, K2: hydraulic condictivity

4. Conclusions and future developments

Borehole temperature measurements are relatively simple, low-cost and reliable investigations, which contribute to the geological and hydrogeological interpretation in deep tunnels.

In the case of the Snowy 2.0 project, a thermal model at the height of the underground waterway has been defined, with temperatures ranging from 11.5°C to 25.2°C. Local geothermal gradients have been assessed for each single borehole or geological sector, showing values ranging from 0.9 to 4.4 °C/100 m. T-logs are used to detect local thermal anomalies along a borehole, related to groundwater flow systems. Three conceptual models have been developed to interpret hydrogeological anomalies based on the shape of the temperature borehole-logs.

The preliminary thermal data can potentially be applied when excavating the tunnels. In case of the occurrence of groundwater bearing zones ahead of the tunnel excavation face, thermal monitoring can be used as a predictive tool. The deviation of actual measurements that can be performed directly behind the advancing face or in the probe hole ahead of the excavation face can be used as a diagnostic tool to detect potential water flows that may be encountered during tunnel advance.

Acknowledgements

The authors thank Snowy Hydro Limited and Future Generations Joint Venture for permission to publish the data contained in this work.

References

Dematteis A., Barla M, Boscaro A., Gargini A., Governa M., Grosso F., Insana A., Marchionatti F., Parisi M.E., Perello P., Ranfagni L., Ruffinatto G., Torri R. Vazzoler S., Vincenzi V. (2020). Guidelines for groundwater and heat management in tunnels. Italian Chapter of IAH, Acque Sotterranee, Italian Journal of Groundwater, AS35, 01-80.

Hasegawa M., Usui M., Gotoh K. (1993). Geological prognosis ahead of a tunnel face. Engineering Geology, Volume 35, Issues 3-4, 229-235.

Maréchal J.C., Perrochet, P. (2010). Theoretical relation between water flow rate in a vertical fracture and rock temperature in the surrounding massif. Earth and Planetary Science Letters, Volume 194, Issues 1-2, 213-219.

Moye, D., Sharp, K., & Stapledon, D. (1954). Engineering Geology of the Snowy Mountains Scheme. Snowy Mountains: Snowy Mountains Hydro Electric Authority.

Wilhelm, J., Rybach, L. (2003). The geothermal potential of Swiss Alpine tunnels. Geothermics 32/4-6, 557-568.

THEME 4 - ENGINEERING GEOLOGY FOR ENGINEERING WORKS

Combination of cementitious and chemical grouting in the transition zone of unlined and concrete-lined tunnel: a case from Upper Tamakoshi Hydroelectric Project, Nepal

Sanjib Sapkota[1], Renos Christakis[2], Jharendra KC[3] & Mahesh Raut[3]

[1]*Upper Tamakoshi Hydropower Ltd., Nepal*
sanjibsapkota@gmail.com

[2]*Tractebel Engineering GmbH, Germany*
renos.christakis@tractabel.engie.com

[3]*JV Norconsult AS – Lahmeyer International GmbH, Nepal*
jharendrakc03@gmail.com, mahesh.raut1218@gmail.com

ABSTRACT: The transition from concrete-lined to unlined (shotcrete-lined) section of a tunnel, always has tendency of water out-leakage from the conveyance system. The main purpose of grouting in transition sections is to mitigate water leakage and maintain seepage below tolerance limits. Cementitious grouting supplemented with chemical grouting has been introduced as an advancement in tunnelling techniques. The cement grouting establishes a radial low-permeability zone within the surrounding rock-mass. Chemical grouting, on the other hand, aims to accommodate concrete shrinkage, and fill any possible fissure or crack of the concrete body. Grouting commenced with thinner grouts, gradually switching to higher viscous grouts. Should Lugeon tests fail to satisfy the 0.5 Lu threshold for each individual hole, split-spacing method was adopted to drill next-round holes at both sides of all failed holes. The gradual reduction of permeability values in successive stages; the achievement of consolidation ratio of 0.4% with a total gout intake of 73,224 litres along with the injection of 2,038 litres of chemicals corroborate the satisfactory outcome of the operation. Additionally, grouting results were validated by conducting water-pressure tests for all drilled holes against a target of very low conductivity (0.5Lu).

Keywords: Cement grouting, chemical grouting, Nepal, tunnel

1. Introduction

Grouting constitutes a technique of pumping fluids aiming to fill voids, fissures, cracks or joints of a targeted material. The targeted material can be rock, soil or even concrete. In general, grout injections are conducted aiming to increase strength, reduce deformability, decrease permeability or a combination of the above. Rock-mass usually constitutes a water permeable “structure” due to existing network of intersecting various-sized discontinuities and other possible primary or secondary voids. On the other hand, despite concrete being considered as water-tight structure; multi-faceted parameters can directly or indirectly influence its porosity and permeability, rendering concrete practically permeable. Permeability of concrete is very low, in the order of 10^{-14} to 10^{-10} metres per second (Bamforth, 1987). Shotcrete properties exhibit relatively higher permeability, however, also in the same order as anticipated within concrete. The main purpose of grouting in transition sections is to create a water-tight zone, which will act as a barrier and prevent loss of water from unlined (shotcrete-lined) tunnel by maintaining seepage below the tolerance limits. This can be achieved either by reducing permeation potential, or mitigate diffusion and migration which might occur through natural or human-induced leakage paths.

Initially, in the history of civil engineering, conventional cementitious grouting was the only available method. The first cementitious injection is considered the one made by the French engineer Charles Bérigny in 1802, wherein he prepared a suspension of pozzolanic cement and water to fill the cavities in a dam foundation

(Ewert & Hungsberg, 2018). Karol (2003) argues that the earliest injection is credited to Marc Brunel, who used Portland cement for grouting in the Thames Tunnel in England in 1838. This literally means, cementitious grouting method has been already utilised since the early years of 19th century (before 1840).

Chemical grouting refers to the injection of Newtonian fluids. On the contrary, cementitious grouting refers to the injection of the Binghamian fluids, where cement particles are suspended in a cement slurry. The first chemical grout can be credited to a European pioneer, Jeziorsky, who injected concentrated sodium silicate in 1886 (Karol, 2003; Heidarzadeh et al., 2007). With the advancement of polymer industries, chemical grouting became quite popular in the 1950s and also developed in its form from inorganic to organic compounds (Karol, 2003; Heidarzadeh et al., 2007).

The practice of grouting in tunnels is emerging in Nepal. Many hydropower developers neglect the fact that every drop of water leaking out from the water conveyance system, is precious. Few works of grouting have been conducted in Nepal, yet not properly documented. Panthi & Nilsen (2005) published a paper based on the grouting works carried out in Khimti-I Hydropower Project and demonstrated how the combination of pre- and post- excavation grouting phases significantly contributed in reducing the permeability of surrounding rock mass, and ultimately the out-leakage of water from the Project's headrace tunnel.

As already mentioned, the purpose of grouting is to establish a radial low-permeability zone within the surrounding rock-mass, and at the same time to improve the major intrinsic rock-mass properties of the peripheral tunnel zone. Notwithstanding this from design to implementation, grouting requires field practitioners to adapt the injection method to the in-situ conditions; anticipating a grouting outcome which still entails some degree of uncertainty; and renders grouting operation a not-easy-to-achieve goal. The prevailing discontinuities within the rock-mass and their interconnections, the dimensions of the aperture, the strength of rock-mass and the encountered groundwater conditions always make grouting a complex goal to accomplish. Low viscosity grouts provide better penetrability but greater shrinkage; on the other hand, high viscosity grouts may set with limited shrinkage effects, but will barely penetrate into the desired area due to decreased pumpability with distance (Kazemian et al., 2010; NTS, 2011).

2. Study area

Upper Tamakoshi Hydroelectric Project (UTKHEP) is located in the eastern region of Nepal (Figure 2). UTKHEP is a peaking run-of-river project with installed capacity of 456 MW. With a gross hydrostatic water head of 822 m, it is designed for 66 m^3/sec discharge. The project consists of surface headworks, 8 km long headrace tunnel, underground powerhouse, 3 km long tailrace tunnel, two access, and several auxiliary underground structures (Figure 1). The headrace tunnel (HRT) is excavated in inverted-D shape with 6 m height, 6 m width and cross-sectional area of 32.1 m^2. Within the HRT, there are altogether five concrete-lined sections namely Section A, Section B, Section C, Section D/E and Power Intake. This paper focuses on the grouting works carried out at the beginning of the very downstream concrete block, the transition from the unlined (shotcrete-lined) section towards the concrete-lined Section A. The overburden of the study tunnel stretch is 566 m.

With respect to geological regime, the project area is located in the kyanite/sillimanite bearing Migmatitic Paragneiss formation of the Higher Himalayan Tectonic Zone (Panthi & Basnet 2017). The surrounding rock-mass is characterized by light grey to dark grey, fine to coarse grained Gneiss, intercalated with biotite-muscovite Schist and quartz & pegmatitic veins.

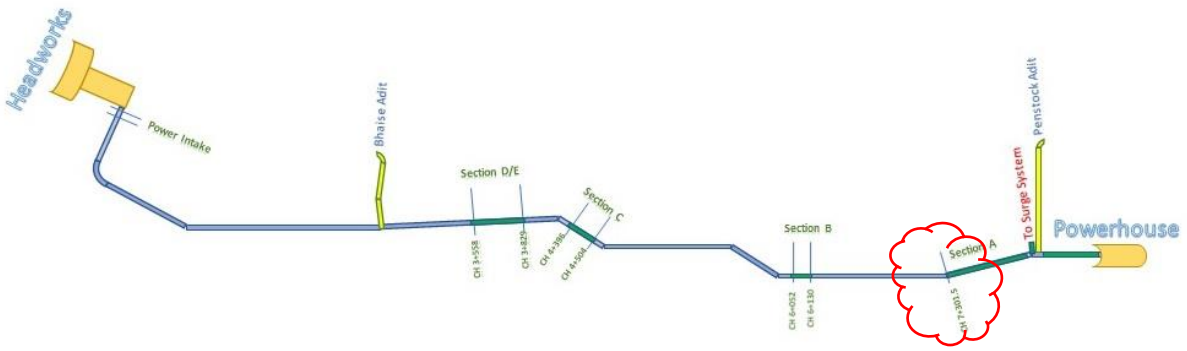

Figure 1. Schematic diagram of the Upper Tamakoshi HEP Headrace Tunnel (study section is marked)

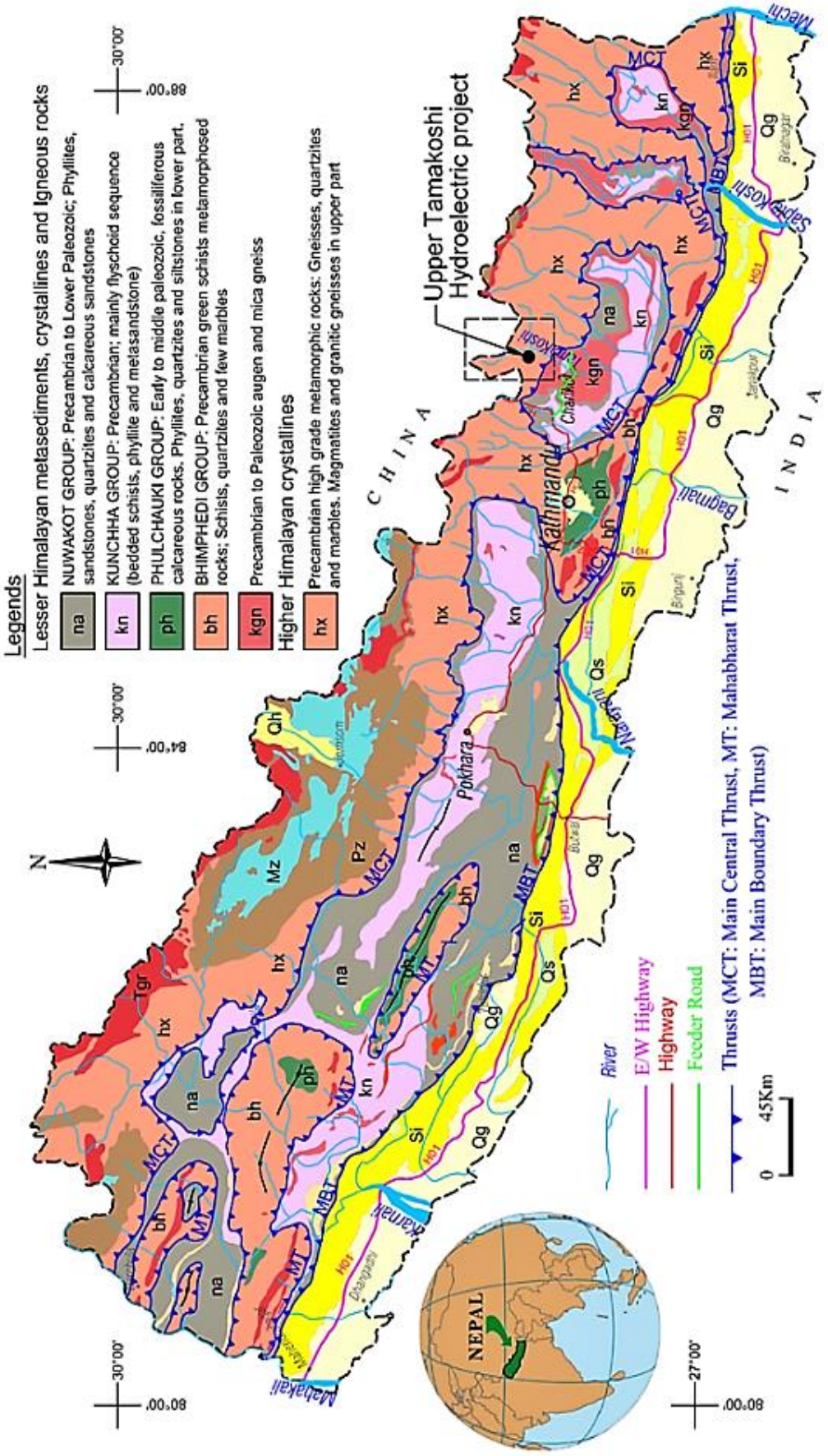

Figure 2. Location of the study area with reference to the geological map of Nepal (Panthi & Basnet 2017)

3. Methodology

Cementitious grouting combined with subsequent chemical grouting was conducted aiming to improve the properties of surrounding rock-mass, achieve the design permeability values and assure long-term water tightness of a transition tunnel stretch which will be subject to high-pressure during powerplant's operation. The methodology framework is presented as process flowchart in Figure 3 and described in the following sub-heads.

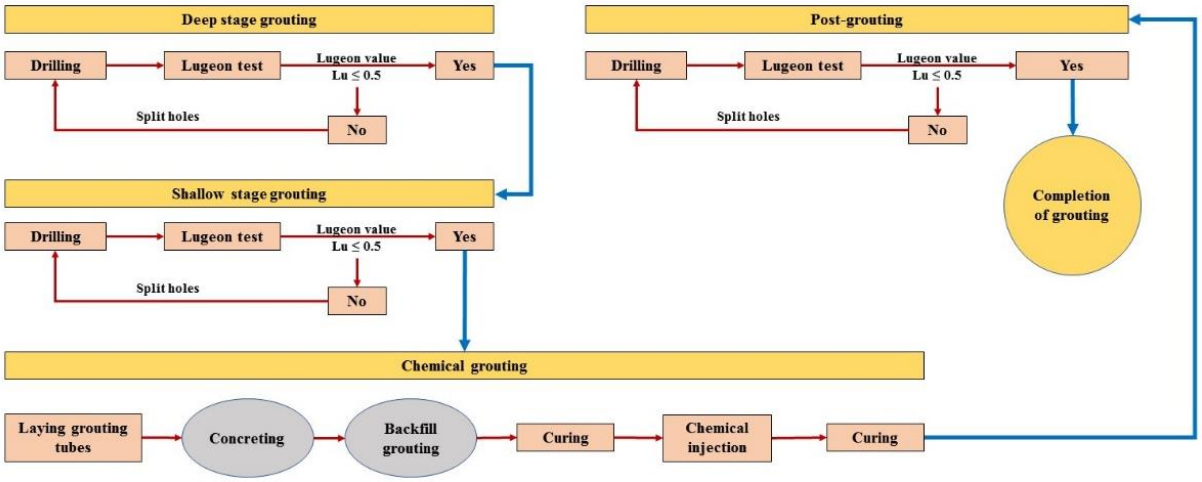

Figure 3. Methodology framework

3.1 High-pressure cement grouting

Grout-holes were drilled in radial staggered patterns and high-pressure injection was carried out in two separate stages which consist of two peripheral zones; an external (deep stage grouting) and an internal (shallow stage grouting).

3.2 Deep stage grouting

During deep grouting stage, 25 m long holes were drilled in radial pattern, in three fans (D1, D2 and D3); each fan consists 8 holes, spaced at 45˚ around the circumference. Permeability tests were performed by setting hydraulic packers at 2 m depth. Grout injection was conducted at 45 bar pressure. Should permeability values of any particular hole be greater than 0.5 Lugeon (Lu), two holes (split holes) at either side of that hole were drilled to 25 m, followed by subsequent permeability tests and grout injection. Similar procedure (i.e. split spacing) was adopted until all holes result to a permissible Lugeon threshold of 0.5 Lu.

3.3 Shallow stage grouting

After completing deep stage grouting, shallow stage was implemented. During shallow stage grouting, 5 m long holes were drilled in radial pattern, similar to the deep stage, and in four fans (S1, S2, S3 and S4). Fans S1 and S3 were drilled in normal pattern whereas fans S2 and S4 were drilled in staggered pattern. Permeability tests were performed by setting hydraulic packers at 1 m depth. Grout injection was carried out at 30 bar pressure. 5 m long additional holes (split holes) were drilled at both sides of any hole where permeability tests did not satisfy the 0.5 Lu threshold. Subsequently, these additional split holes were tested (permeability tests) and grouted under the same principles. Similar procedure (i.e. split spacing) was adopted until all holes result to the permissible Lugeon threshold of 0.5 Lu.

3.4 Concrete casting

Prior to casting of concrete, a network of inflatable tubes was installed onto the rock contour. These tubes were utilised for the injection of chemical components after casting. Special care had taken so that the installed chemical grouting tubes are not damaged or creased. Driver guides made of PVC tubes were inserted in each of the primary and secondary hole positions in order to facilitate the drilling process for the post-grouting stage. The lining segment is reinforced with 301 kg of steel per m^3, and an average concrete lining thickness of 550 mm.

3.5 Low-pressure backfill grouting

After completion of concreting, holes for backfill grouting were drilled on the crown at spacing of 2 m. First ring consisted three holes at 10 o'clock, 12 o'clock and 2 o'clock position whereas second ring consisted two holes at 11 o'clock and 1 o'clock position. Similar staggered arrays were drilled for the whole section. There were drilled six rows and 15 holes in total, for backfill grouting purposes. Backfill grouting was conducted through those holes at 3 bar pressure.

3.6 Chemical grouting

After completing shallow grouting and before commencing concrete placement, a number of inflatable grouting tubes were fixed/attached and nailed onto the rock contour. Altogether eight rings were installed (R1, R2, R3, R4, R5, R6, R7 and R8), spaced 1.5 m apart. For each ring, there were four particular tubes; one at invert, one at crown and two at side walls. Grouting tubes were fixed following the rock contour and nailed properly (maximum distance of 10 cm) to ensure that tubes will follow rock contour, aiming to avoid possible folding or creasing of the tube. For each grout tube its two end tips, lead to a supply line connection. Those supply lines are connected with high pressure hose pipes, fitted with one control valve. Those valves were uniquely labelled so that they could be easily identified during chemical injection.

After installation of grout tubes, casting of concrete took place, followed by backfill grouting. Chemical injection through preinstalled grouting tubes was conducted upon concrete curing completion (i.e. 28 days after backfill grouting). The main purpose of chemical grouting includes the filling of voids/gaps between rock contour and casted concrete due to concrete shrinkage after casting, and ensure the tight bondage between rock and concrete. Moreover, it will also reduce permeability of the surrounding rock-mass by filling chemical components within it. Rings R1, R2, R7 and R8 were grouted with polyurethane (PU) component in order to make a "cushion" and prevent leaking of chemicals from both ends of concrete lining. Subsequently, middle rings i.e. R3, R4, R5 and R6 were injected with epoxy (EPO) component. Polyurethane components were injected under 15-30 bar pressure whereas epoxy components were injected under 30-50 bar pressure.

3.7 Post-grouting

Post-grouting was the final task conducted at the transition area of concrete-lined and shotcrete-lined tunnel section. Two are the major aspects of post-grouting:

- To assess the performance of grouting works conducted earlier (deep and shallow stage of high-pressure grouting; low-pressure backfill grouting and chemical grouting). This literally means; should earlier grouting be properly performed, the anticipated grout volumes during post-grouting would be low or even negligible.
- Further to this, all the voids in rock-mass and concrete which were not filled during previous grouting stages would be compensated during that stage.

During post-grouting stage, eight holes were drilled in radial pattern for each ring, spaced at 45˚ angle around the circumference. Four rings (C1, C2, C3 and C4) were drilled and grouted in total. Rings C1, C3 and C4 were drilled in normal pattern whereas Ring C2 were drilled in staggered pattern. Each hole was drilled 2 m into rock-mass. Hence all 32 holes varied by depth (from 2.8m to 4.0m). Permeability tests were conducted by hydraulic packers set at 0.5 m depth. Grout injection was performed at 30 bar pressure. Split spacing grouting strategy was adopted to drill secondary holes, should any particular hole exhibits Lugeon values greater than 0.5 Lu. Such holes were subsequently tested for permeability and grouted under the same principles. Same procedure continued until all the holes satisfy the design permeability threshold of 0.5 Lu.

The grouting concept for each subsequent stage is illustrated in Figure 4.

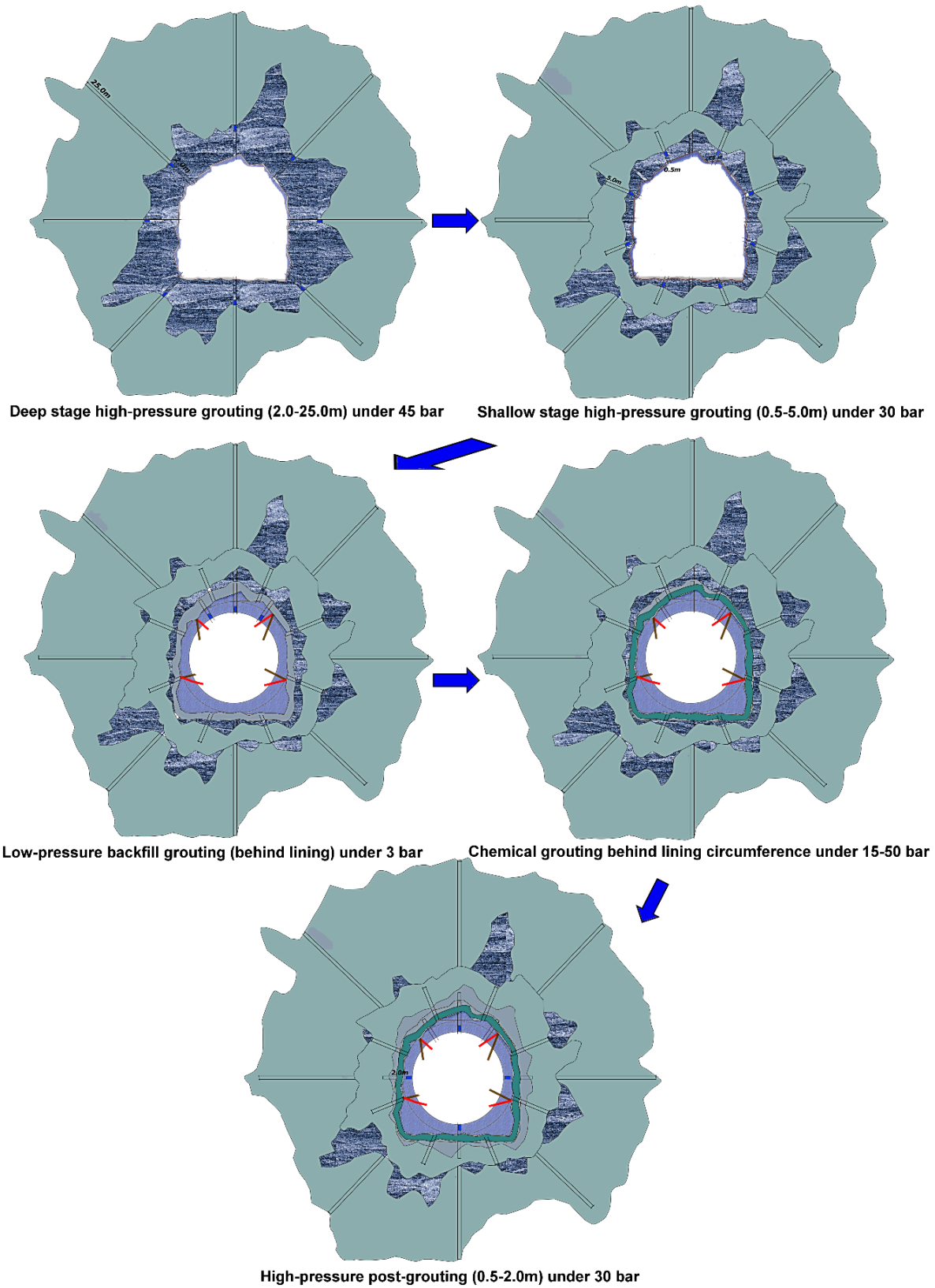

Figure 4. Grouting stages

3.8 Grouting mixes (recipes)

An integral factor for successful grouting relates to the design of the grout mix (i.e. recipe). Since long time, the main debate among grouting designers/field technicians entails continuous arguments whether to utilise a single mix (fixed water/cement ratio of a particular value) or utilising a series of different mixes of variable ratios (Deere & Lombardi, 1985; Lombardi & Deere, 1993; Tolppanen & Syrjänen, 2003; Dalmalm, 2004).

Low viscosity grouting is preferable for better penetrability. However, the decrease in water/cement ratio will result to exponential increase in viscosity (Håkansson, 1993). The development of superplasticizers in recent years paved the road for achieving low viscosity grouts from a thick mix (Dalmalm, 2004).

A series of factors that influence groutability (i.e. the ability of rock-mass to accept a certain grout; Bruce 2006) as well as grout injection should be taken under consideration. The prevailing stress regime in terms of macro-scale and the re-distribution of in-situ stress after the excavation and support of an underground structure mandate the maximum grouting pressure and also influence injection. Gustafson & Stille (1996) suggest that grouting pressure should not exceed the minimum rock stress, aiming to avoid jacking of critical joints. Injection and groutability can be also influenced by the geometry of surrounding rock-mass (strike direction, degree of anisotropy; the joint properties (i.e. type of infilling, spacing, aperture, roughness and continuity); and the groundwater regime (Barton & Choubey, 1977). Another intrinsic parameter which might influence groutability relates to any possible large scale discontinuity or tectonic feature (e.g. shear or fault) in the vicinity. Finally, an extrinsic groutability factor is linked to excavation behaviour (i.e. blasting) and/or possible malpractices (e.g. poor or inefficient blasting, human-induced fragmentation) that might extend the excavation damaged peripheral zone (EDZ) beyond the appropriate depth. These may result to the increase of fragmentation degree.

Considering aforementioned facts, a thinner grout of 1.2:1 water/cement ratio was initially injected in holes exhibiting Lugeon values less than or equal to 3.0 Lu; whereas a relatively thicker grout of 1:1 water/cement ratio was injected for holes exhibiting Lugeon values greater than 3.0 Lu. The water content was gradually lowered to produce thicker mixes. The thickest grout had a water cement ratio of 0.5:1. Recipes used during cement grouting are presented in Table 1. Another important criterion for grouting is the refusal of injection. In order to establish a higher limit that defines excessive injection beyond a targeted area; a certain volume threshold was regarded as cut-off value. The maximum volume of grout for each hole was set to 2000 litres in general and 3000 litres in particular cases where Lugeon values exceeded 8 Lu (Table 1). Super-plasticizer (Sikament®-1016 NS) was used as additive for thinner mixes. For relatively tight joints backfill is anticipated before reaching refusal volume. In such case, pressure is gradually increasing towards predefined maximum value. However, excessive or rapid increase in pressure might result to the hydrofracturing of rock. Therefore, in order to prevent hydrofracturing, a pressure-based refusal criterion was also considered. The grouting operation in a particular hole was designed to be finalised in case of zero intake flow for five minutes and for specified pressure value. Considering the prevailing stress regime and the properties of surrounding rock-mass, the refusal pressure set for deep grouting was 45 bar and that for shallow and post-grouting was 30 bar. For higher penetration results, microfine or ultrafine cements are preferred in rock-mass consisted of thinner fissures and cracks. Since permeability accounts the loss of fluid from fissures and cracks, lower permeability is likely to be associated with thinner cracks/fissures. For improved groutability, ordinary Portland cement was utilised in areas of higher permeability value, and microfine cement was used in rock-mass of lower permeability. The cut-off threshold selected in our case is 3 Lu (Table 1).

Table 1. Grouting recipes

Lugeon value	Cement type	W/C ratio by weight	Super-plasticizer (%)	Maximum volume to be injected (litres)
≤ 3.0	Microfine cement (MFC)	1.2	2.0	300
		1.0	1.5	300
		0.8	1.5	400
		0.5	-	1000
3.0 < Lu ≤ 8.0	Ordinary Portland cement (OPC)	1.2	2.0	300
		1.0	1.5	300
		0.8	1.5	400
		0.5	-	1000
> 8.0	Ordinary Portland cement (OPC)	1.0	1.5	300
		0.8	1.5	500
		0.5	-	2200

4. Results and discussion

4.1 High-pressure cement grouting

All primary (1st round) holes in fans D1, D2 and D3 were drilled to 25 m, tested for permeability, and grouted (Figure 5). All holes for each fan (24 holes) recorded Lugeon values greater than 0.5 Lu. Consequently 24 secondary holes (2nd round) were drilled, tested for permeability, and grouted with cement mixes. 19 holes of this secondary round exceeded the threshold value of 0.5 Lu. Consequently, 35 additional split holes were drilled as tertiary (3rd) round of grouting. All of them were tested for permeability and grouted. Likewise, 22 split holes in quaternary (4th) and 4 holes in quinary (5th) rounds, were drilled, tested and grouted. The majority of permeability tests conducted during the primary stage (approximately two thirds; 62.5%) indicated turbulent flow, whereas 12.5% indicated laminar behaviour. Turbulent behaviour likely corresponds to rock-mass with partly open to moderately wide cracks. Laminar flow likely corresponds to rock-mass of low hydraulic conductivity and relatively low seepage velocities. Further to this, the average permeability of the primary stage was 5.5 Lu, and the range of maximum values is 10.7 to 12.7 Lu, which also corresponds to moderate permeability and partly open discontinuities (Figure 6).

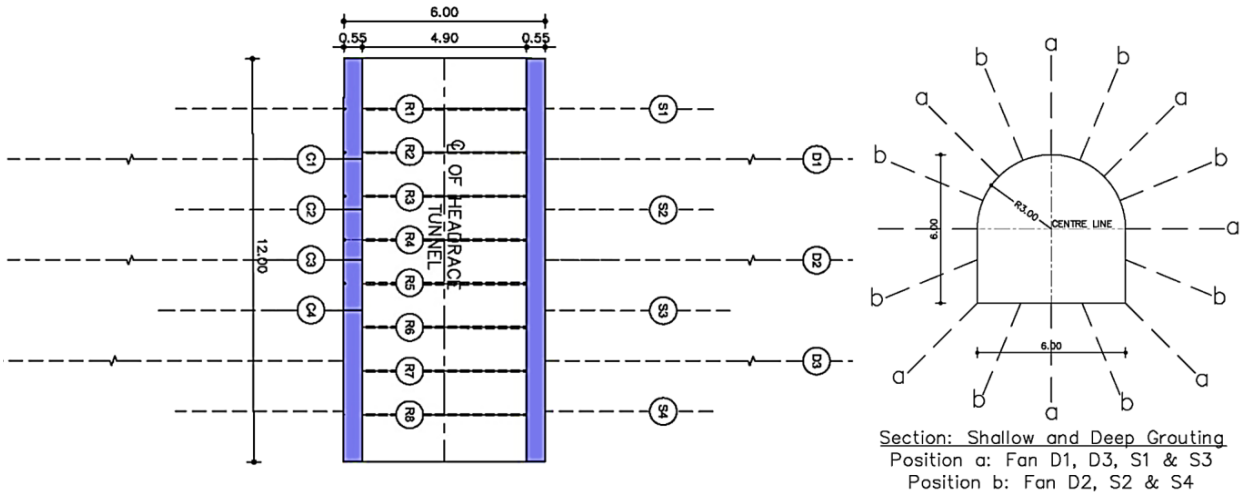

Figure 5. Layout of deep stage and shallow stage barrier grouting

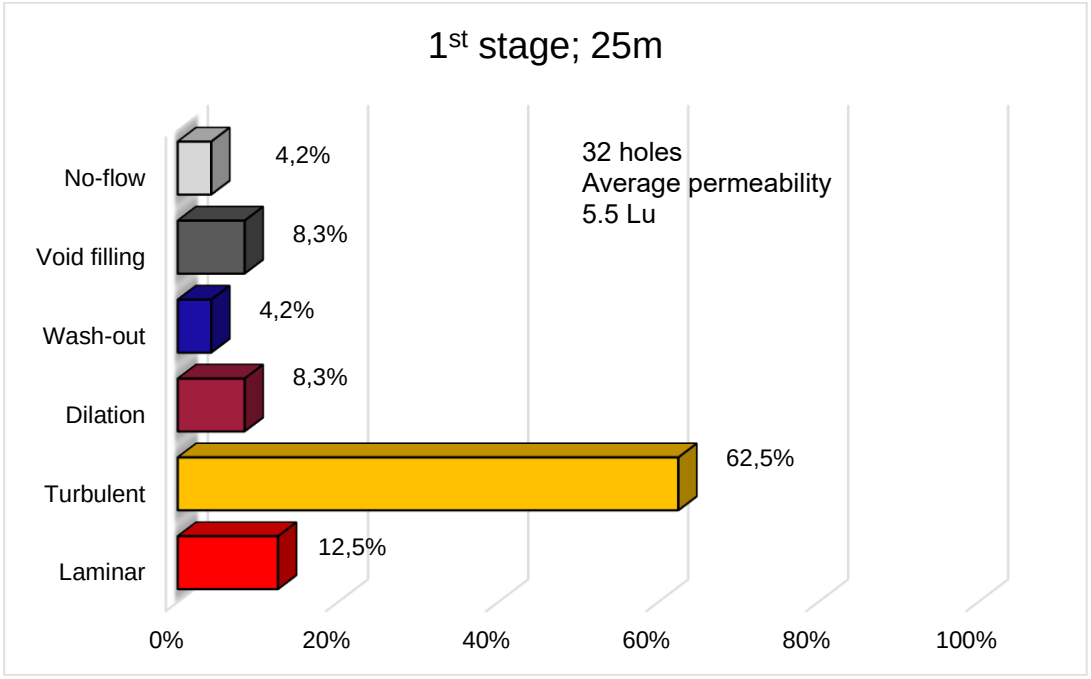

Figure 6. Lugeon behaviour during primary deep stage; 24 holes (tested section 2-25m)

Regarding all supplementary holes that drilled, tested and grouted during the subsequent deep stages (2nd, 3rd, 4th and 5th) nearly half of them showed very low permeability (no flow; 48.2%), whereas 28.2% showed turbulence behaviour with an average value of 1.46 Lu. Behaviour and figures corroborate to low permeability and tight discontinuity conditions. The results of all supplementary stages indicate improvement in terms of hydraulic properties, considering the external peripheral zone (2-25 m) of the tunnel section (Figure 7).

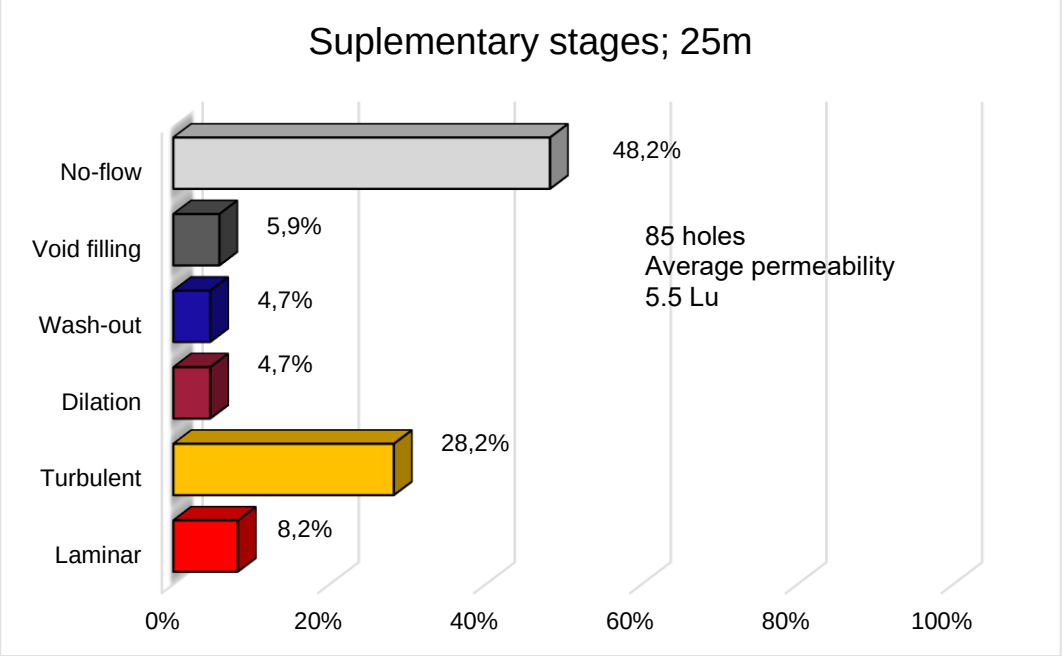

Figure 7. Lugeon behaviour during supplementary deep stages; 85 holes (tested section 2-25 m)

Considering holes in fans S1, S2, S3 and S4, all 32 primary holes recorded Lugeon value below 0.5 Lu threshold. Therefore, all 32 holes were grouted and this stage was terminated at the primary round. Considering that shallow stage (0.5-5 m) was performed as sequential stage to the deep stage, recorded low figures in all 32 holes (no-flow) indicate successful outcome of the deep stages (24 primary and 85 supplementary holes) and efficient propagation of grouts in the internal peripheral zone (0.5-5 m) of the tunnel section (Figure 8).

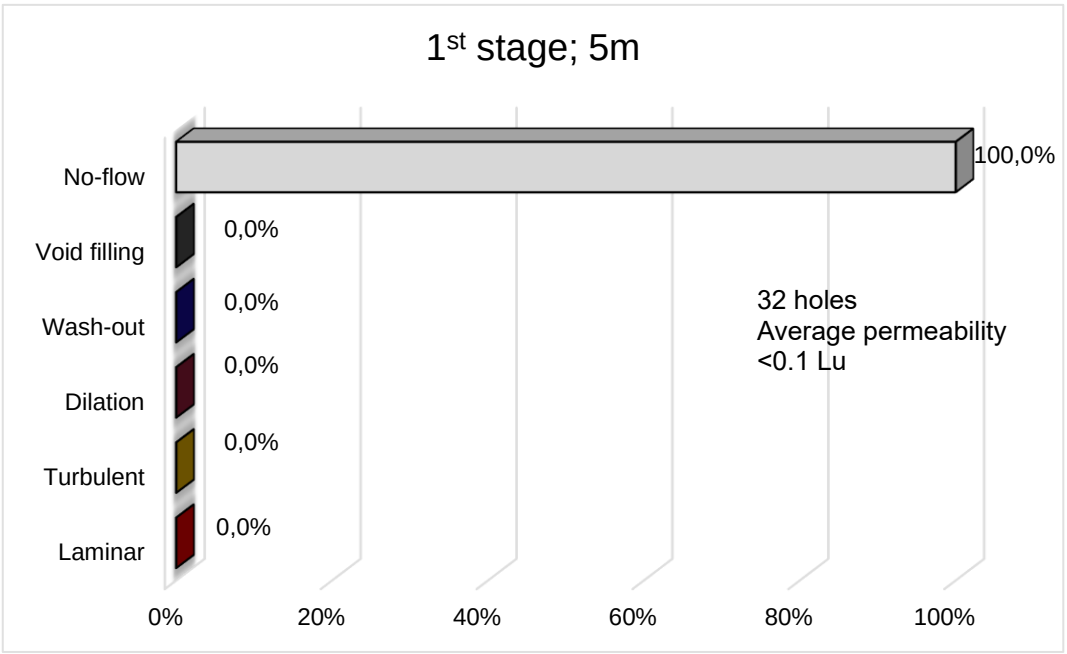

Figure 8. Lugeon behaviour during shallow stages; 32 holes (tested section 0.5-5m)

The number of holes for each consecutive round and the corresponding grout intake for each grouting round is summarised in Table 2. Similarly, a summary of grout-holes with respect to threshold Lugeon value is shown in Table 3.

Table 2. Summary of drill-holes for each round and respective grout intake

Grouting stage	Chainage	No. of holes in each round						Grout intake in each round (litres)					
		I	II	III	IV	V	Total	I	II	III	IV	V	Total
Deep Grouting	7303.0	8	8	12	6		34	9842	4563	3685	1574		19664
	7306.0	8	8	10	8	4	38	10496	4582	5823	3083	690	24674
	7309.0	8	8	13	8	-	37	11407	5974	4299	1731	-	23411
Shallow Grouting	7301.5	8	-	-	-	-	8	1177	-	-	-	-	1177
	7304.5	8	-	-	-	-	8	242	-	-	-	-	242
	7307.5	8	-	-	-	-	8	349	-	-	-	-	349
	7310.5	8	-	-	-	-	8	351	-	-	-	-	351
Grand total		56	24	35	22	4	141	33864	15119	13807	6388	690	69868

Table 3. Summary of drill-holes with respect to threshold Lugeon value

Grouting stage	Chainage	No. of holes, having Lu > 0.5					No. of holes, having Lu ≤ 0.5					Total
		I	II	III	IV	V	I	II	III	IV	V	
Deep Grouting	7303.0	8	6	3	0	-	0	2	9	6	-	34
	7306.0	7	5	5	2	0	1	3	5	6	4	38
	7309.0	5	8	5	0	-	3	0	8	8	-	37
Shallow Grouting	7301.5	0	-	-	-	-	8	-	-	-	-	8
	7304.5	0	-	-	-	-	8	-	-	-	-	8
	7307.5	0	-	-	-	-	8	-	-	-	-	8
	7310.5	0	-	-	-	-	8	-	-	-	-	8
Grand total		20	19	13	2	0	36	5	22	20	4	141

The average grout intake for deep and shallow stages are found to be 23.2 and 9.8 litres per drilled metre, respectively. In general, the average cement mix consumption during high-pressure grouting is 22.5 litres per meter of grouted length. Likewise, the average grout intakes for ordinary Portland cement (OPC) and microfine cement (MFC) are also analysed (Figure 9). The lower values in MFC consumption reflect to the fact that average consumption diminishes with the gradual decrease of Lugeon values of the subsequent grouting rounds, as threshold value for OPC and MFC is set to be 3.0 Lu.

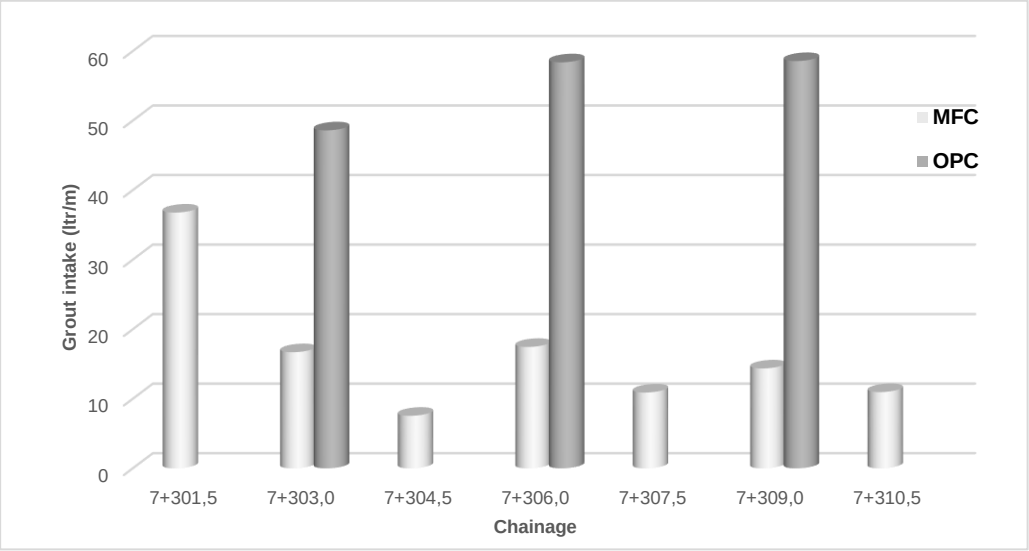

Figure 9. Average grout intake with respect to cement type in high pressure grouting

The mean values of grout intakes for the subsequent grouting series exhibit a decreasing trend, which in turn corroborate to a progressive sealing of the surrounding rock-mass (Ewert & Hungsberg, 2018). Provided that all drilled holes in shallow grouting (rings S1, S2, S3 & S4) were tested and finalised during the primary (1st) round, the average grout consumption for each round is evaluated only considering those holes of deep grouting stage (rings D1, D2 & D3), as presented in Figure 10. From the figures, it is obvious that the average grout intake is counter-proportional to each subsequent grouting round. The average grout intake for all three fans recorded almost same values.

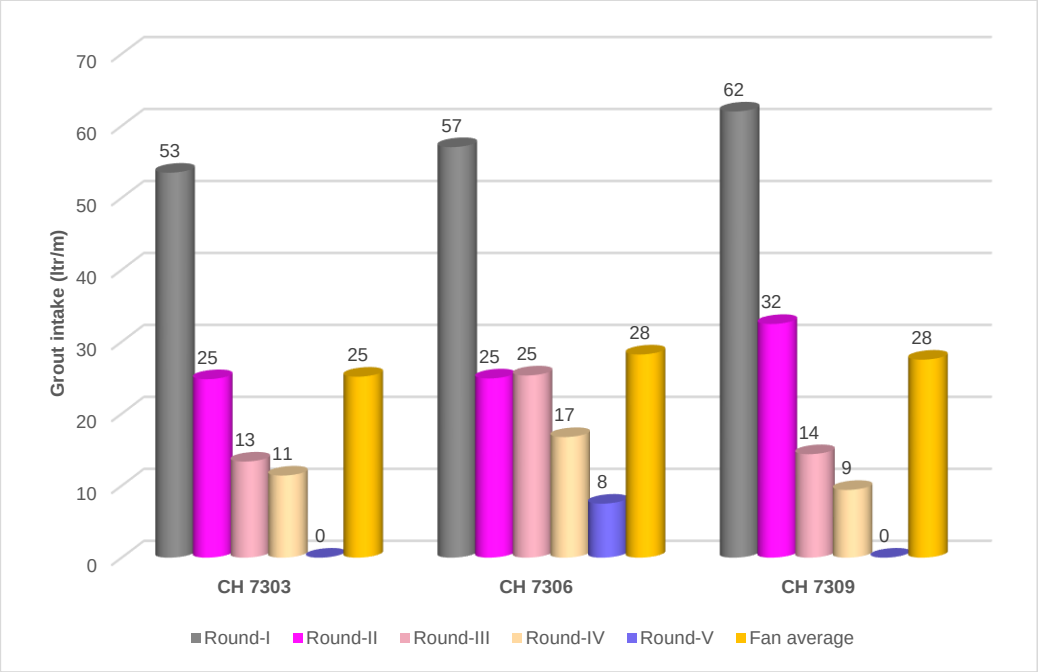

Figure 10. Average grout intake in deep stage grouting

4.1.1 Low-pressure backfill grouting

Low-pressure backfill grouting was conducted for a lined tunnel stretch of 12.0 m, in order to fill all possible remaining gaps between rock contour and the concrete surface, and also compensate all blast-induced fissures or cracks of the excavation damaged zone (EDZ). Moreover, selected components of grout-mix were designed in such way aiming to simulate the properties of casted concrete -and at the same time, to produce a pumpable mix for the targeted area (Table 4). In total, 1503 litres of grout were injected at 3 bar pressure. Therefore, approximately 125 litres were injected per metre of lined tunnel.

Table 4. Grout recipe of backfill grouting

Component	Weight (kg)	Proportion (with respect to cement)
Cement (OPC)	100	1
Water	40	0.4
Fly-ash	10	0.1
Fine sand	10	0.1
Sikament®-1016 NS	2	0.02
Intraplast® EP	1	0.01

4.1.2 Chemical grouting

Initially, two upstream (R1, R2) and two downstream (R7, R8) rings (Figure 5) were grouted with polyurethane (PU) mix (RESOFOAM 1KM of Mapei ©). The setup of grouting tubes is illustrated in Figure 11. The initial mix was produced with 5% accelerator (by weight), wherein reaction started within 8 seconds when mixed with resin. This quick reaction led to clogging of grout hoses and reduced pumpability. To improve pumpability and allow efficient spreading of PU behind concrete segment the accelerator fraction was reduced to 2.5%. In this case reaction started after 15 seconds and the pumping issue was successfully resolved. The remaining four inner rings were grouted with epoxy mix (MapEpoxy BI-R of Mapei ©). The mixing ratio of resin and hardener for this specific task was 1.78:1 (by weight). It shall be highlighted that

setting time and pumpability of both chemical components can be directly influenced by the ambient temperature and humidity. The injection of both chemical products is summarised in Table 5.

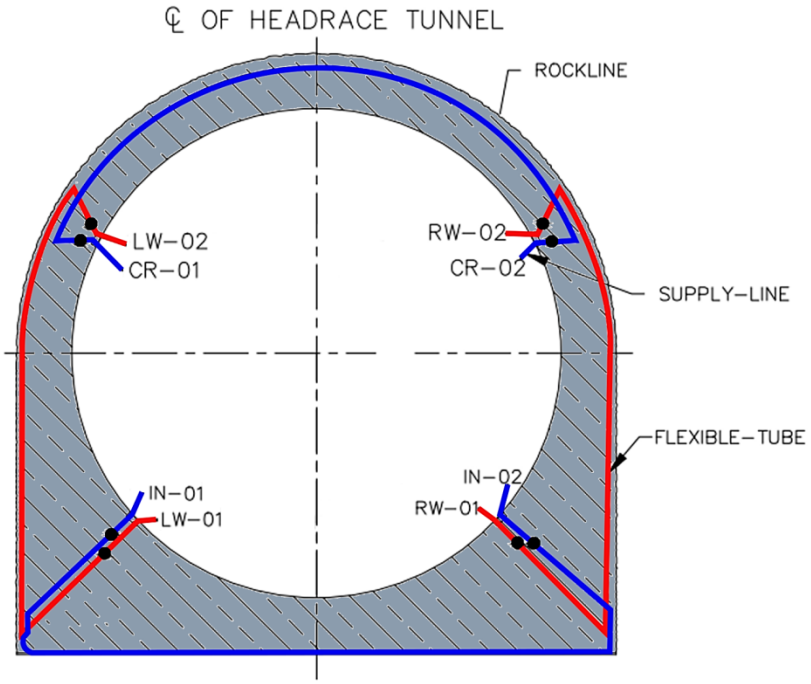

Figure 11. Standard setup of chemical grouting stage

Table 5. Summary of chemical injection

Ring No.	Injected chemical	Grout consumption (litres)
R1	PU	11.7
R2	PU	592.0
R3	EPO	3.9
R4	EPO	75.7
R5	EPO	689.9
R6	EPO	424.0
R7	PU	29.1
R8	PU	212.3
Total		2038.5

4.1.3 Post-grouting

All primary holes (1st round) in fans C1 and C4 were drilled, tested for permeability and grouted. Among these 16 holes, 1 hole in Fan C1 and 2 holes in Fan C4 exceeded the 0.5 Lu threshold. Consequently, another 5 holes were drilled for the secondary round (2nd). Those secondary round holes were tested for permeability, wherein all the holes had Lugeon value within the threshold. All secondary holes were then grouted. Having completed grouting in fans C1 and C4, all primary holes in fans C2 and C3 were drilled, tested for permeability, and grouted. A typical setup for the post-grouting stage is illustrated in Figure 12. During permeability tests, only one hole in the Fan C3 exceeded the 0.5 Lu threshold. Therefore, two holes were drilled as secondary round at Fan C3, tested for permeability and grouted. Both holes in that round satisfied the 0.5 Lu criterion; and post-grouting terminated.

Majority of post-grouting holes showed limited flow (no-flow) that literally mean tight conditions. Only a small fraction of holes showed dilation behaviour with an average very low permeability (approximately 0.6 Lu). Dilation indicates that applied pressure is greater than the minimum principal stress, causing temporary

dilatancy. Considering that tests were carried out close to the excavated profile (0-2 m), blasting activity along with scaling activity possibly affected rock-mass resulting to secondary localised fragmentation (Figure 13).

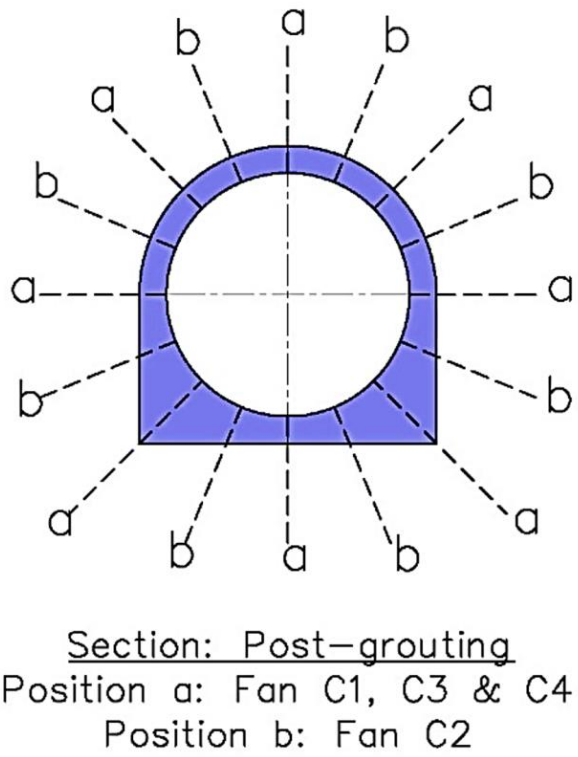

Figure 12. Typical grouting setup for post-grouting stage

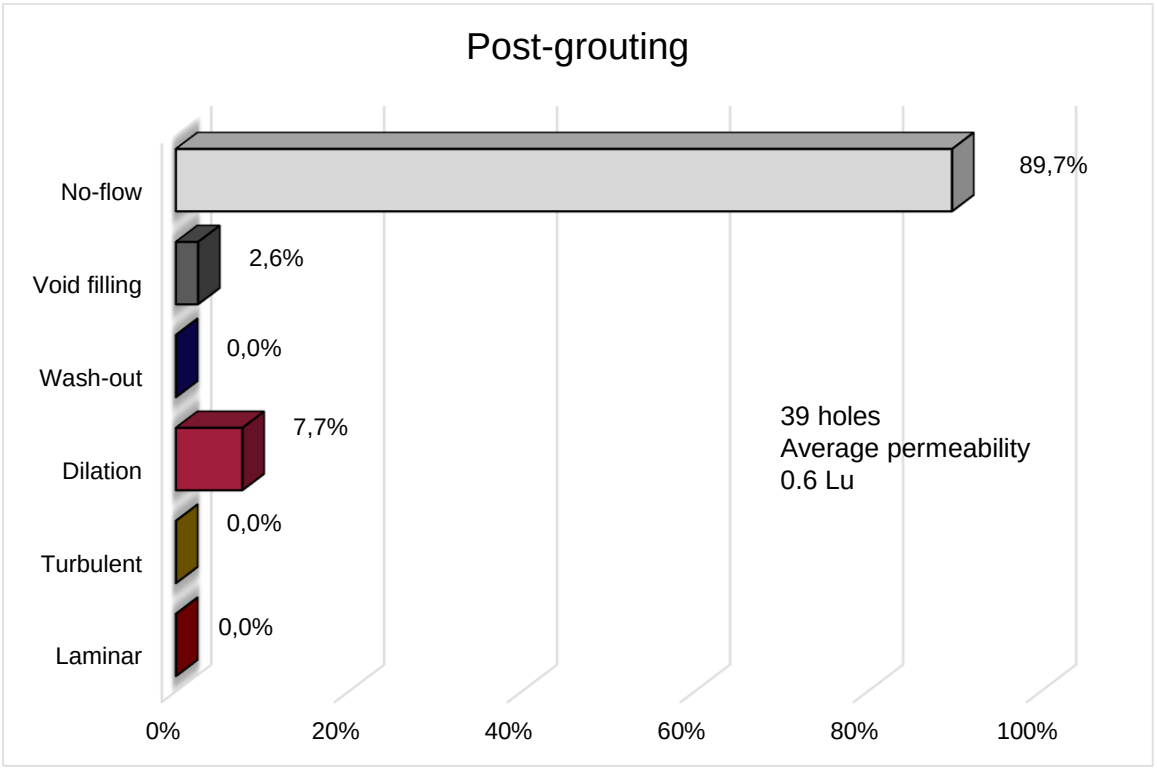

Figure 13. Lugeon behaviour during post-grouting stage; 39 holes (tested section 0-2m)

During post-grouting stage, altogether 39 holes were grouted having an average grout consumption of 35.4 litres per drilled meter. A summary of holes drilled and the respective grout volumes consumed for each round is presented in Table 6.

Table 6. Summary of grouting in post-grouting stage

Chainage	Number of holes			Grout intake (litres)			Average grout intake (l/m)		
	Round-I	Round-II	Total	Round-I	Round-II	Total	Round-I	Round-II	Fan average
7303.0	8	2	10	2570	300	2870	128.5	60.0	114.8
7304.5	8	-	8	78	-	78	3.9	-	3.9
7306.0	8	2	10	123	28	151	6.2	5.6	6.0
7307.5	8	3	11	288	69	357	14.4	9.2	13.0
Total	32	7	39	3059	397	3456	38.2	22.7	35.4

5. Conclusions

109 holes were drilled and grouted for the deep injection stage, 32 holes for the shallow stage, and 39 for the post-grouting stage. Likewise, the respective grout intake for these stages were 67,749 litres, 2,119 litres and 3,456 litres, respectively. This accounts to a total grout injection of 73,224 litres of grout in all 180 grout-holes, within a 9-m tunnel stretch.

Considering the theoretical peripheral zone of 17,850 m^3 where high pressure injection was conducted in three stages (deep stage, shallow stage and post-grouting), and the total grout injection of 73,224 litres; the actual consolidation ratio is approximately 0.4%. The comparative small number of grout-holes required during post-grouting stage (only 21.7% of the aggregate) in conjunction with the limited injected volume (4.7% of the aggregate volume) corroborate the satisfactory outcome of the operation. In addition, 845 litres of polyurethane and 1,193 litres of epoxy were injected (2,038 litres of chemicals) during chemical grouting phase. Grouting results were validated by conducting water-pressure tests for all drilled holes (0.5 Lu threshold; very low conductivity).

The overall rock-mass improvement of the external peripheral zone with respect to its hydraulic properties can be also ascertained by the gradual reduction of permeability figures during each subsequent grouting stage. In brief, the primary average permeability was initially reduced from 5.5 Lu to 1.46 Lu (73% reduction) due to the subsequent deep grouting stages; and the maximum recorded values were also reduced from 10.7-12.7 Lu down to 6.5-8.5 Lu (36% reduction). Further reduction was also achieved after conducting shallow stage injections and post-grouting stage injections where permeability figures dropped down to an average of 0.6 Lu, whereas turbulent behaviour was eliminated, as well.

Nonetheless, it shall be highlighted that the final water tightness of the grouted tunnel segment alongside with the aggregate tightness of the whole waterway will be evaluated upon completion of the first water filling of the HRT.

Acknowledgements

The authors duly acknowledge the various supports from Upper Tamakoshi Hydropower Limited (UTKHPL) as the Owner of the Project; and the Joint Venture of Norconsult AS & Lahmeyer International GmbH (JVNL) as the Engineer of the project.

References

Bamforth, P. B. (1987). The relationship between permeability coefficients for concrete obtained using liquid and gas. Magazine of Concrete Research: Taywood Engineering Limited, England, 39(138), pp. 3-11.

Barton, N., Choubey, V. (1977). The shear strength, of rock joints in theory and practice. Rock Mechanics, 10(b1), pp. 1–54.

Bruce, D. A. (2006). Glossary of grouting terminology. Geotech News, 24(4), pp. 50–59.

Dalmalm, T. (2004). Choice of Grouting Method for Jointed Hard Rock based on Sealing Time Predictions. Royal Institute of Technology, Department of Civil and Architectural Engineering, Stockholm, Sweden.

Deere, D. U., Lombardi, G. (1985). Grout slurries – thick or thin? Issues in dam grouting, proceedings of the session sponsored by the Geotechnical Engineering Division of the American Society of Civil Engineers in conjunction with the ASCE, pp. 156-164.

Ewert, K. A., Hungsberg, U. (2018). Rock Grouting at Dam Sites. Springer International Publishing AG, Switzerland

Gustafson, G., Stille, H. (1996). Prediction of groutability from grout properties and hydrogeological data. Tunnelling Underground Space Technology, 11(3), pp. 325–332.

Håkansson, U. (1993). Rheology of fresh cement based grouts. Division of Soil and Rock Mechanics, Royal Institute of Technology, Stockholm, Sweden.

Heidarzadeh, M., Mirghasemi, A. A., Etemadzadeh, S. M. (2007). Experimental Study of Chemical Grouting of Conglomerate Foundations. International Journal of Civil Engineering, 5 (1), pp. 66-83.

Karol, R. H. (2003). Chemical Grouting and Soil Stabilization. Marcel Dekker, Inc., 3rd edition, USA.

Kazemian, S., Huat, B. B. K., Prasad, A., Barghchi, M. (2010). A Review of Stabilization of Soft Soils by Injection of Chemical Grouting. Australian Journal of Basic and Applied Sciences, 4(12), pp. 5862-5868.

Lombardi, G., Deere, D. U. (1993). Grouting design and control using the GIN principle. Water Power and Dam Construction, pp. 15-22.

NTS (2011). Rock mass grouting in Norwegian tunnelling (Publication No. 20). Norwegian Tunnelling Society, Norway.

Panthi, K. K., Basnet, C. B. (2017). Design review of the headrace system for the Upper Tamakoshi project Nepal. International Journal of Hydropower & Dams 24(1): pp. 60–67.

Panthi, K. K., Nilsen, B. (2005). Significance of grouting for controlling leakage in water tunnels – a case from Nepal. In: Underground Space Use: Analysis of the Past and Lessons for the Future, Erdem & Solak (eds). Taylor & Francis Group, London, UK.

Engineering Geological Aspects of Pipelines, an Australian Prospective

Graeme Jardine[1]

[1]*Jacobs, Brisbane, Australia*
graeme.jardine@jacobs.com

ABSTRACT: Over the past ten years, in Australia, there has been a significant increase in infrastructure development covering both the growth of coal seam gas, mining related operations, and water supply. With the significant distances (some in excess of 400 km) between source location, processing plant, export hub &/or end users. Pipelines have been developed as the most effective delivery infrastructure for these markets. Apart from the typical major potential engineering geological impacts on pipelines, excavatability, trench stability, backfill material reuse, pipe crossing methodology, scour and buoyancy, local conditions of expansive, dispersive/erosive sodic and Acid Sulphate Soils have had to be dealt with. This paper provides an outline of the methods used to identify and evaluate the potential major ground characteristic and behavioural impacts for pipeline design and construction at all stages through a project life cycle. This ranges from remote sensing, site reconnaissance, site investigations and specific design inputs. Of note are the local aspects and related control measures of dealing with problematic soils. In addition, a specific excavatability assessment criteria has been developed based on geotechnical investigations and published papers/plant performance manuals. This provides a coding system that can be presented on interpreted geological long sections or pipeline alignment sheets as and aid for both design and construction contracts.

Keywords: Pipelines, Engineering Geology, Australia

1. Introduction

Over the past approximately ten years in Australia there has been a significant increase in infrastructure development covering both the growth of coal seam gas, mining related operations, and water supply. With the significant distances (some in excess of 400 km) between source location, processing plant, export hub &/or end users, pipelines have been developed as the most effective delivery infrastructure for these markets. In 2020 natural gas pipeline systems in the country equated to an approximate 39,000km transmission network, with other new major gas and water supply pipelines being considered in the coming years.

The major geotechnical drivers for pipeline design & construction have been a variety of integrated characteristics, some with greater weighting than others, in terms of both capital expenditure, constructability & construction program, and operational efficiency & related maintenance. These include:

- Physical nature of the alignment including geomorphological & potential seismological impacts.
- Excavatability & trench stability
- Crossing type, length and existing surface or near surface infrastructure control measures.
- Buoyancy & potential scour issues
- Dealing with adverse inherent soil conditions in terms of backfilling & permanent works.

2. Initial Identification of Optimum Alignments

Defining optimum pipeline alignments requires not just ground engineering considerations, and related constructability issues, but also significant impacts of cost, potential effects on existing infrastructure, environmental and social parameters. Recently, and potentially into the future, environmental impacts &

sustainability with related time and conditions associated with gaining related approvals has for many projects been the critical factor in project development and timelines.

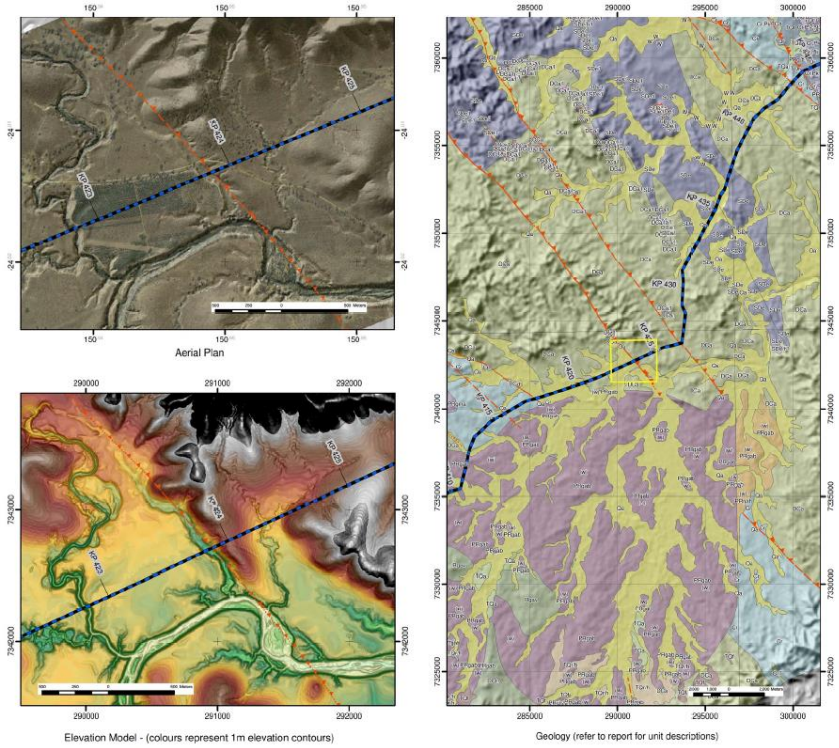

Figure 1. Queensland Gas Pipeline GIS Considerations of Ground Based Datasets

Leaving aside the existing built environment, green and community issues, the impacts of ground characteristics on defining alignments are undertaken at an early stage in a project life cycle. However, this does not mean that tweaks or significant rerouting has not occurred well after optimum alignments were thought to have been fixed.

At these early stages of projects alignment definitions are generally based on a desk study approach, coupled with remote sensing, physical walkover surveys & geomorphological and geological mapping. Data sets used for consideration may include:

- Topography and geomorphological characteristics, including natural terrain hazards); karst; fluvial based events (flooding etc.); coastal erosion (cliff or land loss); height and slope angles; width & nature of valleys & surface drainage features
- Soil types related to main type & chemical/reactive/erodibility characteristics (e.g.vertisols & podosols)
- Potential groundwater depths
- Depth to competent rock and the occurrence and type of major geological structural features
- Tectonic/seismological events & their intensities over available recorded time

It is usually by a Multicriteria Assessment (MCA) process considering all the aforementioned natural features of landscapes coupled with cost, environmental and community aspects that are used to define optimum alignments.

More recently the use of GIS databases, which spatially can map & compare/assess the aforementioned criteria, has been a step change in aiding definition of optimum alignments, including the application of algorithm based approaches such as the Least Cost Path Analysis (LCPA).

An example of the use of GIS datasets of published geology, hillshade and Digital Elevation Models derived from LiDAR surveys is provided in Figure 1. Here the different perspectives provide not only more certainty of the occurrence and nature of a major geological structural feature that could significantly affect the pipeline alignment, but also the nature of fluvial geomorphological features (including ephemeral and abandoned channels, bankfull conditions and depositional/erosional environments), soil depths, the occurrence of rock outcrops, slope heights, angles and stability features, as well as by association potential excavatability assessments.

3. Geotechnical Site Investigation Applications

The scope and applicability of a geotechnical site investigation for pipeline alignments follows the same ethos for other infrastructure projects, i.e.it is dependent on the stage in the life cycle of the project, the outcomes of the desk study gap analysis (linked to uncertainty perspectives), and of course physical character, access, budgetary and time considerations.

In general all main types of investigation techniques can be applied, but based on the often considerable alignment distances involved the application of initial geophysical methods has been found to be of particular value as an aid to determine the value and cost effectiveness of more time consuming intrusive approaches.

3.1 Aerial Electromagnetic Survey (SkyTEM)

Aerial Electromagnetic (AEM) survey is non-intrusive involving the measurement of the varying response of the ground due to the propagation of electromagnetic fields.

In simplified terms, the surveying equipment operates using similar principles as a conventional metal detector. Magnetic fields are generated by passing a current through a loop or coil positioned in the air, referred to as the transmitter loop (see Figure 2).

The transmitter loop is abruptly switched off, causing eddy currents to flow in subsurface conductors. A secondary field is induced in the ground due to the eddy currents which decays rapidly with time. These secondary fields are detected by the alternating currents that are induced to flow in a receiver coil, by a process known as electromagnetic induction. As the induction of current flow results from the magnetic component of the electromagnetic field there is no need to have physical contact between transmitter or receiver and the ground. Consequently, electromagnetic (EM) surveys can proceed effectively by air making them a rapid application technique.

The measured electrical conductivity (the reciprocal of resistivity) of such materials is a measure of how easily an electrical current can pass through a material (which is itself affected by clay composition, dissolved electrolyte concentrations, moisture content, porosity & temperature).

Geotechnical mapping of the precise, high resolution shallow data delivered by the Low Moment configuration of SkyTEM 304 has been successfully used by SkyTEM to assist in mapping depth to bedrock (depths of up to 25 m) for geotechnical investigations and as shallow as the upper few metres in some cases as shown in Figure 3. The SkyTEM 304 system is also capable of lower resolution deep data delivered by the High Moment configuration to depths of up to 100 m depending on the ground conditions.

The AEM data is processed through a SkyTEM proprietary processing sequence to classify the model conductivities into a likelihood of bedrock being present (see Figure 3).

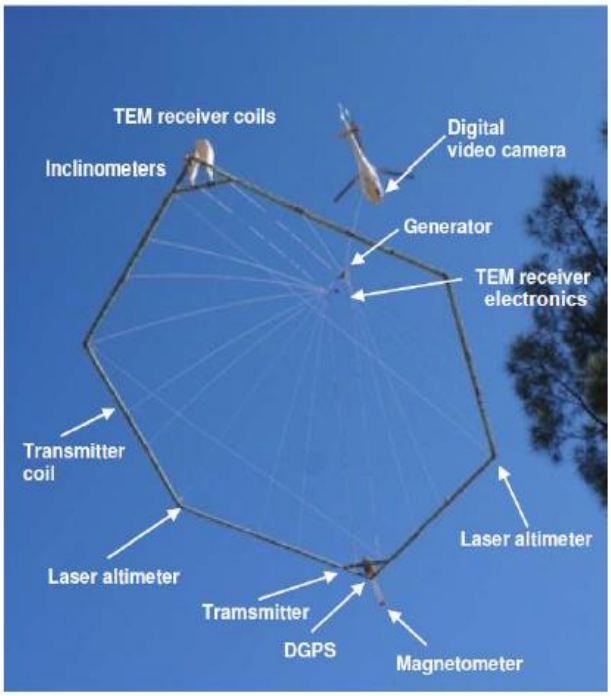

Figure 2. SkyTEM Transmitter Loop

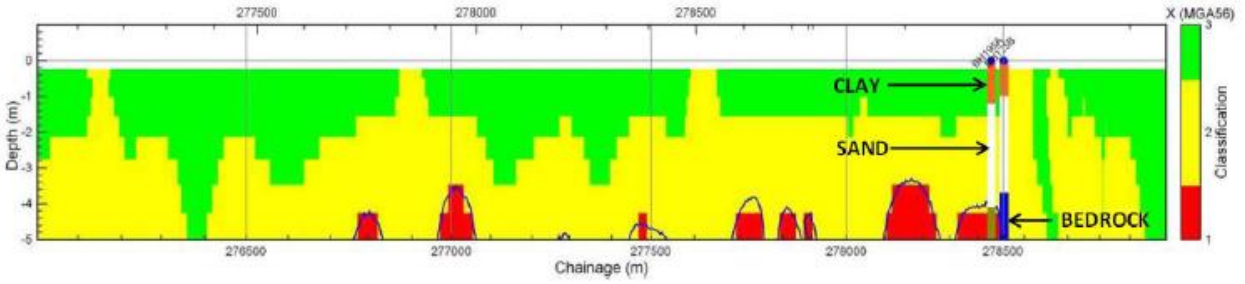

Figure 3. Cross-section of SkyTEM data used for pipeline route assessment

Other marine or terrestrial based geophysical applications can be applied in the same fashion but may be subject to more of the vagaries of physical, environmental and social impacts.

As for all geophysical techniques correlation with intrusive site investigation techniques is vital in gaining the most value from these applications.

3.2 General Investigation Approaches

The full gambit of typical investigation techniques can be applied including, boreholes, test pits and cone penetration testing (CPT). Often for such long liner projects a “type-site” approach is often applicable related to derived project specific terrain models.

In general, the following investigation techniques may be applied:

- Boreholes – for major crossings, pipe bridges, trenchless technology sections and where rockhead is at or near the surface (as well as likely for any major water body traverses); depths at least one pipe diameter below proposed invert level; typically standard penetration tests, undisturbed soil sampling triple tube coring, groundwater sampling form installed wells; possibly borehole vane & televiewer
- CPT – in areas of thick soil cover which could have a complex stratigraphy, high groundwater table or be highly compressible or loose in composition (e.g. wide alluvial floodplains, estuarine or intertidal areas and overwater)
- Test or trial pits – for minor crossings, generally for planned excavations up to 5.0mbgl in soils or extremely weathered rocks; thrust block locations (generally significant changes in pipeline direction); proposed termination depths at least to final excavation level (including bedding material layer under pipe); advantageous to have a dynamic cone penetration (DCP) tests before excavation over pit footprint; hand vane or pocket penetrometer insitu tests, bulk and undisturbed soil samples, as well as groundwater samples; this investigation technique provides a direct method of assessing the excavatability for pipeline installation by considering the effectiveness of the use of a wide variety of excavator plant, bucket width and type, as well as the type of arisings and their possible reprocessing requirements for backfill reuse, an assessment of standing water levels, potential temporary trench wall stability, and bulking factors of materials.

Spacing of investigation locations is dictated by the stage of the project; what approach to investigation is being applied (e.g. “type-site” or for correlation purposed with other techniques), as well as the risk profile of the Client, budget, time and access constraints.

Laboratory testing required can be considerably variable to fit with both the proposed works, the existing character of the ground and its interpreted behaviour traits. Typical testing suites include:

- Soil index and for chemical durability for intended concrete or steel pipelines including organic matter content and resistivity
- Reactive and erodibility assessments of soils including shrink swell and sodic soil suites
- Potential soil remediation related tests including lime and gypsum dosing with associated index, reactivity, erodibility, strength/stiffness and compressibility suites
- Soil earthworks related testing including compactions
- Soil strength & compressibility tests including triaxial, shear box, laboratory vane, oedometers
- Groundwater chemical durability intended concrete or steel pipelines
- Rock strength, stiffness and potentially effective stress

4. Deriving Terrain Models

Following standard engineering geology ground model procedures, long linear pipelines lend themselves to terrain assessments by subdividing alignments by their terrain characteristics, which can be defined by both published and site-specific derived ground engineering characteristics. This approach provides a means of allowing third parties to divide proposed alignments into sections of like construction methodology & programming, as well as for Clients for contract packaging.

5. Assessing Pipeline Excavatability

Any subsurface stratigraphic profile can be excavated, but the “excavatability” of a material, in terms of construction based projects, is the effective and acceptable excavation or production rate for a method or type of plant in operation, for example hydraulic breakers can be used to excavate a competent rock, but blasting may be more time and cost effective. Remembering that the operational state of the plant being used, and the experience of the plant operator are also factors to consider.

The excavatability of a material depends on the method used and material properties. Some properties are not mutually exclusive, for example strength may be affected by rock weathering grade, and run direction is relevant mainly for large open excavations, when dip direction is an issue. In addition, the sensitivity of the work required may influence the excavation method chosen, for example blasting may not be an option for excavation close to a high pressure gas or water mains and therefore hydraulic breaking could be required.

For pipeline excavatability assessments the use of test pitting as previously indicated provides a direct measure. Experience gained from a variety of pipeline projects, has allowed a generic definition of test pit excavation to be defined (see Table 1), and applied to each type of plant used.

Table 1. The Definition of Ease of Excavation from Test Pits

Excavation Term	Type and Speed of Excavation
Very Easy	Bucket to excavate - Fast Excavation
Easy	Bucket to excavate - Slow Excavation
Moderate	Bucket to excavate - Very Slow Excavation
Difficult	Hydraulic breaker used to loosen rock then bucket to excavate
Very Difficult	Hydraulic breaker used to break rock then bucket to excavate

To allow further assessment of excavatability over entire project alignments, it is necessary to quantify the 'ease of excavation' from borehole data. No published correlations exist between the excavatability of soils and the results of drilling. Therefore, an approximate relationship has been derived between the test pit observations and borehole data using the undrained shear strength of cohesive soils. This has then been extended to granular soils using SPT N values. The relationship between the test pit and borehole excavatability assessments is approximate only (see Table 2).

For boreholes in rock the published excavatability assessment method of Pettifer & Fookes (1994) has been applied. This utilises Point Load Strength Index ($Is_{(50)}$) and fracture spacing to determine the 'ease of excavation' associated with potential excavator types.

Pettifer & Fookes emphasise their assessments are for ideal conditions for ripping. Where the rock has tabular or columnar discontinuities, or there is a wide range of block sizes, then ripping will be more difficult and they recommend increasing the Average Fracture Spacing by 20 to 50% to allow for this. Also ripping will be more difficult in the confines of a narrow trench, rather than in a large open road cutting from which most of the data was used to derive their correlations.

The Caterpillar Performance Handbook is widely used to assess excavatability from measured insitu seismic velocities. The Handbook gives degrees of rippability and production rates for various rock types and machine sizes. However, this method is found to be optimistic, and does not correlate well with site experience (MacGregor et al, 1994). Alternative relationships involving seismic velocity combined with various other rock material and rockmass parameters give a better correlation with field experience (MacGregor et al, 1994).

The excavatability codes given in Table 2 are shown for each borehole and test pit on geological long sections or on pipeline sheets/sections. These excavatability assessments are suggested to only be considered as an approximate guideline.

Table 2. Approximate Excavatability Relationship between Test Pits & Boreholes for Pipelines

OBSERVED EXCAVATABILITY DURING TEST PIT EVCAVATION	ASSESSED EXCAVATABILITY FROM BOREHOLE INFORMATION									
	COHESIVE SOIL				GRANULAR SOIL				ROCK	
Description	Code	Description	Approx. SPT N Values	Approx. Borehole Vane Cu kN/m^2	Code	Description	Approx. SPT N Values	Code	Pettifer & Fookes (1994)	Code
Very Easy	1	Very Soft - Firm	< 15	< 75	A	Very Loose - Medium dense	< 30	A	Easy Digging	
Easy	2	Stiff	15 - 30	75 - 150	B	Dense	30 - 50	B		B
Moderate	3	Very Stiff	> 30	> 150	C	Very Dense	> 50	C	Hard Digging	C
Difficult	4								Easy Ripping	D
Very Difficult	5								Hard Ripping	E
									Very Hard Ripping	F
NOT RELEVANT				NOT RELEVANT					Extremely Hard Ripping or Hydraulic Breaking	G
									Blasting or Hydraulic Breaking and Ripping or Digging	H
									Blasting	I

6. Excavation or Trench Temporary Stability

The optimum solution for pipeline installation is open trenching methods, which can also be applied to minor crossings. Depending on the depth of pipe installation required, pipe diameter, along with the subsurface nature of the ground (including the groundwater table depth), open trenching of large diameter pipelines (≥2m) can require a considerable construction corridor. For pipes ≥2m this can be in the region of 40m wide, taking into consideration spoiling and pipe lay down space requirements. A typical excavation trench design for a large diameter water pipe is provided in Figure 4.

The composition and consistency of soils within the pipe excavation and the level of the groundwater table very often dictate the safe temporary excavation batters that can be used during pipe installation. Soft or low densities soils with a high groundwater table (within 1-2m of the existing ground surface) are often the worst case scenarios. Here minimising significant trench side slope instability and providing a dry safe working environment can often require low angle and wide batters with intermediate benching or dewatering.

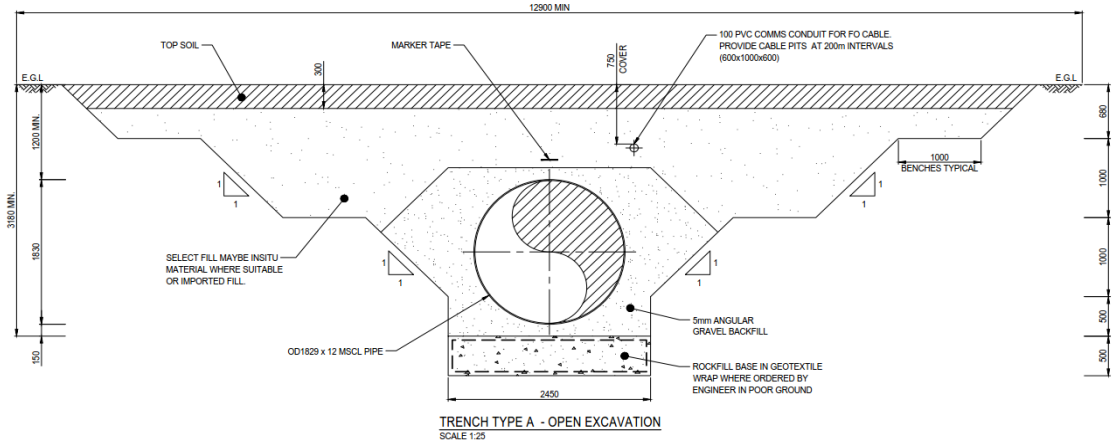

Figure 4. General Pipeline Excavation Design

However, to reduce potential costs and program delays, as well as adverse environmental impacts, the use of trench boxes or more typically sheet piling has been used. This can also have the advantage of reducing the overall construction corridor for large diameter pipes to 20m and is the preferred method for minor road or creek crossings (see Figure 5).

The optimum open trench circumstances are also meet, ie., that of stiff, dense or cemented soil profiles with the groundwater table well below the base of the excavation (see Figure 6). Here excavation profiles can be narrow and pipe laying daily progress rates can be considerable, while in dry season climates backfilling can be left over a matter of days.

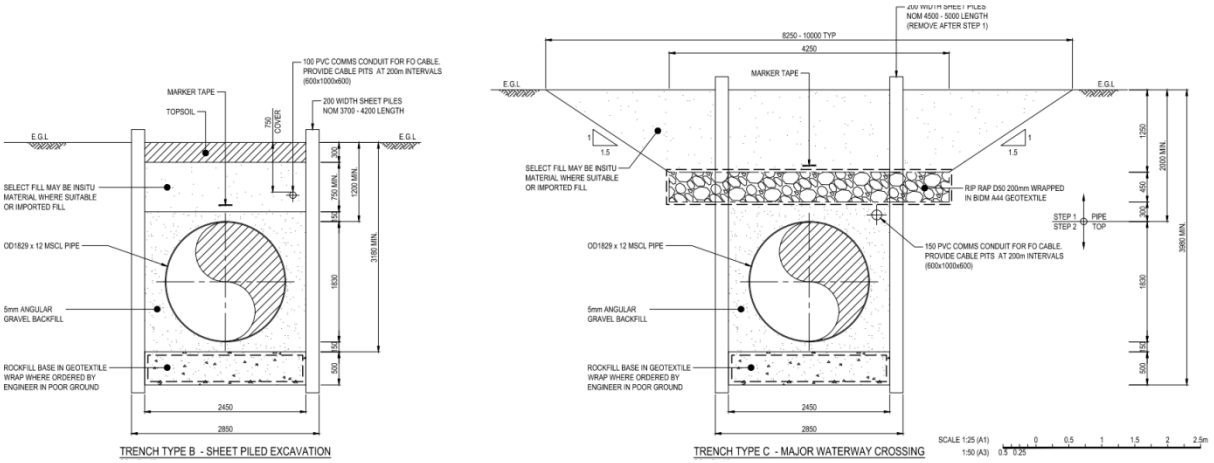

Figure 5. Soft Ground, Minor Road & Creek Crossing Pipeline Excavation Design

Figure 6. Gas pipeline installed in a silcrete subsurface profile, West Queensland

7. Buoyancy & Scour Considerations

7.1 Potential Pipeline Buoyancy

Buoyancy of pipelines within the alluvial floodplains with high groundwater tables can be a significant issue but is dependent on also the depth of pipe below ground level, backfilling material type and specification and the actual pipe material type. The most significant issues may arise if plastic or glass fibre reinforced pipe (GFRP) are used instead of steel pipe. The use of light weight pipes may also require considerable thrust blocks to be installed for restraint purposes.

The restraint of buoyancy could include the following alternatives:

- Concrete linings (see Figure 7)
- The use of sand bagging
- The use of geotextile wrapping (see Figure 8).

Figure 7. Concrete Lining on Steel Pipe

7.2 Potential Scour Considerations

Within main waterway crossings, the potential effects of bed scour can impact installed pipelines. The installation of upper protection layers of rip-rap rock over the pipeline crown to minimise any detrimental effects of scour from flood events (see Figure 5), is seen as the most cost effective and environmentally sensitive approach to potential scour issues. The other alternative that could considered was that of the application of a concrete lining (see Figure 8), but this has been generally dismissed based on cost impacts.

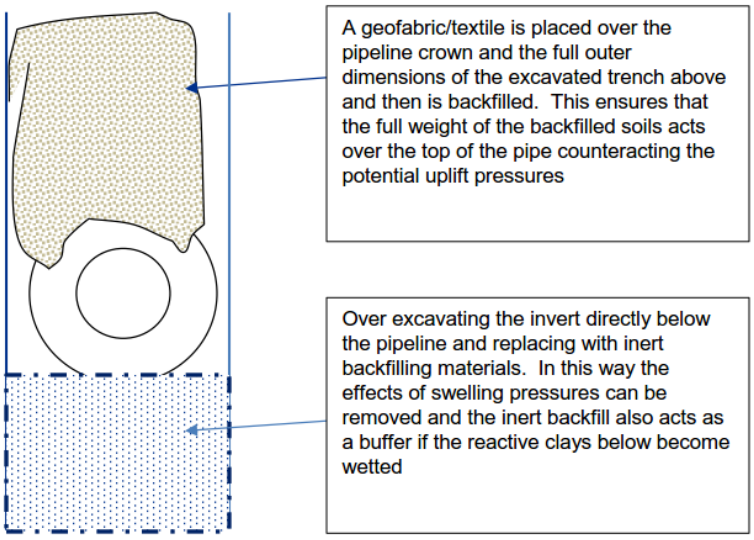

Figure 8. Potential use of Geotextile Wrapping/Soil Pillows to Restrain Uplift

8. Troublesome Soil Impacts

8.1 Reactive Soils

Reactive soils in Australia are associated with vertisol soil types which are commonly derived from the weathering of typically volcanic rocks and most commonly from basalt lava flows. They have a significant shrink:swell potential, can be self-mulching and often formed depressions in the landscape known as “gilgais”, or have open polygoidal/hexagonal cracking at the surface, with a fissured or cracked nature at depth (see Figure 9). When wetted up they can easily have swelling pressures in excess of 250kPa and have seasonal and long term swell of >100mm. The depth of this swelling potentially varies, but the soil moisture or suction profile can be up to 4.00m. By this nature their swelling can impact pipeline installations in a similar manner to buoyancy and generally the geotextile pillowing approach (see Figure 8) to resist such swelling has been employed.

8.2 Dispersive Soils

Dispersive or sodic soils are common soils types in the Australian landscape. These soils are associated with sodium contents, which clog soil pores thereby reducing permeability and when subjected to overland flow often results in piping (see Figure 10). The effects of such sodic dispersive potential on pipeline temporary and permanent works, as well as the possible measures required to reuse these types of soils for fill materials are significant considerations. Tunnelling can be common features after pipeline installation (see Figure 11).

Figure 9. Cracked reactive soils between pipeline inverts

During construction open excavations can be at risk to significant piping in wet seasons, requiring rapid backfilling and reducing pipe laying daily progress rates. This approach often also requires the need for multiple fronts and short lengths of trench excavations.

If these types of soils are considered as reuse within project works, a variety of approaches may be required for this to be enabled, including:

- Additional drainage control measures
- Using a non-reactive covering over the surface of the pipeline

Figure 10. Piping Erosion of Sodic Soils Within Open Pipeline Excavations

Figure 11. Typical Tunnel Erosion of Over Pipeline Backfilled Alignments

- For cohesive dominated backfill soils treat the upper 300-500mm by mixing with potentially between 2 to 5% by weight of gypsum (the calcium replaces the sodium minerals and improves soil permeability and allow water to pass through this layer without erosion occurring – in addition the mixed zone needs to be carefully compacted)
- For granular dominated backfill soils install a geotextile 300-500mm below ground surface and then replace with the excavated soil – the geotextile will act as a barrier in this case
- Installing sand blocks or barriers across/around proven tunnel prone areas (see Figure 12).

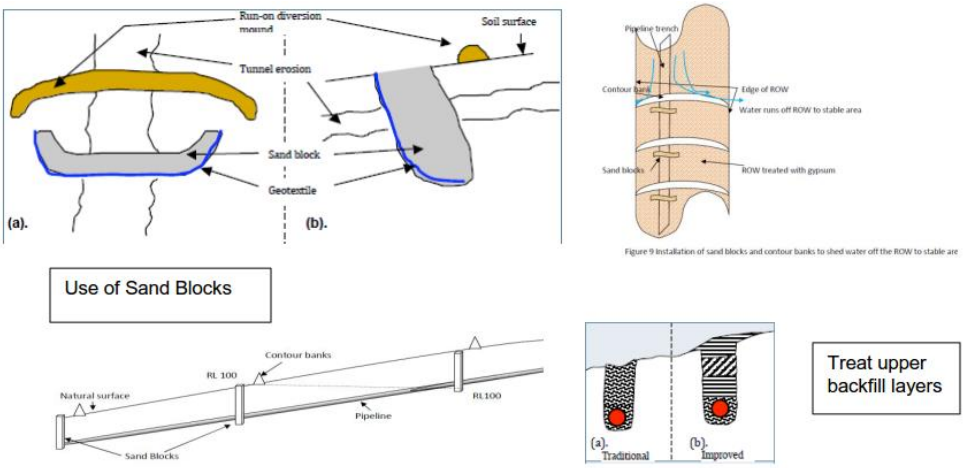

Figure 12. Pipeline Remedial Options for Dispersive Soils

8.3 Acid Sulphate Soils

Acid Sulphate Soils (ASS) are naturally occurring and potentially very acidic soils encountered within coastal and near coastal flat lying areas of Australia. The acidity is derived mainly from accumulated sulphides which in turn when oxidised form sulphuric acid. The extent soils are generally associated with coastal or estuarine areas and those adjacent typically below 10m above the Australian Height Datum (AHD), although a buffer zone of up to 20mAHD is often taken.

Issues of high acidification (to sometimes pH values < 2) are associated with cohesive materials, with granular soils having a benign character. When cohesive soils in these areas are below the water table and subject to reduction conditions then no acidification process occurs. However, when exposed and allowed to oxidise then this subsequentially results in low pH values.

For open trenching (and to a lesser extent trenchless approaches) for pipeline construction this can have significant impacts with the requirement for treatment generally by the addition of quick lime to increase pH and provide a firmer material for backfilling purposes (the reaction being exothermic and resulting in reducing soil moisture content). Dosage rates can be variable from approximately 20kg/tonne to over 100kg/tonne and requires specific treatment pads and time for processing, as well as inevitable cost impacts.

9. Pipeline Trench Backfilling Considerations

The optimum situation for pipeline backfilling is to reuse excavated spoil stockpiled directly adjacent with little if any secondary processing required. In practice often this is not the case with the requirement of either import of backfilling materials, significant reprocessing of spoil (requiring additional treatment pads, including treating dispersive soils and ASS) for backfilling purposes and the cost of transporting and placing unusable excavated materials to offsite disposal facilities.

Typical issues related to backfilling with excavated materials include:

- In alluvial deposits often the variable composition and consistency with cohesive materials interbedded with granular materials makes them difficult to segregate
- Sodic or ASS soils significant costs to render usable (lime or gypsum dosing or additional significant drainage controls)
- With a high water table, excavated materials will have a high moisture content and require drying out before being potentially used in backfilling, within generally only a 40m wide corridor (and perhaps 20m at creek crossings) very little room is available to construct the works, and often no room is available to stockpile spoil material and/or to spread it out for reprocessing/drying out, before being potentially used as backfill material
- It's unlikely to be practical to keep large lengths of excavated trench dewatered throughout the construction and pipeline installation process, therefore it is likely that during backfilling of trenches a highwater table would be re-established; in this event attempting to place cohesive material at the right moisture content and related required compaction density is considered to be impractical

Sometimes with the above considered, spoiling of excavated trench materials is deemed the most practical approach with the use imported granular backfill, in the form of fine grained "pea" gravel, which will be self-compacting underwater. Sources of these materials may be from local commercial quarries, if within economic haul distances, or processed from natural local water courses. The decision of spoiling large volumes of excavated material is a very significant one and has major cost and program implications for projects.

Pipe bedding sand materials are again generally imported from offsite sources again from local natural sources or as an alternative could be the use of crusher dust, which is a by-product of general quarrying processing. The use of these materials requires careful control of the fines content (ie., <10% passing the 475 micron sieve and a PI <5%), but this can be done by appropriate screening by quarries to produce a sand based product at a potentially relatively cheap cost with the added benefit of reducing waste at the quarries.

10. Major Crossing Installation Crossing Techniques

The choice of the most appropriate pipeline installation method for significant crossings of roads, railways or rivers is determined by a range of factors including:

- Length of crossing
- Type and diameter of pipe
- Depth of lowermost point of crossing (and in the case of rivers bed scour potential)
- Subsurface ground profile
- Surface or near surface existing built environment, including utilities, and any related minimum clearances or maximum allowable settlement thresholds by owners/operators
- Physical space available at both sides of the crossing
- Environmental & community considerations
- Cost and construction program

In general, smaller diameter pipes with short drive lengths, in a soil stratigraphy lend themselves to horizontal directional drilling techniques (HDD); however, in certain circumstances offset distances from

crossing points can be considerable. Whereas with thicker steel pipes >1.00m diameter, a practical limit if HDD may be 1km. Larger pipe diameters in soil conditions are often installed by pipe-jacking methods, or by mini-tunnel boring machines (MTBM) if a competent bedrock sequence is present. Both these methods have the advantage of minimal offset distances needed for crossing drives.

As previously stated the use of lighter pipes such as plastic or GFRP for main crossings often may result in the need for considerable thrust blocks for restraint (see Figure 13).

Figure 13. Large excavation & piling required for a railway underbore of a large diameter GFRP water pipeline

The use of bespoke pipe bridges have been used, but generally these are for shorter and steep sided crossings (where the economics of trenchless techniques is impractical); however,often the utilisation of existing road and rail bridges is used as means of crossing these features.

11. Conclusions

Engineering geology plays a key role in the definition of pipeline alignments, their design and construction. The experiences in Australia over the last ten years with various major pipeline projects, have provided the opportunity to develop new methods of identification, investigation, assessment and development of control measures for various engineering geological aspects of encountered ground conditions common to both global & local conditions. In addition, the definition of a specific excavation coding system has allowed a method of ground condition presentation, which has been welcomed by clients and contractors alike.

References

Caterpillar Tractor Company (2018). Caterpillar Performance Handbook 48.

MacGregor et al (1994). The estimation of rock rippability, QJEG v. 27, pp. 123-144

Pettifer, G. S. & Fookes, P. G. (1994). A revision of the graphical method for assessing the excavatability of rock, QJEG, v. 27, pp. 145-164.

Investigation of the Effects of Hydraulic Connection Between Neighboring Valleys and Geologic Structure on Dam Site Selection

Remzi Karagüzel[1], H. T. Yalçın[1] & Cenk Yaltırak[1]

[1]*Istanbul Technical University, Faculty of Mines, Dept of Geological Engineering, Istanbul, Turkey*
karaguzel@itu.edu.tr, yalcint@itu.edu.tr, yaltirak@itu.edu.tr

ABSTRACT: This proceeding discusses the water retaining capacity of a reservoir behind a planned dam on Alara River (Alanya) having a height of 200 m which is 3 km away from the nearest neighboring valley. For this particular purpose, hydrogeological and geological models were constructed between two adjacent valleys. Geological structure comprises folded Miocene series overlying impermeable metamorphic and sedimentary base rocks where the fold axis is perpendicular to valleys and plunging to neighboring valley. Initially, the karstic properties of Aksu and Oymapınar formations at the base of folded structure were investigated aiming to assess possible water leakages from the reservoir of the Alara Dam. Pressured water tests and periodic groundwater level measurements were carried out in boreholes between two valleys to obtain water tightness properties of the geological units. Investigations revealed well-developed, extensive and open karstic structures between layer surfaces of carbonated rocks. It is understood that the chosen site for the Alara Dam at specified height causes increasing water leakages from the reservoir lake at the northern limb of fold and along the karstic system on the syncline axis under changing hydrostatic pressure.

Keywords: Reservoir Lake, Hydraulic Connection, Karst, Water Leakage

1. Introduction

The main aim and decisive investigation of dam sites are their water retaining capacity within a reservoir lake. Engineering geological investigation outcomes such as permeability and slope stability of a reservoir area are effective parameters in determining the dam axis location and even the dam height, besides geological properties such as lithology and structure. The leakage problems especially carry importance in karstified areas. Some researchers discussed the problems originated from karst forms below dam foundations and some discussed how the water losses were treated or the karstification problems in general or in specified localities (Erguvanlı&Yüzer, 1978, Dreybrodt et al 2002, Kocbay and Kilic 2006, Bonaci 2008, Hiller et al 2011, Mozafari and Raesi 2016, Milanaovic 2011 and 2018, Sissakian et al 2020) In this study, the feasibility of a 200 m high dam planned on Alanya-Alara River is discussed. The location of the carbonate rocks having folded and karstic structure is of primary importance in terms of possible water leakage to the neighboring valley, the closest distance of which is 3 km from the planned dam lake.

Within the context of purpose-oriented geological and hydrogeological studies, the hydraulic relationship between the valleys is discussed by use of field observations, pressured water tests and groundwater level measurements in exploration wells.

2. Geological Outlines

Metamorphic and sedimentary units highly deformed in pre-Miocene and having various characteristics, constitute the basement in the Alara Dam water catchment basin. Aksu, Oymapınar, Çakallar, Geceleme and Karpuzçay formations unconformibly overlie the basement (Figure 1). These formations were deposited in fluvial, coastal, shallow marine and reef environments, which are horizontally and vertically transitional. This study is concentrated on water seepages from the Alara Dam basin and a special attention is given to

the Oymapınar and Aksu formations. Hence, the field study is carried out initially on these two formations, their positions and karstic properties are investigated.

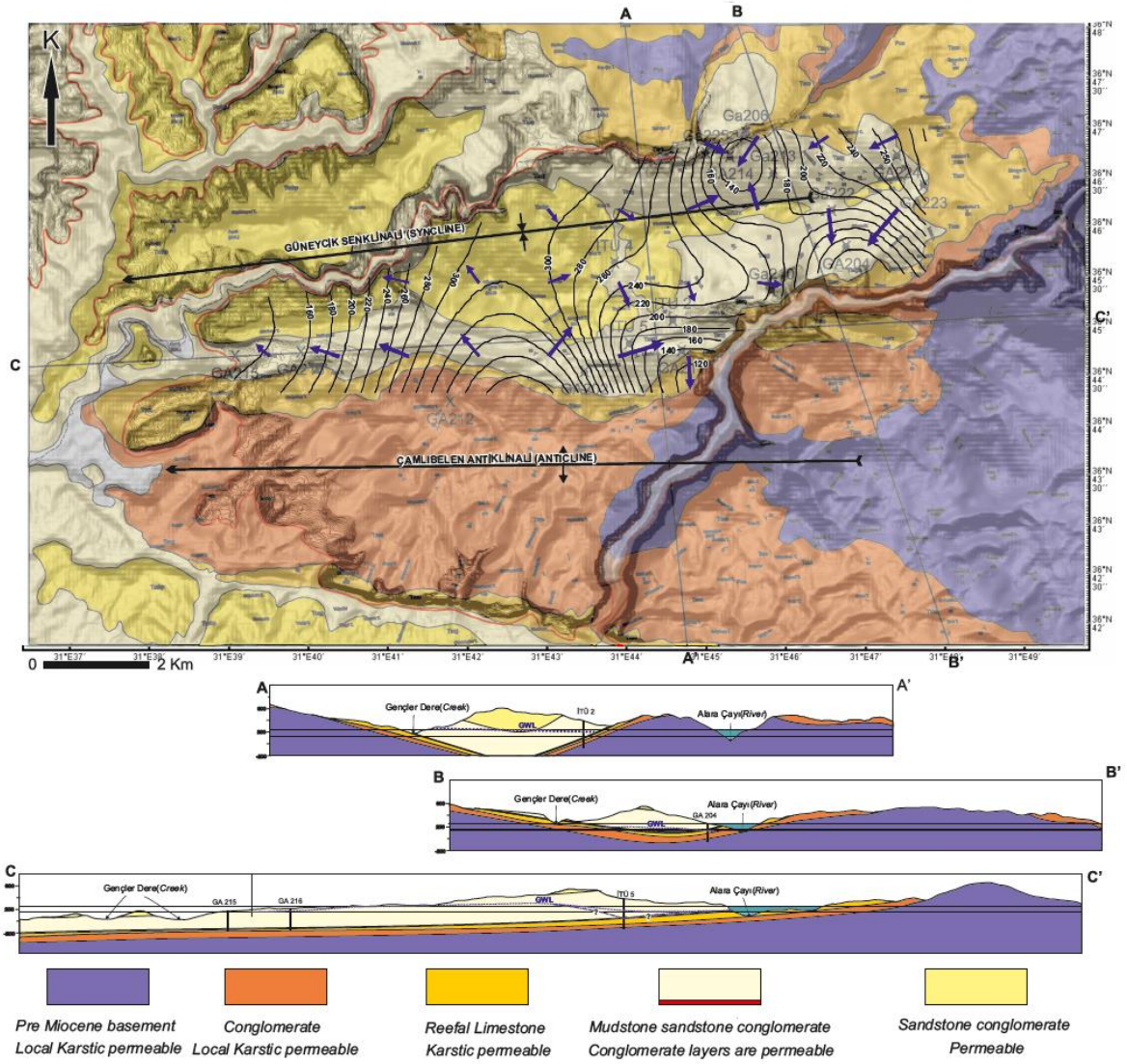

Figure 1. Geological map and cross section of the Alara river and surroundings.

The Aksu formation is made up of carbonate cemented conglomerate (dominantly recrystallized limestone) and sandstone derived from the basement rocks. This unit locally comprises carbonated lenses and limestone lenses. The carbonate content increases upward and gradually passes to the Oymapınar formation. The Oymapınar formation is a carbonate series and its thickness from bottom to top is 60-200 m, which is made up of heterogeneous reef limestone. Taking into consideration the extent and characteristics of this formation in the field, it is a barrier reef that developed in front of a low relief coast. Unlike patch reef, it is continuous and the layer thicknesses are 1-2 m comprising layered limestone that developed in a fore reef facies that can be seen kilometers long in the field. This reef was progressed to the north straight on the basement rock as a result of sea level rise. Therefore, its thickness increases up to 100 m towards south as advanced away from the older coast. The karstic cavities can clearly be observed in the field on both flanks of the Alara River on the two roads heading to the historical bridge. These cavities have the length of 50 cm-1 m in vertical extend and 20-40 m in horizontal extend on the valley slopes shaped by the Alara River within the Oymapınar formation. Similar karstic features in the Oymapınar formation can also easily be seen on the hill slopes where the Alara Castle was constructed.

The Çakallar formation concordantly overlies the Oymapınar formation and comprises siltstone, sandstone and marl, which is horizontally transitional with the Geceleme formation. The importance of the Çakallar formation in this study is that this formation was deposited in a reef front facies, contains carbonated clay and marl and concordant with the Oymapınar formation. These rocks, which are found at the bottom of Çakallar formation, have 10-20 m thickness. These layers separate and insulate the Oymapınar formation

from the overlying clastic formations like an impermeable membrane. There are numerous seasonal springs discharging from the carbonated sandstones over this insulated section.

The Çakallar, Geceleme and Köprüçay formations are vertically and horizontally transitional, their deposition begins dominantly with a trangressive sequence and ends with a regressive sequence. The Miocene sequence observed in the field was deposited in front of a paleogeographic height and comprises shore, fore shore and backshore environments. The Oymapınar formation is made up of rocks originated from the reef that developed parallel to the shoreline in a shallow and warm sea where the width in the sea is more than 20 kms. The Oymapınar formation is above the sea level at least since Messinian and cut by rivers. It is well known that several water resources in this formation are fed by heights on the Middle Taurus Mountains. The development of karstic features started 4 million years ago. Especially by considering the global sea level drop up to -150 m (ice ages of 136- 240 ka and 12-24 ka ago) and submarine fresh water springs discharging from caves in the Mediterranean Sea, it is certain that the Oymapınar formation was developed its karstification in these two latest ice ages.

The Miocene sequence is folded in right side of the Alara River. The position of the Oymapınar formation in this folded structure is interesting. The major folds in the area are the Çambeleni anticline and the Güneycik syncline. The layers of the Oymapınar formation are on the downstream of planned dam axis at the southern limb of the Çambeleni anticline. Conversely, the main axis of the syncline is on the Alara River and constitutes the 4 km long part of both river flanks on the upstream of the planned dam.

3. Hydrogeology

3.1 Hydrogeological Properties of the Geological Units

The west-plunging folded structure that cut by the Alara River carries importance from water leakages and water circulation points of view, especially when the highly permeable Oymapınar formation insulated by the Çakallar formation is considered within the Güneycik syncline. Particularly, when barrier (or fringing) reefs remain above the sea level, they disintegrate and redeposit or when the sea water level rises they drown and cease development. In those cases, the interfingering can be seen with other formations. The horizontal and vertical position of buried Oymapınar formation inside the syncline and formational characteristics generate the primary problems of hydrogeological structure. Even though karstic, groundwater emerges from the Oymapınar formation only at northeast of Uzunlar village closest to the Alara River. Groundwater discharges are not seen from caves inside the outcrops of the Oymapınar formation on the axis of the Alara River (Nov. 2010). Equally, springs are observed in the Çenger Creek side emerging from the contact between Çakallar and Geceleme formations in the same season. This interesting event is due confinement of the Oymapınar formation by impermeable clayey and marly layers. The Oymapınar formation crops out both in Çenger creek and Alara River on the west-plunging Güneycik syncline. In this case, both Alara river and Çenger creek can probably recharge the discharging springs from the Oymapınar formation at the west.

Structurally, the hydrogeological system of the Oymapınar formation that confined by the Çakallar formation in the core of the Güneycik syncline crops out at 100 m altitude in beds of the both Alara River and Çenger creek. From this section to the sea level all the karstic system is exposed all along the limbs of the west-plunging syncline. When the spreading of the Güneycik syncline to the sea is considered, it is highly possible that a link up to -150 m beneath the sea through the karstic system if the Oymapınar formation exists. Consequently, the Oymapınar formation is a karstic and confined hydrogeological system. The upper system that separated by marl from the lower system is a mainly clastic. The lower hydrogeological system cropping out in both Alara River and Çenger creek plunges westwards due to structural reasons. In this case, when the water level in a dam exceeds the 90 m altitude, the Alara river will recharge this system. The hanging fossil karstic cavities on the deeply eroded valley will activate and feed the system to the west if the water level rises.

3.2 Hydraulic Properties Lithological Units

Hydraulic properties of the lithological units in west side of the planned Alara dam are determined using the pressured water tests carried out in exploration boreholes.

The Cebireis Formation: In this formation 0.4 to 1.3 Lugeon (very low permeable) values are measured by pressured water tests in GA-223 borehole.

The Aksu Formation: In this formation 0 to 50 Lugeon (locally highly permeable) values are measured by pressured water tests in GA-201, GA-203, GA-204, GA-206, SG-207 and SL-208 boreholes, and 0 to 5.9 Lugeon (very low permeable) in GA-202 borehole.

The Oymapınar Formation: In this formation 25 Lugeon (locally highly permeable) values are measured in different levels by pressured water tests in GA-222, GA-224, GA-204, GA-206 boreholes, and 0 to 19.4 Lugeon (moderately permeable) in GA-202 borehole. In İTU-5 borehole, water pressure could not be increased between 320 to 316.5 meters where the permeability is very high.

The Çakallar Formation: In this formation 0 to 43.6 Lugeon (locally highly permeable) values are measured by pressured water tests in GA-202, GA-217 boreholes. Generally being impermeable, it is seen that some heavily jointed segments of this formation yield high permeability. In ITU-5 borehole, 0 to 4.5 Lugeon (very low permeability) values are measured between 251 to 302 m depths. Similarly, in ITU-2 borehole, 0 to 4.2 Lugeon (very low permeability) values are measured.

The Geceleme Formation: In this formation 0 to 12.3 Lugeon values are measured between 130 to 251 m depths, however water pressure could not be increased between 130-135m, 170-175 m and 175-210 m where the permeability is very high. Similarly, in ITU-2 borehole, water pressure could not be increased between 35-40m, 150-155 m, 75-85 m and 190-195 m where the permeability is also very high. In other intervals of ITU-2 the values are generally between 0-1.6 Lugeon (very low permeable).

The Karpuzçay Formation: There is no test in this formation.

3.3 Groundwater Level and Hydraulic Gradient

Within the frame of this study the measured groundwater levels in EIE boreholes are given in Figure 2.

The ground water level map is drawn using these data and given in Figure 1. One of the groundwater divide lines is between GA212 and GA202 boreholes. The groundwater flows to Çenger creek at NW direction at the west side of this divide line, to NE at the eastern side to the Alara river. The overall hydraulic gradient is around 7/100 (m/m) and it decreases to 3/100 around GA215 borehole towards to the Çenger creek. Another divide is on the route between GA224 and GA222 boreholes. The groundwater flows to south at the south of this divide and to west and north at the north of this divide. The hydraulic gradient around the GA222 borehole is 8/100. The highest hydraulic gradient is 14/100 at the east of GA202 borehole, and the lowest being 15/1000 at north of ITU-2 borehole. At the north of the route drawn from ITU-2 to ITU-4, a groundwater flow can be seen from Çenger creek to Alara river.

The ITU-4 borehole data that could not encounter the Oymapınar Formation were not considered in the preparation of groundwater level map. The water level of 190 m altitude is used (in uncased borehole) instead of the 90 m water level measured in the cased borehole.

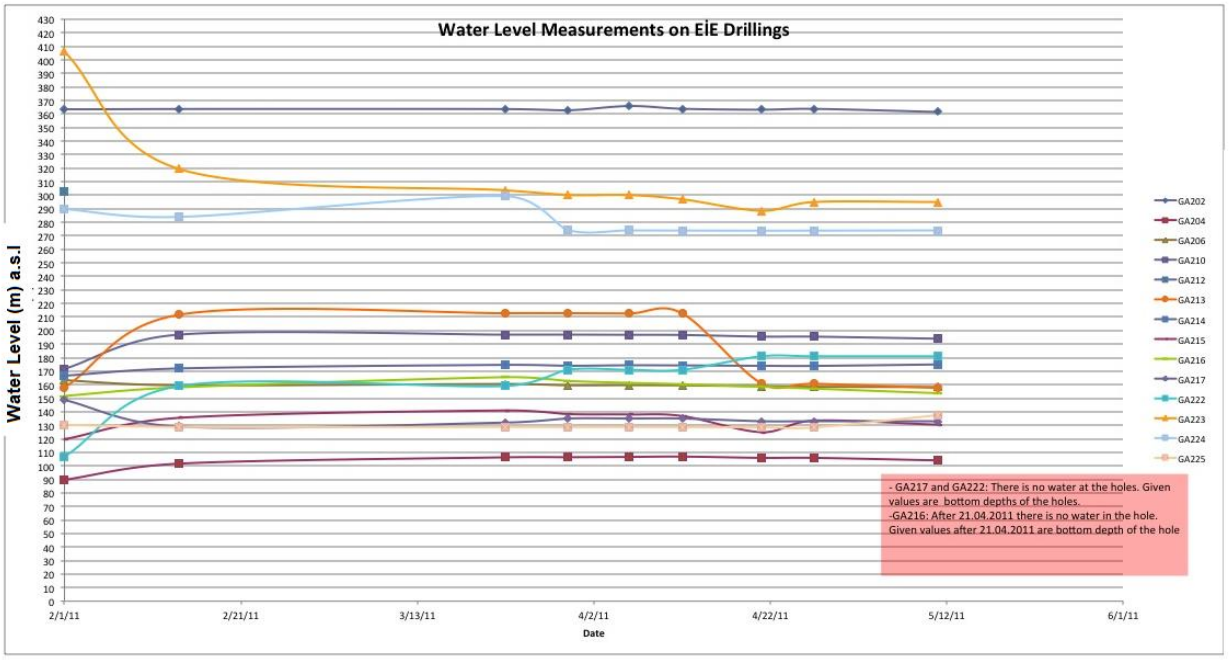

Figure 2. Periodical water level measurements carried out in EIE boreholes

In this situation, the prepared groundwater level map reflects only the combined water level of both lower and upper aquifers. The groundwater level map drawn on a high relief topography (in rocky terrain) should not be expected to be able to reflect the hydraulic structure as reliable as a groundwater level map drawn on an alluvial plain.

3.4 Relationship Between Drilling Depth, Casing and Groundwater Levels in Exploration Wells

The groundwater levels in exploration boreholes and hydrogeological system where the groundwater is found, carry importance in determination of the hydraulic connection between basins. Comparative graphics are prepared relating to time dependent changes in groundwater levels and drilling depth for this purpose.

The measured water levels of ITU-5 during drilling and after the casing was removed are shown in Figure 3. The first sudden drop of water level is seen while the casing is lowered to 54 m deep. This happened due to sealing of the permeable zone within the Geceleme formation. When the borehole reached to the next permeable zone, a sudden water rise was seen followed by a sudden water drop after the lowering of the casing to 171m deep when the borehole reached to highly permeable Oymapınar formation (karstic) another rapid water drop was observed. The water was swallowed by this karstic limestone, furthermore the borehole sucked air from the wellhead. The air circulation was tested using a burning newspaper, and the smoke was observed drawn by the borehole. Another test was done by using a balloon and the vacuum effect on rubber is shown in Figure 4. Even this vacuum effect was so strong that it shaked the drilling rig. These tests showed that the karstic system is well developed, extensive and open.The water level altitude of 90 m in cased borehole was recovered to 241 m altitude following the removal of casing and stabilized at 190-195 m altitude.

A very similar state can be seen when the graphics of EIE for GA202 and GA203 boreholes are scrutinized.

In ITU-2 borehole, after the sealing of the first permeable zone a sudden drop was observed. As the casing did not lowered enough to seal the second and third permeable zones, the change of water level became limited and remained constant after the removal of casing Figure 4. In these boreholes it is evidently seen that the Oymapınar formation with large karstic cavities cannot retain the groundwater but leak the water to other regions. It is also well understood that the Geceleme formation is a good aquifer, which supplies groundwater to the borehole from its permeable zones.

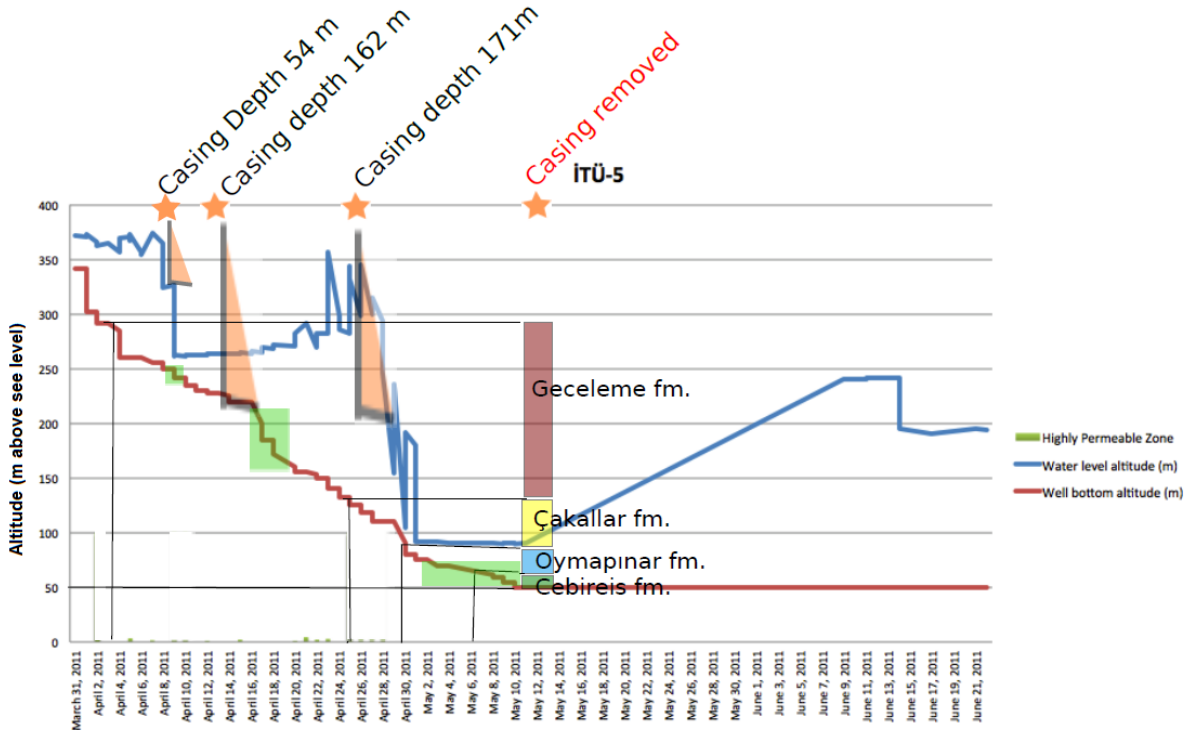

Figure 3. Observed water levels during drilling and after the completion of the ITU-5 borehole

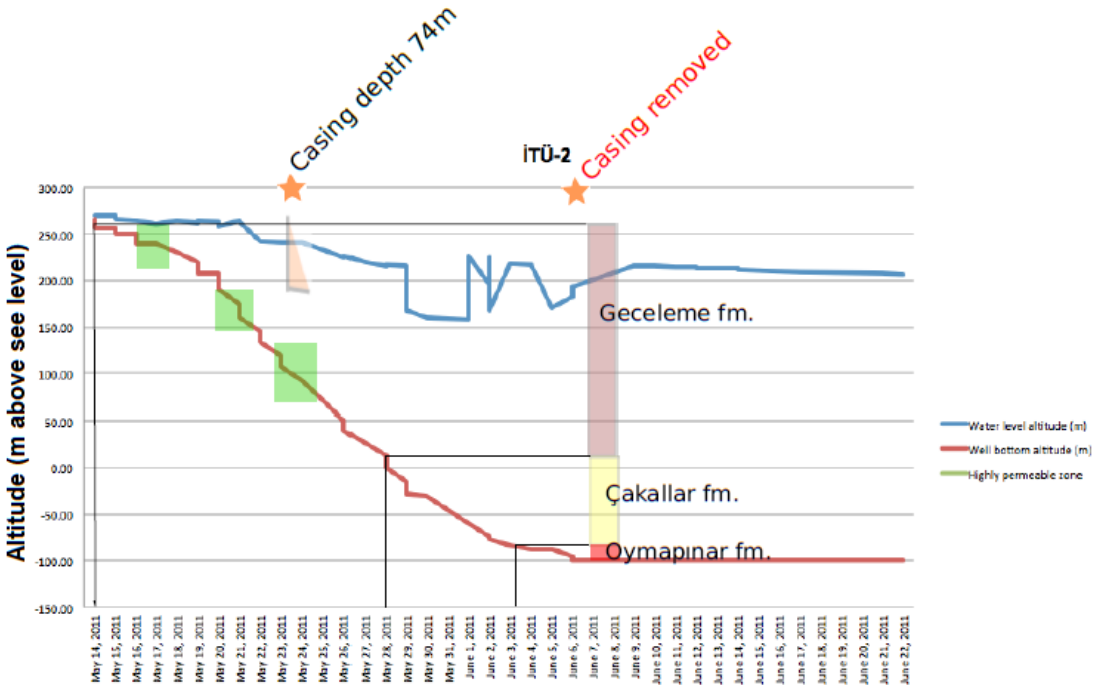

Figure 4. Observed water levels during drilling and after the completion of the ITU-2 borehole

4. Discussion

Metamorphic and sedimentary units, highly deformed in pre-Miocene and having various characteristics, constitute the basement in the Alara Dam water catchment basin. Aksu, Oymapınar, Çakallar, Geceleme and Karpuzçay formations unconformably overlie the basement.

The Miocene sequence is folded in right side of the Alara River. The position of the Oymapınar formation in this folded structure is interesting. Taking into consideration the extent and characteristics of this formation in the field, it is a barrier reef that developed in front of a low relief coast. Unlike patch reef, it is continuous and the layer thicknesses are 1-2 m comprising layered limestone that developed in a fore reef facies that can be seen kilometres long in the field. The major folds in the area are the Çambeleni anticline and the Güneycik syncline. The west-plunging Güneycik syncline has negative effects from water leakages point of view. The horizontal and vertical position of buried Oymapınar formation inside the syncline and formational characteristics generate the primary problems of hydrogeological structure.

For a possible hydraulic connection between the Alara dam lake area and the Çenger creek two different hydrogeological systems carry importance. These are the hydrogeological systems of karstic units lying beneath the impermeable Çakallar formation and the overlying units containing sandstone and conglomerate levels.

In order to determine the hydraulic conductivities and groundwater flow directions of these systems pressured water tests and periodical water level measurements are done inside the exploration boreholes.

Karstic reef limestones and karstic conglomerate levels comprising Aksu formation beneath the impermeable Çakallar formation are highly permeable. Being unable to raise the targeted pressure in tests and having test results greater than 25 Lugeon are the indications of very high permeability. As a matter of fact, the presented groundwater levels are underneath the maximum water level (250 m) of the planned dam at the northern part of the area (north limb of the syncline) on an E-W striking hydrogeological cross section in exploration boreholes of GA-204 (105.3 m), GA-213 (160.69m) and GA-206 (158.45m). Besides, the long-term water level measurement results in these boreholes reveal that the groundwater levels are generally not higher than the upper elevation of the Oymapınar formation. In other words, the groundwater flowing from the upper altitudes leaks from lower karstic and permeable Oymapınar formation. The ground water level map of this study indicates a groundwater flow at northern limb of fold from Çenger creek to the Alara river. The construction of a dam to the selected place at planned height will revert the system and cause water leakages.

The E-W striking hydrogeological cross section showing the hydraulic relationship in southern limb of the syncline reveals that the mapped Oymapınar formation with solution cavities in large areas extends to the Çenger creek. Likewise, the water levels in the exploration wells of GA-217 (<129 m), İTÜ-5 (90 m), GA-212 (160.69 m) and GA-216 (157.07 m) on this cross section line are lower than targeted maximum water level (250 m) of planned dam. On this cross section in ITU-5 borehole, the water level was measured at 90 m altitude when karstic Oymapınar formation was encountered. The vacuum effect by air circulation in karstic solution cavities is very strong to move the drilling rig indicating the karstic system is well developed, extensive and open. The air circulation (suction – pull in) in this borehole was so fast that water level measurements could not be done safely. Following the removal of 175 m long casing that preventing the water discharge from the aquifer over the karstic system to the well, the water level rose to 189 m altitude. The similar groundwater level changes were also determined in GA- 202 borehole of EIE that completed in 2004. The water level dropped to 305 m altitude during drilling rose up to 363 m after the removal of casing. The Oymapınar linked groundwater level in this borehole is most probably at lower altitude. It is observed that in areas where exploration boreholes are available, the Oymapınar formation do not contain groundwater but transmit the water to other regions discharging from upper zones.

The groundwater flow is towards Alara river in the southern limb of the syncline and discharges to the Oymapınar formation. Since there are no springs in this part of the Alara river, the groundwater should recharge the karstic system. If the water level of the dam lake exceeds the 90 m altitude, this lake will also feed the karstic system, and water leakages from dam lake will occur. The hanging fossil karstic cavities on the deeply eroded valley will activate and feed the system to the west if the water level rises.

The springs discharging at the left side of the Çenger creek around Uzunlar village at 30-35 m altitude are thought to be discharge of the Oymapınar karstic system. This hydraulic connection will further progress under hydrostatic pressure of a dam lake at 250 m altitude on the Alara river.

5. Conclusions

Metamorphic and sedimentary units constitute the basement in the Alara dam water catchment area. The basement units are unconformably overlain by Miocene Aksu, Oymapınar, Çakallar, Geceleme and Karpuzçay formations. Remapping the borders of the Oymapınar Formation by field studies, satellite images and digital terrain model revealed the risks of water leakages.

For a possible hydraulic connection between the Alara dam lake area and the Çenger creek two different hydrogeological systems carry importance. These are the hydrogeological systems of karstic units lying beneath the impermeable Çakallar formation and the overlying units containing sandstone and conglomerate levels

The Oymapınar formation is determined as ‘highly permeable’ from pressured water tests either being unable to raise the targeted pressure in tests or having test results greater than 25 Lugeon.

On the E-W striking hydrogeological cross section at the northern limb of the syncline the being of groundwater levels in exploration wells are lower than targeted maximum water level of planned dam and not higher than upper levels of the Oymapınar Formation indicate a hydraulic connection. Consequently, the risk of water leakage from the planned dam reservoir to the Çenger valley is high.

In the areas where exploration boreholes are available, especially in ITU-5 borehole, which drilled in the southern limb of the syncline, encountered large karstic cavities revealed that the Oymapınar formation do not contain groundwater but transmit the water to other regions discharging from upper zones.

The air circulation that strong enough to pull even the drilling rig by vacuum effect is the evidence of a well-developed parallel to bedding, extensive and open karstic system. This also indicates that there does not exist a hydraulic barrier as considered before. Just to be clear, the karstic system will definitely be fed by leakages from the reservoir if the water level in planned dam exceeds the 90 m altitude

The outcropping Oymapınar Formation in the Alara valley extends to the west on the southern limb of the syncline and emerging springs at 30-35 m altitude are considered to be linked with the karstic hydrogeological system.

When all these adverse geological-hydrogeological circumstances are evaluated, the construction of the dam on the selected axis will cause the existing karstic system leak more water by time by increasing hydrostatic pressure.

Acknowledgment

We would like to extend our special thanks to EIE (Electricity Works Survey) and Borusan–EnBW Energy Investments Co. for sharing their years long investigation results and invaluable contributions.

References

Bonacci O (2008). Water losses from a reservoir built in karst: the example of the Boljunčica reservoir (Istria, Croatia). Environ Geol 58(2), pp. 339–345.

Dreybrodt W, Romanov D, Gabrovsek F (2002). Karstification below dam sites: a model of increasing leakage from reservoirs. Environ Geol 42(5):518–524.

EİE, 2006, Alara Barajı ve HES Master Plan Raporu, Ankara Temelsu, (2008). Alara Çayı Havzası Fizibilite Raporu, Ankara (Master Plan Report in Turkish)

Erguvanlı K, Yüzer E (1978). Karstification problems and their effect on Keban Dam foundation and reservoir, IAEG 3. International Congress Section 3, Spain

Hiller T, Kaufman G, Romanov D (2011). Karstification beneath dam sites: from conceptual models to realistic scenarios. J Hydrol 398(3–4), pp. 202–211.

HPI (2009). Hydroprojekt – Alara Hydroelectric Project, Verification and Optimization Report.

HPI (2010). Hydroprojekt - Alara Hydroelectric Project, Request of Permision, First Step Geotechnical Investigation Program (Alara Dam Site, Alara Reservoir).

İslamoğlu (2002). Antalya Miyosen Havzasının Mollusk Faunası ile Stratigrafisi (Batı- Orta Toroslar, GB Türkiye), MTA Dergisi, 123-124, 27-58, Ankara. (Stratigraphy of Antalya Miocene Basin in Turkish)

Kocbay A, Kilic R (2006). Engineering geological assessment of the Obruk dam site, Corum, Turkey. Eng Geol 87(3–4), pp. 141–148.

Milanović P (2011). Dams and reservoirs in Karst. In: van Beynen P (ed) Karst management. Springer, Berlin, pp 47–73. https://doi.org/10.1007/978-94-007-1207-2

Milanović P (2018). Engineering karstology of dams and reservoirs. CRC Press, Boca Raton

Mozafari M, Raeisi E (2016). Salman Farsi Dam reservoir, a successful project on a karstified foundation, SW Iran. Environ Earth Sci. https://doi.org/10.1007/s12665-016-5844-6

Şenel (1997). 1:250 000 Ölçekli Türkiye Jeoloji Haritaları, Isparta Paftası, No:4, MTA Jeoloji Dairesi, Ankara. (Geological Map of Turkey in Turkish)

Sissakian VK, Adamo N, Al-Ansari N (2020). The Role of Geological Investigations.

Performance of different chemical soil stabilisers in the presence of sulphates

Maria Mavroulidou[1], Chris Gray[1] & Mike J. Gunn[1]

[1]*London South Bank University, UK*
mavroum@lsbu.ac.uk

ABSTRACT: Ground improvement of sulphate-bearing soils with calcium-based stabilisers can be severely compromised due to delayed deleterious reactions of the sulphates with calcium, and the consequent formation of expansive crystals of minerals such as ettringite or thaumasite. Amongst other ways to prevent this or mitigate the effects, the literature recommended the use of slags and pozzolanic industrial by-products to replace partially calcium-based stabilisers. This study is thus focusing on assessing whether suitable combinations of such materials partially or fully replacing calcium lime could effectively stabilise sulphate-bearing soils. In addition, the use of magnesium-based additives instead the calcium-based ones is investigated. The added advantage of using these materials is that they are more environmentally friendly than Ordinary Portland Cement and calcium lime, whose production involves high energy input and CO2 emissions. An artificial sulphate bearing soil was treated with mixtures of lime, paper sludge ash (PSA), pulverized fuel ash (PFA), ground granulated blast furnace slag (GGBS) and reactive magnesia cement. Using favourable conditions for the formation of sulphate-induced swelling, compacted soil samples were created and subjected to moisture ingress after 7 and 28 days of curing respectively. Following this, the swelling of the specimens was monitored, and their unconfined compressive strength (UCS) measured. It was found that, although some binder combinations were more successful and showed promise, no binder mix was fully successful in preventing the damage of the samples and suppressing swelling fully. More research is required leading to precise specifications, so that such stabiliser mixes can be used in industrial applications with confidence.

Keywords: ground improvement, sulphates, innovative binders

1. Introduction

In the context of engineering sustainability, chemical ground improvement is becoming an increasingly common practice to improve the hydromechanical properties of unsuitable for construction geomaterials, instead of the traditional practice of replacing them with a more suitable imported material and landfilling them. Some of the most common chemical additives used for ground improvement are cement and lime (the latter stabiliser being mostly used for clay soils). These materials are known to improve considerably the properties of soils in terms of strength and compressibility or plasticity characteristics. However, they could lead to long term problems when used for sulphate-bearing soils. Similar problems can also occur if soils stabilised with calcium-based stabilisers are subjected to a subsequent ingress of sulphates e.g., through water. This is because the calcium they contain can react with the sulphates (or sulphides), leading to the formation of expansive crystals such as ettringite ($Ca_6Al_2(SO_4)_3(OH)_{12}\cdot 26H_2O$) and/or thaumasite ($Ca_3Si(OH)_6(CO_3)(SO_4)\cdot 12H_2O$). This can cause serious and costly damage to roads and pavements founded on stabilised soils, due to heaving caused by these crystals. For instance, sulphate-induced heave damage to Texas highways was reported to have amounted to tens of millions of dollars in one decade (Harris et al, 2004). In the UK some high profile sulphate-induced heave damages were also reported, such as the failure of the Banbury section of the M40, which had resulted from a lack of early design guidance on the use of calcium-based stabilisers for sulphate-bearing soils. The reactions can be very rapid and occur overnight following a single rainfall event but in other cases the reactions are delayed and can take years to occur as e.g. mentioned in Mitchell (1986).

Ettringite /thaumasite expansive crystal formation in calcium stabilised sulphate bearing soils or calcium stabilised soils subjected to a subsequent ingress of sulphates e.g. through water, is a complex phenomenon. Due to the severity of the engineering problem, a lot of research has been carried out on the topic to gain a better understanding of the reactions and mineral formation and to find methods of minimising the risk of such reactions (e.g. Dermatas, 1995; Berger et al, 2001; Harris et al, 2004; Wild et al, 1999 etc.). As a result of this research effort, a number of recommendations were made, e.g. to set a limit of sulphate content beyond which calcium-based stabiliser treatment is not recommended (e.g. a safe limit has been identified as 2,000 ppm or 0.2% of soluble sulphate, whereas for sulphate contents above 7,000 ppm the use of calcium based stabilisers would not be recommended according e.g. to Harris et al, 2004); apply the stabiliser in two stages (Berger et al, 2001); to extend the mellowing periods as much as possible and use a low compaction density, so that expansive crystals have space for growing without disrupting the soil matrix (Harris et al, 2004); mix as much water as practically possible (Little et al, 2010) -for example, Harris et al (2004) suggest that 2% above optimum is better than optimum water content and suggest this as the maximum practical water content above optimum to add, but report that the National Lime Association recommends even higher water contents i.e. 3 to 5% above the optimum water content to give plenty of water for the sulphate to react; finally, it was recommended to use slags and pozzolanic materials such as ground granulated blast furnace slag (GGBS) and pulverised fuel ash (PFA) to replace partially calcium based stabilisers (Chesomi et al, 2017; Wild et al, 1999). However, the reactions and mechanisms of crystal growth (or the lack of it) are very complex and hence the topic constitutes the focus of ongoing research (e.g. Ouhadi & Yong, 2008; Little et al, 2010; Knopp & Moormann, 2016; Chrysochoou et al, 2012 etc.). In addition, with increasing environmental awareness, the use of innovative chemical stabilisers is actively researched. These are based on industrial waste materials (see e.g., Mavroulidou 2018; Mavroulidou et al. 2017; 2019; 2020) or alternatively, materials such as reactive magnesia cement, proposed to be more environmentally friendly than Ordinary Portland Cement in view of the lower temperatures involved in its production. The latter cements showed potential as soil stabilisers. Following early work by Xeidakis (1996), who showed that the addition of $Mg(OH)_2$ could result in expansive clay modification and discussed the theoretical possibility that Mg-based cementitious gels can form, recent research also showed that MgO at 5-20% per dry soil mass can be successful in stabilising clay soils (see e.g. Yi et al, 2014; 2015; 2016 or Gu et al. 2015).

The need has therefore emerged to investigate how these innovative stabilisers behave in the presence of sulphates in soil and whether they could be used without risks of sulphate induced reactions.

This study is thus focusing on assessing whether suitable combinations of such materials used to partially or fully replace lime could effectively stabilise sulphate bearing soils, while also suppressing the formation of expansive crystals.

2. Materials and methods

The soil used as basis for the experiments was an artificial sulphate-rich soil prepared by mixing kaolin clay from the South West of England supplied by Imerys, with 4% per soil mass analytical grade sodium sulphate powder supplied by Fisher Scientific. The clay and the sulphate were mixed in the form of dry powders. This mixture is referred to herein as 'untreated soil'. Sodium sulphate was chosen due to its high solubility (as opposed e.g. to gypsum) to create favourable conditions for ettringite formation. Tests for the total and water-soluble sulphate content based on the gravimetric method of BS 1377-3:1990 (BSI, 1990) showed no evidence of sulphates in the original kaolin soil. The soil stabilisers used were: a) a hydrated lime with a relative $Ca(OH)_2$/CaO ratio of 4.88/1.00; b) Paper Sludge Ash (PSA) provided by a newspaper recycling company from the South-East of England. PSA is mainly a calcium aluminosilicate, as the principal compounds are lime (CaO) (ca 60%), silica (SiO_2) and alumina (Al_2O_3); due to high free lime contents PSA has a pH=12.3-12.4, which is the same as that of the hydrated lime used; (c) ground granulated blast furnace slag (GGBS) from Hanson-Regen; GGBS was used in mixes with other stabilisers, as when used on its own chemical reactions are slow, and Portland cement or lime normally provide the alkalinity to activate and accelerate these; (d) reactive magnesia cement i.e. calcined magnesite containing a minimum of 94 % MgO, supplied by Richard Baker Harrison Ltd. This is a light-coloured non-hazardous free-flowing powder, of a grading 95% finer than the 75 μm sieve, a specific surface area of 15.9 m^2/g and a reactivity of 976s (in terms of time required for the neutralization of an acidic solution) as determined by Jin et al (2015) using the acetic acid test; e) PFA, a by-product of pulverised power station coal, commercially distributed by CEMEX as Cemex-450S. It is a dark grey powder of a grading 12% retained in the 45μm sieve and a specific surface area of 0.6 m^2/g. Typical oxide compositions of the materials based on available suppliers' information and the literature (Spathi, 2015; Bernal et al, 2014; Mozaffari et al, 2009; Mavroulidou et al, 2015

and Mavroulidou, 2018) are shown in Table 1. The particle size distribution of the tested soils and stabilisers based on hydrometer testing or information by the suppliers/literature is shown in Figure 1. For MgO mixes, typical MgO percentages recommended in the literature were used. The minimum required stabiliser dosage (per dry soil mass) for lime and PSA was determined from Initial Consumption of Lime (ICL) tests (Eades & Grim, 1965). These were 4% and 6% respectively. Different percentages were also used in the form of a parametric study, as these materials were partially replaced by PFA and GGBS. Note that the percentage of the stabilizers mentioned are per mass of the artificial sulphate rich soil ('untreated soil') mass.

Table 1. Typical oxide composition (%) of the stabilisers

Oxide	PFA	PSA	GGBS	MgO	Hydrated Calcium lime
SiO_2	45-51	19.20	34.68	1.00	0.70-1.00
Al_2O_3	27-32	8.70	14.16		0.10-0.20
CaO	1-7	60.70	38.74	2.00	95.00-97.00
MgO	1-4	2.80	7.74	94.00 (minimum)	1.40-0.50
Fe_2O_3	7-11	0.50	0.05		0.06-0.10
Na_2O	1	0.15	0.46		
K_2O	3-4	0.20	0.55		
SO_3	0.8	0.48	0.21		
P_2O_5		0.17			
TiO_2	1	0.20			
SrO		0.09			
MnO		0.02			
BaO		0.04			
Li_2O		0.01			
Refractory oxides (R_2O_3)				0.70	

The specimens were prepared so that conditions are most favourable for the formation of expansive minerals. Namely, a) low compaction water contents, adopting a constant liquidity index of IL=-0.05 for all soil mixtures to maintain the same consistency across samples; this IL is below the Proctor optimum –which is around the plastic limit-, thus more critical for expansion due to sulphates (Harris et al, 2004); b) short mellowing periods of 1h; c) a high compaction dry density for the clay, i.e. 1.4 g/cm^3; d) application of stabilisers in one dose.

After mellowing for 1 hour, cylindrical specimens of 50 mm diameter and 100mm height were statically compacted at the required water content and dry density in equal layers, using a monotonic displacement rate of 1mm/min. Specimens still in moulds were wrapped in several layers of cling film and cured at constant moisture in an environmental cabinet (with temperature and humidity control) for the required period of time, i.e. 7 and 28 days. After constant moisture curing, and while still in the cabinet, the specimens (still in moulds) were placed on porous stones in a tray of water where they remained for 1½ months (to cause delayed migration of water); during this period the specimen swelling ΔH was recorded using external dial gauges mounted at the top of the specimens.

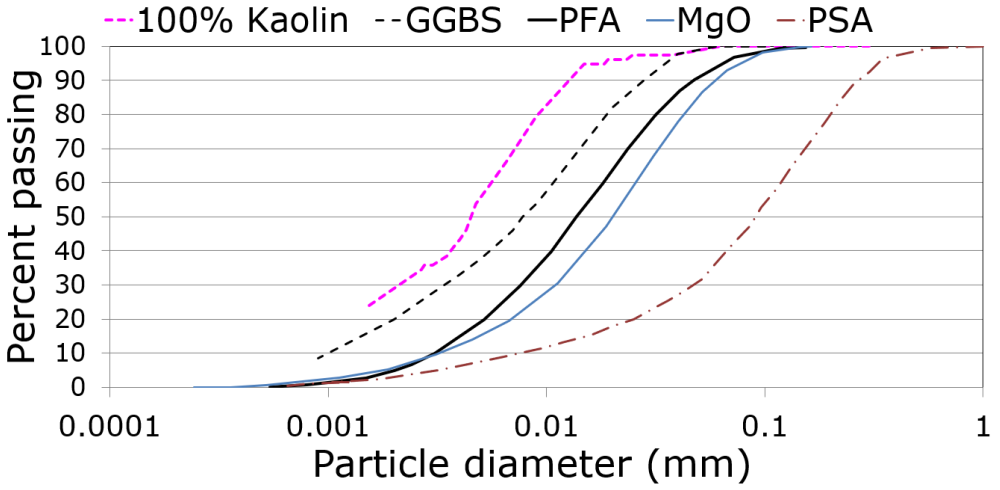

Figure 1. Particle size distribution of the kaolin soil and stabilisers

3. Results

Table 2 shows plasticity characteristics of the untreated and treated soils (at 1 h of mellowing). All stabilisers increased the liquid limit of the untreated soil, consistently with observations on lime-stabilised kaolinitic clay soils (Bell, 1996). Regarding unconfined compressive strength q_u and swelling ΔH of water immersed samples, Figures 2 and 3 show a summary of average values from at least duplicate samples (some tests were replicated in duplicate later). Based on these, there are indications that: a) PSA, rich in CaO, may perform better than lime, presumably due to its aluminosilicates content; b) GGBS improved the performance of lime but not as much that of PSA; c) PFA used at low proportions is not as effective as GGBS, failing to give higher strengths and resulting in higher expansions; d) MgO at high dosages gives relatively high strengths and low swelling but when used in combination with GGBS the results start worsen with higher GGBS dosages presumably due to the calcium in GGBS; e) most 28 day cured samples showed lower strengths than 7-day treated samples as hypothesised. However, the UCS results should be treated with caution as visual observations showed that no stabiliser mix prevented deleterious reactions, as salt crystals formed on the top of all samples (including purely MgO treated specimens, where magnesium sulphate crystals clearly appear to have formed, see Figure 4) so that specimens were cracked before UCS testing (see Figure 4); the adopted compaction characteristics could have contributed to this. As a result of this, there could be large discrepancies in the values of q_u (with some outliers discarded being up to 4 times higher than the mean values shown), presumably depending on the crack pattern.

Table 2. Plasticity characteristics of the soil before and after treatments

Soil type	LL (%)	PL (%)	PI (%)
Untreated soil	52	25	27
4% lime-treated	61	27	34
4% PSA-treated	59	27	32
6% PSA-treated	69	39	29
2% Lime-2% GGBS-treated	58	32	26
2% PSA-2% GGBS-treated	64	40	24
3% PSA-3% GGBS-treated	63	37	26
2% Lime-2% PFA-treated	65	43	22
3% PSA-3% PFA-treated	63	44	19
10% MgO-treated	62	38	24
12% MgO-treated	54	36	18
9% MgO -3% GGBS-treated	60	36	24
3% MgO -9% GGBS-treated	60	37	23

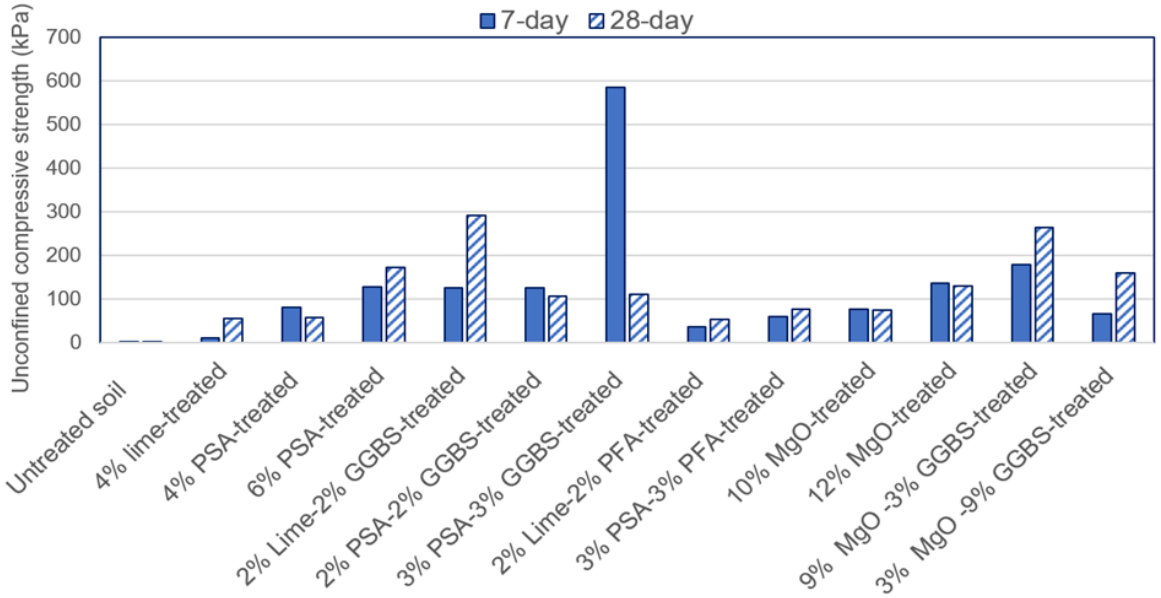

Figure 2. Unconfined compressive strength after immersion in water for 7 and 28 days respectively

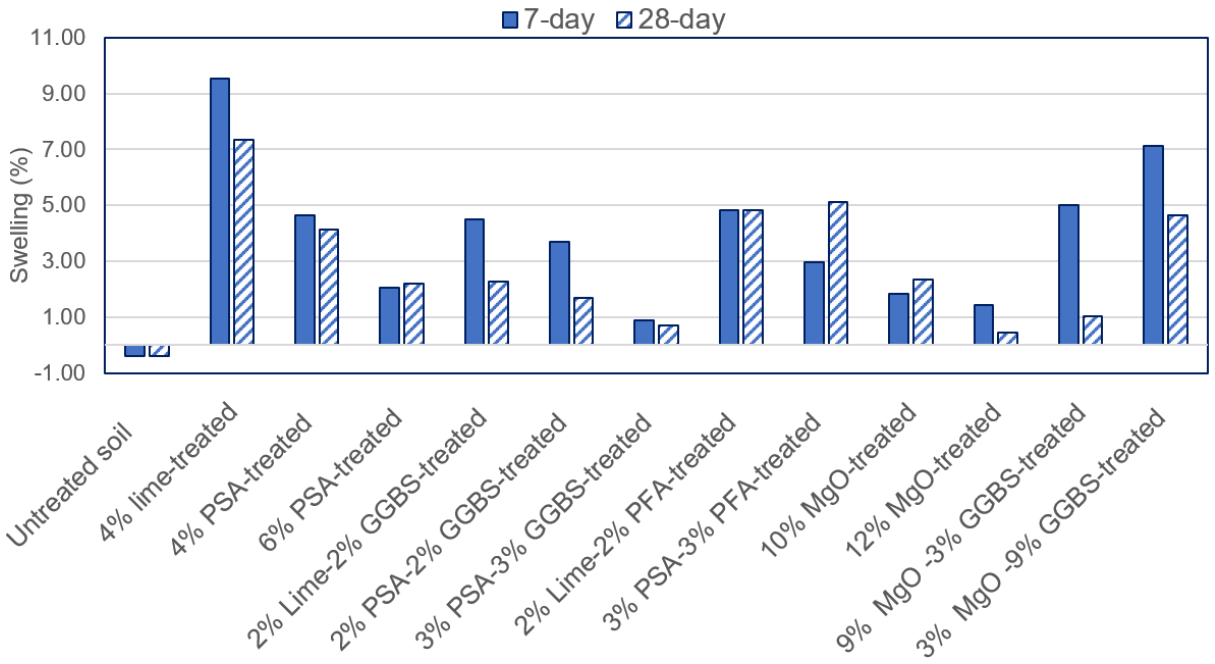

Figure 3. Change in height after immersion in water for 7 and 28 days respectively

Figure 4. Salt formation in MgO mixes and specimen damage (here, MgO-GGBS mix) before UCS testing

4. Conclusions

The results showed that, providing most favourable conditions for the formation of expansive salts and potential resulting damage, no combination of binder was fully successful in preventing the damage of the samples and suppressing swelling. Although rich in CaO, PSA performed better than lime, presumably due to its aluminosilicates content. GGBS improved the performance of lime but not as much that of PSA, whereas PFA used at same proportions as GGBS was not as effective. MgO used on its own gave some promise however crystal forming was observed in all samples. The reactions and mechanisms of expansive crystal growth (or the lack of it) in sulphate bearing soils are very complex. Despite some promising results shown here and in the literature for admixtures with slags and pozzolans or alternative cements, it is the Authors' opinion that more research is required leading to precise specifications, so that such stabiliser mixes can be used in industrial applications with confidence.

References

Bell FG. (1996). Lime stabilization of clay minerals and soils. Engineering Geology, 42(4), pp. 223–37.

Berger, E., Little, D.N., Graves, R. (2001). Technical Memorandum: Guidelines for Stabilization of Soils Containing Sulfates, NLA, http://www.lime.org/publications.html.

Bernal S, Ball R, Hussein O, Heath A & Provis J (2014) Paper sludge ash as a precursor for production of alkali-activated materials. 2nd International Conference on Advances in Chemically Activated Materials, June 1-3 2014, Changsha, China

British Standards Institution (BSI) (1990) BS 1377-3: 1990 Soils for Civil Engineering Purposes. London, UK: British Standards Institution

Cheshomi, A., Eshaghi, A., Hassanpour, J. (2017). Effect of lime and fly ash on swelling percentage and Atterberg limits of sulfate-bearing clay. Applied Clay Science, 135, pp. 190–198.

Chrysochoou, M. Grubb, D.G., Malasavage, N.E. (2012). Assessment of sulfate-induced swell in stabilized dredged material: Is ettringite always a problem? Journal of Geotechnical and Geoenvironmental engineering 138 (3), 407-414.

Dermatas, D. (1995). Ettringite-induced swelling in soils: State-of-the-art. Applied Mechanics Reviews, 48 (10), pp: 659–673.

Eades, J.L., Grim, R.E. (1966). A quick test to determine lime requirements for soil stabilization. Transportation Research Board, Washington, DC Highway Research Record, 139, pp. 61–72.

Harris, P., Scullion, T., Sebesta, S. (2004). Hydrated lime stabilization of sulphate-bearing soils in Texas. Report FHWA/TX-04/0-4240-2, Texas Transportation Institute.

Gu, K., Jin, F., Al-Tabbaa, A., Shi, B., Liu, C, Gao, L. (2015). Incorporation of reactive magnesia and quicklime in sustainable binders for soil stabilisation. Engineering Geology, 195, pp. 53-62.

Jin, F., Gu, K., Al-Tabbaa, A. (2015). Strength and hydration properties of reactive MgO-activated ground granulated blastfurnace slag paste. Cement and Concrete Composites, 57, pp. 8-16.

Knopp J., Moormann C. (2016). Ettringite Swelling in the Treatment of Sulfate-Containing Soils Used as Subgrade for Road Constructions. Procedia Engineering, 143, pp. 28–137. doi:10.1016/j.proeng.2016.06.017

Little, D. N., Nair, S., Herbert, B. (2010). Addressing Sulfate-Induced Heave in Lime Treated Soils, Journal of Geotechnical and Geoenvironmental Engineering, 136 (1), pp. 110-118.

Mavroulidou, M. (2018). Use of paper sludge ash as a calcium-based stabiliser for clay soils Waste Management and Research, 36 (11), pp. 1066–1072.

Mavroulidou, M., Morrison T., Unsworth, C., Gunn, M.J. (2015). Properties of concrete made of multicomponent mixes of low-energy demanding binders. Construction and Building Materials 101, pp. 1122-1141.

Mavroulidou M., Ziniatis A., Gray C, et al (2017). Alternative calcium-based chemical stabilisers for ground improvement: Paper Sludge Ash treatment of London Clay, 15th International Conference on Environmental Science and Technology Rhodes, Greece, 31 August to 2 September 2017

Mavroulidou M., Garelick J., Gray C., Gunn MJ, Youssef A., Hassan S. (2019). A study on the use of paper recycling waste streams for geotechnical applications, XVII ECSMGE European Conference on Soil Mechanics and Geotechnical Engineering, Reykjavik, Iceland 1st- 6th September 2019

Mavroulidou M, Gray, C., Gumbochuma F, Gunn, M.J. (2020). A comparative assessment of chemical stabilisers including waste materials, for the treatment of swelling-shrinking soils, 4th European Conference on Unsaturated Soils (E-UNSAT2020), Lisbon 21-24 October 2020, E3S Web of Conferences 195, 03028 (2020) https://doi.org/10.1051/e3sconf/202019503028

Mitchell, J.K. (1986). Practical problems from surprising soil behavior. Journal of Geotechnical Engineering,112 (3), pp. 255–289.

Mozaffari, E., Kinuthia, J.M., Bai, J., Wild, S. (2009). An investigation into the strength development of Wastepaper Sludge Ash blended with Ground Granulated Blastfurnace Slag. Cement and Concrete Research, 39, pp. 942–949.

Ouhadi, V.R, Yong, R.N. (2008) Ettringite formation and behaviour in clayey soils Applied Clay Science, 42(1–2), pp. 258-265

Spathi, C. (2015) Novel applications for paper sludge ash. PhD thesis, Imperial College, London

Wild, S., Kinuthia, J.M., Jones, G.I., Higgins, D.D., (1999). Suppression of swelling associated with ettringite formation in lime stabilized sulphate bearing clay soils by partial substitution of lime with ground granulated blast furnace slag. Engineering Geology, 51 (4), pp. 257–277.

Xeidakis, G. (1996). Stabilization of swelling clays by Mg (OH)2. Changes in clay properties after addition of Mg-hydroxide. Engineering Geology, 44(1-4), 107–120.

Yi, Y., Liska, M., Al-Tabbaa, A (2014). Properties of two model soils stabilized with different blends and contents of GGBS, MgO, lime, and PC. Journal of Materials in Civil Engineering, 26, pp. 267-274

Yi, Y., Zheng, X., Liu, S., Al-Tabbaa, A. (2015) Comparison of reactive magnesia- and carbide slag-activated ground granulated blastfurnace slag and Portland cement for stabilisation of a natural soil. Applied Clay Science, 111, pp. 21-26.

Yi, Y., Liska, M., Jin, F., Al-Tabbaa, A (2016). Mechanism of reactive magnesia – ground granulated blastfurnace slag (GGBS) soil stabilization. Canadian Geotechnical Journal, 53, pp. 773-782.

A comparative study of different biocementation implementation methods for embankment foundation soil

M.U. Safdar[1], Maria Mavroulidou[1*], Mike J. Gunn[1], D. Purchase[2], I. Payne[3] & J. Garelick[3]

[1]*London South Bank University, UK*
mavroum@lsbu.ac.uk

[2]*School of Natural Sciences, Faculty of Science and Technology, Middlesex University, UK*

[3]*Network Rail, UK*

ABSTRACT: In the context of sustainable ground engineering practices, biocementation has recently attracted the vivid interest of researchers worldwide. The technique utilises the natural biological process of biomineralisation (the biological production of minerals through the metabolic processes of different types of microorganisms/ plants) as a soil stabilisation method. The technique has the potential to be environmentally superior to other common chemical soil stabilisers. This study uses indigenous ureolytic micro-organisms to biocement an organic soil from the UK railway network. The paper focuses on the comparative investigation of different methods of implementation of biocementation treatments. Namely, mixing of all treatments, pressure injection and electrokinetic injection. The success of the techniques is discussed in terms of a) Unconfined compressive strength (UCS); b) calcium carbonate precipitation and c) compressibility and consolidation characteristics. It is shown that electrokinetic treatment is overall more successful as it led to higher strengths and CaCO3 contents, as well as higher stiffness of the treated soil. It also shows promise for a successful implementation of the treatments under existing infrastructure.

Keywords: biocementation, mixing, electrokinetics, pressure injection

1. Introduction

Due to the growing urbanisation and the scarcity of urban space, new infrastructure works in urbanised areas will be increasingly constructed on inferior ground i.e., weak natural or man-made geomaterials (e.g. in waste disposal sites) with increased hazards and impacts of catastrophic failures. Existing infrastructure facilities will also need to be upgraded to meet future needs and changing environmental loads due to climate change. These include ageing transport earthworks in many European countries suffering from serviceability problems and requiring costly maintenance/remediation. Current policies require infrastructure to be provided in an economical and environmentally responsible manner (reducing material use, embedded carbon and other impacts on the natural environment and ecosystems). Improving rather than replacing and landfilling inferior ground or geomaterials (including wastes) for civil infrastructure uses, will thus become critically important in future engineering practice towards low-carbon, sustainable solutions. In line with this, an emerging ground improvement technique, which has recently attracted the interest of researchers worldwide, is soil biocementation. It utilises the natural biological process of biomineralisation (the biological production of minerals through the metabolic processes of different types of microorganisms/ plants) as a soil stabilisation method. The technique was claimed to be environmentally superior to conventional grouts or other common soil stabilisers e.g., cement or lime (linked to high CO_2 emissions) and potentially more sustainable overall, since the non-pathogenic micro-organisms used are natural, readily available and renewable (DeJong et al, 2013). A major challenge however is finding suitable ways to implement treatments under existing infrastructure, as pressure injection can often lead to non-uniform mineral precipitation.

Recent work funded by Network Rail, proved biocementation of a problematic organic foundation soil of UK railway embankments (causing severe settlements), using non-pathogenic, indigenous ureolytic bacteria extracted from the *in situ* soil (Mavroulidou et al, 2019; Safdar et al, 2020a,b). This paper focuses on the

effect of different treatment implementation techniques in successfully biocementing the soil. The success of the techniques is discussed in terms of a) Unconfined compressive strength (UCS); b) $CaCO_3$ precipitation and c) compressibility characteristics.

2. Materials and methods

2.1 Soil type and treatments

The soil used in this study came from two boreholes at an East Anglian railway site in the UK. It was dark grayish brown, had a 50.8% organic matter content, 55.5% natural water content (consistent with a humified/decomposed organic soil), a quasi-neutral pH (7.15) and Liquid Limit and Plastic Limit of 101% and 63% respectively. The soil was identified as amorphous peat. Details on the physico-chemical soil characteristics can be found in Safdar et al, (2000a). Following a microbiological study described in detail in Safdar et al. (2020a,b) four ureolytic indigenous strains were identified as possible candidates for biocementation of the soil (through microbially induced $CaCO_3$ precipitation). These were *Bacillus licheniformis, Rhodococcus erythropolis, Micrococcus luteus, and Lysinibacillus fusiformis,* all of biosafety level (BSL) 1 i.e., not known to consistently cause disease in healthy adults, and of minimal potential hazard to laboratory workers and the environment (U.S. Department of Health and Human Services (CDC/NIH, 2007)). For the hydromechanical property testing, all the test strains were cultivated at pH 7 under aerobic batch conditions in a sterile culture medium of Nutrient Broth (Oxoid, UK) consisting of 5 g/l peptone, 5 g/l sodium chloride, 2 g/l yeast extract and 1 g/l beef extract. Incubation was performed in a shaking incubator at 200 rpm and 37 °C. The strains were grown to an early stationary phase i.e., Optical Density (OD): OD600 ranging from 0.5-0.7 (measured using a Pharmacia LKB Novaspec II spectrophotometer of 325-900 nm Wavelength Range). They were then harvested by centrifuging at 8000g for 10 minutes to achieve the final concentration of approximately $1x10^8$ cfu/mL (optical density 3.3).

The cementing reagents used in this study were equimolar (1M) concentrations of urea and calcium chloride mixed together in one solution. Different equimolar concentrations were also considered in a parametric study described in Mavroulidou et al, (2019) and Safdar et al (2020a). Cementation reagent solutions (or in the case of control samples, nutrient solution+bacteria without cementing reagents) 15 % by weight of the dry soil mass were then added into the soil for all implementation techniques. Samples were then compacted statically to the original field dry density of 0.919 g/cm^3, at a rate of 1mm/min. The samples were wrapped in cling film and were tested after constant moisture curing.

2.2 Implementation methods

Five different treatment implementation methods were used, i.e., biostimulation (with nutrients to stimulate native micro-organism growth and cementing reagent added into the soil) and four bioaugmentation methods (i.e. supplying precultured microorganisms into the soil to enhance favourable microorganism populations). These were (a) mixing with the soil both the nutrients+bacteria solution and the cementing agent solution (urea and calcium chloride); (b) implementation of cementing solution through a flow column under light pressure (nutrients+bacteria were premixed in the soil); (c) Electrokinetic (EK) injection of cementing agents with nutrients+bacteria premixed in the soil; (d) full treatment injected by EK (i.e., nutrients+bacteria and cementing agents). Bacteria were initially premixed to prove biocementation for this soil, circumventing bacteria delivery complications and ensuring better uniformity of treatments. Mixing is however unfeasible under existing embankments unless deep mixing is used with especially designed augers to fit within the rails.

2.2.1 Mixing Method

During implementation by mixing, the soil was mixed with each culture medium containing the urease-producing bacteria, having a concentration of 1 x 10^8 cfu/mL. After thorough mixing with bacteria, the samples were kept in air-tight containers for 24 hours to attain homogeneity of the microorganisms throughout the specimen. Cementation reagent solutions 15 % by weight of the soil sample (made with equimolar concentrations of urea and calcium chloride prepared in Nutrient Broth) were then added into the soil. The cementation reagent was added and mixed thoroughly in three equal portions i.e., each 24 hours, and the samples were again kept in an air-tight container for treatment for 7 days (starting from the mixing of microorganisms); then standard UCS specimens (of 50 mm diameter and 100 mm height) were prepared;

before testing, they were wrapped in cling film and left to cure at constant moisture in a humidity and temperature-controlled cabinet for 2 days.

Pressure flow

The apparatus used consisted of a Plexiglas cylindrical mould (50 mm in diameter and 170 mm in length), a hydraulic pump, a compression frame and an effluent collector (see Safdar et al, 2020a). Aqueous solution of Nutrient Broth with bacteria of a total of 15 % by mass of soil was then supplied for all soil samples. The soil was covered in air-tight seal and left for 48-72 hours to attain homogeneity. Then statically compacted UCS specimens were made and transferred into the Plexiglas mould, where they were sandwiched between the two layers of perforated disks and filter papers (to avoid turbulent inflow and clogging at the inlet and outlet) and were mounted tightly onto the compression frame. The mould inlet was connected to the outlet of the pump. The cementing reagent solution was supplied into the specimen at a constant flow pressure of 150 kPa (the selection of the pressure is explained in Safdar et al, 2020a) and at room temperature (22-27^{o}C) during 3 days; this was followed by 7 days of curing.

Electrokinetic Implementation

For the EK method, a tank of 10 mm thick nonconductive acrylic 'Perpex' sheet with internal dimensions 210 mm length x 160 mm width x 140 mm depth was used. A purpose-built sample extractor internal layer was incorporated to prevent sample disturbance during extraction at the end of the test. The description of the EK cell can be found in Safdar et al. (2020a). The dimensions of the cell allowed for extraction of duplicate UCS specimens (50 mm diameter and 100 mm height cylinders) from three different locations in the soil sample: namely from the areas next to the two electrolyte chambers and from the middle of the sample. The soil sample was statically compacted in the EK tank in five equal layers to its in situ dry density of 0.919 g/cm^3 using a hydraulic compression frame. Bacteria were implemented either (a) by EK injection together with the cementation solutions or (b) were pre-mixed thoroughly with the soil; then the soil-bacteria mix was covered with air-tight seal and left for 48-72 hours to attain homogeneity of treatments throughout the sample and the cementing reagents were then injected by EK. Premixing was mainly used to assess the feasibility of the technique, circumventing complications linked to the bacteria transport and uniformity of bacteria distribution in the sample. However, a more realistic field implementation scenario would use EK injection for all treatments. Bacteria were cultivated directly in the Nutrient Broth solution to the required 1 x 10^8 cfu/mL concentration. A voltage gradient of 0.4 V/cm was maintained throughout the tests as recommended in the literature to prevent potential harm to the bacteria (Mizuno & Hori, 1988; Hassan et al., 2016). Periodic polarity reversal was applied every 24 h, which is recommended for a better uniformity of the treatment but also prevents high pH gradients that could be harmful to the bacteria (Mena et al. 2016). The nutrient broth solution and the cementing reagents were supplied all in one single solution (divided equally in the two electrolyte compartments i.e. 7.5% per dry soil mass per compartment). The EK treatment lasted for two weeks, (i.e. 7 days per electrode polarity), followed by one additional day of curing, which is a typical field treatment length (Mena et al. 2016). At the end of the tests, specimens for unconfined compressive strength (UCS) and oedometer tests were cut from the respective samples.

3. Results

Figure 1 (a) and (b) shows comparative results of the first set of studies (average values of triplicate specimens), using mixing and pressure flow injection of the treatments for the four monocultures, supplied at a concentration of 1x10^8 cfu/mL. It can be seen that, based on the strengths achieved and the $CaCO_3$ contents, mixing did not achieve biocementation, although a slight increase in the $CaCO_3$ content compared to the native soil was observed; on the other hand, similar $CaCO_3$ contents were observed in the control specimens (nutrients+ bacteria cells) and for this reason, the possibility that late compaction could have broken biocementation bonds seems unlikely. Almajed (2017) observed the same for long curing periods and samples treated by enzymatically induced calcite precipitation, and attributed this to a loss of enzymatic activity due to ammonia by-product. The lack of success of mixing was surprising, as it was expected that it would enable more uniform treatments. A change in protocol and shorter mellowing periods could be tried; on the other hand, mixing would not be useful for existing infrastructure and for this reason its study was temporarily suspended, to focus on more successful treatments. Unlike mixing, pressure flow column was successful in increasing the strength and $CaCO_3$ contents of the soil for all monocultures compared to their respective control specimens (nutrients+monoculture). It is interesting that the nutrient+*L.fusiformis* control specimens had strengths as high as biocemented specimens; on the other hand, their $CaCO_3$ content was low and does not concur with biocmentation (which would not have been expected due to the lack of

cementing reagents). Conversely, all specimens with full treatments (incl. cementing reagents) do show an increase in the $CaCO_3$ content pointing at biocementation, with the least well performing strain being *R. erythropolis*. The other monocultures showed similar results for the 1M concentration of cementing agent. However, using equimolar concentrations of lower molarity *B. licheniformis* was found to give better results (see e.g. Figure 4), with the second best strengths (in our parametric study) achieved by *L. fusiformis*. Both *B. licheniformis* and *L. fusiformis*, have elongated cells making it more difficult to flush out during pressure or EK injection, therefore were initially selected as more preferred compared to *M. luteus*. Figure 2 (a) and (b) shows respectively indicative SEM-EDS results from pressure flow column tests with *B. licheniformis*, *L. fusiformis*; well distributed precipitation products have formed on the particles; indicative EDS spectra from sites on the samples show clear Ca and C peaks, concurring to $CaCO_3$ precipitation.

Due to a lack of sufficient sample from the same location one strain was used for further studies. *Bacillus licheniformis* was chosen because: (a) it is widespread in nature and is found in abundance in natural soils; (b) it is motile (using its flagellum) and relatively small (of about 1 μm diameter) which facilitates its motility through smaller pore throats; (c) it is reported to be facultative anaerobic (e.g. Clements et al, 2002) so it can survive in environmental conditions of reduced oxygen supply; (d) it is a spore generating bacterium, therefore potentially appropriate for self-healing of the treatments.

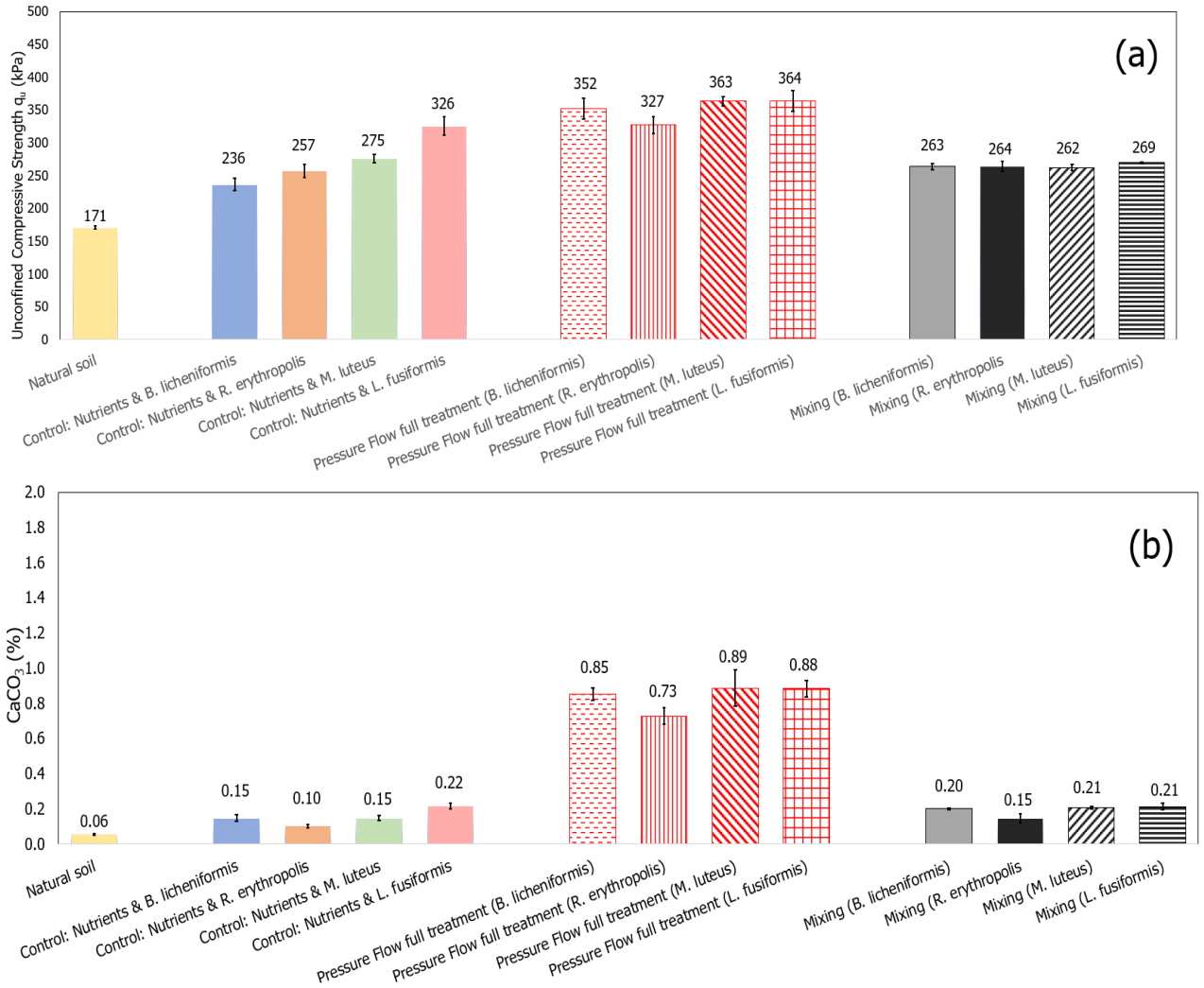

Figure 1. Preliminary testing results with four monocultures: (a) UCS results; (b) CaCO3 measurements

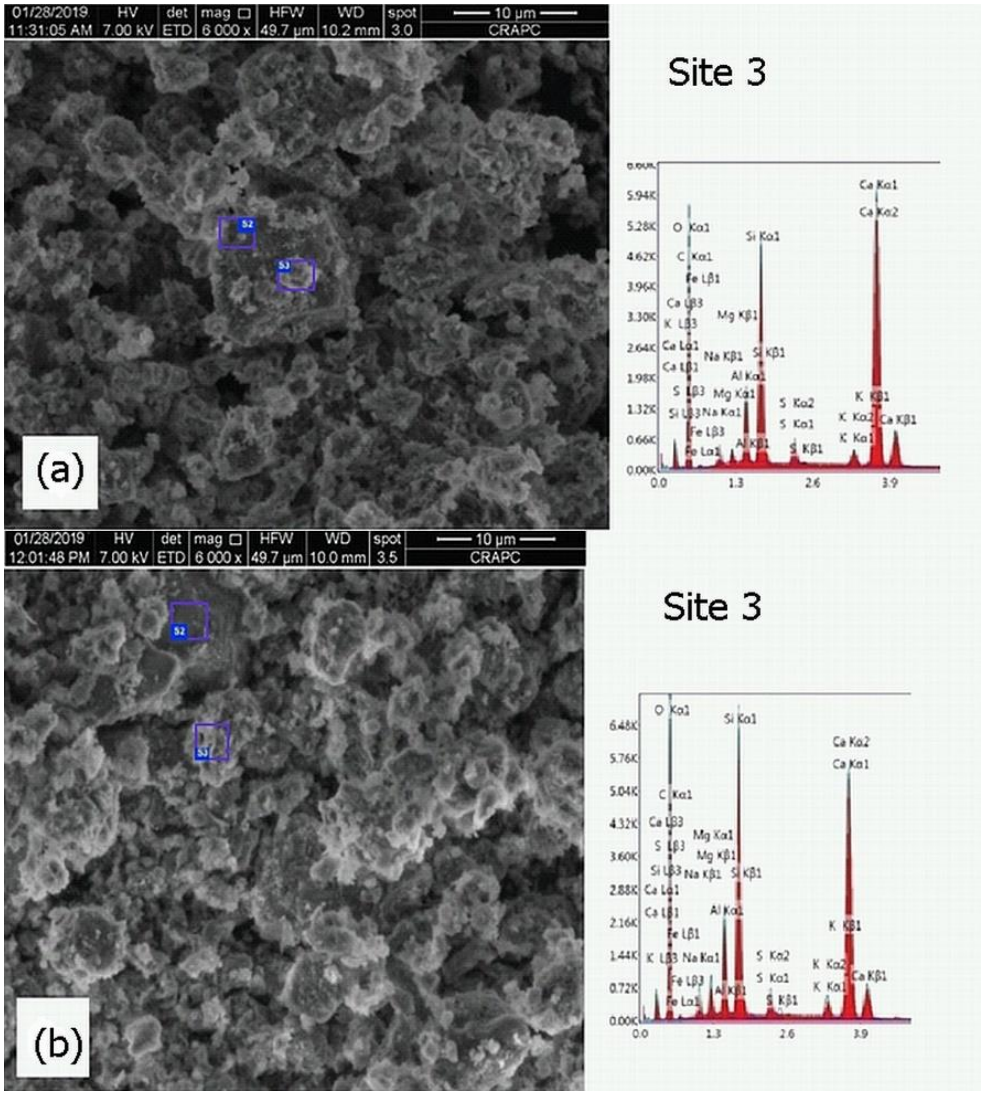

Figure 2. Indicative SEM-EDS results for two monocultures: (a) B. licheniformis;(b) L.fusiformis

Figure 3 shows indicative UCS results of of 1x10^8 cfu/mL *B. licheniformis* specimens with 85% degree of saturation treated with equimolar (1M) reagent solution and different methods. It can be seen that EK injection (with polarity reversal) was the most successful implementation method, superior to the pressure injection; the EK method was studied for degrees of saturation S_r=75-95% with the latter giving the best results (not shown here for brevity). Implementation in wetter periods of the year would therefore be recommended for better success of the treatment. Consistently, the highest $CaCO_3$ contents in the soil (not shown here) were detected for the EK method. Pressure flow led to strength improvement (and increased $CaCO_3$ contents) but to a lesser extent than EK, whilst biostimulation by pressure injection and implementation of full treatments by mixing were not successful. There was obviously a combined effect of biocementation and EK (which is an improvement method *per se*) as EK control samples (not shown here for brevity) had higher strengths than the respective pressure flow ones; however, $CaCO_3$ contents and increased strengths (compared to EK control) when bacteria were used in the EK tests, concur with the conclusion that the strength increase was due to biocementation. Whilst treatment non-uniformity (when bacteria were injected rather than premixed) still needs to be addressed, there is promise that EK could be a viable technique for treating soil under existing infrastructure. The comparatively higher success of the EK method in biocementing the sample can also be testified by the indicative stress-strain behaviour plots in Figure 4. Even with the best performing pressure flow column treatment concentration (0.75M reagent solution), against 1M reagent solution for the EK (which had a rather modest performance for the *B.licheniformis* pressure flow column treatment, as shown in Figure 1 and 3) the EK curves show a more brittle response -and a slight increase in stiffness-, which is consistent with the higher degree of cementation of the EK sample. This is also consistent (with one exception) with the indicative oedometer results in Table 1 showing coefficient of volume compressibility m_v values; both EK and pressure flow led to a reduction in the compressibility of the treated specimens compared to the untreated specimen.

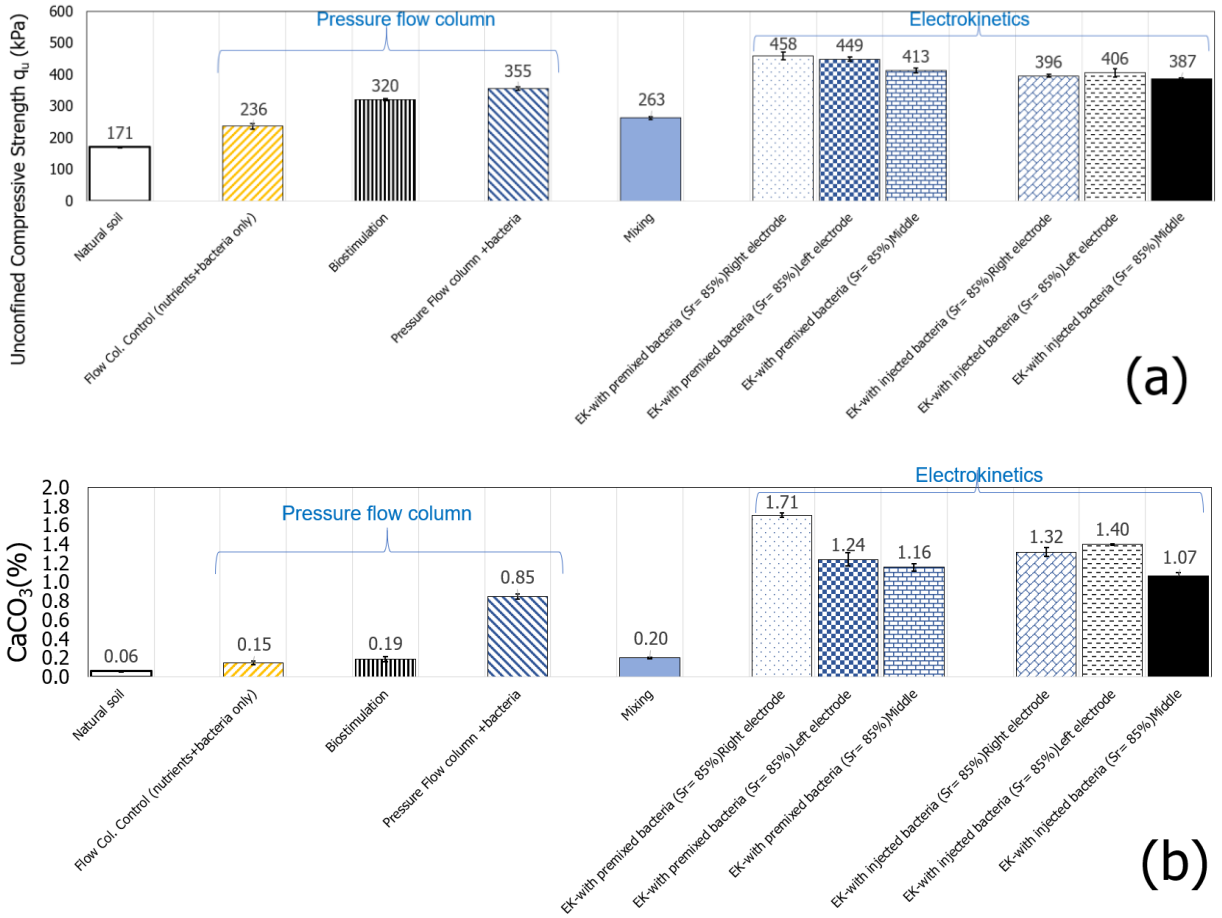

Figure 3. Comparative results for all methods using the selected monoculture (B. licheniformis): (a) UCS results; (b) CaCO3 measurements

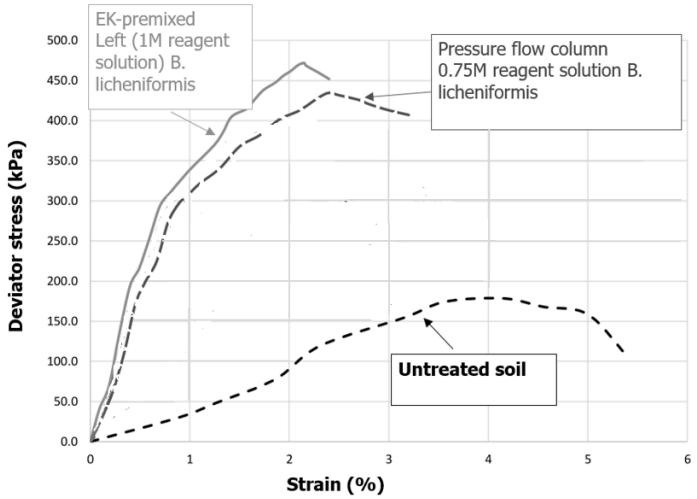

Figure 4. Comparative stress-strain behaviour for the selected monoculture (B. licheniformis)

Table 1. Indicative comparative results of coefficient of volume compressibility, m_v

Effective stress range (kPa)	Untreated (m^2/kN)	Pressure injection (m^2/kN)	EK (m^2/kN)
0-25	0.0009	0.0006	0.0005
25-50	0.0005	0.0002	0.0003
50-100	0.0004	0.0003	0.0003
100-200	0.0003	0.0002	0.0002
200-400	0.0003	0.0002	0.0001

Conclusions

The paper considered comparatively five different implementation methods to realise biocementation of an organic soil; namely, four bio-augmentation implementation methods and biostimulation. Of these, electrokinetics performed the best producing the highest strengths, $CaCO_3$ contents and higher soil stiffness. There was obviously a combined effect of biocementation and electrokinetics; however, $CaCO_3$ contents and increased strengths compared to EK control when bacteria were used in the EK tests, support the conclusion that the strength increase was due to biocementation. Pressure flow did lead to strength improvement and increased $CaCO_3$ contents but to a lesser extent than EK, whilst mixing of the treatments and biostimulation by pressure injection were not successful in this instance. The latter two techniques will be revisited changing the procedure and treatment protocol; in particular, biostimulation is an interesting technique and will be studied further. Whilst treatment non-uniformity (when bacteria were injected rather than premixed) still needs to be addressed, there is promise that EK could be a viable technique for treating foundation soil under existing infrastructure, which is a major challenge for engineers.

Acknowledgements

The authors would like to acknowledge the financial contribution of Network Rail Ltd for this project under research contracts NR-ANG-00164 and ecm_18210_ANG.

References

Almajed, A.A. (2017). Enzyme Induced Carbonate Precipitation (EICP) for Soil Improvement. Ph.D. Thesis, Arizona State University, Tempe, AZ, USA.

CDC/NIH (U.S. Department of Health and Human Services, Centers for Disease Control and Prevention, & National Institutes of Health) (2007). Biosafety in microbiological and biomedical laboratories, 5th edn (eds L. C. Chosewood and D. E. Wilson). Washington, DC, USA: U.S. Government Printing Office. See www.cdc.gov/od/ohs/biosfty/bmbl5/bmbl5toc.htm (accessed 08/04/2020).

Clements, L.D., Miller B.S., Streipsa, U.N.(2002). Comparative Growth Analysis of the Facultative Anaerobes Bacillus subtilis, Bacillus licheniformis, and Escherichia coli. Systematic & Applied Microbiology, 25(2), pp. 284-286

DeJong J. T., Soga K., Kavazanjian E. et al (2013). Biogeochemical processes and geotechnical applications: progress, opportunities and challenges. Géotechnique, 63(4), pp. 287–301.

Hassan, I., Mohamedelhassan, E., Yanful, E.K., Yuan, Z.-C. (2016). A Review Article: Electrokinetic Bioremediation Current Knowledge and New Prospects. Advances in Microbiology, 6, pp. 57-72.

Mavroulidou, M., Safdar, M.U., Gunn, M.J., Payne, I., Garelick, J., Purchase, D. (2019). Innovative methods of ground improvement for problematic transport earthwork materials, 16th Int. Conference on Environmental Science and Technology CEST2019, Rhodes 4-7 September 2019

Mena E, Villaseñor J, Cañizares P and Rodrigo MA (2016) Effect of electric field on the performance of soil electro-bioremediation with a periodic polarity reversal strategy. Chemosphere, 146, pp. 300-307

Mizuno, A., Hori, Y. (1988). Destruction of Living Cells by Pulsed High-Voltage Application. IEEE Transactions on Industry Applications, 24, pp. 387-394. http://dx.doi.org/10.1109/28.2886

Safdar, M.U., Mavroulidou, M., Gunn, M.J., Garelick, J., Payne, I., Purchase, D. (2020a). Innovative methods of ground improvement for railway embankment Peat Fens foundation soil. Géotechnique. https://doi.org/10.1680/jgeot.19.SiP.030.

Safdar, M., Mavroulidou, M., Gunn, M.J., Garelick, J., Payne, I., Purchase, D. (2020b). Biocementation of an organic soil using indigenous ureolytic bacteria, Proceedings of the 6th International Symposium on Green Chemistry, Sustainable Development and Circular Economy (Greenchem6), Thessaloniki, 20-23 September 2020, ISBN:978-618-5494-13-1.

THEME 5 - ENGINEERING GEOLOGY FOR URBAN ENVIRONMENT

Geotechnical Evaluation of Acıpayam Basin (Denizli-Turkey) by Using A Geological and Geotechnical Information System (GEO-GIS)

Halil Kumsar[1], T. Sarayköylü[2] & Y. Say[3]

[1,3]*Department of Geological Engineering, Engineering Faculty, Pamukkale University, Denizli, Turkey*
hkumsar@pau.edu.tr, yigithansay@gmail.com

2DSİ 21. Bölge Müdürlüğü, Aydın, Turkey
tugbasaraykoylu@hotmail.com

ABSTRACT: Geotechnical site investigation studies are essential for urban planning. There is a big amount of geological, geotechnical and geophysical data produced during each site investigation project. There are many site investigation projects used for urban planning of a city. However, different types of data obtained in those projects are not evaluated all together. They are archived in hard copy or scanned in image files on computers. In this study, geological, geotechnical and geophysical data obtained from different site investigation projects in Acıpayam district were evaluated in the same coordinate system by using GEO-GIS computer program written by the first author. According to the results, it was obtained that groundwater was 15 m deeper than ground surface in west and south of Acıpayam basin. In these areas, shear wave velocity (Vs) ranges between 350 m/s and 500 m/s, and the soil amplification values vary between 1.5 and 2.0. It has been determined that the area in the center of Acıpayam district is suitable for urban planning. In the northeast and center of the Acıpayam basin, groundwater is 1m deeper than the ground surface, Vs values vary between 180 m/s and 350 m/s, and soil amplification values vary between 2.1 and 3.1. In this area, soft and weak soil conditions may cause some damages on adobe and masonary buildings in villages in the basin during shaking of strong earthquakes.

Keywords: Geotechnics, Information system, Acıpayam-Turkey

1. Introduction

There are various types of geological and geotechnical data obtained during the site investigation of urban planning and construction projects of building and structures in cities. However, these types of data are stored in individual archive files after each project is completed. Evaluation of all data in one database is not performed in many cities.

A geological and geotechnical information system for urban planning of Denizli (Turkey) was developed by Kumsar et al (2003, 2005) covering geology, geotechnical borehole, laboratory tests, geophysical measurement data types of a geotechnical site investigation project of Denizli. However, the database was not enlarged after the project due to access to archive of Denizli Municipality in the following years. In this study, a geological and geotechnical information system for Acıpayam Municipality (Denizli-Turkey) was developed by using site investigation data extracted from urban planning projects.

2. Structure of Geological and Geotechnical Information System of Acıpayam

Geological and geotechnical information system, called GEO-GIS, for sustainable urban planning is made up of two main parts. Namely, software development and database setting (Figure 1). Software programming of Geological and Geotechnical Information System (GEO-GIS) has been developed by the first author since 1996 in C++ programming language (Kumsar, 1993; Kumsar et al, 2003; 2005).

GEO-GIS for urban settlement is formed by using different types of data extracted from geotechnical site investigation project reports prepared by various consultant companies. A database structure was performed and divided in three parts. These are map, geotechnical and geophysical types of database (Figure 1). Map database includes topography, urban planning, geology and tectonic maps in the same coordinate system. Geotechnical database covers geotechnical logs of bore holes and observation pits, field test data in bore holes, laboratory test results of each soil sample obtained from different level of boreholes and observation pits. Geophysical database contains seismic wave and microtremor measurement results.

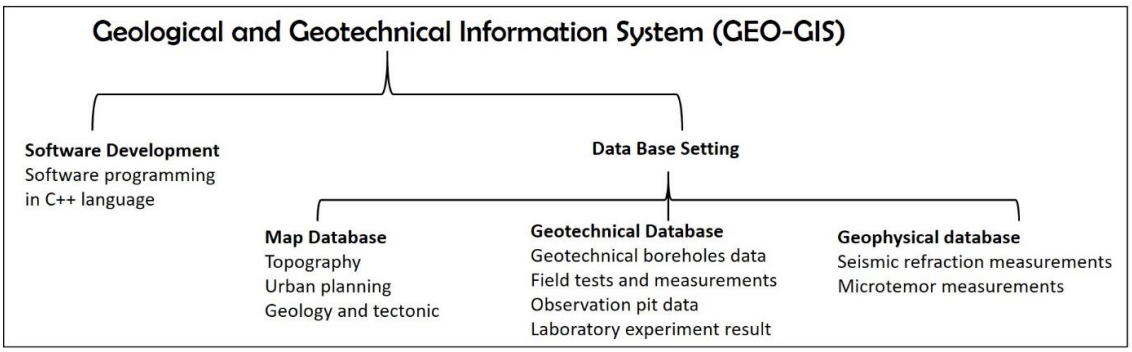

Figure 1. Structure of geological and geotechnical information system GEO-GIS

Each map can be drawn separately or one after on the GEO-GIS. Geology and tectonic map is drawn in the first order as a base map. Later, topography and urban planning maps are drawn depending on the demand of user. Different types of maps, which are used for urban planning, can be produced by using data in GEO-GIS system. These are, groundwater depth, soil liquefaction, shear wave velocity and soil amplification maps.

3. Regional and local geology and tectonics of Acıpayam basin

Acipayam Basin is located in Burdur-Fethiye active fault zone which is one of the important neotectonic and seismic zones of Turkey. There are different studies on paleo-seismology of this neotectonic zone (McKenzie, 1978; Bozcu et al, 2007). Active fault zones in Burdur-Fethiye neotectonic zone (Figure 2) were classified as NE-SW trending, NW-SE trending and N-S trending fault zones 12]. Especially NE-SW trending faults, bounding Burdur Lake from north and south, have left strike slip character.

These faults cut through the Quaternary alluvium sediments in many locations resulting step like morphology with steep slopes. The NW-SE trending faults mostly have normal fault character and they resulted in forming different segments by displacing N-S trending fault zones (Figure 2a) (Bozcu et al, 2007).

The magnitude of the post-1900 earthquakes that occurred in the inner and central parts of this fault zone did not exceed 6.2 (Figure 2a). On the plain of Acıpayam, a 5.3 magnitude earthquake occurred in 1936 centered on Uçarı neighborhood. The epicenter of this earthquake is very close to the 20 March 2019 earthquake, with a recurrence of the earthquake in 83 years (Figure 2b). (Kumsar et al, 2019, 2020)

Acıpayam Basin is a N-S extending Neogene basin in Burdur-Fethiye Fault Zone. Topographic altitude of the basin varies from 850m to 950m and, the surface water of the basin drains out into Dalaman creek at SW. Mesozoic and Cenozoic rocks form high mountains bounding the basin (Figure 2b).

Mesozoic (Triassic-Jurassic-Cretaceous) rocks are composed of carbonated and ophiolite rock groups belong to Lycian nappes (Balcı et al, 1976). The Cenozoic units consist of early Miocene conglomerates, shallow marine limestone and late Miocene-Pliocene period alluvial, fluvial and lake sediments (Erten, 2002; Alçiçek et al, 2004). In the middle of the basin, a normal fault line having a N-S strike and dipping to the west has developed. Bedirbey, Yeniköy and Uçarı (Figure 2b) villages are settled on this fault zone. The epicenter of the 5.5 magnitude earthquake, which occurred at 9.34 am on March 20, 2019, falls on this fault line (Kumsar et al, 2020)

The younger units of the Quaternary period consist of lacustrine, fluvial, alluvial and colluvial deposits along the western slopes of the Malı month (1745 m) in Yumrutaş-Yeşildere-Corum neighborhoods in the east.

After 20 March 2019 earthquake, surface cracks were observed in the south of Yeniköy district, with a direction of N5°E and a length of approximately 1500 m and a width of 1-4 cm (Figure 2b) (Kumsar et al, 2019, 2020).

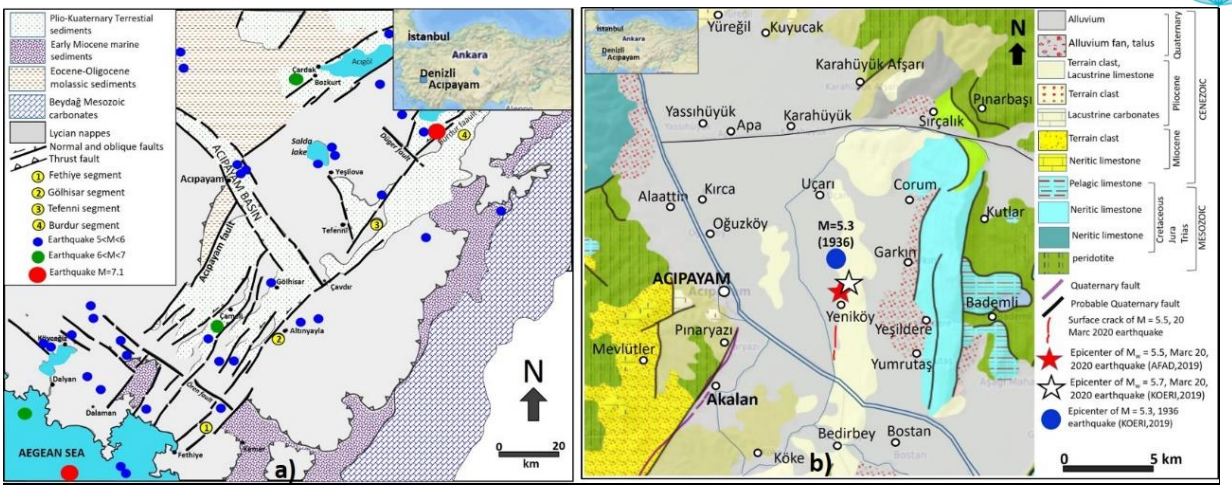

Figure 2. a) Relationship of between tectonic zones located in the Burdur-Fethiye Fault Zone (Bozcu et al, 2007, Kumsar et al, 2020), b) geology and tectonic map of Acıpayam basin (Emre et al, 2013; MTA, 2019; Akbaş et al, 2002, Kumsar et al, 2020).

4. Acıpayam GEO-GIS

Acıpayam GEO-GIS was formed by using eight geotechnical site investigation project reports prepared by various consultant companies. Topography, geology and tectonic maps data was digitized from existing maps, urban planning map was obtained in dxf file format from the Acıpayam Municipality (Kumsar et al, 2021). (Figure 3a). geotechnical database covers data of 82 bore holes 85 observation pits, in-situ test results carried out in bore holes, laboratory test results of soil samples obtained from boreholes and observation pits. Geophysical database contains data of 165 seismic refraction and 82 microtremor measurements (Şekerci, 2013, 2015; Şekerci & Kılınçarslan, 2013; Kocabaş & Şekerci, 2015, 2016a, b; Şekerci & Kocabaş, 2018a,b).

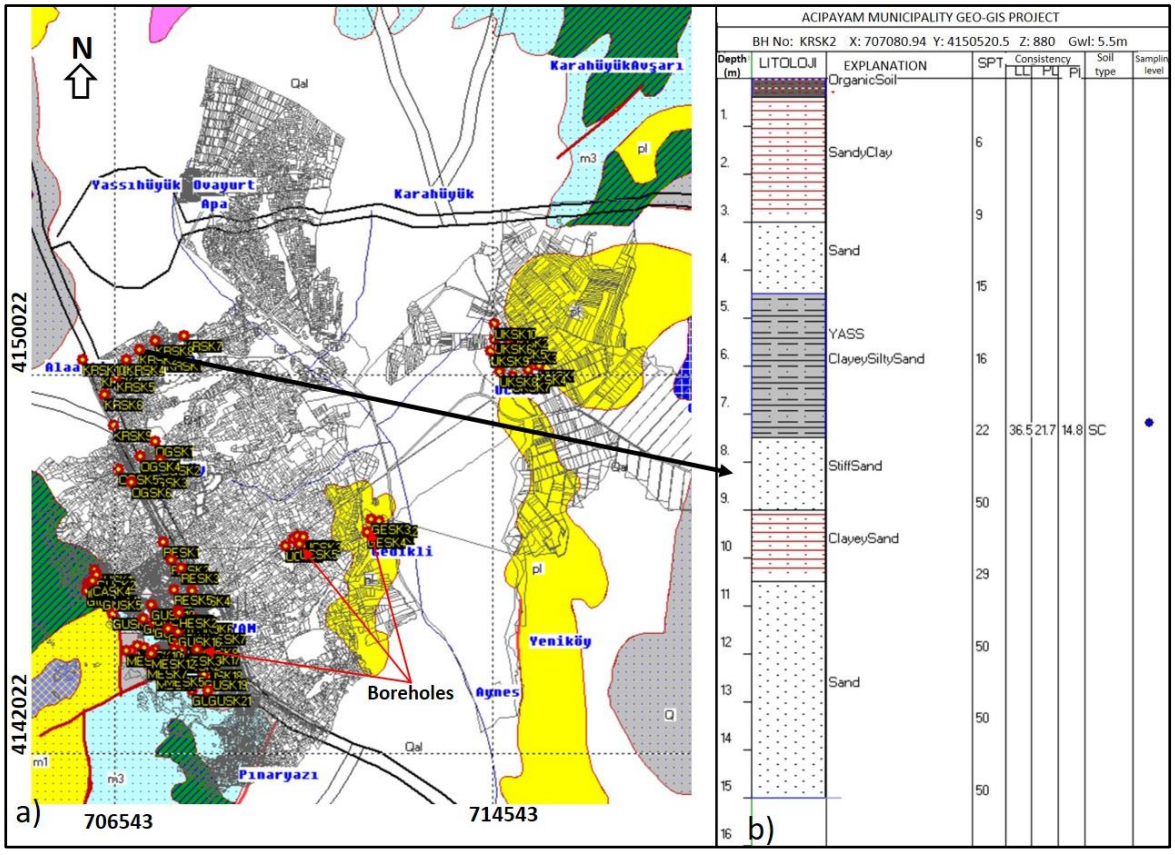

Figure 3. a) Borehole locations on geology, tectonic and urban planning maps (symbols are explained in Figure 2b), b) displaying a geotechnical log of a selected borehole on the maps in GEO-GIS.

Locations of geotechnical boreholes and observation pits can be displayed on different types of maps. As an example, borehole locations are displayed on geology, tectonic and urban planning maps as given in Figure 3a. Geotechnical log of each borehole and trial pit can be displayed on the screen after clicking location of the borehole displayed on the map. Geotechnical log of each borehole contains borehole ID, X, Y and Z coordinates, groundwater depth form ground surface, standard penetration tests (SPT), consistency test results of soil samples were displayed (Figure 3b). Particle size analyses graph of soil samples taken from each borehole and observation pit is drawn and displayed on screen. A cross-section can be taken along a section line from the topographic map of the site (Figure 4a). Boreholes falling in a certain distance to the section line, which is decided by the user, can be displayed on the cross-section (Figure 4b).

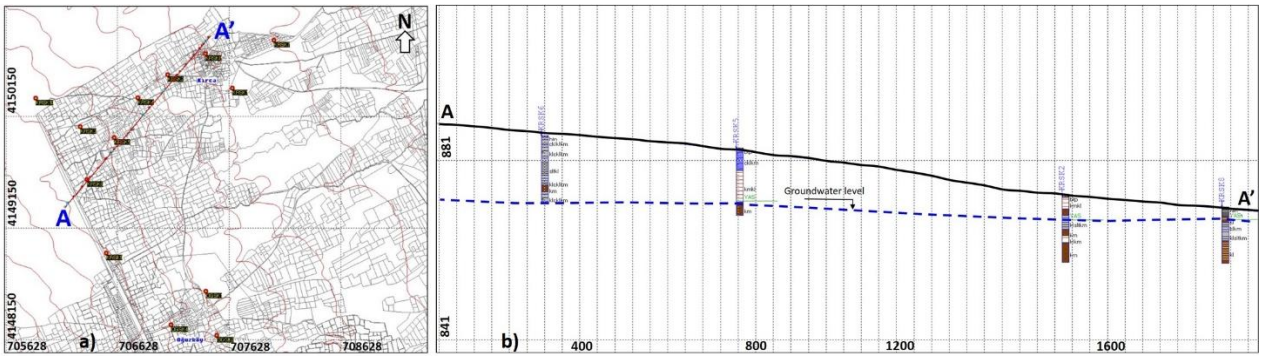

Figure 4. a) Cross-section line define on a topography and urban planning maps, b) drawing of cross-section along A-A' points and boreholes in GEO-GIS.

Four type of maps for geotechnical evaluation of Acıpayam basin area were produced by using Acıpayam GEO-GIS. These are namely groundwater depth from ground surface, liquefaction suceptibility, shear wave velocity and soil amplification maps (Figure 5 and 6).

Figure 5a shows that groundwater level is close to ground surface (1m-3m deep) in middle and northern part of the Acıpayam basin. However, grounwater gets deeper in westenr and southern part of the basin.

Liquefaction analysis of soils in Acıpayam basin was carried out by using Youd et al (2001) method for 5.5 magnitude of earthquake, which occurred on 20 Marc 2020 and caused heavy damages on many adobe houses and slight damages on reinforced concrete buildings in Gedikli, Oğuzköy, Kırca, Uçarı, Apa, Karahöyük villages in Acıpayam basin. The maksimum acceleration of earthquake measured in Acıpayam Station was 361.2 cm/sn^2 in N-S direction (AFAD, 2020). Factor of safety of against liquefaction map given in Figure 5b depicts that there is a liquefaction potential in north east part and southeast part of the basin. However soil liquefaction was not observed in the field after the 5.5 Acipayam earthquake.

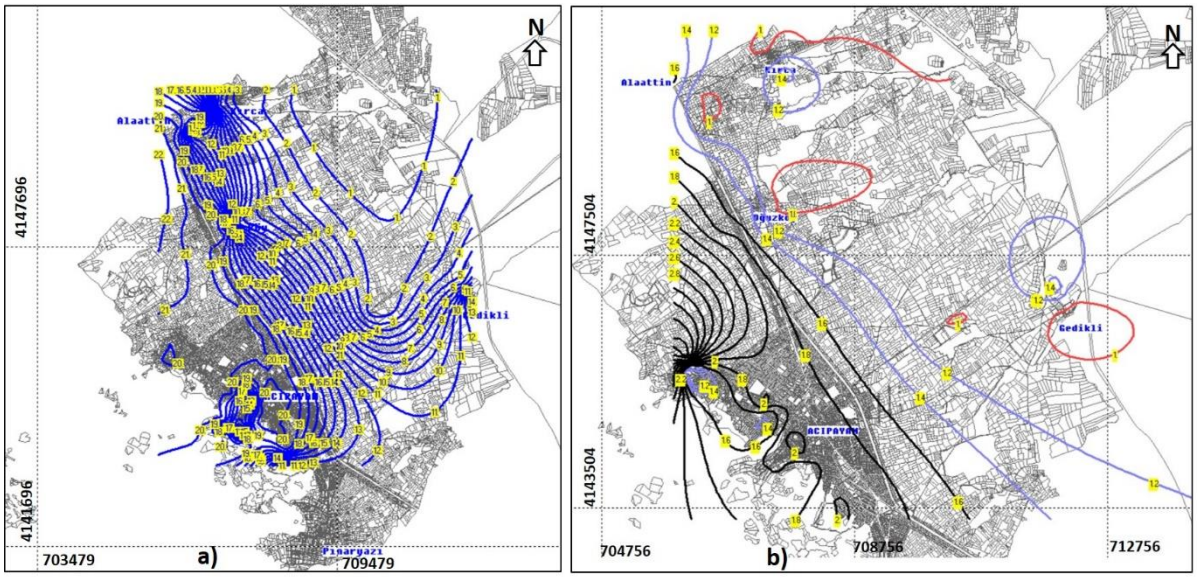

Figure 5. a) Groundwater depth map (in meter), b) liquefaction susceptibility map of Acıpayam basin prepared in GEO-GIS

Shear wave velocity (Vs-m/s) map of the basin shows that, Vs value in Gedikli village is 180 m/s, in Kırca village is 230 m/s, in Oğuzköy village 310 m/s and 280m/s in Alaattin village. The results show that there are weak and soft soils in these areas (Figure 6a).

Amplification factors (A) of soils were obtained from microtremor measurements and also calculated from shear wave velocity measurements in Acıpayam Basin by using $A=68V_S^{-0.6}$ equation (Midorikawa, 1987) where V_S is peak ground velocity of soil Figure 6b.

Amplification factors increase in eastern part of the basin and decrease in southwest of the basin. This values are in good agreement with the 5.5 earthquake damages in the basin. Adobe houses in Gedikli, Kırca and Oğuzköy villages had heavy damages. Same type of structures in Acıpayam district center area had slight damages after the 5.5 earthquake (Figure 7).

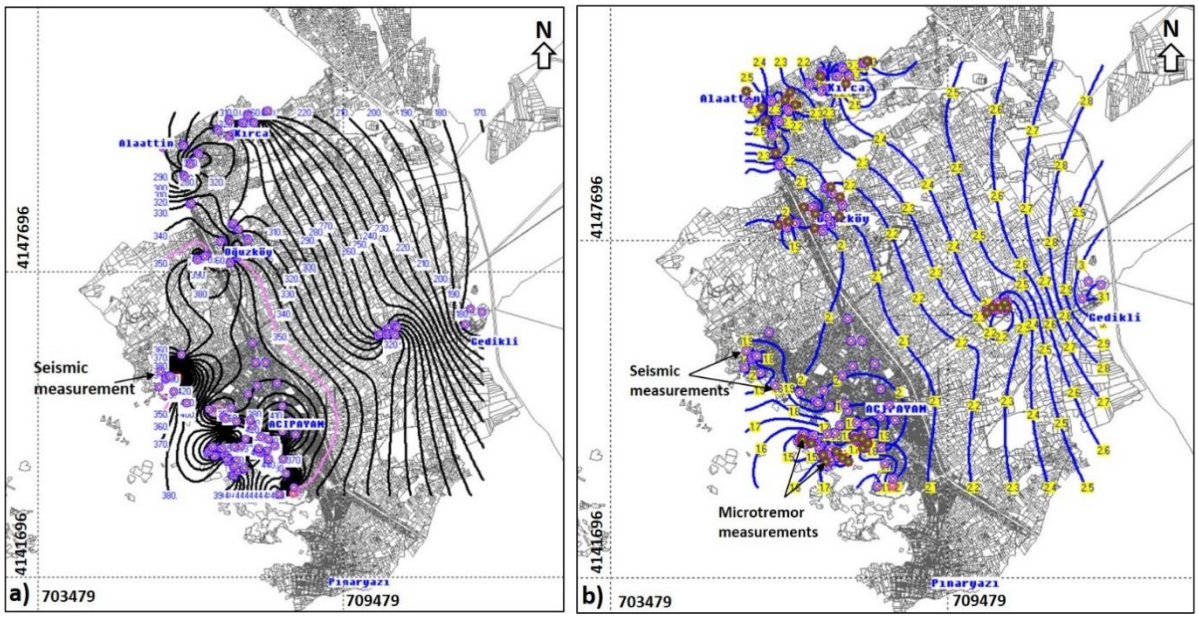

Figure 6. a) Shear wave velocity map (Vs-m/s), b) soil amplification factor map (A) of soil in Acıpayam basin prepared in GEO-GIS

Figure 7. a) Heavily damaged adobe building in Kırca village, b) heavily damaged mosque in Oğuzköy village.

5. Conclusions

Evaluation of geological geophysical and geotechnical data obtained from different site investigation projects in Acıpayam basin was carried out in GEO-GIS system developed by the first author.

The GEO-GIS system gives a facility to geotechnical engineers to bring together all geological, geotechnical and geophysical data of many site investigation projects in one data base. All data can be evaluated together and different resultant maps can be generated to be used as base maps for urban planning. These maps can also be used for detecting expected geotechnical hazards during an expected strong earthquake in existing settlement areas close to active fault zone.

The Acıpayam GEO-GIS, a case study, showed that the damaged buildings due to the 5.5 earthquake were mainly located in clayey soft soils in the area between Oğuzköy, Kırca and Gedikli villages in the existing data area. These damages are in good agreement with the resultant maps generated by using the Acıpayam GEO-GIS. In these areas, amplification factors (A) of soils are between 2.3 and 3.1, shear wave velocities of soils are between 180m/s and 300 m/s, groundwater depth from ground surface is between 7m and 1m, factor of safety against liquefaction is at the limit value of liquefaction phenomena, 1.

Acknowledgements

The authors thank to Acıpayam Municipality, Umut Can Karagöz, Didem Özyurt and Mehmet Reçber for their contribution.

References

AFAD. (2019). Afet ve Acil Durum Yönetimi Başkanlığı. www.deprem.afad.gov.tr (24.03. 2019).

Alçiçek MC, Kazancı N, Özkul M, Şen Ş. (2004). “Çameli (Denizli) Neojen Havzası’nın tortul dolgusu ve jeolojik evrimi (in Turkish),”. MTA Dergisi, 128, 99-123.

Akbaş B, Akdeniz N, Aksay A, Altun İ, Balcı V, Bilginer E, Bilgiç T, Duru M, Ercan T, Gedik İ, Günay Y, Güven İH, Hakyemez HY, Konak N, Papak İ, Pehlivan Ş, Sevin M, Şenel M, Tarhan N, Turhan N, Türkecan A, Ulu Ü, Uğuz MF, Yurtsever A, ve diğerleri. (2002).“Geological Map of Turkey”. Maden Tetkik ve Arama Genel Müdürlüğü Yayını (in Turkish), Ankara, Türkiye.

Balcı M, Sarıkaya A, Yıldız M. (1976). Denizli-Acıpayam Peridotit Masifinin Çatak-Mevlütler Çevresinin Jeolojisi, MTA Raporu (unpublished report in Turkish), Ankara, Türkiye.

Bozcu M, Yağmurlu F, Şentürk M. (2007). “Fethiye-Burdur Fay Zonunun Bazı Neotektonik ve Paleosismolojik Özellikleri GB-Türkiye (in Turkish)”. Jeoloji Mühendisliği Dergisi, 31(1), 25-48, 2007.

Emre Ö, Duman, TY, Özalp S, Elmacı H, Olgun Ş, Şaroğlu F. (2013). ”1/1.250.000 Ölçekli Türkiye Diri Fay Haritası”. Maden Tetkik ve Arama Genel Müdürlüğü Özel Yayınlar Serisi (in Turkish), Ankara, Türkiye.

Erten H. (2002). Acıpayam-Çameli Karasal Neojen İstifinin Stratigrafisi ve Mikromemeliler Yönünden İncelenmesi, MSc thesis (in Turkish), Pamukkale Üniversitesi, Denizli, Türkiye.

Kocabaş A., Şekerci, H. (2015). Denizli ili Acıpayam İlçesi Güneybatısında Yer alan Çalışma Alanının Revize İmar Planına Esas Jeolojik-Jeoteknik Etüt Raporu (unpublished report in Turkish).

Kocabaş, A., Şekerci, H. (2016a). Denizli İli Acıpayam İlçesi Uçarı Yolu Üzeri N22B08A2C, N22B08B1D Paftalarında Yer alan Çalışma Alanının İmar Planına Esas Jeolojik-Jeoteknik Etüt Raporu (unpublished report in Turkish).

Kocabaş A., Şekerci, H. (2016b). Denizli ili Acıpayam İlçesi Mevlütler yolu üzeri, N22B07C1B, N22B07C1C, N22B07C2A N22B07C2B, N22B07C2C, N22B07C2D, N22B07D1A, N22B07D1D Paftalarında Yer alan 285415 m2’lik Alanının İlave İmar Planına Esas Jeolojik-Jeoteknik Etüt Raporu (unpublished report in Turkish).

KOERI. 2019. “Kandilli Observatory and Research Institude”. www.koeri.boun.edu.tr, (28.03.2019).

Kumsar, H. (1993) Mine Slope Stability Assessment by Using Iner-Slice Force Transmission Theory. PhD Thesis, Deparment of Mineral Resources Engineering, Nottingham University, UK.

Kumsar, H, Çelik, SB, Kaya, M. (2004). Denizli il merkezi yerleşim alanının jeolojik, jeoteknik kent bilgi sistemi (JEO-KBS) (in Turkish), Pamukkale Üniv. Mühendislik Bilimleri Dergisi, 10(4), 25-31.

Kumsar H, Özkul M, Semiz B. (2019). “Geological and Geotechnical Investigation of 20 March 2019 Mw 5.5 Acıpayam (Denizli) Earthquake”. National Symposium on Engineering Geology and Geotechnics–ENGGEO’2019, H. Kumsar, SB. Çelik, T. Çan, M. Mutlutürk (Eds.), pp 701-710, ERS press, Denizli, Turkey.

Kumsar, H., Özkul, M., Semiz, B. (2020). Geotechnical Site Investigation and Evaluation of 20 March 2019 Mw 5.5 Acıpayam (Denizli) Earthquake, Pamukkale Univiversitesi Muhendislik Bilimleri Dergisi, 26(8), 1343-1352.

Kumsar, H., Çelik, S .B., Kaya, M. Topaloğlu, S. (2005). Geological-geotechnical urban information system for Denizli, (Denizli için jeolojik-jeoteknik kent bilgi sistemi), Mühendislik Jeolojisi Bülteni-Bulletin of Engineering Geology, 21, 35-47.

Kumsar, H., Say, Y., Özyurt D., Karagöz, U.C., Sarayköylü, T., Reçber, M. (2021). Sürdürülebilir Kentleşme İçin Jeolojik Jeoteknik Coğrafi Kent Bilgi Sistemi (JEOKBS), Acıpayam Belediyesi (Denizli) Uygulaması,(in Turkish), 73. Türkiye Jeoloji Kurultayı (http://tjk.jmo.org.tr/), 24-28 Mayıs 2021, Ankara, JMO Yayınları, 509-510.

McKenzie DP. (1978). Active tectonics of the Alpine-Himalayan Belt: The Aegean sea and its surronding regions, Geophysical Journal of the Royal Astronomical Society, 55, 217-254.

Midorikawa S. (1987). Prediction of isoseismal map in the Kanto Plain deu to hypotetrtical earthquake. Journal of Structural Engineering, 33B, 43-48.

MTA. (2019) “Maden Tetkik ve Arama Genel Müdürlüğü“ http://yerbilimleri.mta.gov.tr/anasayfa.aspx, (30.04.2019).

Şekerci, H. (2013). Denizli İli Acıpayam İlçesi Oğuz Mahallesi N22B07B2C, N22B07B2B, N22B07B3C, N22B07B3D, N22B08A4D, N22B08A4A, N22B08A4C, N22B08D1A, N22B08D1B, Paftalarında Yer alan Çalışma Alanının İmar Planına Esas Jeolojik-Jeoteknik Etüt Raporu (unpublished report in Turkish).

Şekerci, H. (2015). Denizli İli Acıpayam İlçesi N22B07B2C, N22B07B3B, N22B07B3C, N22B07B3D, N22B08A4D, N22B08A4A, N22B08A4C, N22B08D1A, N22B08D1B Paftalarında Yer alan Çalışma Alanının Revize İmar Planına Esas Jeolojik-Jeoteknik Etüt Raporu (unpublished report in Turkish).

Şekerci, H., Kılınçarslan, N. (2013). Denizli İli Acıpayam İlçesi Acıpayam Belediyesi, Çamlık Mahallesi 20L-I Paftasında Yer alan Çalışma Alanının İmar Planına Esas Jeolojik-Jeoteknik Etüt Raporu. Nisan (unpublished report in Turkish).

Şekerci, H., Kocabaş, A. (2018a). Denizli İli Acıpayam İlçesi Kırca Mahallesi N22B02B3C, N22B02B3D, N22B02B4C, N22B02B4D, N22B02C1A, N22B02C1B, N22B02C1C, N22B02C1D, N22B02C22A, N22B02C2B, N22B02C4B, N22B03A4D Paftalarında Yer alan Çalışma Alanının İmar Planına Esas Jeolojik-Jeoteknik Etüt Raporu . Ekim, 247s.

Şekerci, H., Kocabaş, A. (2018b). Denizli İli Acıpayam İlçesi Oğuz Mahallesi N22B02C3A, N22B02C3B, N22B02C3C, N22B02C3D, N22B02C4AD, Paftalarında Yer alan Çalışma alanının İmar Planına Esas Jeolojik-Jeoteknik Etüt Raporu (unpublished report in Turkish).

Youd TL, Idriss IM, Andrus RD, Dobry R, Ishihara K, Martin, GR, Arango I, Finn WDL, Koester JP, Mitchell JK, Robertson PK, Castro G, Harder Jr LF, Liao SSC, Christian JT, Hynes ME, Marcuson III WF, Moriwaki Y, Seed RB, Power MS, Stokoe II KH. (2001). Liquefaction resistance of soils: summary report from the 1996 NCEER and 1998 NCEER/NSF Workshops on Evaluation of Liquefaction Resistance of Soils, Journal of Geotechnical and Geoenvironmental Engineering, 127 (10), 817-833.

THEME 6 - ANALYSIS AND MITIGATION OF GEO-HAZARDS

Merge historical documents digitalisation with LiDAR: a method for assessing and disseminating rockfall mitigation strategies

Davide Notti[1], Daniele Giordan[1] , Diego Guenzi[1] & Rosa Lasponara[2]

[1]*CNR-IRPI, Strada delle Cacce 73, 10135 Torino, Italy*
davide.notti@irpi.cnr.it, daniele.giordan@irpi.cnr.it

[2]*CNR-IMAA, C.da S. Loja - Zona Industriale, 85050 Tito Scalo (PZ), Italy*
rosa.lasaponara@imaa.cnr.it

ABSTRACT: In this work, we present a methodology to improve the rockfall risk assessment and the population preparedness for small communities. Lauria town, southern Italy, is shown as a case history. We used traditional digitalisation of the paper archive to reconstruct and geocoding the history of mitigation works. We coupled this with the very-high resolution orthophotos and DTM derived from the LiDAR-RPAS survey. The aim was to create a reliable state of the art, resumed in an operative monography, for experts who need to design affordable and efficient new rockfall mitigation structures. The very-high resolution DTM is also aimed to improve rockfall modelling. Moreover, we made webGIS and 3-D interactive views to disseminate rockfall hazard and mitigation strategies among the population and local authorities.

Keywords: Rockfall risk assessment, RPAS-LiDAR, WebGIS, dissemination

1. Introduction

The rockfall mitigation is a sum of several strategies (, Scavia et al., 2020) that includes: event inventory and susceptibility mapping (Depountis et al., 2020; Cingetti et al., 2020), modelling (Agliardi et al., 2009;), the evaluation of the affordability of the different scenarios (Galve et al., 2016), and the design of mitigation structures (Toe et al., 2018).

Often, rockfalls that affect small town or villages are studied only at a limited scale. However, even if limited to a very local scale, rockfalls can threaten several people's lives and limited access to significant portions of small villages and urbanised area.

The local authorities (e.g. small municipalities) sometimes do not have enough resources and technical background to define a long term strategy that could stabilise large rockfall prone areas. For this reason, the risk that local authorities can be focused only on the immediate resolution of the localised problem without a general overview over a large area is very high.

If the general overview is missing, several studies on rockfall risk assessments are commissioned to different companies that worked autonomously on a single small site. These studies are usually stored in the local archive and (particularly in the past) only in paper format in the town hall. One of the critical effects of this approach is that an interesting amount of acknowledgement is not accessible and could be lost or not used when new studies and projects are made.

Another critical point is the correct maintenance of infrastructures realised for the reduction of the rockfall risk. Actually, several regulations define the redaction of maintenance plans that have to be provided during the design and realisation of rockfall protection. These plans are not easy to apply and, in the past were not provided by the companies that realised the works. For this reason, even good remedial works can be affected by critical degradation that is not carefully considered for the lack of a dedicated background and a clear maintenance plan.

In these cases, the first important element that should be considered is a correct management of acquired information. The digitalisation of old archive study is the first low-cost solution to creating a (geo)database

of available information. Unfortunately, digitalisation is not always the resolutive solution because the number of information can be very high. It can be hard to have a general overview of what has already been investigated and what is still unknown. For this reason, the use of a dedicated document that has been developed to make a reasoned collection of most essential information organised in a predefined structure can be a good add value. Giordan et al. (2018) proposed using Operative Monography (OM) to acquire and organise all available information using a reasoned and codified approach. OM can be considered a good solution for the organisation of large and complex datasets that can be adopted to manage large slope instability monitored by local authorities or for the study of rockfall prone areas.

Another important element that could help analyse rockfall prone areas is the availability of high-resolution DTMs. In recent years, LiDAR (Saroglou et al., 2018) and RPAS (Giordan et al., 2020; Santagelo et al., 2019) offered the opportunity to map at very-high resolution and relatively low cost the slope affected by rockfall. Proximal remote sensing techniques also reduce the risk for the operator that could limit the direct access to the most dangerous areas (Menegoni et al., 2019).

In this work, we present a methodology based on the digitalising of an old archive and the use of RPAS-LiDAR survey aimed to create a state of the art of rockfall mitigation of a sector of the Lauria municipality, a small town of southern Italy (Basilicata region).

The proposed methodology has been adopted to acquire all available documents and studies made in the last 40 years. The creation of a database that identifies all the infrastructures built in the studied area and collects all the available information is the first step for the evaluation of the general condition of the infrastructure and for a better definition of a long term strategy aimed to reduce the rockfall risk in a complex area. The adopted methodology also considered disseminating products like WebGIS and 3-D models that aim to increase the preparedness among the population and simplify the access to the available information.

2. Study area

The town of Lauria (Basilicata region, southern Italy) is located in the southern Apennine Chain.

From the geological point of view, the town is on the northern border of the Lauria Mountains structural unit (Canora et al., 2019), mainly made by Mesozoic limestone formation. The lower part of the town (Lauria Inferiore) was built at the base of Sant'Elia Ridge. On this slope, outcrops cretaceous dolomitic limestone, with layers of marl, conglomerate and calcareous sandstone (Figure 1 B).

The main structural lineament and sub-vertical faults are oriented NNW-SSE and NW-SE and N-S. The main dipping of the formation is to NW, and some karst processes enhance the rock mass fractionation.

The high acclivity of the slope and the complex fracture systems isolate unstable blocks subject to frequent rockfall/toppling events of small-medium volumes. The slope affected by rockfall show a length of about 1 km, the slope height reaches the 200 m. The average slope is about 60° in the sector just above the old part of Lauria town. Several buildings measure less than 20 m from the toe of the cliff.

Some events like extreme rainfall (2002), wildfire (1996, 2017) or earthquake (Michetti et al.,1998) caused significant rockfall events that sometimes affected the closest buildings and the road. Fortunately, there is no notice of fatalities in recent years.

3. Material and Methods

We have created a methodological approach (Figure 2) that helps to create a database of previous knowledge and data for future study and dissemination for the population. The methodology is made of four steps: i) data collection; ii) organised geo-database setup; iii) OM reduction; iv) result dissemination.

In the first step, the data collection, we have two main inputs data:

1. The digitalisation of old studies from the archive of Lauria municipality (Figure 3) and the geocoding of project maps on a GIS.
2. Very high-resolution LIDAR data (DTM and Orthophotos) of the study area. The LIDAR survey was made by an external enterprise. The LiDAR used is a Riegl miniVUX-1 with Applanix APX-20 and Sony A7R Mk.III loaded on a DJI MATRICE 600 RPAS. The area covered is about: 609,260 m^2, Points: 107,301,741 Point Density: 176 pt/m^2. The use of some GCPs measured with RTK GNSS allowed validating the cloud points, that have an accuracy of 2 cm in Z. . From the clouds, points were processed to obtained DTM

and DSM at 0.5 m of spatial resolution and the orthophotos at 0.02 m of spatial resolution. The single photo frames not orthorectified acquired by the RPAS were delivered as part of raw data.

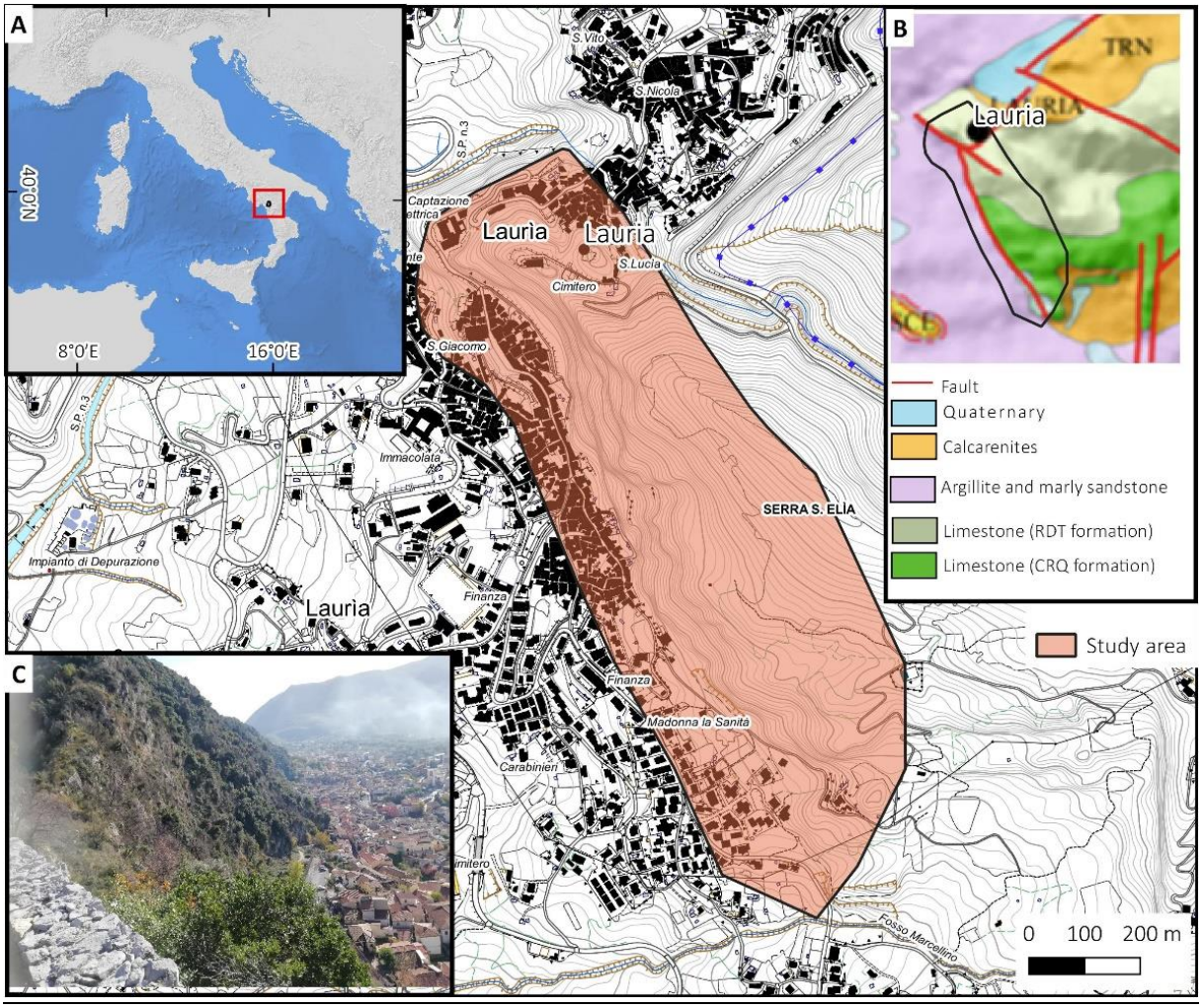

Figure 1. The study area (Serra Sant'Elia ridge) overlapped on topographic (data source: Regione Basilicata). Panel A) Location of Lauria; B) Geological map modified from (Canora et al., 2019); C) a Photo of Serra Sant'Elia ridge with the most exposed buildings just close to the base of the cliff.

The second step is creating an organised database, in which the studies and project materials were allocated in different folders on the base of the year of production, works certification and typology.

At the same on GIS software, we create a geo-database of the main rockfall mitigation works, geomechanical data, and other ancillary data. The mitigation structure was geolocated also using the high-resolution LiDAR orthophoto. We also did a ground survey to take photos of the most representative mitigation structures. In a third step, we create the OM that represents a practical (and standardised) organisation of what we already know about the studied phenomenon is the first fundamental step for better management of a possible emergency related to an increase of the activity of the slope instability.

The setup of the geo-database of mitigation works combined with high-resolution LIDAR and RPAS surveys could be the base for future and detailed rockfall modelling. (e.g. precise impact energy estimation for new structures).

The last step is dissemination. This phase is aimed to increase the population preparedness and knowledge about the rockfall risk. The main products consist of a WebGIS with free-cost software and 3-D models for interactive visualisation of the affected areas.

To create the WebGIS of Lauria rockfall mitigation works, we used GeoServer and MapStore services.

The GeoServer (http://geoserver.org/) is a web mapping server for the dissemination of GD. GeoServer is a FOSS server written entirely in Java that allows users to store, view and edit geospatial data. Designed

for interoperability, it publishes data from any major spatial data source using open standards (Cignetti et al., 2019).

MapStore (https://www.geosolutionsgroup.com/technologies/mapstore/) is a professional open-source cartography and geographical information platform based on the topological map model that allows creating WebGIS service using the WMS obtained from GeoServer.

To create a 3-D interactive view of the mitigation works (that can be used with any browser without installing GIS or other software), we used the Qgis2threejs plugin for QGIS and LIDAR DTM as an elevation layer to create the 3-D view model.

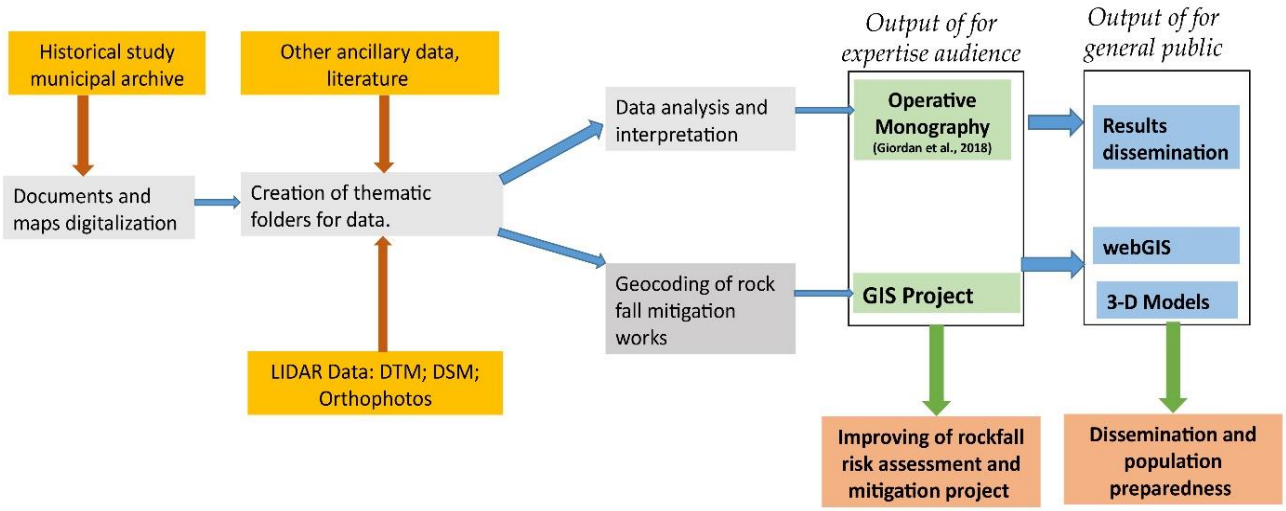

Figure 2. The methodology flow-chart

4. Results

4.1 A digital archive of past mitigation works

We digitalised about 70 documents and maps from the Lauria town hall archive, and we organised them in structured folders (Table 1). The maps of the ubication of the rockfall mitigation structures were digitised in geo-database (Figure 3), containing more detailed information than the paper map. For instance, for each installation, it is possible to know the type and the number of anchors, eyebolt anchor or the mesh used (e.g. double-twisted hexagonal wire mesh). When it was possible, we also classified the barrier using the photos taken on the ground (Figure 4).

The digitalisation of the archives allowed us to reconstruct the mitigation work history. Since the late 80's the municipality of Lauria and the regional civil engineering board set up a series of studies and mitigation works. The most important work took place from 1997 to 2001, when several rockfall events occurred after a wildfire (1996) and the 1998 earthquake (Michetti et al., 1998).

For these mitigation work, geo-structural surveys, borehole investigation, rockfall modelling were commissioned, and most of them are archived only in the analogic format in the Lauria town hall.

In January 2002, a few weeks after remedial works conclusion, a rockfall partially destroyed the new barriers and nets. The infrastructures were restored a few months later. These are the last documented works and studies done on the unstable cliff of Sant'Elia Ridge.

In the last 20 years, no new risk mitigation projects were done, and no maintenance work was planned for the installed structure. In 2017, another wildfire that hit the area of Mount Sant'Elia caused new small rockfalls.

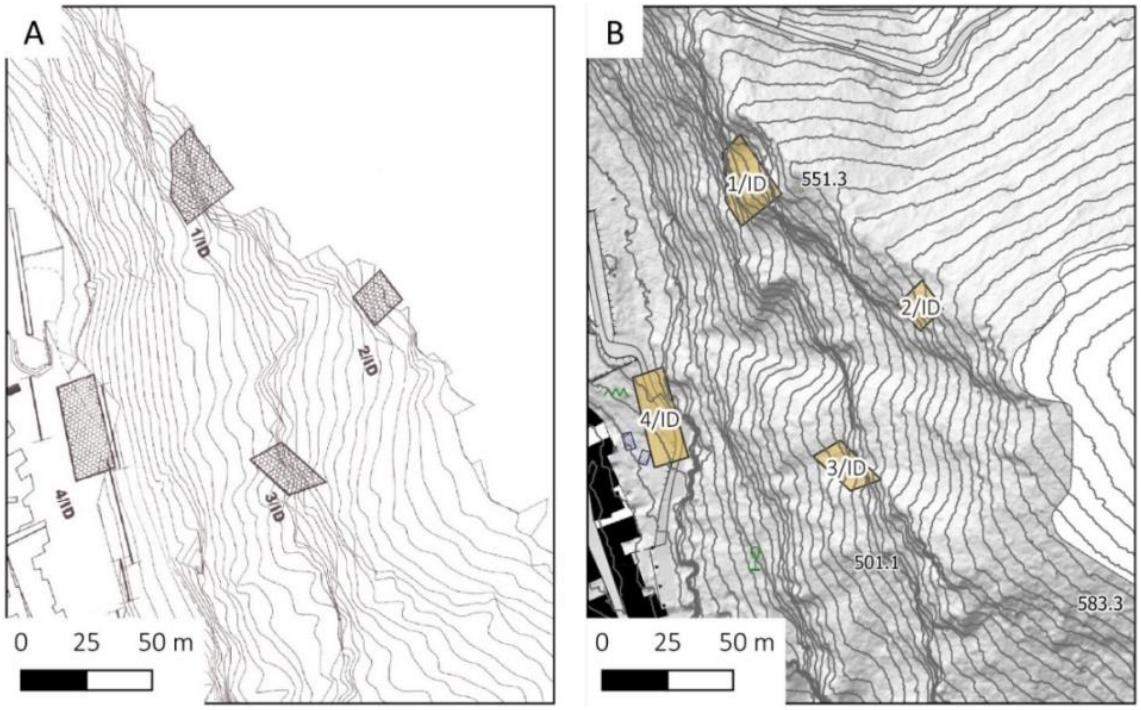

Figure 3. a) Original document showing the location of some mitigation structure for widespread rockfall. B) the digital version overlapped to hillshade derived from LIDAR DTM.

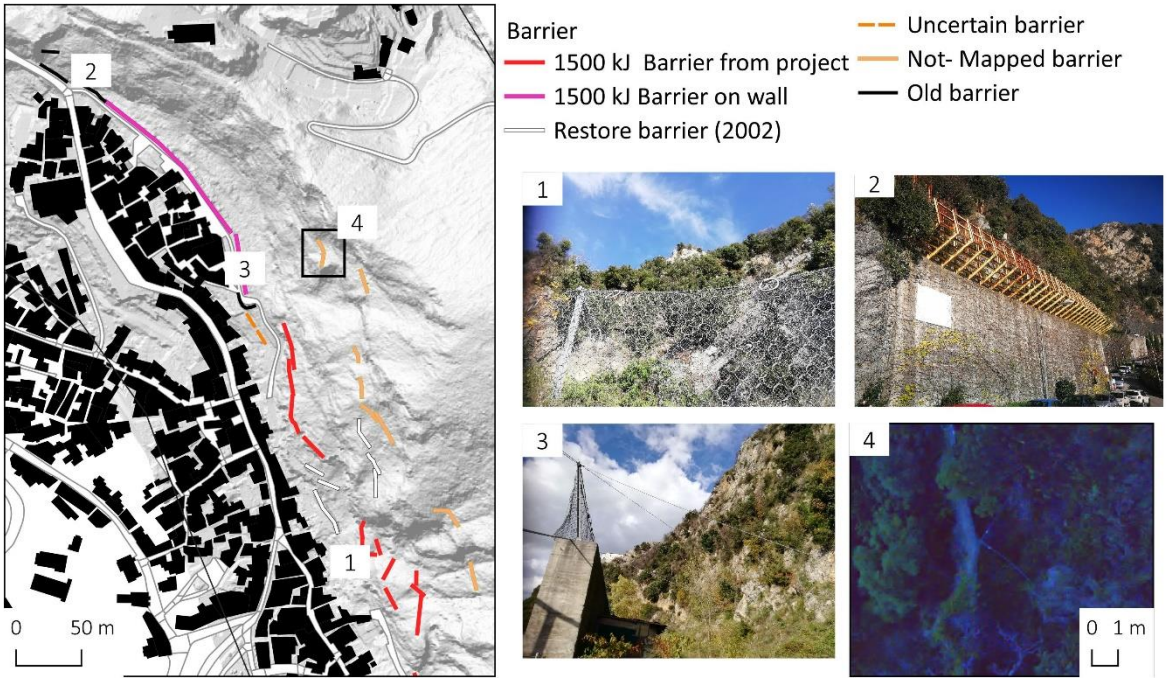

Figure 4. Map of barriers classified on the base of available documents. 1) An example of a certified barrier (1500 kJ energy); 2) An old type of barrier not reported in any documents; 3) A certified barrier installed over an older concrete wall; 4) A Detailed view of a barrier partially masked by vegetation in LiDAR orthophoto

Table 1. An Example of the organisation of the digitalised materials

Folder	Name	Description	Format
01 1997 projects	Barrier specification	Design specification required for barriers	PDF document
	Impact test	Impact test to evaluate the energy load on barriers	PDF document
02 1998 studies	Geomechanical stations	Resume of the main geomechanical parameters for each station	PDF document/ Table
	Maps of geomechanical stations	Approximativve ubication of geomechanical stations	Geo-database on GIS
03 2000 final projects	Spread instability mitigation	Ubication of the mitigation works for widespread rockfall instability	Geo-database on GIS
	Spot instability mitigation	Ubication of the mitigation works for local rockfall instability	Geo-database on GIS
04 2002 Restoration work	Geological settings reports	Geological and survey report on 2002 rockfall event	PDF document
	1-D Rokcfall modelling	Results of 1-D Rokcfall modelling on collapsed areas	PDF document
	Restoration of barrier	Maps of the design of the restoration of barriers, nets damaged by the 2002 event	Geo-database on GIS

4.2 The RPAS-LiDAR DTM and their consequence on modelling

The RPAS-LiDAR survey allowed us to obtain very-high-resolution Orthphto and DTM. The derived product like the slope gradient (Figure 5) and the hillshade have unprecedented details that allowed to identify the area most probably affected by potential rockfall. The very high-resolution DTM also increases the accuracy rockfall model. For example, using a quick test on the QPROTO plugin for QGIS (Castelli et al., 2021), the outputs show improved resolution and accuracy of modelling the runout velocity of fallen blocks from 5-m to 0.5m based on DTM. The orthophoto and the single photo frames taken from RPAS allowed improving the geocoding of most of the rockfall barrier and some net and mesh.

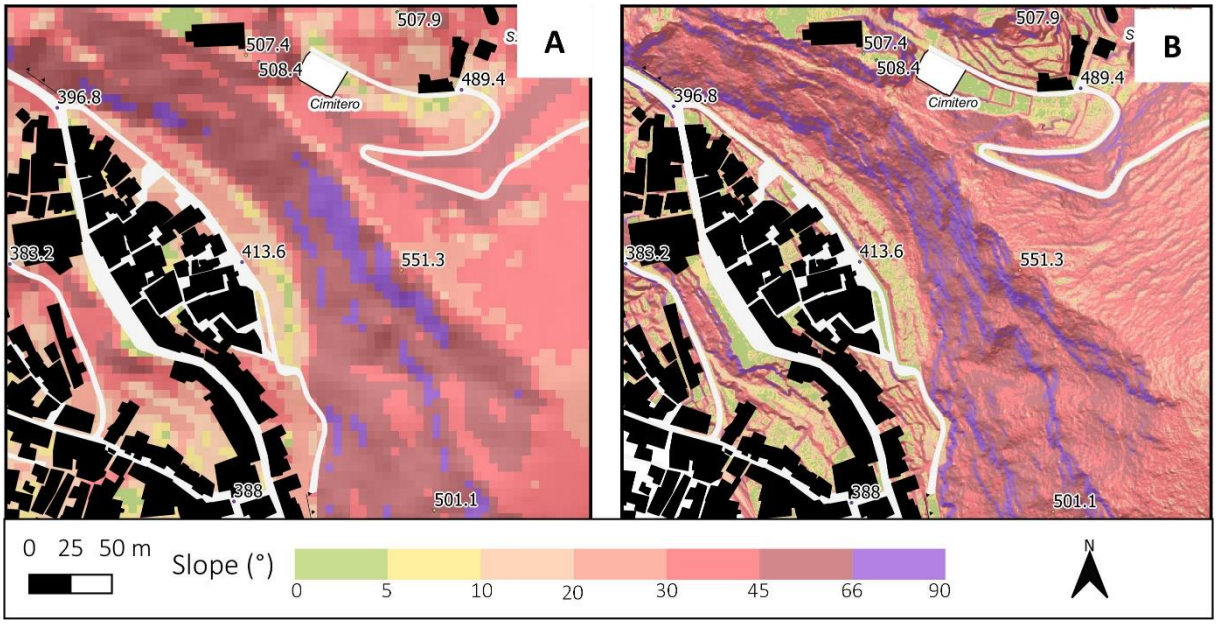

Figure 5. Slope and shaded relief based on: A) 5-m DTM of Regione Basilicata; B) 0.5 m 2020 LIDAR

4.3 Operative Monography and the dissemination of results

We resume all the acquired data in an operative monography specifically adapted for the Lauria case study (Table 2). The production of a WebGIS (actually access-restricted for Lauria municipality administration, Figure 6) and the creation of some 3-D models allow an easy consultation of the database also for non-expert people.

Table 2. Operative Monography chapter organization

Section	Chapter	Sub-Chapter
1 Summary	Summary of the study area	
2 Ancillary data	2.1 Geological and geomorphological settings	
	2.2 Rockfall events	Historical Rockfall event; Collapses related to the earthquake of 9 September 1998; Collapse event January 2002
	2.3 Geomechanical Surveys 1998	
3 Mitigation structure	Type of mitigation structure installed	Undocumented antecedent works; Restoration works following the collapse 23 January 2002; Photo documentation
4 New data	4.1 LiDAR and derived product description	
	4.2 GIS, WebGIS and 3-D model note	
5 Summary	Summary and integration proposals	

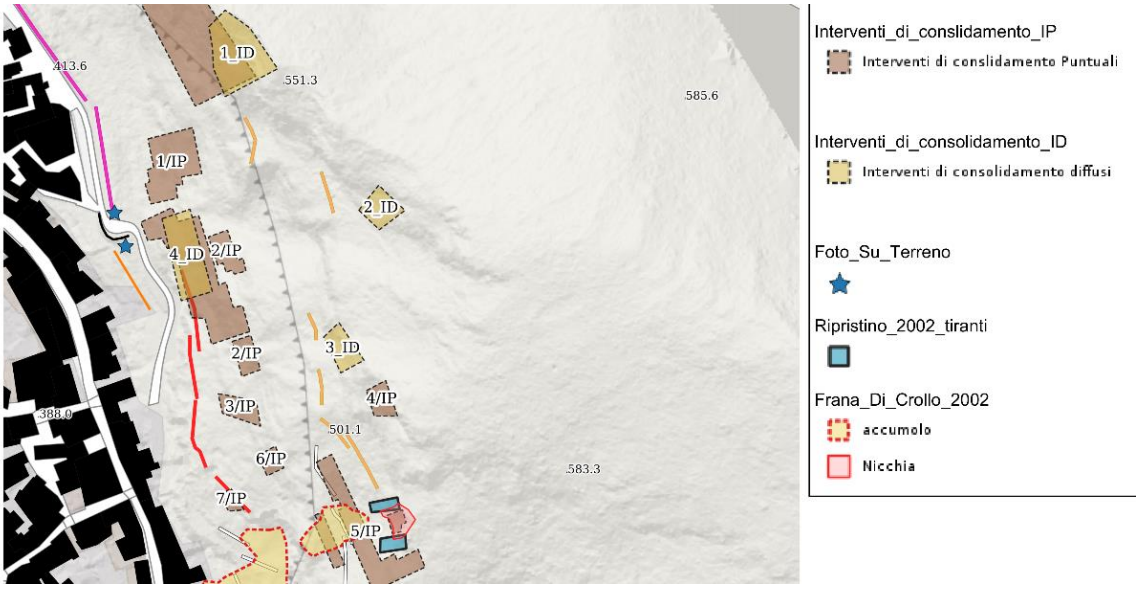

Figure 6. A screenshot of webGIS of the mitigation works in Lauria (Italian legend).

5. Discussion and conclusion

In this work, we presented a low-cost methodological approach to creating a state of the art rockfall mitigation for small public administration. We tested our methodology in the town of Lauria. The approach combined a traditional archive digitalisation with a high-resolution LIDAR survey of the slope affected by rockfall.

We obtained a detailed state of the art and the maintenance conditions of the mitigation works made until now. The results show that the most recent studies have more than 20 years, and no maintenance works were made on structures. The acquired knowledge, resumed in an operative monography, joint with DTM LiDAR will allow the expertise to make more accurate modelling and to design a more appropriate structure to mitigate rockfall risk.

We also create products more focuses on the general public, like the WebGIS and interactive 3-D model. We believe that population preparedness and knowledge about the natural hazard and risk mitigation strategy are essential for choosing the best affordable and safe measure by decision-makers.

Acknowledgements

The authors would acknowledge the municipality of Lauria and its Major for the support in document archive research.

References

Agliardi, F., Crosta, G.B. and Frattini, P., 2009, Integrating rockfall risk assessment and countermeasure design by 3-D modelling techniques. Natural Hazards and Earth System Sciences, 9(4), pp.1059-1073.

Canora, F., Rizzo, G., Panariello, S. and Sdao, F., 2019, Hydrogeology and hydrogeochemistry of the Lauria mountains northern sector groundwater resources (Basilicata, Italy). Geofluids, 2019

Castelli, M., Torsello, G. and Vallero, G., 2021., Preliminary Modeling of Rockfall Runout: Definition of the Input Parameters for the QGIS Plugin QPROTO. Geosciences, 11(2), p.88.

Cignetti, M., Guenzi, D., Ardizzone, F., Allasia, P. and Giordan, D., 2020, An open-source web platform to share multisource, multisensor geospatial data and measurements of ground deformation in mountain areas. ISPRS International Journal of Geo-Information, 9(1), p.4.

Cignetti, M., Godone, D., Bertolo, D., Paganone, M., Thuegaz, P. and Giordan, D., 2020, Rockfall susceptibility along the regional road network of Aosta Valley Region (northwestern Italy). Journal of Maps, pp.1-11.4

Depountis, N., Nikolakopoulos, K., Kavoura, K. and Sabatakakis, N., 2020, Description of a GIS-based rockfall hazard assessment methodology and its application in mountainous sites. Bulletin of Engineering Geology and the Environment, 79(2), pp.645-658.

Galve, J.P., Cevasco, A., Brandolini, P., Piacentini, D., Azañón, J.M., Notti, D. and Soldati, M., 2016, Cost-based analysis of mitigation measures for shallow-landslide risk reduction strategies. Engineering Geology, 213, pp.142-157.

Giordan, D., Cignetti, M., Wrzesniak, A., Allasia, P. and Bertolo, D., 2018, Operative Monographies: Development of a New Tool for the Effective Management of Landslide Risks. Geosciences, 8(12), p.485.

Giordan, D., Adams, M.S., Aicardi, I., Alicandro, M., Allasia, P., Baldo, M., De Berardinis, P., Dominici, D., Godone, D., Hobbs, P. and Lechner, V., 2020. The use of unmanned aerial vehicles (UAVs) for engineering geology applications. Bulletin of Engineering Geology and the Environment, 79(7), pp.3437-3481.

Menegoni, N., Giordan, D., Perotti, C. and Tannant, D.D., 2019, Detection and geometric characterisation of rock mass discontinuities using a 3-D high-resolution digital outcrop model generated from RPAS imagery–Ormea rock slope, Italy. Engineering geology, 252, pp.145-163.

Michetti, A.M., Ferreli, L., Esposito, E., Porfido, S., Blumetti, A.M., Vittori, E., Serva, L. and Roberts, G.P., 2000, Ground effects during the 9 September 1998, Mw= 5.6 Lauria earthquake and the seismic potential of the “aseismic” Pollino region in southern Italy. Seismological Research Letters, 71(1), pp.31-46.

Santangelo, M., Alvioli, M., Baldo, M., Cardinali, M., Giordan, D., Guzzetti, F., Marchesini, I. and Reichenbach, P., 2019, Brief communication: Remotely piloted aircraft systems for rapid emergency response: road exposure to rockfall in Villanova di Accumoli (central Italy). Natural Hazards and Earth System Sciences, 19(2), pp.325-335.

Saroglou C, Asteriou P, Zekkos D, Tsiambaos G, Clark M, Manousakis J. UAV-based mapping, back analysis and trajectory modeling of a coseismic rockfall in Lefkada island, Greece. Natural Hazards and Earth System Sciences. 2018 22 January;18(1):321-33.

Scavia, C., Barbero, M., Castelli, M., Marchelli, M., Peila, D., Torsello, G. and Vallero, G., 2020, Evaluating rockfall risk: Some critical aspects. Geosciences, 10(3), p.98.

Toe D, Mentani A, Govoni L, Bourrier F, Gottardi G, Lambert S. Introducing meta-models for a more efficient hazard mitigation strategy with rockfall protection barriers. Rock mechanics and rock engineering. 2018, Apr;51(4):1097-109.

The application of empirical rainfall thresholds towards shallow landslide probability estimation in fire-affected areas

Spyridon Lainas[1], Nikolaos Depountis[1] & Nicholas Sabatakakis[1]

[1]*University of Patras, Greece*
splainas@upatras.gr, ndepountis@upatras.gr , sabatak@upatras.gr

ABSTRACT: A methodology for the estimation of the probability of shallow rainfall-induced landslide activation in burned areas is proposed. As a study area has been selected the Ilia regional unit in Western Greece which has been suffered one of the most devastating wildfires in European level with severe social-economic damages in infrastructures and properties. Throughout detailed landslide and daily rainfall data recordings, the rainfall conditions that favoured landslide trigger are identified in detail and as a result annual exceedance statistics of the threshold values for the specific landsliding conditions are defined. This approach can aid landslide hazard assessment under certain climatic and engineering geological conditions and especially in areas that have been affected by wildfires. The topic of landslide forecasting by means of rainfall threshold exceedance has also an exceptional interest in the concept of Climate Change and its direct or indirect impacts on the human and physical environment.

Keywords: Shallow landslide forecasting, Rainfall thresholds, wildfires, Greece.

1. Introduction

There is an obvious tendency for landslide frequency to increase as rainfall volume or intensity increases and it is also clear that any critical rainfall conditions that may trigger the slope failure depend on climate, local ground conditions, built-up of pore water pressure, geomorphology, land use pattern as well as human intervention. Several efforts have been made on the temporal forecasting of landslides, often aiming to create landslide warning systems (Alleoti, 2004; Farina et. al., 2020). The temporal occurrence and forecasting of landslides can be modeled by the use of empirical rainfall thresholds by using the corresponding critical rainfall values after statistical analysis of rainfall events that have resulted in landslides under certain conditions (Naidu & Oommen, 2017; Valenzuela et. al., 2018).

This paper aims to contribute to the clarification of the role of rainfall in the activation of shallow landslides in burned areas and to provide annual probabilities for landslide activation by using the lower-bound rainfall values of an empirical Cumulative Event-Duration threshold proposed for the study area, following the suggestions provided by Lainas et.al. (2016). Given also the unequivocal warming of the climate system and the anticipated effects on the stability of natural and engineered slopes every attempt towards the quantification of the probability of rainfall-induced landslides can be an important aspect in landslide hazard analysis and forecasting.

2. Geological features and rainfall patterns of the study area

The study area belongs in the Ilia Regional Unit, Western Greece, one of the most well–known and popular archaeological and touristic destinations in Greece. Towards the end of August 2007, extensive wildfires burned many regions in the Greek mainland. The study area was one of the most affected areas, with approximately 870 km^2 of burned mainly rural and residential land, covering approximately 33% of its overall extent.

The burned areas were extended along the center of the region and divided into two discrete sections, one at the North (a) and the other at the South (b) (Figure 1), separated by the valley of the Alfeios river. The

northern burned section is mainly characterized by agricultural, hilly areas of smooth relief and altitudes up to 800m. On the other hand, the southern section of the burned areas (b) has slightly different, more mountainous and forest terrain, with altitudes up to 1335m. In a recent research conducted by Depountis et al. (2021), the rate of increase in the soil erosion rate at the Northern part of the study area, immediately after the fire event, was found to be equal to 36.2%, with the percentage reducing to 31% after a decade. This is an important circumstance for the study area since soil erosion accelerates landslide occurrence, especially when rainfall infiltrates eroded areas. It must be noted that soil erosion rate is commonly calculated with the combined use of the RUSLE equation and GIS (Depountis et al., 2018).

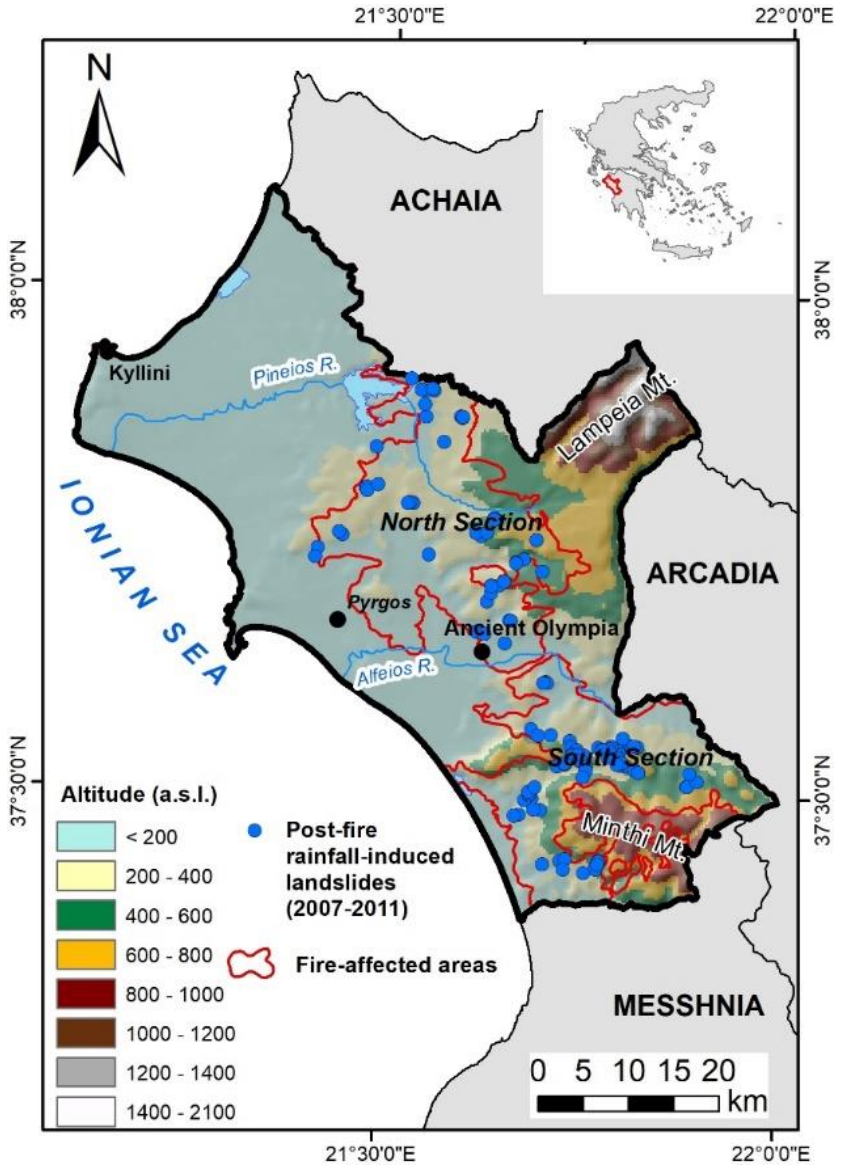

Figure 1. Location and landslide inventory map, showing recorded rainfall-induced landslides in the study area. The area is divided in the Northern (a) and Southern (b) sections.

Typical geological formations within the study area (Figure 2) consist mainly of marls, sandy clays, thick sequences of sandstones and mudstones and a lower percent of conglomerates. Quaternary loose deposits consist of 18.61% and 38.59% of the sections (a) and (b), respectively, while bedrock outcrops range from 28.4% in the southern section to only 1.1% in the northern section. Bedrock consists of alpine rock formations belonging to the Olonos-Pindos and Gabrovo Geotectonic Units, part of External Hellenides Orogenetic belt (Bonneau 1984). Main bedrock rock types include typical “flysch-type” sequences of shales, siltstones and sandstones, as well as thinly-bedded to massive limestones, schists and cherts. The aforementioned rock types and post-Miocene sediments, due to differential response to weathering processes and intense fracturing are the most susceptible to landslide phenomena geological formations, with heavy rainfall and climate pattern to be considered as the main controlling factors (landslide predictors) for landslide activation in the wider area and in Greece (Sabatakakis et al. 2005, 2013;).

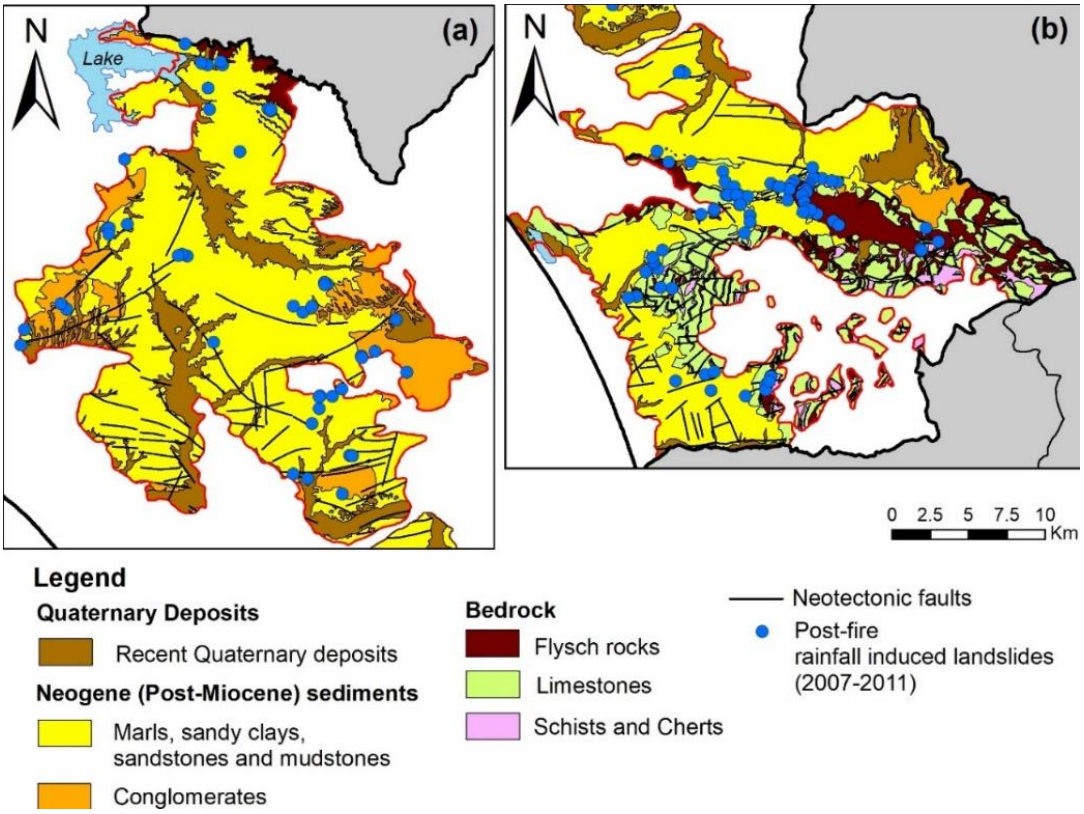

Figure 2. Simplified geological map of a) North and b) South section of the burned areas with landslide positions (modified from Lainas et. al., 2016)

Annual rainfall in the affected areas ranges approximately between 600 and 1400mm (Figure 3) with the lower values along the plain areas at the west and the higher at the easternmost mountainous areas. Long-term variation of mean annual rainfall during the 1977-2019 period shows that the study area is characterized by dry periods 2 to 5 years long, alternating with rainy periods lasting from 2 to 3 years. The Mean Annual Precipitation (MAP) in the burned areas is approximately 1070mm. It is also observed that, even if the overall annual rainfall trend seems to be steady during the whole above time frame, after examining the periods before and after 2007, respectively, it seems to be a change in the rainfall trend. A general trend of decreasing annual rainfall up to 2007 it can also be observed, followed by an increasing trend after 2007 (Figure 3).

3. Data and Methodology

3.1 Landslide dataset

Landslides and soil erosion phenomena induced by rainfall affected the burned areas in the study area, particularly road network and inhabited areas (Koukis et al. 2008; Koukis et al. 2010; Rozos et al. 2008). Local authorities focused their attention on mitigating the problem by implementing small-scale remedial measures. To aid this planning a systematic detailed engineering geological survey was carried out (Depountis et al. 2010) throughout an approximately 4-year post-fire period (up to May 2011) including: (a) field surveys to identify and map the occurred instability phenomena, (b) detailed engineering geological and geotechnical investigations in selected landslide zones and (c) landslide recording by applying an appropriately designed Landslide Inventory Form (Sabatakakis et al. 2013).

A total number of 122 well defined and documented, rainfall-induced landslides were recorded within the fire-affected areas, which were activated at least once during the period from August 2007 up to May 2011. Most landslides (56%) were recorded within the Post-Miocene (Neogene) sediments, with the most of them (82%) occurring in fine grained and mixed facies that represent 46% of the total recorded cases (56/122). The rest were recorded in the bedrock (44%) with the majority occurring in the weathered flysch and cherts (83%) that represent 37% of the total recorded cases (45/122). The main type of movement, according to the classification given by Cruden and Varnes (1996) is the rotational sliding (81%) with a smaller number occurring as translational and composite slides, earth flows and falls. In respect of the landslide volume,

according to the classification given by Fell (1994), most recorded cases represent very small landslides (72%).

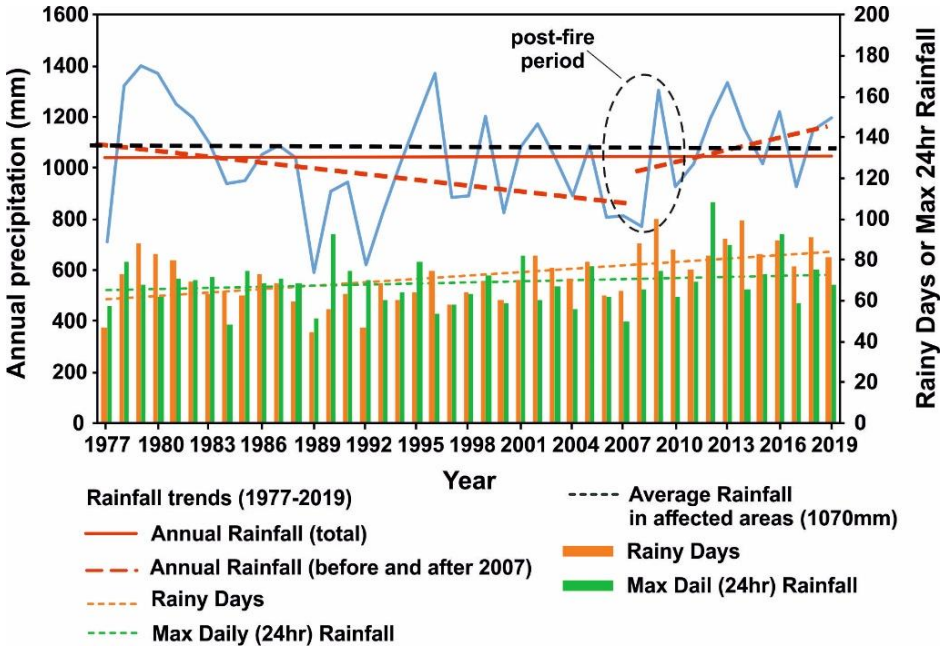

Figure 3: Average annual rainfall, rainy days and maximum daily (24hr) rainfall trends from 1977 to 2019. A change in the precipitation trend is being observed during 2007-2010.

3.2 Selection and definition of rainfall events

For every landslide occurrence, daily rainfall data obtained from a selected meteorological station based on its proximity to the landslide location, the local morphological setting and the reliability of the station records. Priority was given to meteorological stations that were located within the same watershed and had elevation close to the elevation of the respective landslide.

Having as a reference the number of days that each landslide had been activated the detailed analysis of the daily rainfall data allowed the identification of distinct rainfall events with defined duration and cumulative amount of rainfall. The definition of each rainfall event resulted in the identification of specific time windows (in days) of rainfall with the corresponding values of cumulative rainfall (E, mm) and the recorded maximum daily (R24hr, mm) rainfall (Table 1). Rainfall events that have triggered landslides in the affected areas had a duration between 2 and 13 days, cumulative rainfall between 50.0 and 251.5mm and maximum daily (24hr) rainfall within the range from 22.6 to 71.4mm.

Table 1: Number and rainfall patterns (Duration, cumulative rainfall and maximum 24hr rainfall) of the rainfall events that triggered landslides in the fire-affected areas.

Number of rainfall events	Recorded landslides	Meteorological Station (No)	Rainfall Duration (Days)	Cumulative rainfall (E) (mm range)		Max R_{24h} (mm range)	
2	2	3,9	2	50	106.6	31.6	57.2
2	7	1,3,8,9	3	64.9	112.8	25.4	58.2
4	8	2,5,9	4	73.4	133.4	27.4	58.6
3	8	2,5,9	5	71.9	134.6	23.8	62.4
3	22	2	6	145.6	188.2	62.4	71.4
8	36	2,3,5,9	7	95.6	214.4	22.6	57.2
1	6	2	8	119	119	25.4	25.4
2	13	2,3,5,9	9	109	232.1	30	62.4
2	4	2,3	10	202.8	251.5	41.8	57.2
3	8	2,6,9	11	110.3	164.8	23.2	49.2
1	8	5	13	112.8	112.8	40.4	40.4

4. Exceedance Statistics – Probability estimate

The recorded landslides were associated with the cumulative rainfall event (E) in respect of a certain rainfall duration (D) that was responsible for landslide activation by using the Cumulative Event- Duration (EDD) empirical threshold equation proposed by Lainas et. al (2016).

$E = 10.95\ x\ D^{0.423}$ (1), when 48<D<312hrs [1]

where,

E is the cumulative (total) event rainfall (in mm) and *D* is the duration of the rainfall event (in hours)

The distribution of the recorded landslide cases during the post-fire period in respect of the rainfall data (E and D) is shown in Figure 4, together with the corresponding rainfall threshold. In Figure 4 it can also observed that the majority of rainfall-induced recorded landslides were triggered after 144hrs (6 days) of cumulative rainfall) and, more precisely, between 6 and 7 days.

By using the threshold equation, the corresponding threshold rainfall values have been calculated for every duration class. In this way, the rainfall value was used to estimate annual landslide probability when the corresponding threshold is being reached or exceeded. If the frequency of these triggering thresholds can be determined from the statistical analysis of the rainfall data, this can be used as a basis for estimating landslide probability. However, in any case, it is important to recognize that the occurrence of a landslide event that exceeds the threshold value may not necessarily lead to slope failure. Some events may be redundant or even ineffective, depending on the status of the slope development and the local landslide history.

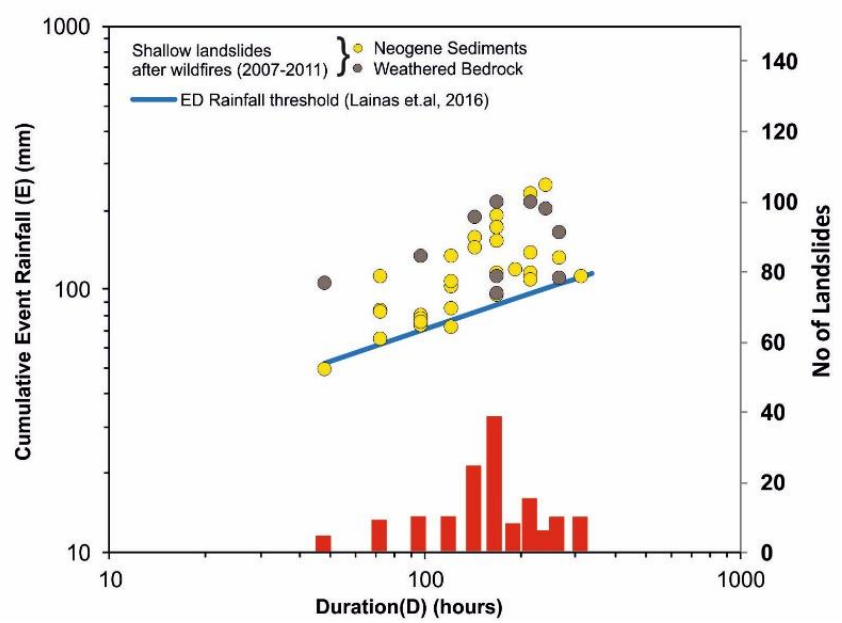

Figure 4. Rainfall threshold for possible shallow landslide trigger in fire affected areas (modified from Lainas et. al., 2016). Post-fire landslides are shown in both Neogene sediments and weathered bedrock along with the landslide distribution in respect to the rainfall duration.

The probability of occurrence of a rainfall-induced landslide can be expressed as the product of the annual probability of the trigger (i.e. the rainfall threshold) and the conditional probability of the slope failure. The conditional probability is defined as the probability of slope failure once the rainfall threshold has been exceeded. If P(A) is the annual probability of the rainfall event exceedance and P(B) is the probability of landslide activation, the landslide probability $P[A \cap B]$ is expressed as (Floris and Bozzano, 2008)

$P[A \cap B] = P(A) \times P[B \mid A]$ [2]

This equation states the probability of occurrence of both events A and B (intersection probability) and is equal to the probability of occurrence of event A multiplied by the probability of occurrence of event B in the condition that event A has already occurred (conditional probability).

P(A) is determined based on the assumption that

$P(A) = P[E > E_{th})$,

where,

$P[E > E_{th}]$ is the annual probability of the rainfall threshold (E_{th}) exceedance, with E_{th} corresponding to the calculated threshold for each rainfall duration class, according to equation (1).

As a result, the return period (T) of each threshold value can be also expressed as

$$T = \frac{1}{P[E>E_{th}),} \quad [3]$$

For the calculation of annual probability P(A) for every rainfall threshold value, all rainfall events during the period 1977-2019 for each duration class between 2 and 13 days were first identified for every meteorological station with associated landslide events.

Following this, P(A) was then calculated by applying the Generalized Extreme Value Distribution Function (GEV) (Gumbel method) to the series of the cumulative rainfall for every rainfall duration class in order to finally obtain the exceedance probability for every rainfall threshold value.

The determination of P[B│A] relied on the landslide frequency after rainfall exceeded the given threshold value for every duration class and the corresponding landslide set. Calculations of the annual probability of landsliding for every rainfall duration class are given in Table 2 and Figure 5 in regard to the classification proposed by Fell (1994). It can be concluded that shallow landslide response in fire-affected areas has higher annual probability for rainfall events with total duration between 6 and 9 days. Furthermore, it can be observed that higher annual probabilities for landslide trigger are observed in the central and easternmost parts of the affected areas. Both aforementioned areas have both similarities and differences in respect to the conditions that may favor landslide trigger.

Table 2: Annual probability estimates and classification of shallow rainfall-induced landslides in terms of the Cumulative Event and Duration (ED) threshold exceedance per rainfall duration class (D).

D (Days)	Eth (mm)	No of landslides	T (years)	(P(A)	P(B|A)	P(A∩B)	Landslide probability classification (Fell, 1994)
2	56.31	2	1.31	0.763	0.763	0.016	Medium
3	66.84	7	1.38	0.725	0.705	0.057	Medium - High
4	75.49	8	1.24	0.806	0.864	0.067	High
5	82.97	8	1.41	0.709	0.709	0.067	High
6	89.62	22	1.00	1.000	0.999	0.18	High
7	95.66	36	1.14	0.877	0.964	0.295	High-Very High
8	101.22	6	1.01	0.990	0.990	0.049	High
9	106.39	13	1.41	0.709	0.776	0.107	High
10	111.24	4	1.04	0.962	0.973	0.033	Medium
11	115.81	8	1.18	0.847	0.719	0.066	Medium - High
13	124.29	8	1.81	0.552	0.552	0.066	Medium

5. Conclusions

This paper presents a methodology for landslide forecasting by applying an empirical rainfall threshold model. Its aims to contribute to the clarification of the role of rainfall in the activation of shallow landslides which have been triggered by heavy rainfall in either natural or excavated slopes within areas that have been previously affected by wildfires. As a study area was selected the Ilia regional unit in Western Greece and the landslide dataset used for this purpose included several well-defined and documented, rainfall-induced shallow landslide occurrences of small extent which were recorded within the fire-affected areas. It has been concluded that shallow landslide response in fire-affected areas with the geological characteristics of the study area (Neogene sediments and weathered bedrock) has higher annual probabilities for rainfall events with a total duration between 6 and 9 days.

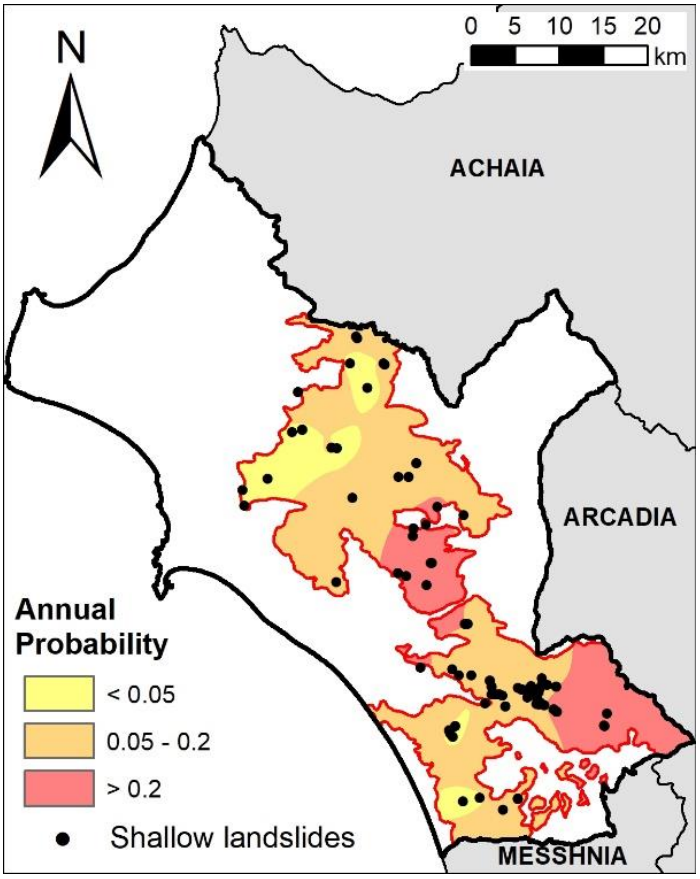

Figure 5. Annual Probability map for shallow landslide trigger in the study area in regards to the classification proposed by Fell (1994).

This research aims to act as a basis for landslide forecasting, especially by pointing landslides triggered by heavy rainfall. The application of the proposed methodology in an area that has previously suffered a significant natural disaster under specific geological and climatic conditions, represents a useful example in the context of rainfall-induced landslide research and it aims to a better understanding of the role of rainfall in the landslide hazard. Finally, it is noted that the outcomes of this research apply to the recorded landslides before remedial works were implemented aiming to investigate the immediate and short-term response of the affected slopes in heavy rainfall. The effects of the landslide remedial works in the affected areas represents a task of further research which is in progress by the authors.

References

Aleotti, P., Baldelli. P., Bellardone, G., Quaranta, N., Tresso, F., Troisi, C., Zani, A. (2002). Soil slips triggered by October 13–16, 2000 flooding event in the Piedmont Region (Northwest Italy): critical analysis of rainfall data. Geologia Tecnica e Ambientale, 1, pp.15–25.

Alleoti, P. (2004). A warning system for rainfall-induced shallow failures. Bulletin of Engineering Geology, 73, pp. 247-265.

Bonneau, M. (1984). Correlation of the Hellenide nappes in the southeast Aegean and their tectonic reconstruction. Dixon, J.E. and Robertson, A.H.F. (eds). The geological evolution of the Eastern Mediterranean, Geological Society of America, Special Publication, (17), pp.517–527.

Cruden, D.M, Varnes, D. J. (1996). Landslide types and processes. Turner, A.K., Shuster, R.L. (eds). Landslides: Investigation and Mitigation, Transportation Research Board, U.S. National Academy of Sciences, Special Report (247), pp.36–75.

Depountis, N., Lainas, S., Pyrgakis, D., Sabatakakis, N., Koukis G. (2010). Engineering Geological and geotechnical investigation of landslide events in wildfire affected areas of Ilia Prefecture, Western Greece. Proceedings of the 12th International Congress of the Geological Society of Greece, Bulletin of the Geological Society of Greece, (3), pp.1138-1148. Patras, Greece.

Depountis, N., Vidali, M., Kavoura, K., Sabatakakis, N. (2018). Soil erosion prediction at the water reservoir's basin of Pineios dam, Western Greece, using the Revised Universal Soil Loss Equation (RUSLE) and GIS. WSEAS Transactions on Environment and Development (14), pp.457–463.

Depountis, N., Michalopoulou, M., Kavoura, K., Nikolakopoulos, K., Sabatakakis N. (2021). Estimating Soil Erosion Rate Changes in Areas Affected by Wildfires. International Journal of Geoinformation, 9(10), pp.562.

Farina, P., Catani, F., Rosi, A., Setiawan, I., Junaidi, A., Afrizal, K., & Wijayanto, A. (2020). Development of an early warning system for shallow landslide hazard in the Grasberg area, Indonesia. May, pp.1425–1438.

Floris, M., Bozzano ,F. (2008) .Evaluation of landslide reactivation: A modified rainfall threshold model based on historical records of rainfall and landslides. Geomorphology, (94), pp. 40-57.

Gostelow, P. (1991). Rainfall and landslides, Prevention and Control of Landslides and Other Mass Movements, Almeida-Teixeira, M.E., Fantechi, R., Gomes Coelho, A., (Eds), Commission European Communities, Brussels, Belgium, pp. 139–161.

Koukis, G. (2008). Geological and Geotechnical Investigations in fire-affected municipalities of Ilia State for the reconnaissance and remediation of post-fire landslides - Design of landslide remedial measures. Scientific Research Project, Region of Western Greece, Patras, Greece (in Greek).

Koukis, G., Sabatakakis, N., Lainas, S., Depountis, N., Skias, S. (2010). Engineering geological investigation of heavy rainfall induced landslides in wildfire affected areas, western Greece. Proceedings of the 11th IAEG Congress, Geologically Active, Williams et al. (Eds), pp. 331–338, Auckland, New Zealand.

Lainas, S., Sabatakakis, N. and Koukis, G. (2016). Rainfall thresholds for possible landslide initiation in wildfire-affected areas of western Greece. Bulletin of Engineering Geology and the Environment, 75(3), pp.883-896.

Meyer, G.A. (2002). Fire in western conifer forests–geomorphic and ecologic processes and climatic drivers. Geological Society of America, Abstracts with Programs, (34), p.46.

Morton, D.M. (1989). Distribution and frequency of storm-generated soil slips on burned and unburned slopes, San Timoteo Badlands, Southern California. Sadler, P. M. and Morton, DM (Eds), Landslides in a Semi-Arid Environment with Emphasis on the Inland Valleys of Southern California, Publications of the Inland Geological Society, (2), pp. 279-284.

Naidu, S., & Oommen, T. (2017). Early warning system for shallow landslides using rainfall threshold and slope stability analysis, (9), pp.1871–1882.

Rozos, D., Georgiadis, P., Leivaditi, A., Kyrousis, I., Marinos, P., Rondoyanni, Th., Tsiambaos, G., Lykoudi, E., Markantonis, K., Tsangaratos, P. (2008). Engineering geological consideration of the wildfire site of Zacharo municipality, Peloponnesus Greece, Meeting of pilot approach for the reconstruction of wildfire areas, 12pp. NTUA, Athens, Greece (in Greek).

Sabatakakis, N., Koukis, G., Vassiliades, E., Lainas, S. (2013). Landslide susceptibility zonation in Greece. Natural Hazards, 65(1), pp.523 – 543.

Sabatakakis, N., Koukis, G., Mourtas, D. (2005). Composite landslides induced by heavy rainfalls in suburban areas of City of Patras and surrounding area, western Greece, Landslides, (2), pp202 – 211.

Valenzuela, P., Zêzere, J. L., Domínguez-Cuesta, M. J., Mora García, M. A. (2019). Empirical rainfall thresholds for the triggering of landslides in Asturias (NW Spain). Landslides, 16(7), pp.1285–1300.

Rock mass characterisation for rock slope instabilities using aerial photogrammetry and 3D Point Cloud Model interpretation

Charalampos Saroglou[1], Deheng Kong[2], Faquan Wu[2,3], Vassilis Kallimogiannis[1], Athina Tsirogianni[1] & Neil Bar[4]

[1]*National Technical University of Athens, Athens, Greece000*
saroglou@central.ntua.gr

[2]*Department of Geotechnical Engineering, College of Civil Engineering, Tongji University, Shanghai 200092, China*
kongdeheng@tongji.edu.cn

[3]*Key Laboratory of Rock Mechanics and Geohazards of Zhejiang Province, Shaoxing University, Shaoxing 312000, China;*
shapeng@usx.edu.cn

[4]*Gecko Geotechnics, Cairns, Australia*
neil@geckogeotech.com

ABSTRACT: In the current paper, a methodology of rock mass characterisation of rock slope instabilities using aerial photogrammetry and 3D point cloud model interpretation, is presented. The methodology is demonstrated through a case study, where a large rock slope instability occurred in 2019 leading to a rockfall with total volume of the detached rock blocks of 1000m3. To characterise the rock slope failure, field mapping was performed with measurement of discontinuity characteristics and rock mass properties. Additionally, UAV photogrammetry was utilized to assess the properties of the discontinuities obtained through automatic identification algorithms. Using the 3D point cloud model, the discontinuity pattern and the rock block distribution on the failed slope was defined. These were used to accurately determine the geometry of the slope failure and potential rock block sources of future instabilities.

Keywords: Rock mass, Point cloud model, slope, rockfall

1. Introduction

Techniques such as terrestrial laser scanning (TLS) and digital terrestrial photogrammetry (DTP) for rock mass characterisation are increasingly being used in the last two decades. TLS and DTP allow accurate representation of rock outcrops by means of 3D textured point clouds and interpolated models.A limitation of terrestrial remote sensing is related to the survey of high slopes and complex morphologies where the site of acquisition, generally at the bottom of the slopes, results in omitted zonesand shadows in the output data where no line-of-sight was available. Such limitation can however be overcome using aerial reconnaissance, from which high-detail images can be acquired from multiple angles for high and steep slopes.

In the current paper, a methodology of rock mass characterisation of rock slope instabilities using aerial photogrammetry and 3D point cloud model interpretation, is presented. The methodology is demonstrated through a case study in Greece, where a large rock slope instability occurred in 2019 leading to a rockfall with total volume of the detached rock blocks of 1000m^3.

2. Rock mass characterisation for rock slope instabilities

Aerial reconnaissance using UAV is routinely used to inspect and study unstable or failed slopes in bothcivil and mining engineering applications. High resolution imagery and video are captured while ensuring the engineer remains at a safe distance from potential rock falls or unstable zones (Bar et al., 2020). Digital surface models (DSMs), orthophotos and three-dimensional (3D) models derived from processed UAV images allow accurate mapping of joint geometries and their degree of uncertainty (Salvini et al., 2017).

Several commercial software packages are available for modern photogrammetry (e.g., ShapeMetriX, Agisoft, Pix4D). All work in a similar way and provide comparable DSM results. Software such as ShapeMetriX and Gem4D have functionality that enables an engineer or geologist to map the location and orientation of geological features.

An accurate understanding of block geometry is critical in different rock slope engineering applications such as stability evaluation and support design of slopes or excavations in jointed rock masses (Dong et al., 2020) and rockfall barrier design (Umili et al., 2020). Ruiz-Carulla and Corominas (2020) established a rockfall fractal fragmentation model (RFFM) for the transformation of the in-situ block sizedistribution (IBSD) into the resultant rockfall block size distribution (RBSD), to predict the change in block volume distribution and increase of the number of blocks by fragmentation.

The size, shape, and spatial distribution of rock blocks have a significant impact on the engineering properties of rock masses (Kim et al., 2006) and the failure scale and mode in most natural rock collapse hazards (Mavrouli et al., 2015). Kong et al. (2021) developed a semi-automatic procedure, in which several mathematical algorithms were designed and programmed for discontinuity interpretation and block characterization. The procedure is based on the point cloud model and the deterministic discontinuity network on rock exposures (PCM-DDN) to extract the in-situ rock blocks on a slope. The flow chart of methodology is illustrated in Figure 1.

As the PCM of rock outcrop surfaces usually contain large-size waviness and small-size roughness, theraw point cloud is directly employed in PCM-DDN method without meshing which will cause irregularities at these uneven surfaces. The Nesti-Net algorithm (Ben-Shabat et al., 2019) is applied first for the normal vector estimation using convolutional neural networks (CNNs). The related orientations of eachpoint are plotted in stereographic projection, and clustered by the fuzzy k-means algorithm. The main discontinuity sets are classified, and every single spatial cluster of joint surfaces can be identified basedon density-based spatial clustering of applications with noise (DBSCAN) method (Schubert et al., 2017).The visual inspection is performed manually to reduce errors at this step.

Then, a global search of block candidates is conducted as follows: (1) intersecting discontinuities group,

(2) block vertex detection, and (3) block candidate extraction. The random sample consensus (RANSAC) algorithm (Fischler, et al., 1981) was applied for executing plane fitting of respective joints. The polyhedral modelling including all vertices, edges and faces can be established from mutual intersections of these planes. One principal issue of PCM-DDN method is that there are inevitably someparts of blocks invisible from rock exposures. Usually, a logical extension of existing joint planes can bemade into rock mass to form 3D block geometry. For some special cases, artificial planes are needed to generate blocks based on field conditions and the geological expertise of researchers. A multi- dimensional block indicator system for systematic block characterization, i.e., in-situ block size distribution (IBSD), block shape distribution (BSD), and block orientation distribution (BOD), is calculated, and the exposed block spatial distribution (EBSD) is mapped. More details can be found in the original paper (Kong et al., 2021).

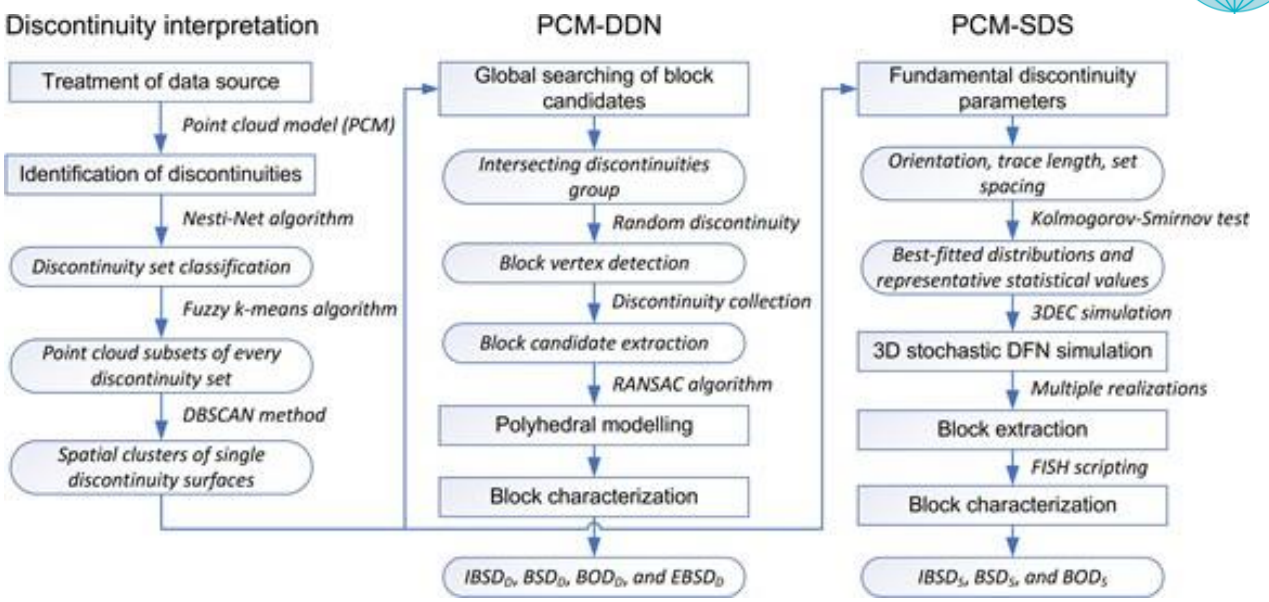

Figure 1. Flow chart of PCM-DDN method (Kong et al., 2021)

3. Case study: Engineering geological and rock mass conditions

The case study is a limestone rock slope, located in Voiotia prefecture in Greece (shown in Figure 2), where a failure occurred in 2019. The rockfall event was triggered by intense rainfall and has affected the adjacent house settlement at the base of the slope and put in risk the structural integrity of an archaeological site founded on the slope crest. The total volume of the detached rock blocks reached approximately 1000 m^3 and the largest blocks were up to 50 m^3. The size distribution of the fallen blockswas directly controlled by the spacing of the main discontinuity sets. The majority of the fallen blocks has volume smaller than 50 m^3. Very few blocks have volume up to 150 - 250 m^3.

The steep slope was found to be unstable well before the failure occurred, as an open tensile crack, filled with clay, existed parallel to the slope. The main triggering factor of the instability was the continued rainfall prior to the event (75mm in 4 days). The total precipitation in the previous month was 190mm, which was the maximum mean monthly rate that has been recorded in the past 13 years.

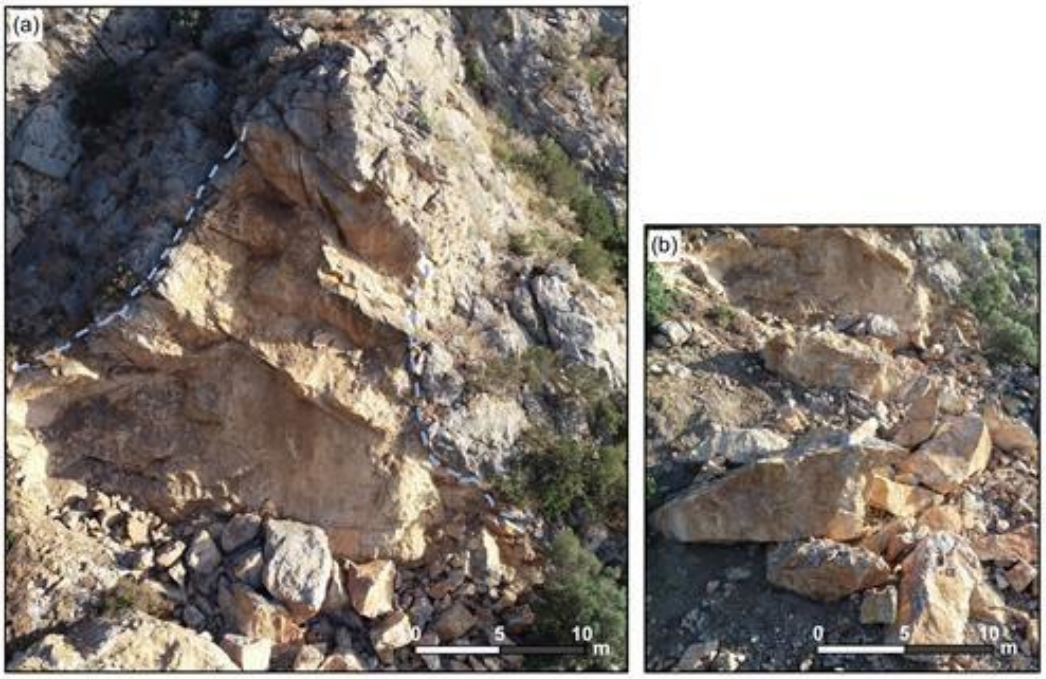

Figure 2. a) View of the failed rock slope, b) view of fallen blocks

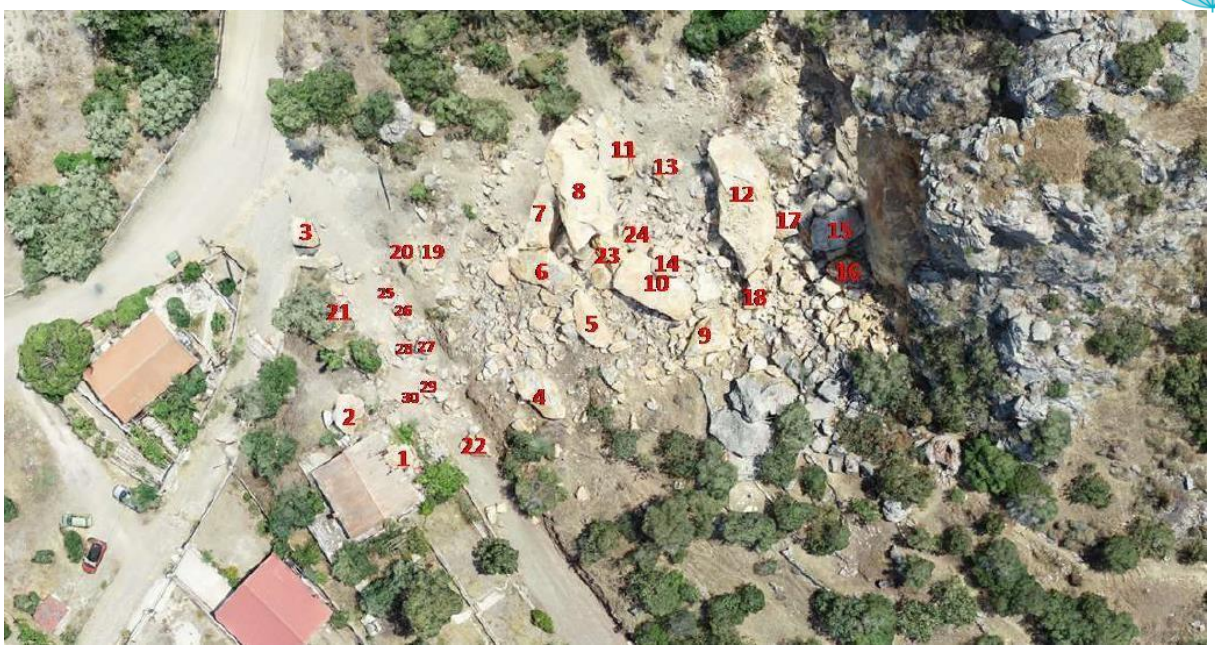

Figure 2. c) Plan view with count of most significant fallen blocks.

In the study area, the limestone is underlain by a schist – chert formation, approximately at the base ofthe slope (Figure 3). The steep slope is intersected by a fault dipping at 70^0 towards it, which is encountered 5 m upslope and parallel to the slope face, controlling the overall stability. The area belongsto the very seismically prone region of northern Corinthian golf, in which earthquakes with a magnitudeof Mw = 6 to 7 Richter have occurred in the past. The limestone is intersected by three to four discontinuity sets, moderately fractured, resulting in a blocky to very blocky rock mass (GSI = 55-65). The discontinuity surfaces are moderately weathered, open to very open, partially filled with clay. The tensile cracks are open (approx. 20cm) and filled with clay material.

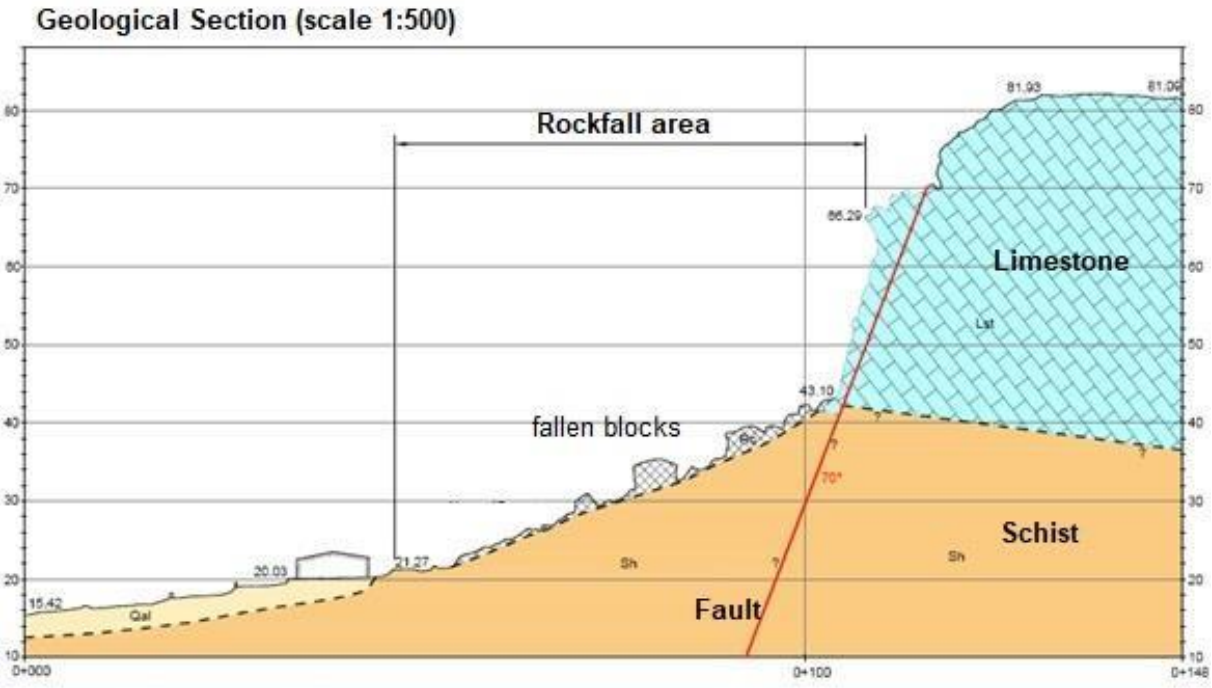

Figure 3. Engineering geological section of the study area.

4. Automatic detection of discontinuities for slope stability

Due to the high risk of instabilities in the rock failure area, the orientation and traces of discontinuity planes were obtained using automatic detection from point clouds and Structure from Motion technique(Gaich & Potsch, 2015; Saroglou et al. 2019). Discontinuities were then mapped deterministically in detail. For comparison, a traditional survey was only performed in the accessible and relatively secure areas of the slope. Photographs were taken close to the slope and a dense three-dimensional (3D) pointcloud was obtained through image processing to rebuild the slope geometry. Figure 4 illustrates the 3DDSM generated from over 100 photographs captured using a 9 millimeter digital camera mounted on aDJI Phantom 4 drone overlain with mapped geological structures in the failure area. The model computed in less than 30 minutes on a mobile workstation (*2017 Alienware 17 R4*). It consists of over 2million surface points and has a ground sample distance (GSD) of 5 centimeters per pixel.

ShapeMetriX software (3GSM GmbH) has been used to generate the DSM and map the location, orientation and length or surface area of visible discontinuities. ShapeMetriX software allows direct analysis of geometric entities such as volumes, areas, distances, sections, and the measurement of point coordinates. A total of 197 orientations, traces and surface areas were interpreted are shown in Figure 4. The stereographic projection of the interpreted discontinuities is presented in Figure 5a and includes four major, and four minor sets.

The mechanism of failure was controlled by the steep morphology, the open tensile crack (set J5) parallel to the slope filled with clay and the main discontinuity (set J1) dipping opposite to the slope at an angle of 64^0 (Figure 6a). The volume distribution of the most significant fallen blocks captured in Figure 2c is presented in Figure 6b. Most of the blocks (40%) have volume less than 10 m^3, which resulted from the breaking of larger blocks into smaller ones. A significant percentage of fallen blocks (25%) have volume greater than 30 m^3, which is controlled by the high persistence of the main discontinuity sets. Two of the biggest blocks have a volume of 195 and 211 m^3. The slope is still in a marginally stable condition. An open tensile crack exists parallel to the slope at 15 m, which creates unfavorable conditions for a future instability.

For this purpose, it was considered important to determine the rock block characteristics of post-failureslope using the PCM-DDN method. Pix4Dmapper was utilized in this study and the key points were generated from all the images acquired from UAV photogrammetry by the feature matching algorithm (SIFT, scale-invariant feature transform). Then, a sparse (low-density) point cloud was created by employing the bundle adjustment system. A final dense point cloud model (PCM) was constructed usingmulti-view stereo (MVS) algorithms.

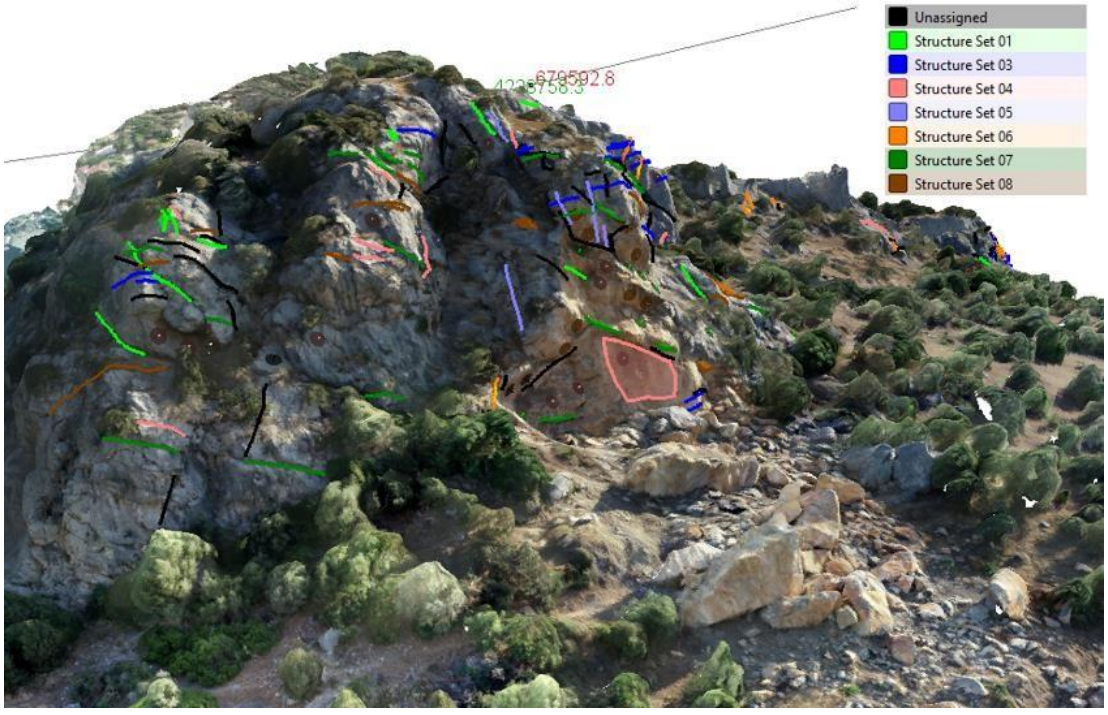

Figure 4. 3D DSM and mapped geological structures from UAV photogrammetry (ShapeMetriX software)

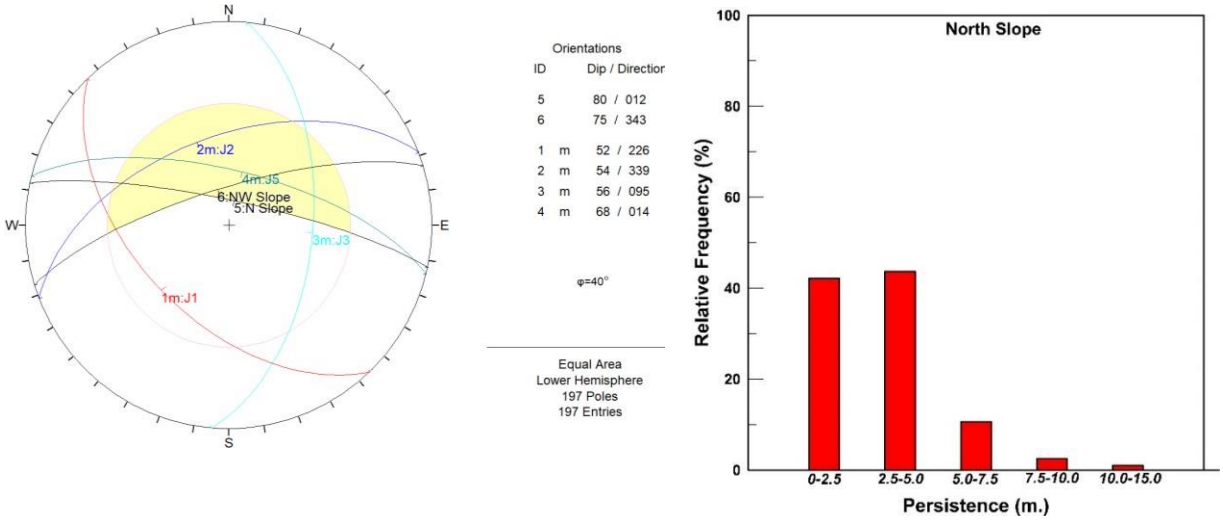

Figure 5: Stereographic projection from a) interpretation in ShapeMetriX b) Relative frequency distribution of discontinuities' persistence in North slope

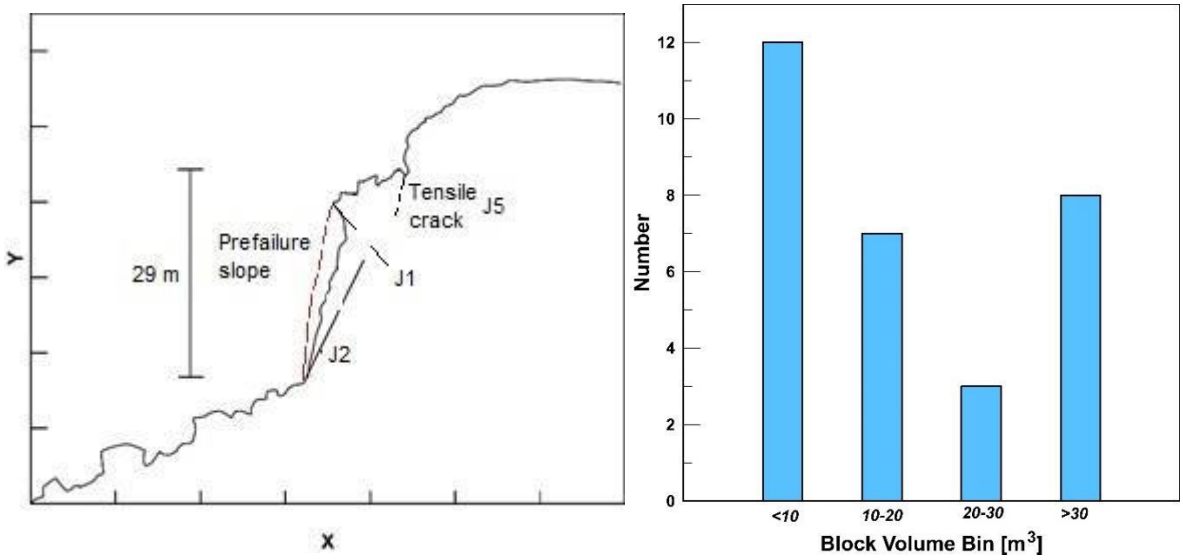

Figure 6: a) Failure mechanism of slope b) Block volume distribution of fallen rock blocks.

5. Rock mass characterisation using PCM-DDN

The PCM-DDN methodology was applied on the post-failure slope to determine the block characteristicsof the rock mass, as shown in Figure 7a. The blocks formed by the main discontinuity sets are exposedafter the previous rockfall activity and these extracted blocks on the upper parts of the slope can be potential rockfall sources in the future. The volume of approximately half of these blocks is at the rangeof 10 - 20 m^3 (Figure 7b), while the average volume is 22.96 m^3, and the maximum volume is 78.51 m^3.

The blocks mainly have an elongated shape due to the pervasive nature of the joint set dipping towardsthe slope (Figure 7c and d). The result of application of the PCM-DDN are as expected.

A comparison by visual investigation of the volume distribution and shape of the blocks on the slope with those which have fallen previously was performed (Figure 6b). This comparison shows most of the extracted blocks

and the previous fallen blocks have the same elongated shape, which indicates the main discontinuity set (J5) controls not only the overall slope stability but also the shape of major blocks.

Regarding the block size comparison, the statistical distribution of fallen blocks presents, as expected, a higher proportion of small-size blocks (with a range of 0 - 10 m^3), since these are formed by the breaking up of the larger blocks encountered on the slope (with a range of 10 - 20 m^3).

Most of extracted blocks are bounded and detached by pre-existing joint surfaces. The increase in blocksize distribution of fallen blocks (also called rockfall block size distribution, RBSD) reflects the fragmentation and disaggregation of initial blocks during the rockfall event and impact on the ground. This transition from IBSD to RBSD invariably leads to a decreasing of the block volume, and simultaneously, reduces the kinetic energy of individual blocks. This relationship is quite essential to beincorporated into rockfall trajectory simulation, risk assessment and barrier design in the future (Ruiz- Carulla and Corominas 2020).

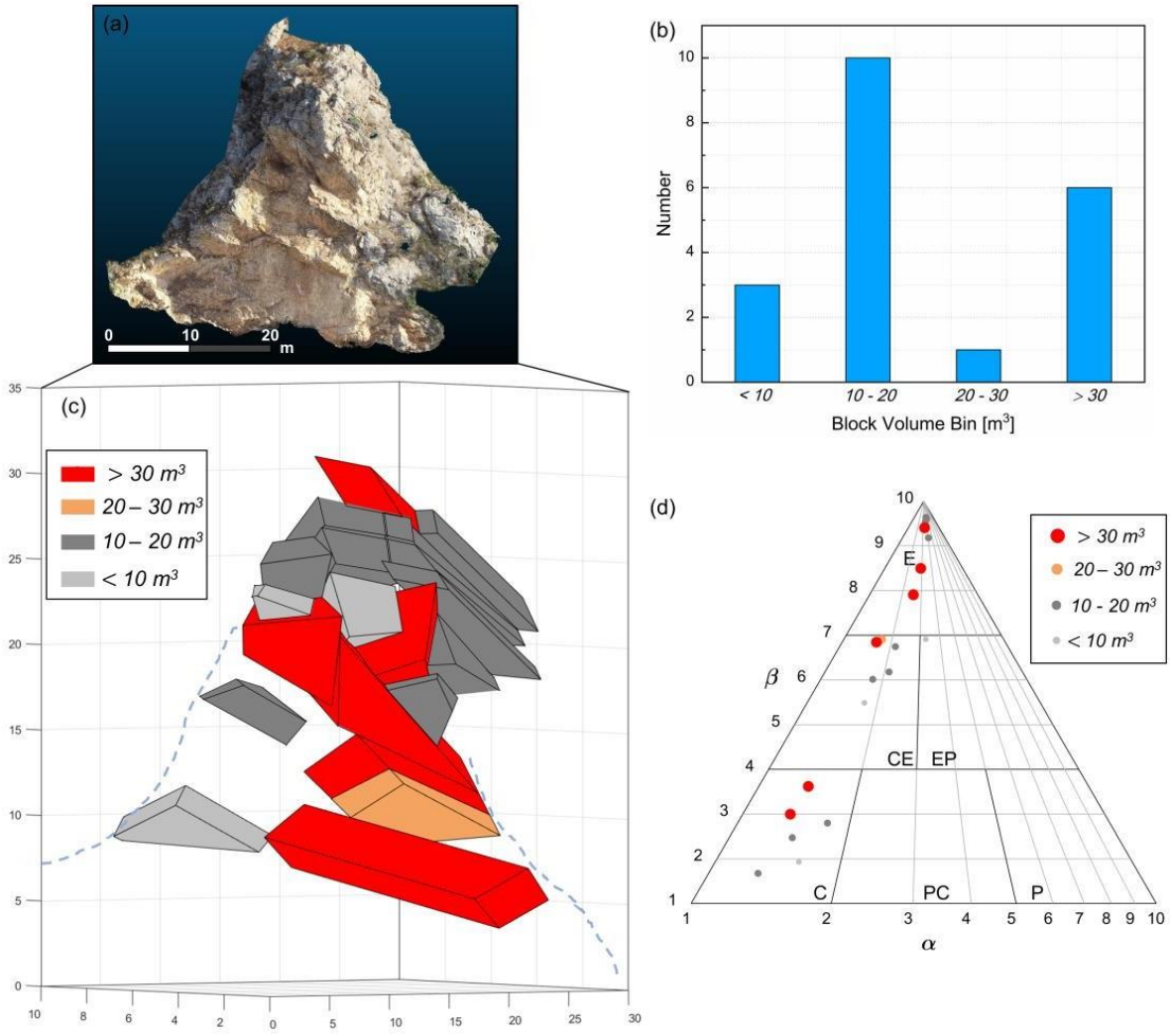

Figure 7. (a) PCM of the rockfall site, Greece. (b) Block volume distribution of extracted rock blocks. (c) The EBSDD of rock blocks extracted from PCM-DDN. (d) The block shape distribution from PCM-DDN.

6. Conclusions

Modern photogrammetric systems are advantageous in producing detailed orthophotos as they allow accurate mapping in areas difficult to access which is one of the main limitations of traditionaltechniques. Other advantages of using UAV systems in the study of rock slope stability are linked to thepossible acquisition of multi-temporal data and the ability to update data frequently, and rapidly. The results highlight the benefits of integrating photogrammetric data with those collected through classicalmethods: the resulting knowledge of the site is crucially important in stability analyses.

However, field mapping is essential since it is not possible to reliably estimate discontinuity properties and rock mass structure only based on remote sensing data.

In the present paper, a methodology of rock mass characterisation using aerial photogrammetry and 3Dpoint cloud model interpretation, was presented using a case study, where a large rock slope instabilityoccurred in 2019 leading to a rockfall with total volume of the detached rock blocks of 1000m^3.

Due to the high risk of instabilities in the rock failure area, the orientation and traces of discontinuity planes were obtained using automatic detection from point clouds and Structure from Motion technique.Additionally, the PCM-DDN method was used to determine the rock block characteristics of the post-failure slope and compare their block volume characteristics with the block size distribution of the fallenblocks. The results from this comparison led to the determination of the transition from IBSD to RBSD which led to a decrease of the block volume distribution.

Acknowledgements

The first author would like to thank the Ministry of Culture (Ephoria of Voiotia) and Giannis Manousakisfrom ElxisGroup SA who has performed the UAV aerial mapping for the study area.

References

Bar N, Kostadinovski M., Tucker M., Byng G., Rachmatullah R., Maldonado A., Pötsch M., Gaich A., McQuillan A., Yacoub T.,2020, Rapid and robust slope failure appraisal using aerial photogrammetry and 3D slope stability models. Int. Journal of Mining Science and Technology 30,651–658.

Dong, X.; Xu, Q.; Huang, R.; Liu, Q.; Kieffer, D.S., 2020, Reconstruction of Surficial Rock Blocks by Means of Rock Structure Modelling of 3D TLS Point Clouds: The 2013 Long-Chang Rockfall. Rock Mech. Rock Eng., 53, 671–689, doi:10.1007/s00603-019-01935-0.

Gaich, A., Potsch, M.,2019, 3D images for data collection in tunnelling - applications and latest developments. Geomechanik und Tunnelbau 8(6):581-588.

Kim, B.H.; Cai, M.; Kaiser, P.K.; Yang, H.S., 2006, Estimation of Block Sizes for Rock Masses with Non-persistent Joints. Rock Mech. Rock Eng., 40, 169, doi:10.1007/s00603-006-0093-8.

Kluckner, A.; Söllner, P.; Schubert, W.; Pötsch, M., 2015, Estimation of the in-situ Block Size in Jointed Rock Masses using Three-Dimensional Block Simulations and Discontinuity Measurements. In Proceedings of the 13th ISRM International Congress of Rock Mechanics, Montreal, Canada, 10–13 May 2015.

Kong, D.; Saroglou, C.; Wu, F.; Sha, P.; Li, B., 2021, Development and application of UAV-SfM photogrammetry for quantitative characterization of rock mass discontinuities. Int. J. Rock Mech. Min. Sci., 141, 104729, doi: 10.1016/j.ijrmms.2021.104729.

Kong D., Wu F., Saroglou C., Sha P., Li B.,2021, In-situ Block Characterization of Jointed Rock Exposures Based on a 3D Point Cloud Model. Remote Sensing. MDPI.

Kong, D.; Wu, F.; Saroglou, C., 2020, Automatic identification and characterization of discontinuities in rock masses from 3D point clouds. Eng. Geol., doi:10.1016/j.enggeo.2019.105442.

Lato, M.; Diederichs, M.S.; Hutchinson, D.J.; Harrap, R., 2009, Optimization of LiDAR scanning and processing for automated structural evaluation of discontinuities in rockmasses. Int. J. Rock Mech. Min. Sci., 46, 194–199, doi:10.1016/j.ijrmms.2008.04.007.

Macciotta, R.; Gräpel, C.; Skirrow, R., 2020, Fragmented rockfall volume distribution from photogrammetry-based structural mapping and discrete fracture networks. Appl. Sci., 10, 6977; doi:10.3390/app10196977.

Mavrouli, O.; Corominas, J.; Jaboyedoff, M.,2015, Size Distribution for Potentially Unstable Rock Masses and In Situ Rock Blocks Using LIDAR-Generated Digital Elevation Models. Rock Mech. Rock Eng., 48, 1589–1604, doi:10.1007/s00603-014-0647-0.

Riquelme, A.J.; Abellán, A.; Tomás, R.; Jaboyedoff, M., 2014, A new approach for semi-automatic rock mass joints recognition from 3D point clouds. Comput. Geosci., 68, 38–52, doi:10.1016/j.cageo.2014.03.014.

Ruiz-Carulla, R.; Corominas, J., 2020), Analysis of Rockfalls by Means of a Fractal Fragmentation Model. Rock Mech. Rock Eng., 53, 1433–1455; doi:10.1007/s00603-019-01987-2.

Salvini R., Mastrorocco G., Seddaiu M., Rossi D., Vanneschi C., 2017, The use of an unmanned aerial vehicle for fracture mapping within a marble quarry (Carrara, Italy): photogrammetry and discrete fracture network modelling, Geomatics, Natural Hazards and Risk, 8:1, 34-52, DOI: 10.1080/19475705.2016.1199053.

Saroglou, C., Kallimogiannis, V., Bar, N., Manousakis, G., Zekkos, D., 2019, Analysis of slope instabilities in the Corinth Canal using UAV-enabled mapping. In Proc. ICONHIC 2019: 2nd International Conference on Natural Hazards & Infrastructure.

Umili, G.; Bonetto, S.M.R.; Mosca, P.; Vagnon, F.; Ferrero, A.M., 2020, In Situ Block Size Distribution Aimed at the Choice of the Design Block for Rockfall Barriers Design: A Case Study along Gardesana Road. Geosciences, 10, 223.

THEME 8 - ENGINEERING GEOLOGY AND CULTURAL HERITAGE PROTECTION

Profiling of the recent deposits of Nafplio coastal plain (Greece) from engineering geological modelling and geophysical surveys

Charalampos Saroglou[1], Francesca Bozzano[2], Salvatore Martino[2], Aggelos Mouzakiotis[3], Vassilis Karastathis[3], Athina Tsirogianni[1], Benedetta Antonielli[2], Paolo Ciampi[2], Matteo Fiorucci[2], Roberto Iannucci[2], Daniele Inciocchi[2], Charilaos Maniatakis[1], Stefano Rivellino[2], Andreas Antoniou[1], Achilleas Papadimitriou[1], Renzo Carlucci[4] & Alessio Di Iorio[4]

[1]*National Technical University of Athens, Athens, Greece*

saroglou@central.ntua.gr, apapad@civil.ntua.gr, andreasan19@yahoo.com

[2]*Sapienza Università di Roma, Rome, Italy*

francesca.bozzano@uniroma1.it, salvatore.martino@uniroma1.it, benedetta.antonielli@uniroma1.it, paolo.ciampi@uniroma1.it, matteo.fiorucci@uniroma1.it, roberto.iannucci@uniroma1.it, inciocchi.1702351@studenti.uniroma1.it, stefano.rivellino@uniroma1.it

[3]*Geodynamic Institute of Athens, Athens, Greece*

aggelmo@noa.gr, karastathis@noa.gr

[4]*Alma Sistemi S.r.l.*

rca@alma-sistemi.com, adi@alma-sistemi.com

ABSTRACT: In the current paper, some preliminary results from the research performed in the EU funded project “STABLE: Structural Stability risk assessment”, which aims to develop a methodology and tools to determine the seismic vulnerability of buildings in historical centres, are presented. The area of the historical centre of Nafplio was selected as case-study since it is one of the most important historical centers in Greece and a not negligible local seismic response may be expected based on the geological and geomorphological setting. The geological - geotechnical conditions in the study area were collected and evaluated and a geological model was identified. For this study, seismic noise measurements have been performed in the coastal plain where the town is built and processed with output resonance varying from 1 Hz up to 5 Hz, moving from the coastline towards the Acronafplia ridge. The results will be used to perform a structural stability analysis of the historical buildings using a simplified approach for specific earthquake scenarios in the future.

Keywords: engineering-geological model, geophysical investigation, local seismic response, Nafplio.

1. Introduction

The paper presents results from research performed in the EU funded project “Stable: Structural Stability risk assessment”, which aims to develop a methodology and tools to determine the seismic vulnerability of buildings in historical centres. In this context, the engineering geological conditions and seismic response of

the ground in the historical centre of Nafplio is studied. For this purpose, relevant geological and geotechnical data have been collected, the seismotectonic conditions and the local seismicity has been studied and geophysical investigations have been performed in the field. The preliminary results of the study and a discussion on the main findings are presented.

2. Engineering geological model

From a geomorphological point of view, the study area is characterized by the mountainous landscape prevailing in the south and the flat landscape dominating to the north. The prominent topographic features are the Palamidi hill on the southeast (223 m), the Acronafplia peninsula (85 m) on the south and the Bourtzi island 600m NW from the harbour (Figure 1). The north slopes of Acronafplia present a relatively low angle. On the contrary, the northwestern and the southern slopes of Acronafplia are very steep. The altitude in the area where the old and the new city extend, varies from 0.50 m in the plain area to 60 m on Palamidi slopes.

To better understand the geological and engineering-geological features, geological and geophysical field surveys were integrated with previously available data.

A seismic reflection campaign was carried out by the Hellenic Survey of Geology & Mineral Exploration (HSGME) in 2006. HSGME also conducted a series of seismic reflection surveys, electrical resistivity tomography (ERT), boreholes with associated crosshole analysis in the coastal area and in the mainland with the aim of detecting the depth of the bedrock and the possible presence of tectonic elements (Apostolidis & Koutsouveli, 2010). Furthermore, 21 boreholes were drilled from various contractors (Triton SA, 2003, 2017) both in the sea and in the mainland to determine the thickness of recent soft-soil deposits and the depth of the bedrock. The stratigraphy obtained is consistent in the geotechnical investigations.

Figure 1. Satellite view of the Nafplio historical centre, harbour and modern town

Geological and engineering-geological surveys were directly conducted in the field during 2020 to provide a detailed geological model that is functional to reconstruct the local seismic response model of the study area. The results revealed that Acronafplia peninsula composes of limestone bedrock (Cretaceous), except for the SW side in which conglomerates (of Pleistocene age) outcrop. The latter are heavily eroded by the marine action on the coast, with the consequent retreat of the coastline. In this area, metric to decimetric limestone blocks are evident, which have fallen from the slope above and testify the high susceptibility of the southern slope to evolve due to rock fall phenomena. Palamidi hill is composed of limestone (Cretaceous), affected by the presence of a NW-verging thrust and an inverted stratigraphic series. In the thrust footwall, corresponding to the connection area between Palamidi and Acronafplia reliefs, the bedrock is composed from intensely fractured limestone (Cretaceous) and clayey-marly flysch (Upper Cretaceous-Eocene). It is also evident that, from west to east, there is a repetition of the outcropping formations with the identification of calcite steps that suggest the presence of a fold in the footwall and of a normal fault that lowers the western sector (Acronafplia peninsula). The northern slope of the Palamidi hill is also characterized by the presence of Pleistocene gravels and breccias, that surround its base, in erosional unconformity with the underlying Eocene flysch. The base of the slope is also characterized by the presence of limestone blocks placed above the breccias, testifying active rock fall phenomena. The flat landscape of the Nafplio historical and modern city is characterized by recent soft soil materials and man-made ground (Sabatakakis & Koukis, 2010).

The combination of information deriving from previous data and field surveys has allowed to reconstruct nine detailed engineering-geological sections and an engineering-geological chart that highlighted the presence of three main geological units: bedrock, recent soft soil materials, man-made ground (Figure 2). Furthermore, to perform future numerical modelling for local seismic response analysis, the characteristic geotechnical parameters were attributed to each geological unit defined in terms of natural weight per unit volume, shear stiffness and damping properties (G/G0 and D% curves) and seismic wave velocity.

3. Seismotectonic context and local seismicity

The area of Nafplio demonstrates a vertical diversity consisting of the slab of the Hellenic subduction zone and the Aegean plate on top of it. The subduction of the African plate lies several tenths of kilometres under the study area producing earthquakes of intermediate, mostly, depth. Like seismological and geodetic data suggest, the overriding Aegean plate is stretched in a N-S direction in the Gulf of Corinth, and changes in a E-W direction while moving southwards to the South Peloponnesus.

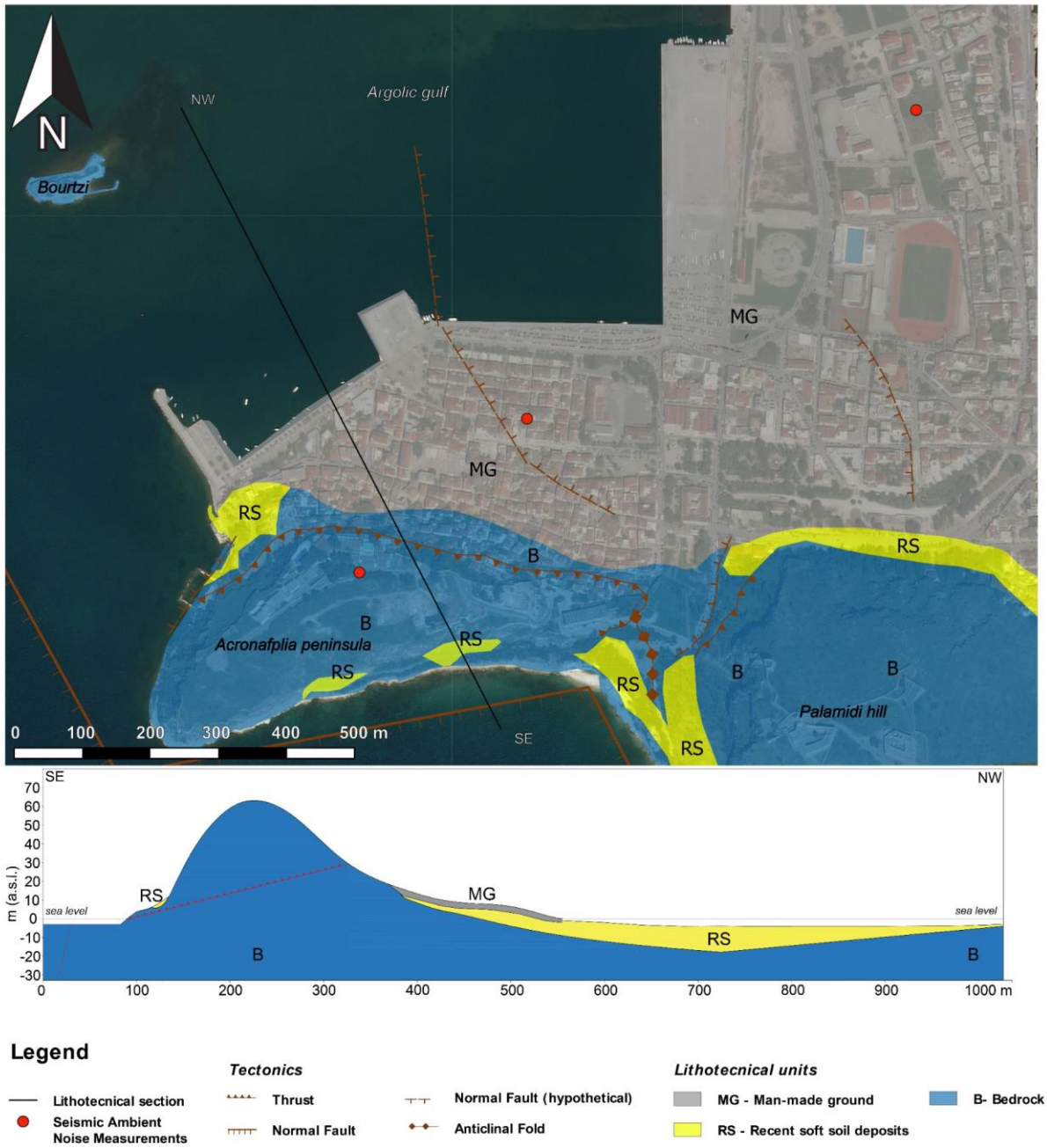

Figure 2. Engineering-geological map and simplified geological section of Nafplio study area.

Seismic activity in the broader region in historical times is characterized by several events with proposed magnitudes >M6 (Figure 3a), according to the earthquake catalogue of Papazachos & Papazachou (2003). The occurrence of many of these events, as well as their possible location and magnitudes are highly debated, since they are based on historical observations, rather than actual recorded data (Ambraseys, 2009). Despite this fact, most of these events have been associated with known regional fault zones. The most notable of them are:

- The Xylokastro fault zone (e.g., Ferentinos et al., 1988; Armijo et al., 1996), located in the southeastern coast of the Gulf of Corinth and associated with a M6.7 event that occurred in 1742, as well as several other events with magnitudes of M6.0.

- The Athikia and Kechriae fault zones, south of the Corinth canal (e.g., Goldsworthy & Jackson, 2001; Roberts et al., 2011), possibly related to the M6.5 event of 1858.
- The Iria and Epidaurus fault zones to the east of the city of Nafplio (e.g., Papazachos & Papazachou, 2003; Karakaisis et al., 2010) which are the most probable candidates for the strong M6.4 event of 1769, as well as several others in their region, shown in Figure 3a. Both these faults are provided by Papazachos & Papazachou (2003) as linear sources, since they are based only on proposed focal mechanisms in combination with scaling laws relating their length with the proposed magnitudes.
- The Tyros fault to the south of the study area (e.g. Papanikolaou et al., 1988), with a highly debatable activity however. Also presented as alinear source in Figure 3a, since no detailed information about its characteristics is available.

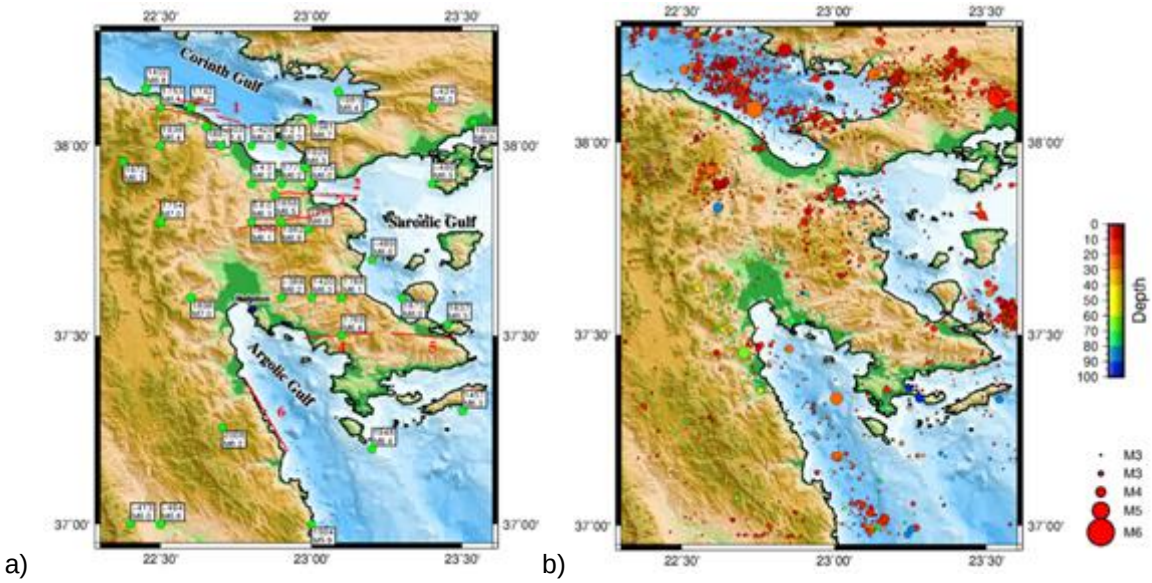

Figure 3. a) historical seismicity according to Papazachos & Papazachou (2003) and most notable faults in the broader area of Nafplio (1: Xylokastro fault zone, 2: Kechriai fault, 3: Athikia fault zone, 4: Iria fault, 5: Epidaurus fault and 6: Tyros fault) and b) modern seismicity in the as recorded by NOA for the period of 2000-2021 (showing events with magnitude M>3).

Recent seismicity in the region around the city of Nafplio is characterized mostly by low magnitude events (< M5.0 Figure 3b). Most of these events have a depth >40km, indicating that they are associated with the Greek subduction zone and not with shallow local faults. Some events with larger magnitudes appear further to the NNE, in the Athikia fault zone and towards the North, within the Gulf of Corinth, which shows a significant seismic activity (Figure 3b).

4. Seismic ambient noise measurements

Single-station seismic ambient noise measurements were performed in several sites distributed between the historical centre of Nafplio, the modern town and the Acronafplia ridge (Figure 2). Seismic ambient noise was recorded for 1 hour in each site using LE-3D/5s 3-component seismometers by Lennartz Electronic GmbH coupled with REFTEK 130-01 dataloggers set to a sampling frequency of 250 Hz.

The seismic ambient noise measurement was analyzed by the Horizontal-to-Vertical Spectral Ratio (HVSR) technique (Nakamura, 1989) that is commonly used to derive the fundamental frequency (f0) of sites

characterised by a stratigraphy with a marked impedance contrast, traditionally a soft soil on a stiff bedrock (Bour et al. 1998; Haghshenas et al. 2008). Using Geopsy software (Wathelet et al., 2020), each 1-h record was divided in non-overlapping windows of 40 s with 5% cosine taper; the Fast Fourier Transform (FFT) was computed for the three components (North-South, East-West and Up-Down) in each window and the obtained FFT spectra were smoothed by the Konno and Ohmachi (1998) function; the single-window spectra and HVSR ratio were averaged to obtain mean FFT spectra for each component and the HVSR function.

It is possible to observe that the HVSR functions obtained by analyzing the seismic ambient noise measurements on the Acronafplia ridge do not show any significant peak (Figure 4, right panel), indicating that this limestone acts as seismic bedrock. On the contrary, the HVSR functions are characterized by marked peaks for the measurements carried out on the recent deposits of the Nafplio coastal plain, with frequency values that vary between 1 and 2 Hz in the modern town area (Figure 4, middle panel) and 2 and 5 Hz in the historical centre (Figure 4, left panel). These resonance values can testify to a lower thickness of the recent deposits in the historical centre area.

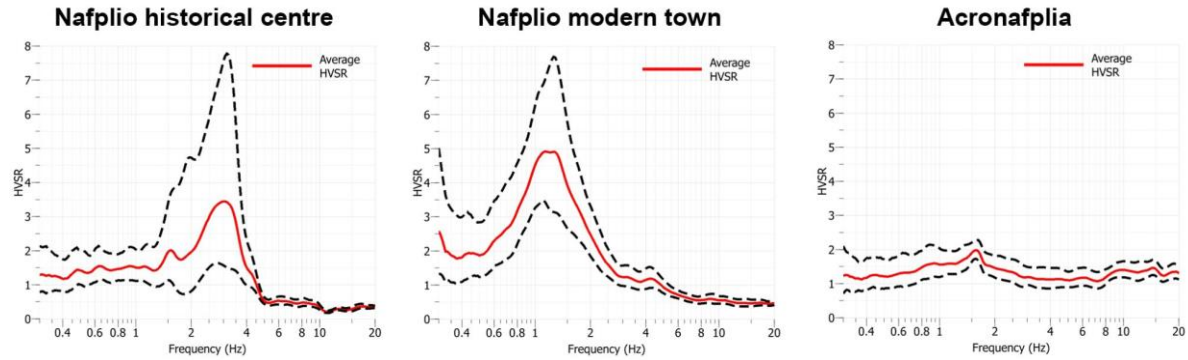

Figure 4. Examples of HVSR function (the dashed black lines show the standard deviation of the curve) obtained for Nafplio historical centre, Nafplio modern town and Acronafplia.

5. Conclusions and future activities

In future perspective, two-dimensional numerical modelling (for seismic input at different return periods) will be carried out to obtain the amplification functions along different engineering geological sections that will allow to analyze the distribution of site amplification effects due to both morphological and stratigraphic characteristics in Nafplio's municipality. Furthermore, it will be possible to obtain:

- elastic response spectra for the characterization of the site response in the design of seismic vulnerability mitigation interventions.
- specific amplification factors that will allow to perform a zonation of the seismic local response as a useful tool for urban planning and seismic risk mitigation.

The generation of a three-dimensional multi-source model is one of the most challenging aspects among the future developments of the project. The data modelling activities proceed through the construction of a geodatabase, a sort of data storage model used for geospatial analysis in a GIS environment and editing. The processing activities on point data, employing appropriate interpolation algorithms, may aspire to build a 3D mesh capable of storing and representing site-specific geological-geophysical aspects. The overlapping of geological, engineering, and geophysical knowledge within a solid geo-referenced model can potentially lead

to both the manipulation of spatial information and the extraction of useful elements for the decision-making process.

Based on preliminary results from the STABLE project research which is carried on at Nafplio town area (Greece), a not negligible local seismic response was observed from HVSR computed after seismic noise measurement. In particular, the town area closest to the coastline reveals a resonance due to recent deposits (marine and continental) at almost 1Hz. On the contrary, the portion of the plain closest to the Acronafplia ridge shows a resonance up to 5Hz. It is not possible to exclude 2D amplification effects due to the lateral contact between the seismic bedrock outcropping along the ridge and the soft soil which fills the plain. In view of structural stability analysis, a quantitative evaluation of the local seismic amplification will be performed through numerical modelling. A 3D geological model of the subsoil will be derived to support the conceptual model for local seismic response, allowing the extrapolation of effects where only indirect data are available.

Acknowledgements

This work was prepared in the framework of the STructural stABiLity risk assEssment project (STABLE), H2020-MSCA-RISE-2018 with Grant Agreement number: 823966. The Authors wish to thank Luigi Marino for his technical co-operation in the geophysical field surveying. The first author thanks Dr. C. Georgiou from HSGME and Mr. A. Kokoromytis for providing previous geological and geotechnical data for Nafplio.

References

Ambraseys, N. (2009). Earthquakes in the Mediterranean and Middle East: A Multidisciplinary Study of Seismicity up to 1900. Cambridge University Press, New York, 968 pp.

Apostolidis, E., Koutsouveli, A. Hellenic Survey of Geology & Mineral Exploration (HSGME), (2010). Engineering geological mapping in the urban and suburban region of Nafplio city (Argolis, Greece). Bulletin of the Geological Society of Greece, XLIII, No 3, p.1418-1427, Proceedings of the 12th International Congress, Patras

Armijo, R., Meyer, B. G. C. P., King, G. C. P., Rigo, A., Papanastassiou, D. (1996). Quaternary evolution of the Corinth Rift and its implications for the Late Cenozoic evolution of the Aegean. Geophys. J. Int., 126(1), 11-53.

Ferentinos, G., Papatheodorou, G., Collins, M. B. (1988). Sediment transport processes on an active submarine fault escarpment: Gulf of Corinth, Greece. Mar. Geol., 83(1-4), 43-61.

Goldsworthy, M., Jackson, J. (2001). Migration of activity within normal fault systems: examples from the Quaternary of mainland Greece. J. Struct. Geol., 23(2), 489-506.

Bour M., Fouissac D., Dominique P., Martin, C. (1998). On the use of microtremor recordings in seismic microzonation. Soil Dyn. Earthq. Eng., 17(7-8), 465-474.

Haghshenas, E., Bard, P.-Y., Theodulidis, N. (2008). SESAME WP04 Team Empirical evaluation of microtremor H/V spectral ratio. Bull. Earthq. Eng., 6, 75-108.

Hellenic Survey of Geology & Mineral Exploration (HSGME) (2007-2009). Project 7.3.1.3.''Urban Geology'', Subproject 3 ''Integrated geological, geotechnical, hydrogeological, geochemical, geophysical and marine studies of the urban and suburban pilot area of Nafplio, Argolis prefecture''.

Karakaisis, G. F., Papazachos, C. B., Scordilis, E. M. (2010). Seismic sources and main seismic faults in the Aegean and surrounding area. Bulletin of the Geological Society of Greece, 43(4), 2026-2042.

Karastathis, V.K., Karmis, P., Novikova, T., Roumelioti, Z., Gerolymatou, E., Papanastassiou, D., Liakopoulos, S., Tsombos, P., Papadopoulos, G.A. (2010). The contribution of geophysical techniques to site characterisation and liquefaction risk assessment: Case study of Nafplio City.Journal of Applied Geophysics Vol. 72, p. 194–211

Papanikolaou, D., Lykousis, V., Chronis, G., Pavlakis, P. (1988). A comparative study of neotectonic basins across the Hellenic arc: the Messiniakos, Argolikos, Saronikos and Southern Evoikos Gulfs. Basin Research, 1(3), 167-176.

Papazachos, B., Papazachou, C. (2003). The earthquakes of Greece. Ed Ziti, Thessaloniki.

Roberts, G., Papanikolaou, I., Vött, A., Pantosti, D., Hadler, H. (2011). Active Tectonics and Earthquake Geology of the Perachora Peninsula and the Area of the Isthmus, Corinth Gulf, Greece. 2nd INQUA-IGCP 567 International Workshop on Active Tectonics, Earthquake Geology, Archaeology and Engineering, 19-24 September 2011, Corinth (Greece), Field Trip Guide, 70 pp.

Konno, K., Ohmachi, T. (1998) Ground-motion characteristics estimated from spectral ratio between horizontal and vertical com-ponents of microtremor. Bull. Seism. Soc. Am., 88, 228-241.

Nakamura, Y. (1989). A method for dynamic characteristics estimation of subsurface using microtremor on the ground surface. Quarterly Report of Railway Technical Research Institute (RTRI), 30(1), 25-33.

Sabatakakis, P., Koukis, G. (2010). Aqueous environment and effects on the civil areas: the case of Nafplio, Bulletin of the Geological Society of Greece, XLIII, No 3, p.1508-1519, Proceedings of the 12th International Congress, Patras

Triton Consulting Engineers S.A. (2003). Geotechnical report for the excavatability conditions of the harbour basin in front of the commercial pier of Nafplio port. Project ‘’Nafplio Port’’. Athens, June 2003.

Triton Consulting Engineers S.A. (2017). Geotechnical report for the geotechnical investigation with submarine boreholes and the classification of the materials that were excavated in the framework of the Nafplio harbour deepening project. Athens, June 2017

Wathelet, M., Chatelain, J.-L., Cornou, C., Di Giulio, G., Guillier, B., Ohrnberger, M., Savvaidis, A. (2020). Geopsy: A User-Friendly Open-Source Tool Set for Ambient Vibration Processing. Seismol. Res. Lett., 91(3), 1878-1889.

THEME 10 - AGGREGATES AND CONSTRUCTION MATERIALS

Importance of Engineering Geological Studies in Resource and Reserve Reporting for Aggregates

Atiye Tuğrul[1], Murat Yilmaz[2]

[1]*President, IAEG Aggregate Commission, Istanbul University-Cerrahpasa, Geological Engineering Dept., Istanbul, Turkey*

tugrul@iuc.edu.tr

[2]*Secretary, IAEG Aggregate Commission, Istanbul University-Cerrahpasa, Geological Engineering Dept., Istanbul, Turkey*

yilmazm@iuc.edu.tr

ABSTRACT: Aggregates as construction raw materials, including the materials used for cement, are mainly made up of crushed stone, gravel and sand. In this study, the importance of engineering geological researches and new perspectives on the resource and reserve reporting made for aggregates according to International Mining Standards is presented. Expected quality of rocks that have been used in many areas, such as concrete and cement raw material, asphalt and embankment aggregates, railway ballast, change according to their using areas. In many quarry areas there are changes in some parameters in very short distances such as; composition and texture of rock, organic material and shell content, effect of structural characteristics on rock quality, different weathering types and their products, harmful and dangerous substances related with origin of rocks etc. That's why, to determine changes in rock quality by conducting engineering geological studies have an important role in resource and reserve reporting for aggregates. The aim of this study; is to attract attention to objections related to quarry sites without engineering geological studies before reporting and quarrying. Therefore, engineering geological studies that should be conducted in locations of the quarries were mentioned.

Keywords: Aggregate, engineering geology, resource, reserve

1. Introduction

The global aggregate industry has grown every year. This growth has also caused a more professional and technical approach to aggregate mining, both in the exploration phase and in the operation of Aggregate quarries. Aggregate producers should Increase their attention to the environmental impacts and safety risks associated with mining. Every quarry site has its own geological and engineering geological characteristics.

The significant features of a successful aggregate project are; the right rock type having suitable quality for the market, quality continuity, correct evaluation of reserves according to the real market value, low transport costs to the market, correct professional market evaluation and preliminary tests, sector-specific market knowledge

and suitable quarrying method and equipment (crushing, screening, washing etc.) according to the target material's geological characteristics.

In general, aggregates can be produced by using typical mining methods including drilling and blasting, crushing, and screening, if necessary, washing. Once extracted from the quarry, aggregates are processed based on both the characteristics of the rock and the market strategy of the company, to produce various size of aggregates. Producing the best material, in terms of size, shape and quality, is the key to a successful Aggregate project. This depends on, professional geological evaluation, good knowledge of the market demand, professional mining design in line with the target stone geo-structural features, appropriate mining methods and equipment.

If the quarry production plan is not associated with a detailed engineering geological model, unexpected problems may occur during production. Most of the productions are generally made by considering the average quality of the aggregates in the quarry without the need for engineering geology maps. In many quarries, different rock units are frequently extracted, broken, and mixed with each other to minimize the production of low strength rocks. However, there are some losses of high-quality aggregate in the meantime. If the quality change at the quarry site has been investigated before and the material to be produced is wide enough and the quarry area is also large enough, higher quality materials can be produced separately. (Raisanen, 2005). As stated by Van Loon (2002); production quality in an aggregate quarry depends on the local geological characteristics of the area where the quarry is located. The shape of the aggregate depends on the structural and textural properties of the rock, as well as the production technique (Ramsay et al., 1974). Also, tests given in many standards do not adequately characterize aggregate sources (Langer, 2001). Therefore, geological investigations should be done. In determining whether the quality of the aggregate produced in a region is due to the mechanical properties of the aggregates or the production processes, the experience of the geological engineer who researches the geology of the quarry site is also very important.

The geological, structural, and metamorphic histories of rocks have a high impact on their quality (Persson, 2002). If the planning and production of an operated quarry is not based on geological data about the quarry site, it is inevitable that it will be less efficient (Raisanen, 2005). The characteristics of the rocks in the pit area and the change of these properties affect the selection and cost of the quarry equipment. In addition, as Lizotte and Scoble (1994) stated, although the influence of the geological properties of rocks on production processes (blasting, crushing, etc.) is known, the information on this is not sufficient. As a result of blasting and crushing, some rock types have a very fine material ratio, some have a high proportion of elongate and/or flat grains, but some do not have any problems (Jern, 2001). The surface geometry and shape of the crushed grain is related to the behavior of the rock against the crushing and blasting process (Briggs and Bearman, 1996; Evertsson, 2000). Especially in heterogeneous rock conditions, while evaluating the quarry site, considering the geological and mechanical properties of the rock, will provide economic benefits to the business (Stubbs ve Smith, 1997; Houston and Smith, 1997; Lolcama, 2002; Persson, 2002; Raisanen, 2005). According to Smith and Collis (1993), the production system and its economic conditions should be evaluated as well as environmental and geological factors while planning a quarry site. These evaluations are carried out with engineering geology studies.

In experimental studies, which are another important step in Engineering Geology research, an appropriate test program should be applied regarding the usage area of the aggregate. According to the data obtained from these experiments; the materials produced from the quarries should be classified as much as possible according to their properties. Also, it is necessary to determine the harmful substances in aggregates and the property changes (weathering, dispersion, etc.) that may occur in aggregates during storage. Especially in

igneous and metamorphic rocks, dangerous substances are likely to be present. Therefore, it is important to determine the concentrations of metal elements containing toxic properties for human health before the exploitation of such rocks.

Environmental impacts of aggregate quarries cannot be ignored. The most prominent environmental impacts of these quarries are changes in morphology and land use pattern. Especially forests and agricultural lands are transforming into a wide area. Other effects are the reduction of the residential areas and vegetation of the living creatures in the region, the change of surface and groundwater regime, the pollution of water resources and air due to the dust emitted to the environment, noise, blasting effects, erosion and deterioration of the image. Therefore, the environmental impact levels of such quarries should be investigated in detail. Unfavorable environmental conditions can limit the utilization of reserves. Due to mining, geology has a significant influence on the intensity of environmental impacts. Some geological conditions are well understood and easily characterized. It is easy to determine the environmental impact of such conditions and to control them within the natural system. However, it is more difficult to predict the extent and intensity of environmental impacts of some conditions such as riverbeds, karstic and potential landslide areas. Engineering geology studies are required to determine the instabilities that may occur in the quarry slopes in advance and to evaluate the environmental impacts of the quarries.

2. Important factors to evaluate the Aggregates Projects

The significant features of a successful aggregate project are; the right rock type having suitable quality for the market, correct evaluation of reserves according to the real market value, low transport costs to the market, correct professional market evaluation and preliminary tests, sector-specific market knowledge and suitable quarrying method and equipment according to the target material and its geological characteristics.

Changes in aggregate quality are a very important problem in the quarries. Variability in aggregate quality causes an increase in incremental costs in production of concrete and asphalt. In other words, when the aggregate quality is reduced, for production of concrete or asphalt in the same quality, we must use more cement/bitumen or additives.

Test methods given in the standards do not represent the material quality exactly every time. Petrographic, mineralogical, and chemical analyses should be conducted. According to the usage area, if necessary, durability tests should be performed. In addition, aggregate and cement reaction products and special reaction products related to using different aggregates having different compositions together are also important for concrete durability. Therefore, special investigations are needed related to both aggregate type and usage area.

Local geological features of the area where the quarry is located, especially structural and textural properties of rock, affects the production quality in quarries. Product quality (size, grain shape, fine content, physical and mechanical characteristics of the aggregates etc.) is related with the production techniques (quarry planning, blasting design, crusher type etc.). The quality continuity in an aggregate quarry controls the product quality continuity. It is relatively straightforward to determine if the material is of low, medium, or high quality in relation to market demand.

In general, aggregates can be produced by using typical mining methods including drilling and blasting, crushing and screening, if necessary, washing. Once extracted from the quarry, aggregates are processed based on both the characteristics of the rock and the market strategy of the company, to produce various sizes of aggregates. Producing the best material, in terms of size, shape and quality, is the key to a successful

Aggregate Quarrying project. This depends on, professional geological evaluation, good knowledge of the market demand, professional mining design in line with the target stone geo-structural features, appropriate mining methods and equipment.

3. Common Constraints in Aggregate Projects

Some conditions may affect accessing the resource at some point within the licensed area. Some of these constraints may not be related to the area studied and some other constraints may be added to the list. These common constraints are given below.

- Geology: Overburden, material quality, quality continuity, structural effects / continuity, hydrogeology, geotechnics, hydrology etc.
- Land use / permitting: Areas under evaluation, time limit (permit/lease), output limit (permit / lease), other permit restrictions, zoning, no working rights, other restrictions
- Technical Studies: Access to excavated and filled slopes in the quarry, plant location, capacity and capability, site infrastructure, stockpiles, sewage lagoons, access to quarry, managing slope stability, rock slope excavation stability, fill slope stability, slope design, working plan,
- Environmental effects: Water, wastewater, air/dust, noise, vibration effects, visual pollution, flora and fauna, habitats/wetlands
- Market Demand/Economy: Valuation of the reserve, production cost, sales price, transportation cost, dispossession, return of investment
- Social Effects: Landscape, protected property, dispossession, social/community effects, archaeology, ancient monuments, ancient structures

4. Resource and Reserve Reporting for Aggregates

Petrographical, mineralogical and chemical analyses may not always be relevant, and other quality and performance characteristics may be more applicable and acceptable as the basis of the reporting. As indicated in CRIRSCO (2019) Template (UMREK Code, 2018), some aggregate resources may be capable of yielding products suitable for more than one application and/or specification. If considered material by the Competent Person, such multiple products should be quantified either separately or as a percentage of the bulk deposit. Unless it is a specific aspect of his or her instructions to reflect the range of product mixes and target markets for the deposit, the Competent Person should normally report the reserves and resources within the framework of an existing mining plan or established set of product and market assumptions and objectives. If there is potential for ancillary products, or mining or process waste, to be sold off site for subsidiary uses in addition to the planned sales of primary products (i.e. other uses for non-saleable quarry production, such as secondary aggregate or engineering or other fill), the Competent Person should reflect this in his report and comment on any significant implications (e.g. reductions in the amount of non-saleable material that could otherwise be used as a restoration material). For aggregates, it is common practice to report the saleable (or usable) product rather than the 'as mined' product.

5. The resources estimation (inferred, indicated and measured) and the reserves calculation

As a first stage, resources are estimated using various data and field evaluation techniques, such as geological and geophysical exploration, core drilling, pits, and sampling. As a second stage, taking into consideration the CRIRSCO (2019) Template (PERC, UMREK Code etc.), correlation scheme for the transformation of resources into reserves (Figure 1), the following modifying factors scheme for aggregate reserves calculations are proposed.

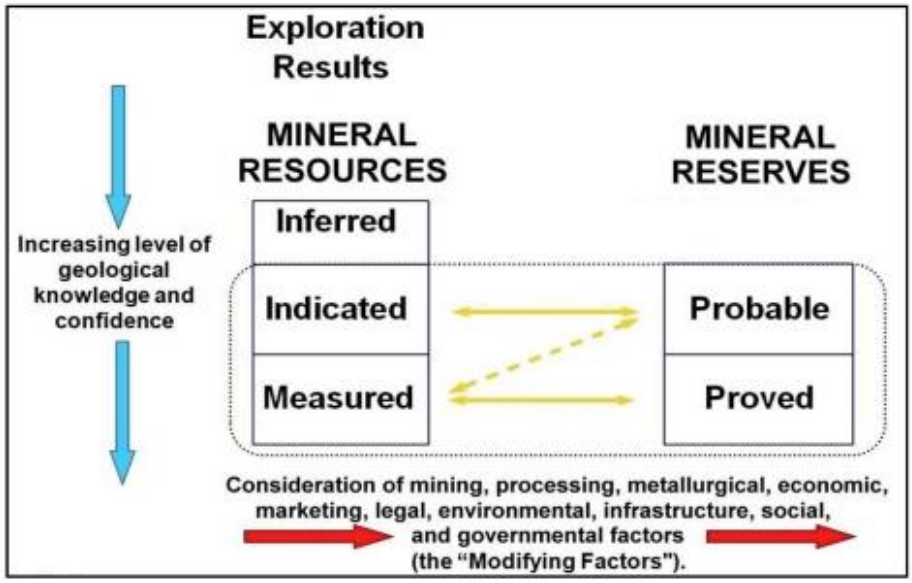

Figure 1. General relationship between Exploration results, mineral resources, and mineral Reserves (CRIRSCO, 2019 Template)

As indicated by CRIRSCO (2019); Modifying Factors are considerations used to convert Mineral Resources to Mineral Reserves. These factors include mining, processing, metallurgical, infrastructure, economic, marketing, legal, environmental, social, and governmental factors.

As written by Cosi (2015); the concept is necessary in order to quantify the estimated percentage of volumetric reserves of target rock that can realistically be considered as marketable reserves, and as such, to assign a more accurate real market value to a Dimension Stone project. This is nearly the same as in aggregate projects. He also indicated that; Market quality can be calculated as a single 'Market Quality Factor' (MQF), and this factor cannot be evaluated by chemical or any other laboratory analyses. This situation is also nearly the same for aggregate projects. It should also be confirmed by comparison with comparable materials already priced and sold in the aggregate market, as well as by the expert on Aggregates (Competent Person on aggregates). Benchmark analysis of similar materials should be included in an Aggregate project during the evaluation of market quality factor.

As indicated in UMREK Code (2018); within the scope of reporting, it is possible to utilize core drilling and if necessary geophysical methods in aggregate exploration. In Mineral Resource and Mineral Reserve reporting, all the Mineral Resources identified in the field need to be identified (geo-stratigraphic analyses by considering market probabilities and describing the geological unit planned for production). Measured Resource estimation (containing data acquired from drilling and if necessary geophysics through geological prospecting, outcrop sampling, preparing geological cross and longitudinal sections, 3D resource modelling and engineering

geological modelling), and the Proven Reserves should be identified by defining the following six Attenuation Factors and including in the report (Modified from Cosi, 2015 and UMREK Code, 2018).

MIF (Mineral Impact Factor): The estimated volume percentage of within rock mass/gravel sand deposit which cannot be produced due to some unusable layers/parts containing harmful/dangerous minerals/elements.

DF (Discontinuity Factor): The estimated volume percentage within rock mass/gravel sand deposit which cannot be produced due to some unusable layers, bedding planes, faults, joints, fissure and openings (this is usually described for limestones and marbles not directly produced by karstic phenomena).

KF (Karstification Factor): Karstic openings within rock mass (Determined by field studies, core logging and if necessary, by geophysical exploration).

WF (Weathering Factor): The estimated volume percentage of weathered material within rock mass/gravel and sand deposit, which cannot be produced.

MF (Mining Factor): The estimated volume percentage that cannot be produced due to mining design and planning (the volume fraction of the resource quantity that will be left unproduced and is not producible in economic terms due to the final slope design shaped by the pit type).

QF (Quality Factor): The estimated volume percentage that does not meet the quality traits related with the rock/gravel-sand composition (such as color, weathering products and their distribution etc.).

The quality of aggregates, formed by a mix of these parameters, directly influences the demand and the selling prices. From the resource quantity to be identified in the reporting, reserve quantities determined by also considering the above specified reduction factors must be identified. The recovery rate may vary in relation to the final target product (type, shape and size) and may also depend on the company's market strategy. Petrographical characteristics, mineralogical and chemical composition and physico-mechanical properties are the key parameters for the classification of aggregates.

An aggregate CP Report should include all available information on the safety, environmental and social aspects of the project, with comments and evaluation on the project's sustainability from these and any other relevant non-financial perspectives. The products of mining need to be sustainable.

An aggregate project should be coordinated and evaluated by an Aggregate Competent Person, with sufficient knowledge and experience in the geology and mining of aggregates and in the relevant market areas. Project report should contain information, if the aggregate is of low, medium or high quality in relation to market demand and/or to define the content of the mineral in a unit volume or length.

6. Valuation Methodologies in the Aggregate Sector

The aggregate sector is very particular, with its own rules, features and driving factors. As a result, the valuation of Aggregate projects needs to be approached and evaluated using sector specific methodologies and tools, different from those used in other sectors. Resource estimation and reserve calculations of aggregate projects should also be made considering generally different factors than other mining projects. Aggregate projects cannot be evaluated and valuated like all other mining projects. They are completely different. In an aggregate quarrying project, the rock mass/gravel, sand deposits should be evaluated. Defining the geometrical characteristics (volume) of the rock mass/gravel, sand deposits is not enough. Considering the market quality is much more necessary. Detailed market and price benchmark analyses should always be included in

Competent Person Report to estimate the quality of the identified resources, so that the final economic reserves can be accurately calculated.

7. Conclusion

The global aggregate industry has grown every year. This growth has also triggered a significant general trend in many countries towards the adoption of a more professional and technical approach to aggregate mining, both in the exploration phase and in the operation of Aggregate quarries. Production technologies have developed rapidly over the past three decades, particularly in the developed world where labor costs are high and developing countries have also developed their own equipment manufacturing industries in the last years. Furthermore, this development trend has been accompanied by a period of increased attention to the environmental impacts and safety risks associated with mining, and many of these regions have experienced increased regulation during the past decade. The Engineering Geological investigations conducted in quarry sites have an important role during these studies.

References

Bobrowsky, P.T. (1998). Aggregate resources-A global perspective: A.A. Balkema, Rotterdam, Netherlands, pp. 470

Briggs, C. A., Bearman R. A. (1996). An investigation of rock breakage and damage in comminution equipment. Minerals Engineering, 9, pp. 489–497.

Cosi, M. (2015). The dimension stone sector: new perspectives on the global market and on the reporting of international mining standards, EFG Magazine, pp. 24-30.

CRIRSCO Template. (2019). CRIRSCO international reporting Template, http://www.crirsco.com/template.asp

Evertsson, C. M. (2000). Cone crusher performance. PhD Thesis, Chalmers University of Technology, Goteborg.

Houston, E. C., Smith, J. V. (1997). Assessment of rock quality variability due to smectitic alteration in basalt using X-ray diffraction analysis. Engineering Geology, 46, pp. 19–32.

Jern, M. (2001). Determination of the damaged zone in quarries, related to aggregate production. Bulletin of Engineering Geology and the Environment., 60, pp. 157–166.

Langer, W.H. (2001). Geological considerations affecting aggregate specifications. 9th Annual Symposium of the International Center for Aggregates Research, Austin, Texas, April 23-25.

Langer, W. H. (2020). The role of the geologist in managing the development of aggregate resources, European Geologist, Proceedings of 1st International Professional Geology Conference, Alicante University, Spain, pp. 52-54.

Lizotte, Y.C., Scoble, M.J. (1994). Geological control over blast fragmentation. Can Mining Metallurgical Bull. 87(983), pp. 57–71.

Lolcama, J. L., Cohen, H. A., Tonkin, M. J. (2002). Deep karst conduits, flooding, and sinkholes: lessons for the aggregates industry. Engineering Geology, 65, pp. 151–157.

Lüttig, G.W. (1994). Aggregates-Raw materials' giant: Report on the 2nd International Aggregate Symposium, Erlangen, pp. 346

PERC Code. (2017). Pan-European Code for reporting of Exploration Results, http://percstandard.org/about.asp

Persson, L. (2002). Rock materials for construction: Resources, Properties, Heterogeneity and suitability for use: Examples and Issues from the Precambrian of Sweden, Proceedings of 9th IAEG Congress, Durban, South Africa, pp. 105-120.

Powell, J.D. (1999). Aggregate properties-Do we know what we want?. Proceedings, Seventh Annual Symposium of the International Center for Aggregates Research, University of Texas, Austin, Texas, p. A1-4-4 -A1-4-6.

Raisanen, M. (2005). Quality assessment of a geologically heterogeneous rock quarry in Pirkanmaa county, southern Finland, Bulletin of Engineering Geology and the Environment, 64, pp. 409-418.

Ramsay, D. M., Dhir, R. K., Spence, I. M. (1974). The role of rock and clast fabric in the physical performance of crushed-rock aggregate, Engineering Geology, 8, pp. 267-285.

Smith, M. R., Collis, L. (1993). Aggregates. Geological Society Engineering Geology Special Publication, Vol 9. pp. 339

Stubbs, B. J., Smith, J. V. (1997). Weathered bedrock as a source of sand and gravel aggregate in north-eastern New South Wales, Australia. Environ Geol., 32(1), pp. 64–70.

UMREK Code. (2018). National Resources and Reserves reporting Committee of Turkey (UMREK), First Edition, http://www.umrek.com.tr/index.php?id=umrekcode

Van Loon, A. J. (2002). The complexity of simple geology. Earth Sci Rev., 59, pp. 287–295.

Author Index

A

Alvarado F. 50
Antonielli B. 140
Antoniou A. 140

B

Balint A. 41
Bar N. 130
Bozzano F. 140

C

Carli G. D. 50
Carlucc R. 140
Chortis F. 33
Christakis R. 56
Ciampi P. 140

D

Dematteis A. 50
Depountis N. 122
Di Iorio A. 140

F

Fiorucc M. 140

G

Garelick J. 98
Georgiannou V. 33
Giordan D. 114
Gray C. 91
Guenzi D. 114
Gunn M. J. 91, 98

I

Inciocchi D. 140

J

Jardine G. 71

K

Kallimogiannis V. 27, 130
Karagüzel R. 83
Karastathis V. 140
KC J. 56
Kong D. 130
Kumsar H. 106

L

Lainas S. 122
Lannucci R. 140
Lasponara R. 114

M

Maniatakis C. 140
Martino S. 140
Matveev V. 19
Mavroulidou M. 91, 98
Mouzakiotis A. 140

N

Notti D. 114

P

Papadimitriou A. 140
Pavlopoulou E. M. 33
Payne I. 98
Purchase D. 98

R

Raut M. 56
Rivellino S. 140
Russo G. 11

S

Sabatakakis N. 122
Safdar M. U. 98
Sapkota S. 56
Sarayköylü T. 106
Saroglou C. 27, 130, 140
Say Y. 106
Shanina V. V. 19

T

Thuering M. 50
Tsirogianni A. 130, 140
Tuğrul A. 149

V

Verzani L. P. 11

W

Wu F. 130

Y

Yalçın H. T. 83
Yaltırak C. 83
Yilmaz M. 149

EUROENGEO ATHENS 2020

3RD EUROPEAN REGIONAL CONFERENCE OF THE INTERNATIONAL ASSOCIATION FOR ENGINEERING GEOLOGY & THE ENVIRONMENT

Leading to Innovative Engineering Geology Practices